Journal of Radioanalytical and Nuclear Chemistry
https://doi.org/10.1007/s10967-024-09513-7

Extension of evaluated cross section database for charged particle monitor reactions

F. Tárkányi[1] · A. Hermanne[2] · A. V. Ignatyuk[3] · F. Ditrói[1] · S. Takács[1] · R. Capote-Noy[4]

Received: 18 March 2024 / Accepted: 17 April 2024

Abstract
The evaluation and deduction of recommended cross section values allowing extension of the database to monitor energy and intensity parameters of charged particle beams is presented. Included are 53 charged particle (p, d, ^{3}He, ^{4}He) induced reactions on suited C, Al, Ti, Fe, Ni, Cu, Nb and Au targets. The new data allow more systematic simultaneous use of multiple reactions on the same target and promote the backings of electrodeposited and sedimented targets as monitoring aids. Where possible the energy range is extended to above 100 MeV. Integral yield curves over the studied energy range are derived and compared to experimentally measured yields at specific energy points. A comparison with the theoretical excitation curve prediction of the TALYS-code as available in the TENDL 2021–2023 libraries is shown.

Keywords Monitor reactions · Charged particle (p, d, ^{3}He, ^{4}He) beams · Recommended cross sections · TENDL predictions · Thick target yield

Introduction

The development and optimization of radionuclide production routes for industrial and medical applications are of considerable and indisputable interest to the IAEA and to the user community. Cyclotrons and other particle accelerators, available in recent years in an increasing number of countries, often with the support of the IAEA, are being used for the production of radioisotopes for medicinal diagnostic and therapeutic purposes, thin layer activation for industrial wear studies, and nuclear analytics. Besides commercial or in-house medical radionuclide production, reactions with low-energy charged particles are of primary importance for several industrial and scientific applications.

The physical basis for radioisotope production is the nuclear interaction of charged particles, such as protons, deuterons and alphas, with matter atoms. The different contributing processes and reactions have to be well quantitatively understood to obtain useful and high-purity radioisotopes efficiently and safely. For this reason, knowledge of well-evaluated numerical data for excitation functions (cross sections depending on particle energy) and thick target yields over verified energy domains are needed. Both for efficient production of radioisotopes in the different applications and for physics on nuclear reaction characteristics a good control on bombarding beam parameters is essential. A technique applied on-site is the use of monitor reactions. Although cross section data for basic and usefull monitor reactions are available and were evaluated earlier the further development of radionuclide production requires broader and self-controlling possibility of choices for monitors. In this study an extension of the evaluated number of reactions and their critical evaluation is discussed. An overview of basic characteristics and requirements of beam monitoring by charged particle-induced reactions on well-identified and selected targets, followed by measurement of the decay of the activation products is presented in the next sections.

✉ F. Ditrói
ditroi@atomki.hu

1 HUN-REN Institute for Nuclear Research, Debrecen, Hungary

2 Vrije Universiteit, Brussels, Belgium

3 Institute for Physics and Power Engineering, Obninsk, Russia

4 IAEA, Vienna, Austria

Published online: 13 May 2024

Monitor reactions

The usefulness of monitor reactions for controlling or investigating different beam parameters [1], defined more precisely later, is summarized in Table 1 for three specific types of applications where their importance and requirements are different.

The definitions of the above-listed beam parameters and the methods of determination and measurement are explained here:

Ion species and charge state

Definition: (Z, N).
Determination: by parameters of ion source, accelerators, bending magnets.
Application of monitor reactions: possible.

Current

Definition: time dependence of the beam current.
Type: macro pulse, bunch, mean current: DC or AC.
Determination: Faraday cup, calorimetric measurement, beam current transformers, secondary particles (electrons, ions, neutrons).
Application of monitor reactions: possible.

Beam profile

Definition: intensity distribution in transverse directions.
Determination: Viewing screens (optical, thermographic), profile grids, scanners or harps, residual gas ionization, slits + Faraday cup measurement, monitor reactions.
Application of monitor reactions: possible.

Beam energy, beam energy spread

Energy:
Definition: Nominal energy of a single particle within this beam; in practice the average.
Energy spread:
Definition: Energy distribution of the beam particles.
Determination: Magnetic spectrometers, Telescopes, TOF technique (capacitive pick-ups, coaxial cups, etc.), monitor reactions.
Application of monitor reactions: yes.

Table 1 Beam parameters

Beam parameters	Applications		
	Accelerator technology	Isotope Production	Radiation therapy
Ion species, charge state	Yes	Yes	Yes
Current	Yes	Yes	Yes
Macro	Yes	No	No
Bunch	Yes	No	No
Mean	Yes	Yes	Yes
Beam profile	Yes	Yes	Yes
Emittance and brilliance	Yes	(Yes)	(Yes)
Beam energy, beam energy spread	Yes	Yes	Yes
Beam pulse frequency, width	Yes	No	No

The basic idea for the use of monitor reactions is the activation technique by irradiation of a target sample and measurement of the amount of radioactive reaction products via direct in-beam counting or their nuclear decay. It is based on the use of the general equation:

$$A \sim N \sim s(E, q)F(t)\ n$$

where A is the activity in Bq, N is the number of produced nuclei,ϕ(t) is the total number of incident particles on the surface of the target (fluence, flux and irradiation time), σ(E, θ) is the energy and angle-dependent reaction cross section, n is the number of irradiated target nuclei (depends on target thickness, density and atomic mass).

Based on this equation the following mean parameters can be determined after activity measurement:

- Number of incident particles (fluence) or irradiation time.
- Number of target nuclei (thickness).
- Incident particle energy.

In most cases, a single unknown parameter can be extracted, in special circumstances several parameters can be obtained simultaneously (e.g. energy, intensity).

A series of general and special conditions have to be respected and maintained for the optimal choice of targets, activation reactions and their cross sections, irradiation conditions to successfully and reliably apply the activation technique.

The target.

- The target material should be of a single element or impurities should not result in the formation of activated contaminating isotopes that significantly disturb the quantitative determination of the reaction products of the primary target. The target material should be obtained without difficulty at a reasonable price.
- The target should be prepared in final form in an easy way to get stable uniform thickness.
- The target material and the prepared target should stand in normal laboratory circumstances without chemical or physical changes (recrystallization, oxidation, etc.).

- The target should be stable during irradiation. Targets having low melting points or chemical instabilities by heating should be avoided.
- The same type of target could be used for broad energy and flux ranges and different bombarding particles.
- The target should have high thermal conductivity to allow higher intensities and effective cooling.

The reaction cross section.

- The absolute cross section for the chosen reaction should be known precisely in a wide range of incident particle energy.
- The activation effect of the secondary particles induced by the primary process should be small (cf. neutron production and activation).
- The cross sections have to be "high" in the investigated energy region.
- For improvement of the energy measurements range the cross sections should change sharply in the investigated energy (preferably around the energy of the maximal cross section) and preferably several reaction channels have to be open with a different slope of the excitation functions.
- For reliable flux measurements, the cross section should be constant or change slowly in the investigated energy range to minimize the uncertainty of energy.
- The reaction products (measurement of activation).
- The emitted radiation should be easily measurable (energy, intensity, type of radiation, form of the reaction products).
- The reaction products (decay) have to remain in the irradiated sample (gas, recoil effects).
- The activity of simultaneously produced "contaminating" reaction products, not used in the monitoring process, should be limited (reduction of background, overloading and increase of dead time).
- The half-life of the reaction products should be not too short to limit important decay during unloading, transport to detector set up and measurement of several targets and not very long as compared to irradiation time to get proper activity. But in the case of using parallel monitor reactions on the same target, the half-life of the products can differ significantly.
- An internationally accepted database for nuclear decay data (half-life, energy and abundance of emitted γ-lines) should be used for deriving cross section from the activity measurements performed at the site. The data as mentioned in Table 4 are the reference values.

The irradiation

- The irradiation parameters ($\phi(t)$, E) and thickness should be well-known, controlled and fixed during the time of irradiation.
- The monitor should be placed at a known and constant angle with the beam direction and in the energy region of interest if degraders are involved.

Main characteristics of beam monitoring via monitor reactions

Advantages

- Simple and cheap, performed in combination with irradiation of production targets.
- Require small space compared to other methods.
- Local monitor.
- The number of incoming nuclei is controlled.
- Any beam shape can be monitored.
- Both absolute and relative measurements are possible.
- Broad range of energies and intensities can be monitored.
- Good accuracy for determination of the beam fluence.
- The results could be corrected for later changes in nuclear data.
- Nondestructive, the beam passes through, without significant changes.
- The beam could be followed by extended targets inside (by inserting monitor foils through the target to follow the energy degradation and the beam broadening).

Disadvantages

- Moderate accuracy for determination of the energy.
- Highly depend on the quality of the available nuclear decay data.
- The quality of the recent data base is very poor.
- No online information on the measured parameters.
- It is difficult to install at accelerators and beam lines (temporarily installed)??
- Give only average intensity over irradiation time (time variations couldn't be followed).
- High doses during installation and separation.
- Not independent from the particle species, from energy, their range, etc., compared to other monitor methods.
- The particles have to hit the monitor under well-known conditions.
- Automation, feedback to control during irradiation are impossible.

Main application fields of monitor reactions

- Medical isotope production.

- Parameters of accelerators.
- Nuclear data measurement.
- Irradiation for analytical purposes and thin layer activation technique.
- Research type of works.

Problems when using monitor reactions

- Data base still needs to be extended, especially at higher energies.
- Very few intercomparisons and validations.
- Definition of the used cross sections (direct, cumulative). Problems in case of cumulative having not very significant parent-daughter half-life.
- To place the monitor foil in the proper position (E, geometrically, single monitors in front of the target or series of monitors to follow the beam parameters).
- Uniformity of the monitor targets.
- Irradiation time vs half-lives of product targets.
- Effect of time variation of the fluence (integral).
- Effect of finite thickness (integral).
- Low energy gamma-rays, background lines.
- Effect of energy spread of the beam.
- Comparison of results of monitor reaction and other direct beam current measurement.
- Cumulative effects.
- Correction for recoils.
- Secondary particles.

Evaluation of experimental data and generation of the recommended cross section for standard monitor reactions

At present, the IAEA database [2] contains recommended data for monitor reactions for 4 types of light charged particles: 11 reactions for protons, 11 for deuterons, 6 for ^{3}He, 6 for alpha particles (Table 1) [2–4]. It is however to be mentioned that, according to recent publications, the monitor reactions used in new research or production studies continuously change and are often not the recommended standard reactions.

In this work evaluation and proposal for a large number of new recommended cross sections over a wide energy are discussed and an update is presented for 4 earlier evaluated reactions. The new reactions were selected based on reported experimentally determined cross sections, decay properties of the product nuclei and the suitability of target materials as monitors. Attention was paid to discuss similar reactions leading to different activation products on interesting separate isotopes of multi-isotopic targets, allowing direct confirmation in a single experiment (Cu, Ti, Ni, Fe, Mo targets). The different conditions for appropriate target material and irradiation conditions have been summarized in earlier sections. In addition to the 19 new reactions proposed in the IAEA Technical Meeting in 2018 [5], 38 reactions were evaluated/re-evaluated and all are collected in Table 1.

The monitor reactions on C were used extensively earlier up to high energy and they were included in the earlier IAEA compilation [6] but are at present not in the database.

The Nb, Au target materials are new while a reaction on Fe is only present once. The cross sections in Fe are very well measured, the only drawback is the possible corrosion. Nuclear reactions on Au and Nb were used already earlier to monitor charged particle beams. In the case of Nb the low melting point has to be taken into account.

For several of the presently used monitor targets often only two, or even a single, reaction is recommended for a specific incoming particle. Now additional reactions were included for the different incident particles, allowing often comparison and confirmation based on differences in the excitation functions:

- A different energy slope of the excitation functions of different reaction products gives a better possibility to determine the energy of the bombarding particle.
- A nearly constant cross section over a broad energy range gives the possibility to avoid the need for exact energy knowledge for the determination of the number of incident particles.
- The different half-lives of the reaction products give the possibility to separately measure monitor data at optimized times after EOB for each activation product.
- A few reactions on monoisotopic elements or natural targets are common with reactions for the production of medical isotopes. They can be included in both lists of the IAEA database.

4.1 Summary of the method of evaluation

Detailed information on the method of collection and selection of experimental data, followed by Padé fitting methodology and obtaining uncertainties of the fit, can be found in relevant IAEA publications.

We repeat here the main steps and attention points of the compilation and evaluation:

- The experimental cross section data, often without uncertainties, were found in EXFOR [7] and/or in the original publications.
- The EXFOR/published datasets were corrected for up-to-date monitor cross sections or nuclear decay characteristics. Unrealistic low uncertainties in publications were enlarged based on other experimental data and the practice of the compilers.

- The experimental data show in many cases very large disagreements between different publications. This is mainly because they were measured in poor experimental circumstances, without strict rules being agreed upon and information was not always complete (beam current and detector efficiency measurements, nuclear data used,…). It was hence impossible to use the standard evaluation method based on pure statistical methods.
- In practice, the evaluation contains several steps. Collection, if needed correction on the decay data to the values of [8, 9] and of the energy scale, and selection of published experimental data sets by an experimentalist. Fitting of the selected data by an expert on model calculation and data evaluation. During this step often further deselection of a few separate data, outlying more than the uncertainties when compared to the neighboring selected sets, in contradiction to the theoretical predictions and below the reaction thresholds, occurred.
- By investigating the experimental circumstances several corrections can be necessary: rescaling the energy in case of long stacks, normalization of some large sets to ensure data in unmeasured regions, deleting complete data controversy data sets, giving larger weight to data from well-proved authors, detail investigate the used technology (long stacks, coincidence losses, use only one monitor foil, unreliable primary beam energy, measurement of beam intensity with not Faraday cups, detector efficiencies at low energies, etc.)
- Problematic cases occur when only a few (two or three) experimental data sets are available with contradicting results. In this case, to fill the energy range where only one data set was available, selection and correction, and normalization were done based on many facts: on the earlier results of the authors, the used experimental techniques, etc.
- For particle-induced reactions in several cases, the data from some publications are too low by a factor of two. We observed this fact already earlier while evaluating monitor reactions. Our experimental data show that the sets with too low cross sections result from an improper estimation of the number of incident particles (measured by the incoming charge) due to neglecting the double electron charge of the α-particle.
- For the selection of the best monitor reaction by practical users, the most important information is the figures of the excitation function and the yield curves.
- Presently at least two independent data sets are needed before selection and fitting are considered. Reactions for which only a single experimental data set was found in EXFOR or literature are not included or discussed in this article.
- Differential yield data are used only if the yields are given from the threshold on and if the mentioned energy steps are small (depending on the behavior of the excitation function).
- For the selection of data sets earlier evaluations and the results of model calculations were taken into account. An important factor in the selection of sets for contradicting data is the quality of the results and the experience in research of the concerned group.
- Fit of the selected experimental data was done using Padé approach (approximant by rational function) [10–12].
- Uncertainties in the fitted results were estimated via a least-squares method with an addition of a 4% systematic uncertainty, an expert estimate of overall unrecognized uncertainties as discussed in earlier evaluations.
- Calculation of so-called physical integral production yields [13] is based on the obtained recommended cross section data.
- We decided to include 2021 and 2023 versions of the TENDL library to show and discuss the change and possible improvement of the theoretical predictions by the evolution of the TALYS code [14].

Some other points on problems encountered during the evaluation process are:

- In a few problematic reactions different Padé fits were done, with the question of which to select: the one based strictly on experimental data or include theory and systematics.
- For practical production the shape of the excitation function and the tabulated yields are important. Hence no covariance calculations were done.
- According to our experience, the pure statistical evaluation methods only work well in cases where a large number of data sets with realistic uncertainties, detailed knowledge of the experiments and the used nuclear data, are available.
- The reason for disagreement of different data sets lies essentially in:

  Estimation of number of incident particles (Faraday cup, beam stop, monitor in single energy point, monitor in all energy range, etc.).

  Quality of targets in case of different target preparation techniques.

  The technique of spectra measurement, distance, dead time, coincidence losses, and corrections.

  Determination of incident energy and control of the energy degradation.

  Properties of the single foil, stacked foil, and rotating wheel irradiation technique.

  Direct measurement vs after chemical separation.

Table 2 List of the evaluated monitor reactions with energy range is included presently on the IAEA Web

Protons	Deuterons	^{3}He-particles	Alpha-particles
^{27}Al(p,x)^{22}Na (20–1000)	^{27}Al(d,x)^{22}Na (20–100)	^{27}Al(^{3}He,x)^{22}Na (8–100)	^{27}Al(α,x)^{22}Na (30–150)
^{27}Al(p,x)^{24}Na (20–200)	^{27}Al(d,x)^{24}Na (10–100)	^{27}Al(^{3}He,x)^{24}Na (20–130)	^{27}Al(α,x)^{24}Na (30–160)
^{nat}Ti(p,x)^{48} V (2–100)	^{nat}Ti(d,x)^{48} V (2–50)	^{nat}Ti(^{3}He,x)^{48} V (5–100)	^{nat}Ti(a,x)^{51}Cr (5–50)
^{nat}Ti(p,x)^{46}Sc (5–60)	^{nat}Ti(d,x)^{46}Sc (2–80)	^{nat}Cu(^{3}He,x)^{66} Ga (6–40)	^{nat}Cu(a,x)^{66} Ga (7–67)
^{nat}Ni(p,x)^{57}Ni (14–100)	^{nat}Fe(d,x)^{56}Co (8–50)	^{nat}Cu(^{3}He,x)^{63}Zn (10–44)	^{nat}Cu(a,x)^{67} Ga (14–49)
^{nat}Cu(p,x)^{62}Zn (14–100)	^{60}Ni(d,x)^{61}Cu (2–7)	^{nat}Cu(^{3}He,x)^{65}Zn (8–96)	^{nat}Cu(a,x)^{65}Zn (14–48)
^{nat}Cu(p,x)^{63}Zn (4–100)	^{nat}Ni(d,x)^{56}Co (2–55)		
^{nat}Cu(p,x)^{65}Zn (4–100)	^{nat}Ni(d,x)^{58}Co (2–50)		
^{nat}Cu(p,x)^{56}Co (4–100)	^{nat}Cu(d,x)^{62}Zn (17–50)		
^{nat}Cu(p,x)^{58}Co (20–1000)	^{nat}Cu(d,x)^{63}Zn (6–50)		
^{nat}Mo(p,x)$^{96m+g}$Tc (4–45)	^{nat}Cu(d,x)^{65}Zn (4–50)		

List of evaluated nuclear reactions and the main decay data

An overview of the monitor reactions evaluated earlier is presented in Table 2 [2] while the reactions discussed at present are in Table 3. Table 4 [8] contains the used decay data of the reaction products, Table 5 lists, for each reaction, the number of available experimental data sets, the maximal energy of the available experimental data (fitted only in an energy range useful for practical production), the parameters of the final Padé fit and the number of available experimentally determined yield publications.

Results and discussion of the studied reactions

All available corrected experimental data in comparison with the TENDL 2021 and 2023 predictions, the selection and the selected data are presented with the obtained recommended data and uncertainties. Integral yield data were deduced from the recommended cross section data and compared with the directly measured experimental integral yield data reported in the literature. In some publications yield data derived from the measured cross section data (so-called DERIV yields) are available. As these data are not independent, they are not included in the comparison.

Evaluated proton-induced nuclear reactions

^{nat}C(p,x)^{7}Be reaction

Two reactions contribute to ^{7}Be formation: ^{12}C(p,3p3n)^{7}Be (^{12}C abundance is 98.90% in ^{nat}C) and ^{13}C(p,3p4n)^{7}Be (^{13}C

Table 3 List of the new evaluated monitor reactions (*4 reactions are re-evaluated*)

Protons	Deuterons	^{3}He-particles	Alpha-particles
^{nat}C(p,x)^{11}C	^{nat}Ti(d,x)^{43}Sc	^{nat}C(^{3}He,x)^{11}C	^{27}Al(α,x)^{28}Mg
^{27}Al(p,x)^{7}Be	^{nat}Ti(d,x)^{47}Sc	^{nat}Ti(^{3}He,x)^{44m}Sc	^{nat}Ni(α,x)^{57}Ni
^{nat}Ti(p,x)^{43}Sc	^{nat}Fe(d,x)^{55}Co	^{nat}Ti(^{3}He,x)^{46}Sc	^{nat}Ni(α,x)^{57}Co
^{nat}Fe(p,x)^{55}Co	*^{nat}Fe(d,x)^{56}Co*	^{nat}Ti(^{3}He,x)^{47}Sc	^{nat}Ni(α,x)^{60}Cu
^{nat}Fe(p,x)^{56}Co	^{nat}Fe(d,x)^{57}Co	^{nat}Ti(^{3}He,x)^{48}Cr	^{nat}Ni(α,x)^{61}Cu
^{nat}Fe(p,x)^{57}Co	^{nat}Fe(d,x)^{58}Co	^{nat}Ti(^{3}He,x)^{51}Cr	^{nat}Ni(α,x)^{62}Zn
^{nat}Fe(p,x)^{58}Co	^{nat}Ni(d,x)^{55}Co		^{nat}Ni(α,x)^{63}Zn
^{nat}Ni(p,x)^{55}Co	^{nat}Ni(d,x)^{56}Ni		^{nat}Ni(α,x)^{65}Zn
^{nat}Ni(p,x)^{56}Ni	*^{nat}Ni(d,x)^{56}Co*		^{nat}Mo(α,xn)^{95}Ru
^{nat}Ni(p,x)^{56}Co	^{nat}Ni(d,x)^{57}Ni		^{nat}Mo(α,x)^{96}Tc
^{nat}Ni(p,x)^{57}Ni	^{nat}Ni(d,x)^{57}Co		^{nat}Mo(α,xn)^{97}Ru
^{nat}Ni(p,x)^{57}Co	*^{nat}Ni(d,x)^{58}Co*		^{197}Au(α,x)^{196}Au
^{nat}Ni(p,x)^{58}Co	^{93}Nb(d,x)^{93m}Mo		^{197}Au(α,x)^{199}Tl
^{nat}Cu(p,x)^{61}Cu	^{nat}Mo(d,x)^{96}Tc		^{197}Au(α,x)^{200}Tl
^{93}Nb(p,x)^{90}Mo	^{197}Au(d,x)^{194}Au		
^{nat}Mo(p,x)^{95m}Tc	^{197}Au(d,x)^{196}Au		
^{197}Au(p,x)^{194}Au	^{197}Au(d,x)^{198}Au		
^{197}Au(p,x)^{196}Au			

Table 4 Decay data of the reaction products

Isotope	Half life	E_γ (kev)	I_γ (%)	Reaction	No of exp.dat	$E_{max.}$exp (MeV)	E_{max}fit (MeV)
^{11}C	1221.8 s	511.0	199.534	$^{nat}C(p,x)^{7}Be$	13	162	165
^{11}C	1221.8 s	511.0	199.534	$^{nat}C(p,x)^{11}C$	26	980	200
^{11}C	1221.8 s	511.0	199.534	$^{nat}C(^{3}He,x)^{11}C$	6	485	40
^{7}Be	53.22 d	477.6035	10.44	$^{27}Al(p,x)^{7}Be$	31	2605	800
^{28}Mg	20.915 h	400.6	35.9	$^{27}Al(\alpha,x)^{28}Mg$	12	170	160
		941.7	36.3				
		1342.2	54				
^{43}Sc	3.891 h	372.9	22.5	$^{nat}Ti(p,x)^{43}Sc$	10	192	200
^{43}Sc	3.891 h	372.9	22.5	$^{nat}Ti(d,x)^{43}Sc$	4	23.6	25
^{47}Sc	3.3492 d	159.381	68.3	$^{nat}Ti(d,x)^{47}Sc$	8	49.2	50
^{44m}Sc	58.61 h	271.241	86.74	$^{nat}Ti(^{3}He,x)^{44m}Sc$	4	133.4	140
^{46}Sc	83.79 d	889.277	99.984	$^{nat}Ti(^{3}He,x)^{46}Sc$	4	134	100
		1120.545	99.987				
^{47}Sc	3.3492 d	159.381	68.3	$^{nat}Ti(^{3}He,x)^{47}Sc$	4	134	140
^{48}Cr	21.56 h	112.31	96.0	$^{nat}Ti(^{3}He,x)^{48}Cr$	5	134	100
		308.24	100				
^{51}Cr	27.704 d	320.0824	9.910	$^{nat}Ti(^{3}He,x)^{51}Cr$	3	134	140
^{55}Co	17.53 h	931.1	75	$^{nat}Fe(p,x)^{55}Co$	23	2600	180
		1408.5	16.9				
^{56}Co	77.236 d	846.770	99.9399	$^{nat}Fe(p,x)^{56}Co$	43	2900	200
		1037.843	14.05				
		1238.288	66.46				
^{57}Co	271.74 d	122.06065	85.60	$^{nat}Fe(p,x)^{57}Co$	17	200	200
		136.47356	10.68				
^{58}Co	70.86 d	810.7593	99.450	$^{nat}Fe(p,x)^{58}Co$	16	177	85
^{55}Co	17.53 h	931.1	75	$^{nat}Fe(d,x)^{55}Co$	7	49	50
		1408.5	16.9				
^{58}Co	70.86 d	810.7593	99.450	$^{nat}Fe(d,x)^{58}Co$	7	30	25
^{57}Co	271.74 d	122.06065	85.60	$^{nat}Fe(d,x)^{57}Co$	8	49	49
		136.47356	10.68				
^{58}Co	70.86 d	810.7593	99.450	$^{nat}Fe(d,x)^{58}Co$	7	30	25
^{55}Co	17.53 h	931.1	75	$^{nat}Ni(p,x)^{55}Co$	27	2600	200
		1408.5	16.9				
^{56}Co	77.236 d	846.770	99.9399	$^{nat}Ni(p,x)^{56}Co$	16	1600	130
		1037.843	14.05				
		1238.288	66.46				
^{57}Co	271.74 d	122.06065	85.60	$^{nat}Ni(p,x)^{57}Co$	15	385	150
		136.47356	10.68				
^{58}Co	70.86 d	810.7593	99.450	$^{nat}Ni(p,x)^{58}Co$	13	384	180
^{56}Ni	6.075 d	158.38	98.8	$^{nat}Ni(p,x)^{56}Ni$	23	2605	150
		269.50	36.5				
		480.44	36.5				
		749.95	49.5				
		811.85	86.0				
		1561.80	14.0				
^{57}Ni	35.60 h	127.164	16.7	$^{nat}Ni(p,x)^{57}Ni$	47	2605	200
		1377.63	81.7				
^{55}Co	17.53 h	931.1	75	$^{nat}Ni(d,x)^{55}Co$	8	50	50
		1408.5	16.9				

Table 4 (continued)

Isotope	Half life	E_γ (kev)	I_γ (%)	Reaction	No of exp.dat	$E_{max.}$exp (MeV)	E_{max}fit (MeV)
^{56}Co	77.236 d	846.770	99.9399	^{nat}Ni(d,x)^{56}Co	12	50	50
		1037.843	14.05				
		1238.288	66.46				
^{57}Co	271.74 d	122.06065	85.60	^{nat}Ni(d,x)^{57}Co	9	50	50
		136.47356	10.68				
^{58}Co	70.86 d	810.7593	99.450	^{nat}Ni(d,x)^{58}Co	10	50	
^{56}Ni	6.075 d	158.38	98.8	^{nat}Ni(d,x)^{56}Ni	4	50	50
		269.50	36.5				
		480.44	36.5				
		749.95	49.5				
		811.85	86.0				
		1561.80	14.0				
^{57}Ni	35.60 h	127.164	16.7	^{nat}Ni(d,x)^{57}Ni	7	50	50
		1377.63	81.7				
^{57}Co	271.74 d	122.06065	85.60	^{nat}Ni(α,x)^{57}Co	9	50	50
		136.47356	10.68				
^{57}Ni	35.60 h	127.164	16.7	^{nat}Ni(α,x)^{57}Ni	10	161	150
		1377.63	81.7				
^{60}Cu	23.7 m	826.4	21.7	^{nat}Ni(α,x)^{60}Cu	7	50	50
		1332.5	88.0				
^{61}Cu	3.336 h	282.956	12.7	^{nat}Ni(α,x)^{61}Cu	13	170	100
		656.008	10.4				
^{62}Zn	9.193 h	548.35	15.3	^{nat}Ni(α,x)^{62}Zn	12	122	120
		596.56	26.0				
^{63}Zn	38.47 m	669.62	8.2	^{nat}Ni(α,x)^{63}Zn	9	50	50
		962.06	6.5				
^{65}Zn	243.93 d	1115.539	50.04	^{nat}Ni(α,x)^{65}Zn	8	87	90
^{61}Cu	3.336 h	282.956	12.7	^{nat}Cu(p,x)^{61}Cu	20	1500	200
		656.008	10.4				
^{90}Mo	5.67 h	122.370	64	^{93}Nb(p,x)^{90}Mo	6	2605	100
		162.93	6.0				
		203.13	6.3				
		257.34	77				
		323.20	6.3				
		445.37	6.0				
		941.5	5.5				
		1271.3	4.1				
^{93m}Mo	6.85 h	263.049	57.4	^{93}Nb(d,x)^{93m}Mo	5	48	50
		684.693	99.9				
		1477.138					
^{95m}Tc	61 d	765.789	93.8	^{nat}Mo(p,x)^{95m}Tc	12	67	70
^{96}Tc	4.28 d	778.22	99.760	^{nat}Mo(d,x)^{96}Tc	6	49.5	50
		812.54	82				
		849.86	98				
		1126.85	15.2				
^{95}Ru	1.643 h	336.40	69.9	^{nat}Mo(α,xn)^{95}Ru	8	40	40
		626.83	17.8				
		1096.80	20.9				

Table 4 (continued)

Isotope	Half life	E_γ (kev)	I_γ (%)	Reaction	No of exp.dat	E_{max}exp (MeV)	E_{max}fit (MeV)
^{97}Ru	2.83 d	215.70	85.62	$^{nat}Mo(\alpha,xn)^{97}Ru$	7	67	70
		324.49	10.79				
^{96}Tc	4.28 d	778.22	99.760	$^{nat}Mo(\alpha,x)^{96}Tc$	3	67	70
		812.54	82				
		849.86	98				
		1126.85	15.2				
^{194}Au	38.02 h	293.548	10.58	$^{197}Au(p,x)^{194}Au$	5	2600	160
		328.464	60.4				
^{196}Au	6.1669 d	147.81	43.5	$^{197}Au(p,x)^{196}Au$	8	2600	150
		168.37	7.8				
		188.27	30.0				
^{197m}Hg	23.8 h	133.98	33.5	$^{197}Au(d,2n)^{197m}Hg$	7	50	
^{194}Au	38.02 h	293.548	10.58	$^{197}Au(d,x)^{194}Au$	4	86	90
		328.464	60.4				
^{196}Au	6.1669 d	147.81	43.5	$^{197}Au(d,x)^{196}Au$	8	80	80
		168.37	7.8				
		188.27	30.0				
^{198m}Au	2.272 d	180.31	49	$^{197}Au(d,x)^{198}Au$	12	80	80
		204.10	39				
		214.89	77.3				
		333.82	18				
^{199}Tl	7.42 h	158.359	5.0	$^{197}Au(\alpha,x)^{199}Tl$	18	116	116
		208.20	12.3				
		247.26	9.3				
^{200}Tl	26.1 h	367.942	87	$^{197}Au(\alpha,x)^{200}Tl$	18	94	100
		579.300	13.7				
		28.27	10.8				
^{196}Au	6.1669 d	147.81	43.5	$^{197}Au(\alpha,x)^{196}Au$	11	100	100
		168.37	7.8				
		188.27	30.0				

Gamma lines 100–1500 keV

abundance is 1.10%). The lowest threshold for the clustered particle emission reaction ^{12}C (p,αd)^{7}Be is 26.06053 MeV.

A total of 13 cross section data sets, covering the energy range from threshold up to 170 MeV, were found in literature: Dickson [15], Lefort [16], Gauvin [17], Brun [18], Rayudu [19], Vdovin [20], Williams [21], Aleksandrov [22], Bodeman [23], Michel [24], Fassbender [25], Baumer [26], Baecker [27].

As a large disagreement is observed and no TENDL predictions are available for this low Z element, the data of Michel [24] were considered as reference values (Fig. 1). The whole set of Dickdon 1951, the single point of Rayudu 1964 (130 MeV, too low) and of Vdovin 1979 (50 MeV, too low) were deselected. As the sets of Williams 1979 and Aleksandrov 1990 agree well in overall shape with Michel 1997 but show lower values, they were multiplied by, respectively, a factor 1.35 and of 1.2. The data of Lefort 1961 and Brun 1962 were linearly decreased in energy to correspond with the shape of the Michel 1997 excitation curve. The outlying point of Brun 1962 at 42.18 MeV was deselected. As the uncertainties given in the publications of Michel 1997, Gauvin 1962 and Baecker 2019 are well below 10%, for selection they were systematically increased to 12%. The original and corrected datasets of ten publications were selected and fitted (Fig. 2). The calculated yields, based on the recommended values from the Padé fit, are shown in Fig. 9. No experimental yield data were found in the literature. No TENDL predictions are available for this low Z-value target.

$^{nat}C(p,x)^{11}C$ reaction

Two reactions contribute to ^{11}C formation in proton bombardment of C targets: $^{12}C(p,pn)^{11}C$ (^{12}C abundance is

Table 5 Parameters of the evaluated and fitted nuclear reactions

Reaction	Data sets	E_{max} recom. (MeV)	Pade parameters	Exp yield
Protons				
$^{nat}C(p,x)^{7}Be$	13	162	Pade 11, N = 144, $\chi^2 = 1.12$	No data
$^{nat}C(p,x)^{11}C$	24	980	Pade 9, N = 208, $\chi^2 = 0.88$	2
$^{27}Al(p,x)^{7}Be$	31	800	Pade 13, N = 390, $\chi^2 = 1.07$	No data
$^{nat}Ti(p,x)^{43}Sc$	8	192	Pade 19, N = 175, $\chi^2 = 0.99$	1
$^{nat}Fe(p,x)^{55}Co$	22	180	Pade 14, N = 175, $\chi^2 = 1.81$	1
$^{nat}Fe(p,x)^{56}Co$	43	200	Pade 12, N = 512, $\chi^2 = 2.98$	4
$^{nat}Fe(p,x)^{57}Co$	16	200	Pade 10, N = 288, $\chi^2.21$	2
$^{nat}Fe(p,x)^{58}Co$	15	85	Pade 14, N = 306, $\chi^2 = 3.53$	No data
$^{nat}Ni(p,x)^{55}Co$	22	200	Pade 15, N = 518, $\chi^2 = 1.96$	3
$^{nat}Ni(p,x)^{56}Ni$	23	150	Pade 8, N = 266, $\chi^2 = 1.5$	No data
$^{nat}Ni(p,x)^{56}Co$	15	130	Pade 14, N = 230, $\chi^2 = 1.62$	2
$^{nat}Ni(p,x)^{57}Ni$	28	200	Pade 17, N = 505, $\chi^2 = 1.50$	3
$^{nat}Ni(p,x)^{57}Co$	15	150	Pade 15, N = 313, $\chi^2 = 2.27$	3
$^{nat}Ni(p,x)^{58}Co$	13	180	Pade 13, N = 254, $\chi^2 = 1.25$	3
$^{nat}Cu(p,x)^{61}Cu$	20	200	Pade 14, N = 218, $\chi^2 = 1.33$	2
$^{93}Nb(p,x)^{90}Mo$	6	100	Pade 8, N = 40, $\chi^2 = 1.79$	No data
$^{nat}Mo(p,x)^{95m}Tc$	10	70	Pade 17, N = 247, $\chi^2 = 1.31$	4
$^{197}Au(p,x)^{194}Au$	5	160	Pade 10, N = 95, $\chi^2 = 1.16$	1
$^{197}Au(p,x)^{196}Au$	7	150	Pade 8, N = 121, $\chi^2 = 1.65$	3
Deuterons				
$^{nat}Ti(d,x)^{43}Sc$	4	25	Pade 5, N = 30, $\chi^2 = 0.60$	2
$^{nat}Ti(d,x)^{47}Sc$	8	50	Pade 13, N = 218, $\chi^2 = 1.12$	2
$^{nat}Fe(d,x)^{55}Co$	7	50	Pade 17, N = 284, $\chi^2 = 1.01$	2
$^{nat}Fe(d,x)^{56}Co$	12	50	Pade 9, N = 206, $\chi^2 = 1.73$	2
$^{nat}Fe(d,x)^{57}Co$	8	49	Pade 9, N = 167, $\chi^2 = 1.26$	3
$^{nat}Fe(d,x)^{58}Co$	7	25	Pade 11, N = 101, $\chi^2 = 1.15$	2
$^{nat}Ni(d,x)^{55}Co$	11	50	Pade 15, N = 204, $\chi^2 = 1.16$	2
$^{nat}Ni(d,x)^{56}Ni$	7	50	Pade 5, N = 72, $\chi^2 = 1.50$	No data
$^{nat}Ni(d,x)^{56}Co$	13	49.8	Pade 17, N = 241, $\chi^2 = 0.98$	3
$^{nat}Ni(d,x)^{57}Ni$	11	50	Pade 9, N = 192, $\chi^2 = 1.28$	3
$^{nat}Ni(d,x)^{57}Co$	12	50	Pade 10, N = 184, $\chi^2 = 1,44$	3
$^{nat}Ni(d,x)^{58}Co$	8	50	Pade 10, N = 196, $\chi^2 = 1.44$	3
$^{93}Nb(d,x)^{93m}Mo$	5	50	Pade 14, N = 116, $\chi^2 = 1.79$	1
$^{nat}Mo(d,x)^{96}Tc$	6	50	Pade 13, N = 180, $\chi^2 = 0.93$	3
$^{197}Au(d,x)^{194}Au$	4	90	Pade 7, N = 43, $\chi^2 = 1.01$	No data
$^{197}Au(d,x)^{196}Au$	8	80	Pade 9, N = 93, $\chi^2 = 2.06$	1
$^{197}Au(d,x)^{198}Au$	12	80	Pade 13, N = 154, $\chi^2 = 2.51$	1
^{3}He-particles				
$^{nat}C(^{3}He,x)^{11}C$	6	40	Pade 20, N = 194, $\chi^2 = 5.50$	2
$^{nat}Ti(^{3}He,x)^{44m}Sc$	4	140	Pade 17, N = 130, $\chi2 = 1.20$	No data
$^{nat}Ti(^{3}He,x)^{46}Sc$	4	100	Pade 10, N = 129, $\chi^2 = 1.45$	No data
$^{nat}Ti(^{3}He,x)^{47}Sc$	4	134	Pade 12, N = 136, $\chi^2 = 1.28$	No data
$^{nat}Ti(^{3}He,x)^{48}Cr$	5	100	Pade 12, N = 158, $\chi^2 = 0.87$	No data
$^{nat}Ti(^{3}He,x)^{51}Cr$	3	140	Pade 11, N = 68, $\chi^2 = 1.44$	No data
Alpha-particles				
$^{27}Al(\alpha,x)^{28}Mg$	12	160	Pade 17, N = 148, $\chi^2 = 1.43$	3
$^{nat}Ni(\alpha,x)^{57}Ni$	10	161	Pade 11, N = 89, $\chi^2 = 1.98$	1
$^{nat}Ni(\alpha,x)^{57}Co$	9	50	Pade 19, N = 110, $\chi^2 = 1.71$	1
$^{nat}Ni(\alpha,x)^{60}Cu$	7	50	Pade 8, N = 42, $\chi^2 = 1.03$	1

Table 5 (continued)

Reaction	Data sets	E $_{max}$ recom. (MeV)	Pade parameters	Exp yield
$^{nat}Ni(\alpha,x)^{61}Cu$	13	100	Pade 13, N = 161, χ^2 = 2.34	3
$^{nat}Ni(\alpha,x)^{62}Zn$	12	120	Pade 19 s, N = 126, χ^2 = 1.68	2
$^{nat}Ni(\alpha,x)^{63}Zn$	9	50	Pade 16, N = 89, χ^2 = 1.13	No data
$^{nat}Ni(\alpha,x)^{65}Zn$	8	90	Pade 20, N = 107, χ^2 = 1.16	No data
$^{nat}Mo(\alpha,xn)^{95}Ru$	8	40	Pade 20, N = 103, χ^2 = 1.66	1
$^{nat}Mo(\alpha,x)^{96}Tc$	3	70	Pade 9, N = 38, χ^2 = 0.84	1
$^{nat}Mo(\alpha,xn)^{97}Ru$	7	67	Pade 9, N = 87, χ^2 = 1.29	1
$^{197}Au(\alpha,x)^{196}Au$	11	100	Pade 6, N = 145, χ^2 = 1.53	No data
$^{197}Au(\alpha,x)^{199}Tl$	18	116	Pade 20, N = 200, χ^2 = 2.35	No data
$^{197}Au(\alpha,x)^{200}Tl$	18	100	Pade 12, N = 169, χ^2 = 1.92	No data

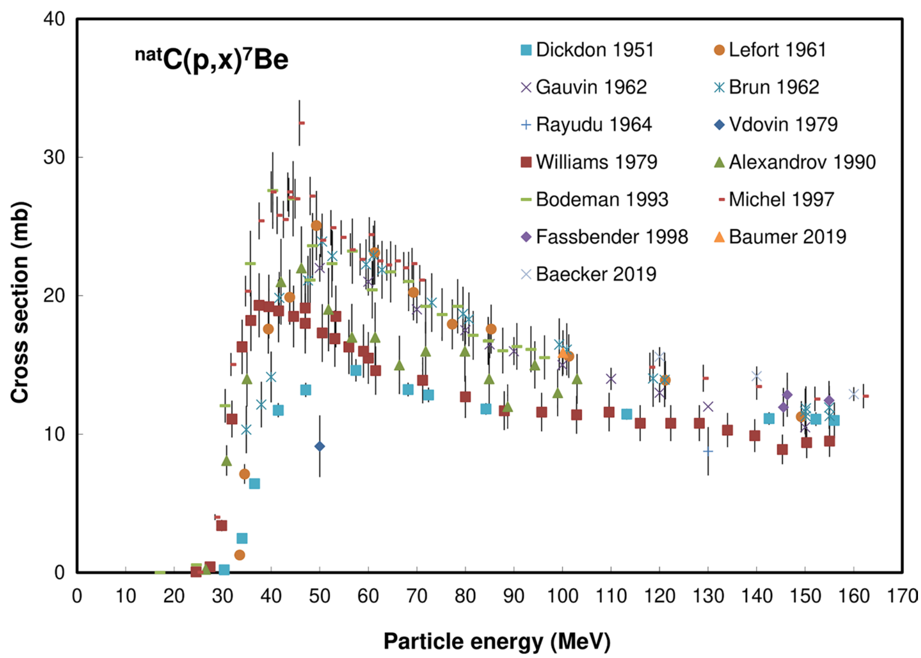

Fig. 1 $^{at}C(p,x)^7Be$ reaction: all experimental data No TENDL is available, for targets with Z below 9

98.90% in ^{nat}C) and $^{13}C(p,p2n)^{11}C$ (^{13}C abundance is 1.10%). The lowest threshold for clustered particle emission reaction is 16362.54 keV.

A total of 26 cross section data sets up to 1000 MeV incident proton energy were found in literature and are presented in Fig. 3: Hintz [28], Aamodt [29], Burcham [30], Crandall [31], Measday [32], Symonds [33], Rosenfeld [34], Whitehead [35], Parikh [36], Goebel [37], Gauvin [17], Brun [18], Cumming [38], Kavanagh [39], Andrews [40], Hogstrom [41], Kostjuchenko [42], Kettern [43], Akagi [44], Matsushita [45], Baumer [26], Baecker [27], Horst [46], Rodriguez-Gonzalez [47].

As some disagreement is observed and as no TENDL predictions are available for this low Z element, the recent data over the whole energy range of interest by Rodriguez-Gonzalez [47] and the sets of Hintz 1962 and Cuming 1963 were accepted as reference values.

Five sets show too low values over a rather extended energy region and were deselected Whitehead 1958 ser1, Gauvin 1962 (also not independent measurements), Akagi 2013, Matsusita 2016, Horst 2019.

Additionally, some data points at energies under 18 MeV are too low and were deleted: Aamodt 1952 ser1 (3 points) Hintz 1952 (4 points), Kettern 2004 (1 point at 12.3 MeV).

As remarked in the previous section for several sets the uncertainties given in the original publication are well below 10% and were systematically increased to 12% for selection. The original and corrected datasets of fourteen publications

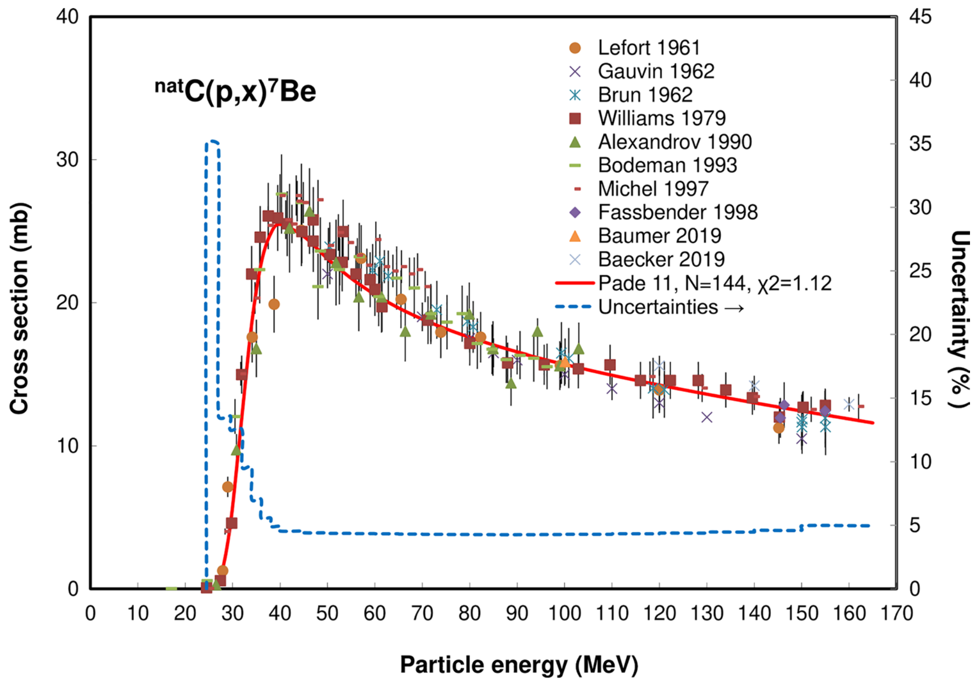

Fig. 2 $^{nat}C(p,x)^7Be$ reaction: selected experimental works and Padé fit (solid line) with total derived uncertainties, including 4% systematic uncertainty (dashed line, right-hand scale)

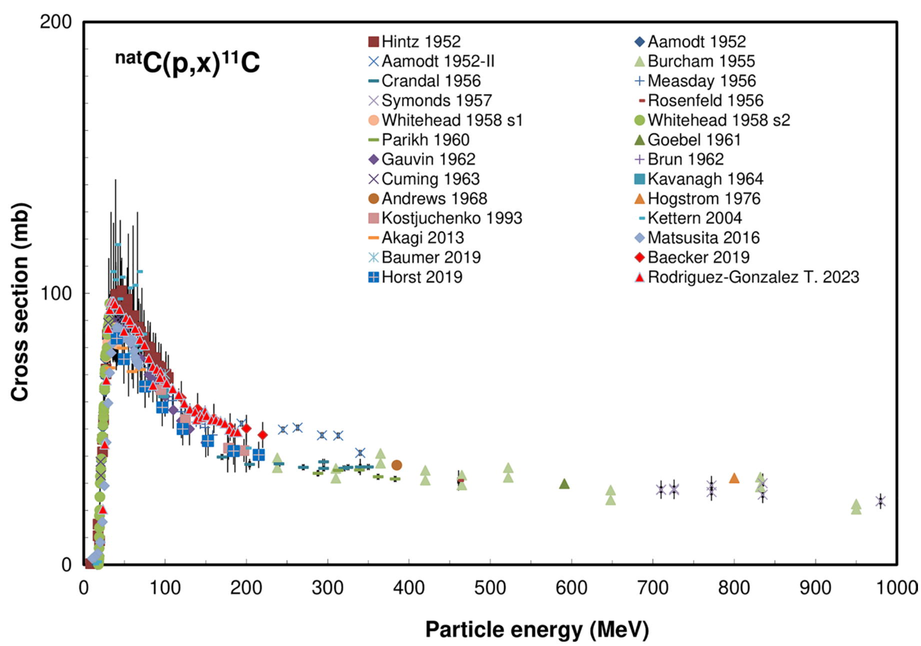

Fig. 3 $^{nat}C(p,x)^{11}C$ reaction: all experimental data

were selected and fitted (Fig. 4). The integral yields calculated from the recommended cross sections are shown in Fig. 9, together with the experimental yield data of Krasnov [48] and Dmitriev [49].

$^{27}Al(p,x)^7Be$ reaction

As Al is monoisotopic only the $^{27}Al(p,10p11n)$ reaction can contribute to ^7Be formation by activation. The lowest threshold for the maximally clustered light particle emission $^{27}Al(p, 5\alpha n)^7Be$ reaction is 47.59 MeV. As experimentally formation of ^7Be is observed at lower energies probably other reaction mechanisms are involved (fission, fragmentation, Be particle emission). The TENDL 2021 and 2023 prediction exists but predict very low cross sections probably because only light particle emission is included in the model (Fig. 5).

A total of 31 cross section data sets, covering the energy range from threshold up to 1000 MeV, were found in literature: Marquez [50], Lavrukhina [51], Neuzil [52],

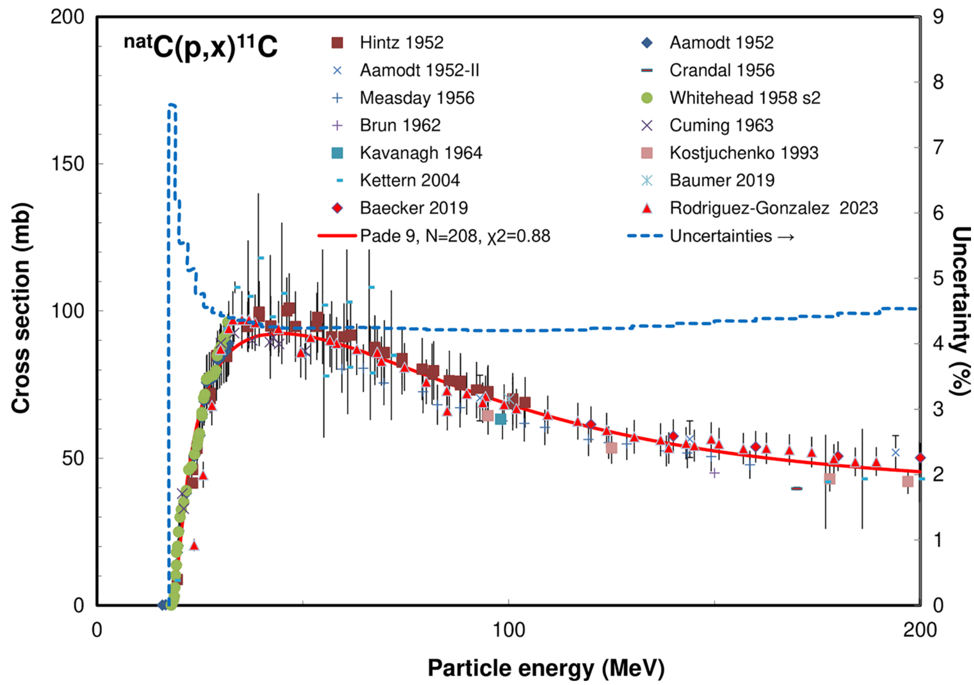

Fig. 4 $^{nat}C(p,x)^{11}C$ reaction: selected experimental works and Padé fit (solid line) with total derived uncertainties, including 4% systematic uncertainty (dashed line, right-hand scale)

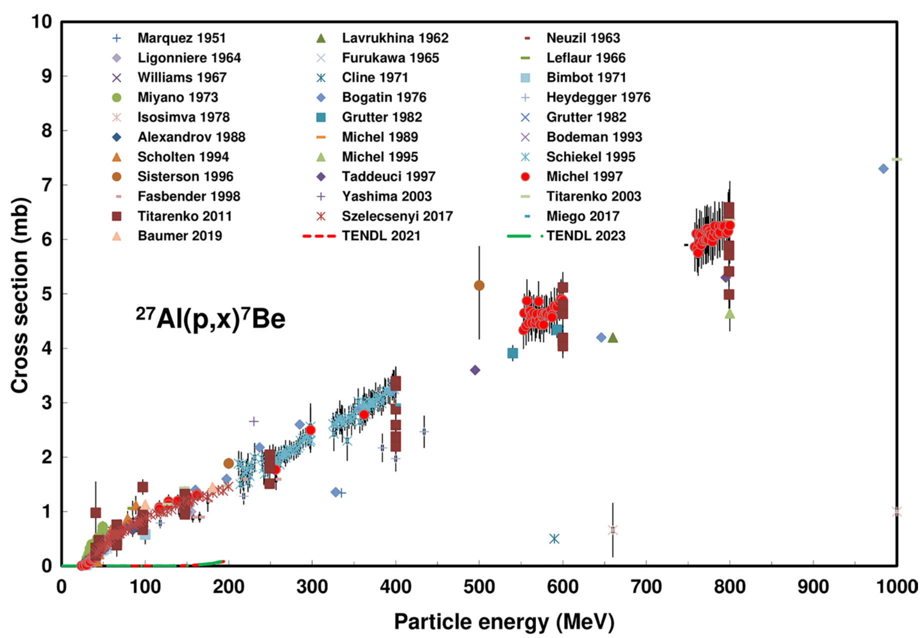

Fig. 5 $^{27}Al(p,x)^{7}Be$ reaction: all experimental data

Ligonniere [53], Furukawa [54], Lafleur [55], Williams [21], Cline [56], Bimbot [57], Miyano [58], Bogatin [59], Heydegger [60], Grutter [61], Grutter [62], Aleksandrov [22], Michel [63], Bodemann [23], Scholten [64], Michel [65], Schiekel [66], Sisterson [67], Taddeuci [68], Michel [24], Fassbender [25], Yashima [69], Titarenko [70], Titarenko [71], Szelecsenyi [72], Meigo [73], Baumer [26].

The originally published set by Titarenko 2011 consists of multiple, spreaded, measured data at 9 distinct energy points. Only a single representative value at each energy, corresponding best to the numerous datapoints over the whole energy range of Schiekel 1995 and Michel 1997, was selected. The spread data of Bugatin 1976 and the single outlying point of Michel 1995 at 800 MeV were deselected. Additionally, 8 sets, each containing only a few datapoints that are all outlying, were deselected: Marquez, Lavruskhina, Sisterson, Cline, Heydeggern, Isosimva, Schiekel, Yashima. The original and corrected datasets of the remaining twenty-two publications were selected up to 800 MeV and fitted (Fig. 6). The integral yields calculated from the

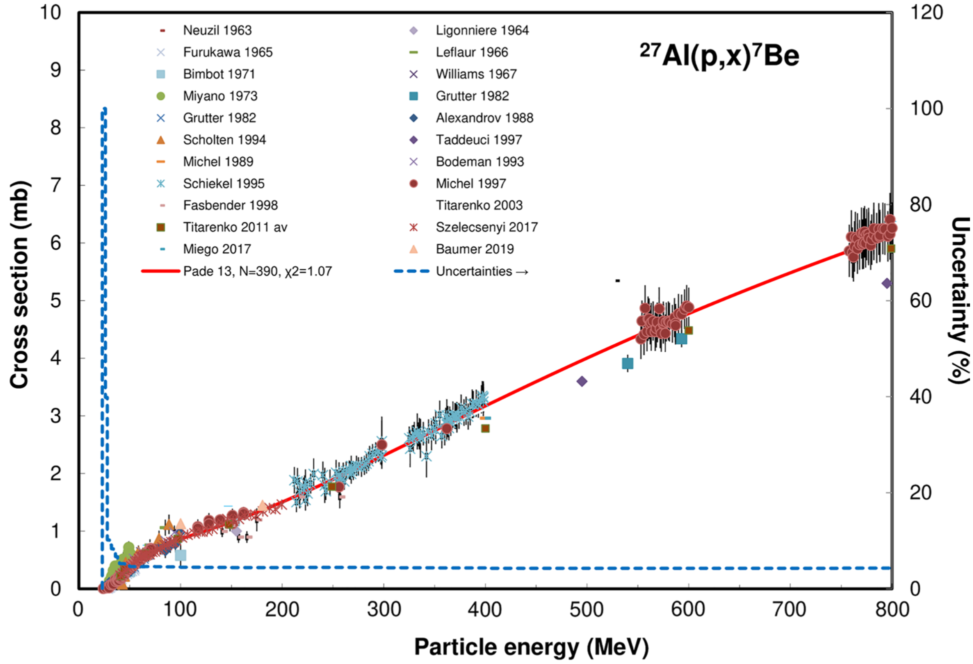

Fig. 6 ^{27}Al(p,x)^{7}Be reaction: selected experimental works and Padé fit (solid line) with total derived uncertainties, including 4% systematic uncertainty (dashed line, right hand scale)

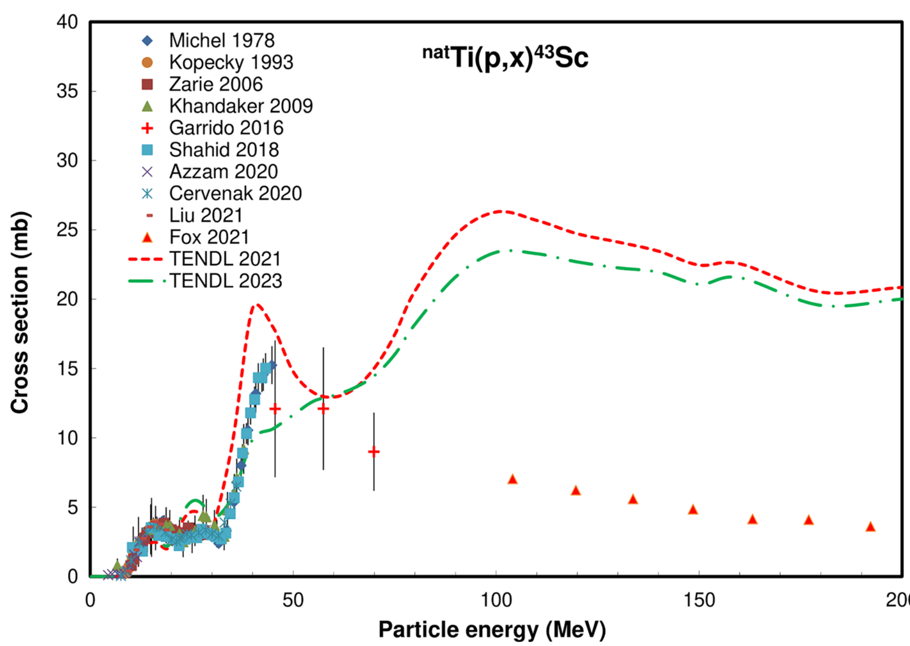

Fig. 7 ^{nat}Ti(p,x)^{43}Sc reaction: all experimental data and the TENDL theoretical excitation functions

recommended cross sections are shown in Fig. 9. No experimental yield data were found.

^{nat}Ti(p,x)^{43}Sc reaction

Reactions of the general shape (p,αxn), with x between 2 and 6, on the five stable isotopes of Ti can contribute to direct ^{43}Sc formation (^{46}Ti abundance is 8.25%; ^{47}Ti abundance is 7.44%, ^{48}Ti abundance is 73.72%, ^{49}Ti abundance is 5.41%, ^{50}Ti abundance is 5.18%). The lowest threshold is for the ^{46}Ti(p,α2n)^{43}Sc reaction at 3.144 MeV. The contribution of the interaction with the other isotopes occurs at higher energies and results in an excitation function with multiple local maxima. The formation of ^{43}Sc at energies above 32 MeV is always cumulative as it contains the full decay of very short-lived ^{43}Ti ($T_{1/2}$ = 0.5 s) produced by (p,pxn) reactions on the different stable Ti isotopes. The threshold for ^{46}Ti(p,p3n)^{43}Ti reaction is 31.21 MeV.

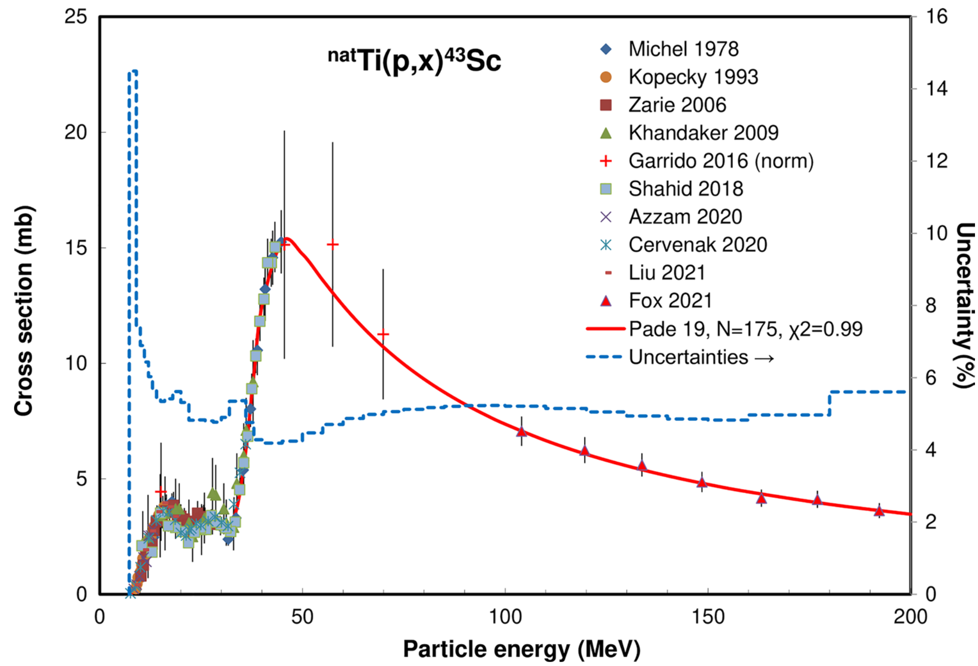

Fig. 8 $^{nat}Ti(p,x)^{43}Sc$ reaction: selected experimental works and Padé fit (solid line) with total derived uncertainties, including 4% systematic uncertainty (dashed line, right hand scale)

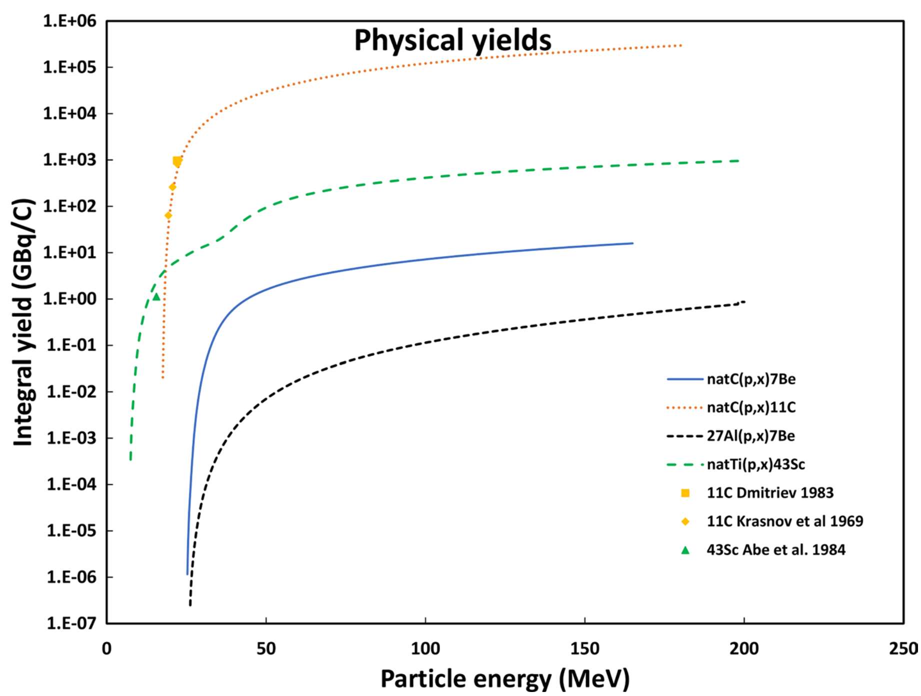

Fig. 9 Yield calculated from the recommended cross sections of the $^{nat}C(p,x)^{7}Be$, $^{nat}C(p,x)^{11}C$, $^{27}Al(p,x)^{7}Be$ and $^{nat}Ti(p,x)^{43}Sc$ reactions

A total of 10 cross section data sets, covering the energy range from threshold up to 200 MeV, were found in the literature and are displayed in Fig. 7: Michel [74], Kopecky [75], Zarie [76], Khandaker [77], Garrido [78], Shahid [79, 80], Cervenak [81], Liu [82], Fox [83]. The 4 datapoints of Garrido 2016 were multiplied by a factor of 1.25 to agree with the values of Shahid 2018 and Michel 1978 near the local maximum at 45 MeV. The 4 data points of Azzam 2020 below 8 MeV and the point at 6.7 MeV of Khandaker 2009 were considered as outlying and deselected. The original and corrected datasets of the 10 publications were selected and fitted (Fig. 8).

While the TENDL 2021 prediction represented in a more pronounced way the multiple contributions of the reactions on the five stable target isotopes the 2023 version is ignoring the dominant local maximum in the 40–50 MeV domain. Both versions seem to overestimate the cross sections above 60 MeV.

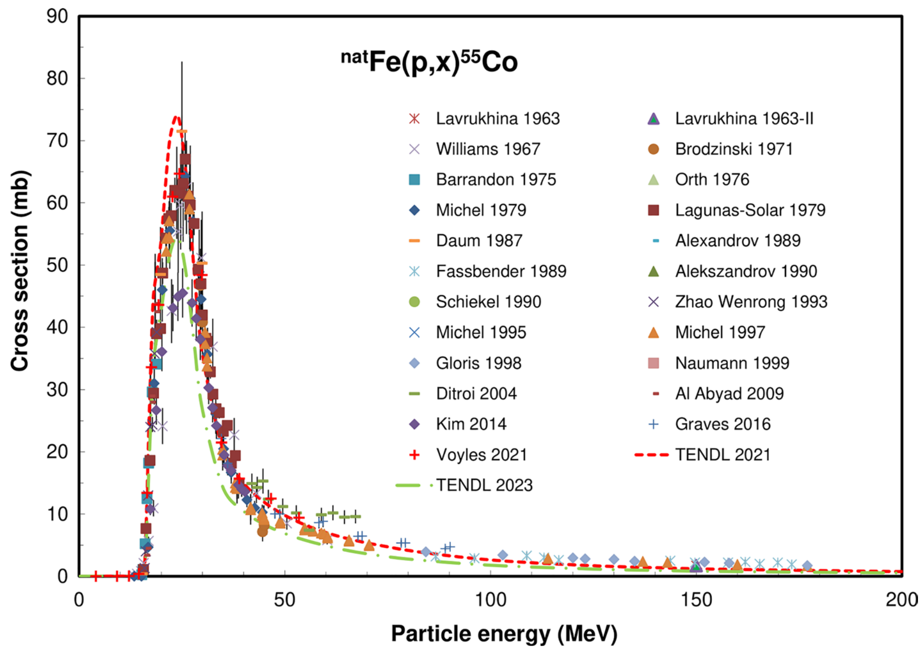

Fig. 10 $^{nat}Fe(p,x)^{55}Co$ reaction: all experimental data and the TENDL theoretical excitation functions

The integral yields calculated from the recommended cross sections are shown in Fig. 9. One experimental yield data was found: Abe [84].

^{nat}Fe(p,x)^{55}Co reaction

Three (p,xn) reactions on the stable target isotopes ^{56}Fe(abundance 91.754% in ^{nat}Fe), ^{57}Fe (2.119%) and ^{58}Fe (0.282%) contribute to the formation of ^{55}Co. Due to the predominance of the ^{56}Fe isotope, the (p,2n) reaction with a threshold of 15.71 MeV will in practice be the single contribution.

A total of 23 cross section data sets, covering the energy range from threshold up to 200 MeV, were found in literature and are displayed in Fig. 10: Lavrukhina [85], Williams [86], Brodzinski [87], Barrandon [88], Orth [89], Michel [90], Lagunas-Solar [91], Daum [92], Aleksandrov [93], Fassbender [94], Aleksandrov [95], Schiekel [66], Zhao Wenrong [96], Michel [65], Michel [24], Gloris [97], Neumann

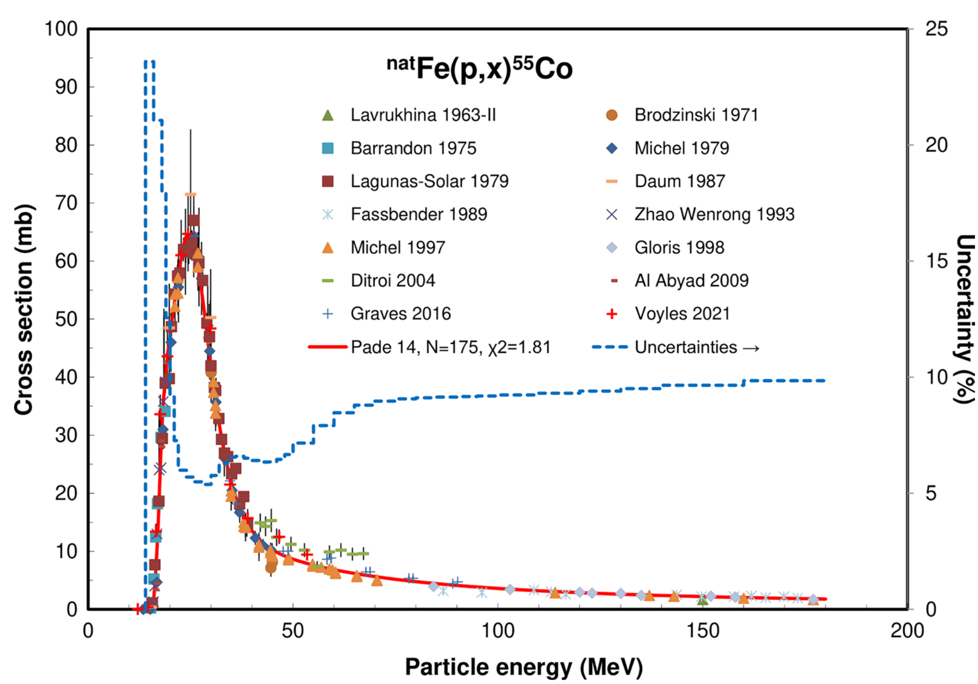

Fig. 11 $^{nat}Fe(p,x)^{55}Co$ reaction: selected experimental works and Padé fit (solid line) with total derived uncertainties, including 4% systematic uncertainty (dashed line, right-hand scale)

[98], Ditroi [99], Al Abyad [100], Kim [101], Graves [102], Voyles [103].

The four sets by Orth 1976, Aleksandrov 1989, Schiekel 1990, and Neumann 1999 only contain data above the 200 MeV energy limit considered as being appropriate for practical use and are hence not presented in the figure.

The data sets of Williams 1967 and Kim 2014 are too low over the whole energy domain and are deselected. The two datapoints of Voyles below 12 MeV are deleted. We accepted the value at 12.11 MeV of Voyles and 13.43 MeV of Michel, both below the threshold mentioned earlier, as indications of the presence of contribution of the ^{54}Fe(p,γ)^{55}Co reaction.

The errors of all Laguna-Solar data were increased to 8% and the error of Michel 1979 point was corrected to 10%. The first two low-energy points were omitted.

The original and corrected datasets of 14 publications were selected up to 180 MeV and fitted (Fig. 11). The two TENDL predictions enhance the predominance of the ^{56}Fe(p,2n)^{55}Co reaction. While the TENDL 2021 slightly overestimates the maximal value the TENDL 2023 predictions are systematically lower over the whole energy range. The integral yields calculated from the recommended cross sections are shown in Fig. 18. One experimental yield data was found by Talebi 2013 [104].

^{nat}Fe(p,x)^{56}Co reaction

Three (p,xn) reactions on the stable target isotope ^{56}Fe(abundance 91.754% in ^{nat}Fe), ^{57}Fe (2.119%) and ^{58}Fe (0.282%) contribute to the formation of ^{55}Co. Due to the predominance of the ^{56}Fe isotope the (p,n) reaction with a threshold of 5.44 MeV will in practice be the single contribution.

A total of 43 cross section data sets, covering the energy range from threshold up to 100 MeV, were found in literature and are displayed in Fig. 12: Remsberg [105], Tanaka [106], Read [107], Lavrukhina [85], Lavrukhina [108], Rayudu [109], Williams [86], Rayudu [19], Jenkins [110], Cline [56], Brodzinski [87], Gadioli [111], Barrandon [88], Orth [89], Lagunas Solar [91], Michel [90], Schoen [112], Michel [113], Michel [114], Antropov [115], Michel [63], Aleksandrov [93], Neumann [98, 116], Levkovskii [117], Jung [118], Zhao Wenrong [96], Takacs [119], Sudar [120], Michel [65], Schiekel [66], Michel [24], Daum [92], Gloris [97], Ditroi [99], Sisterson [121], Al Abyad [100], Titarenko [71], Kim [101], Graves [102], Zherebchevsky [122], Uddin [123], Lawriniang [124], Voyles [103].

The too low set of Williams 1967 was deselected and all datapoints of several publications below the threshold mentioned earlier were deleted.

The original and corrected datasets were selected up to 50 MeV, the energy limit for interesting practical applications, and fitted (Fig. 13).

The two TENDL predictions are enhancing the predominance of the ^{56}Fe(p,n)^{56}Co reaction and are well estimating the maximal value and shape.

The integral yields calculated from the recommended cross sections are shown in Fig. 18. Three experimental yield data were found: Acerbi [125], Dmitriev [126], Isshiki [127], Abe [84]. Acerbi data are differential yields, and not presented in the figure.

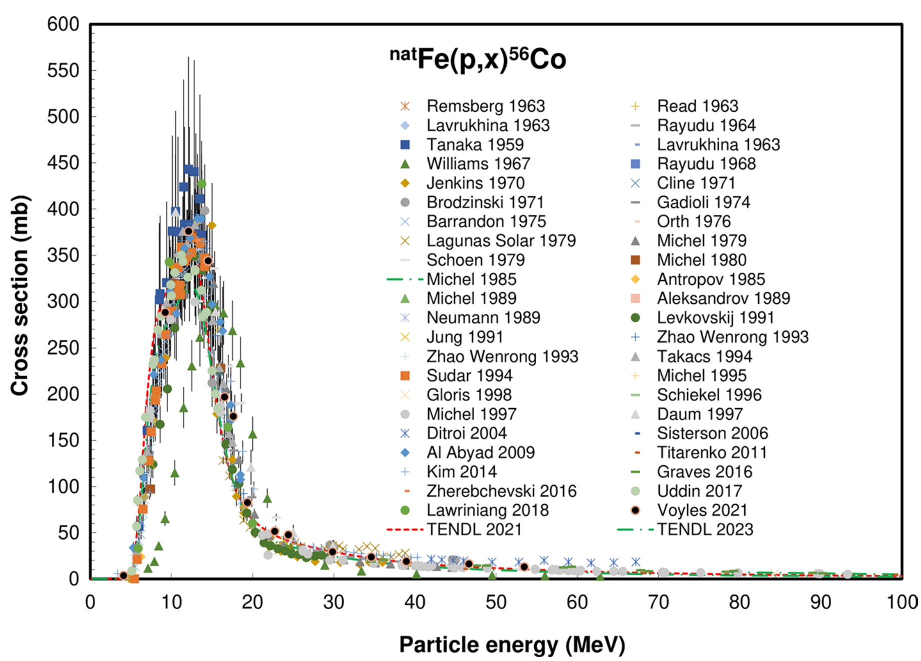

Fig. 12 ^{nat}Fe(p,x)^{56}Co reaction: all experimental data and the TENDL theoretical excitation functions

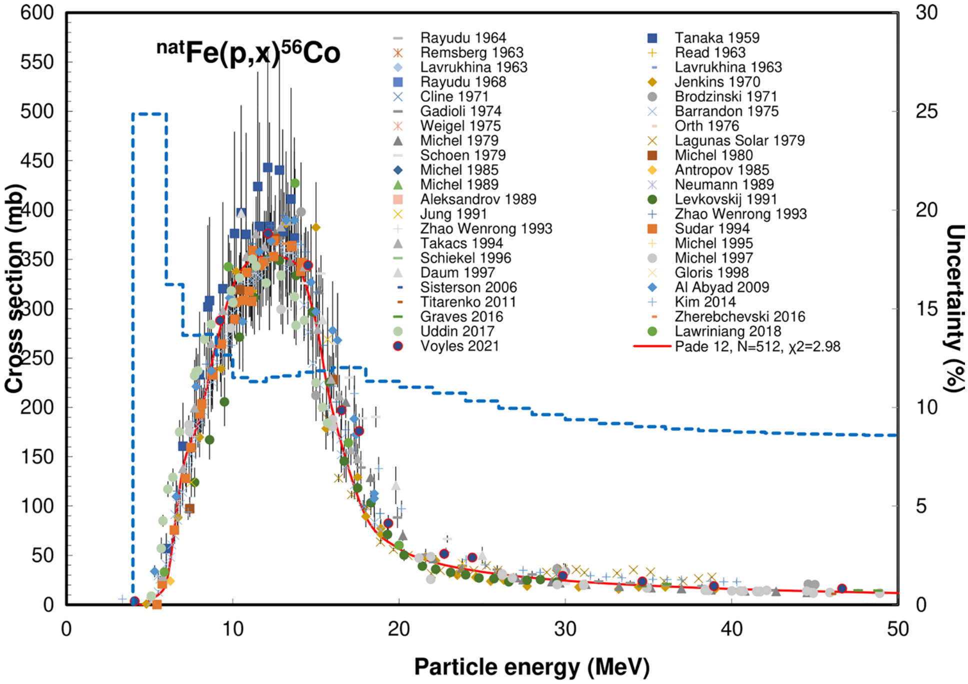

Fig. 13 $^{nat}Fe(p,x)^{56}Co$ reaction: selected experimental works and Padé fit (solid line) with total derived uncertainties, including 4% systematic uncertainty (dashed line, right-hand scale)

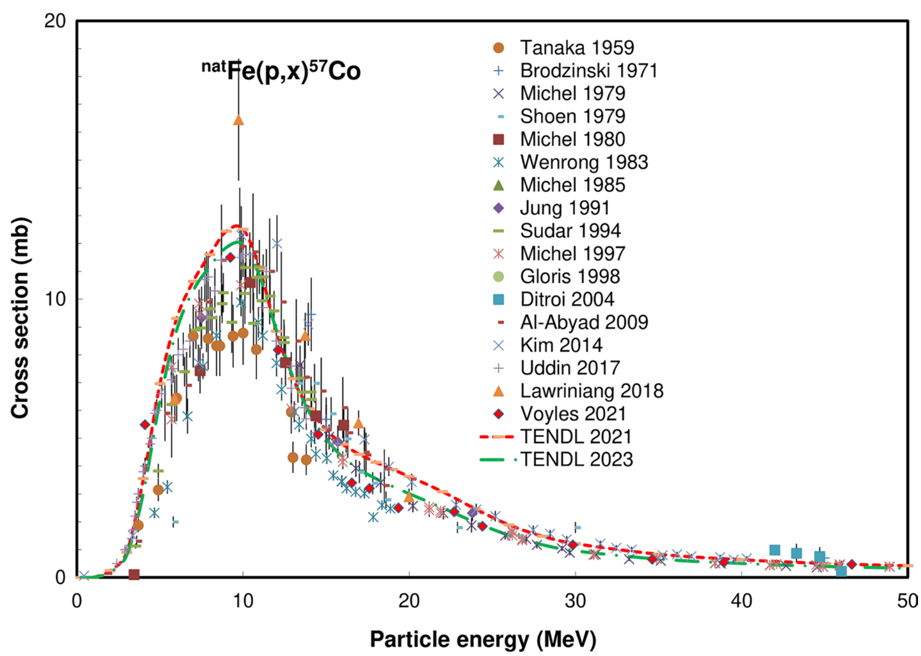

Fig. 14 $^{nat}Fe(p,x)^{57}Co$ reaction: all experimental data and the TENDL theoretical excitation functions

$^{nat}Fe(p,x)^{57}Co$ reaction

Two reactions $^{57}Fe(p,n)$ reaction (abundance 2.119%, threshold of 1.647 MeV) and $^{58}Fe(p,2n)$ (lower abundance 0.282%, threshold 11.87 MeV) contribute to the formation of ^{57}Co when irradiating ^{nat}Fe targets.

A total of 17 cross section data sets, covering the energy range from threshold up to 50 MeV, were found in the literature and are displayed in Fig. 14:

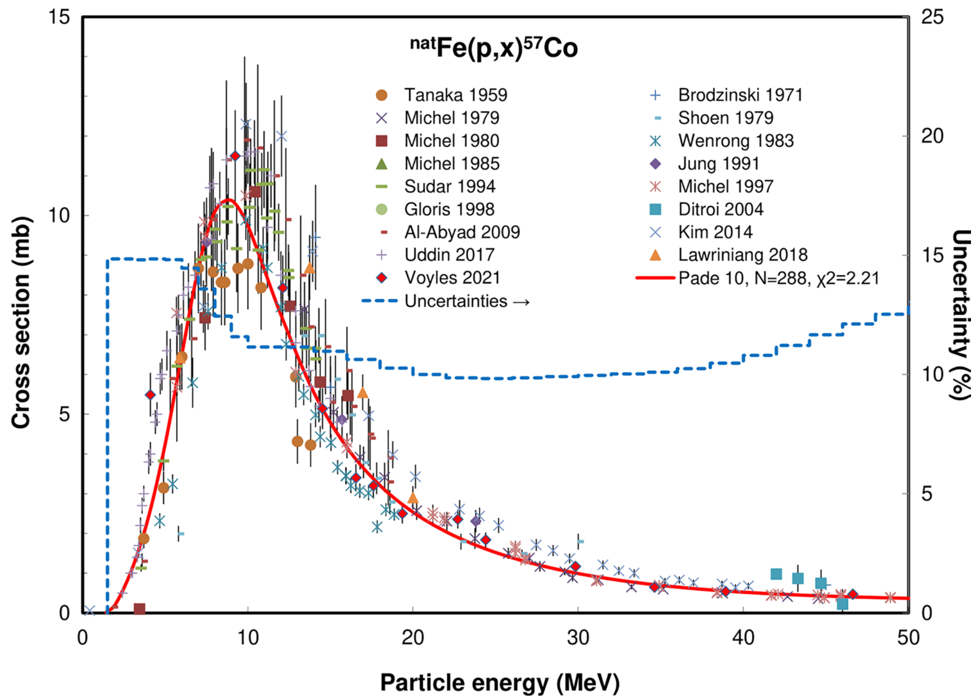

Fig. 15 $^{nat}Fe(p,x)^{57}Co$ reaction: selected experimental works and Padé fit (solid line) with total derived uncertainties, including 4% systematic uncertainty (dashed line, right-hand scale)

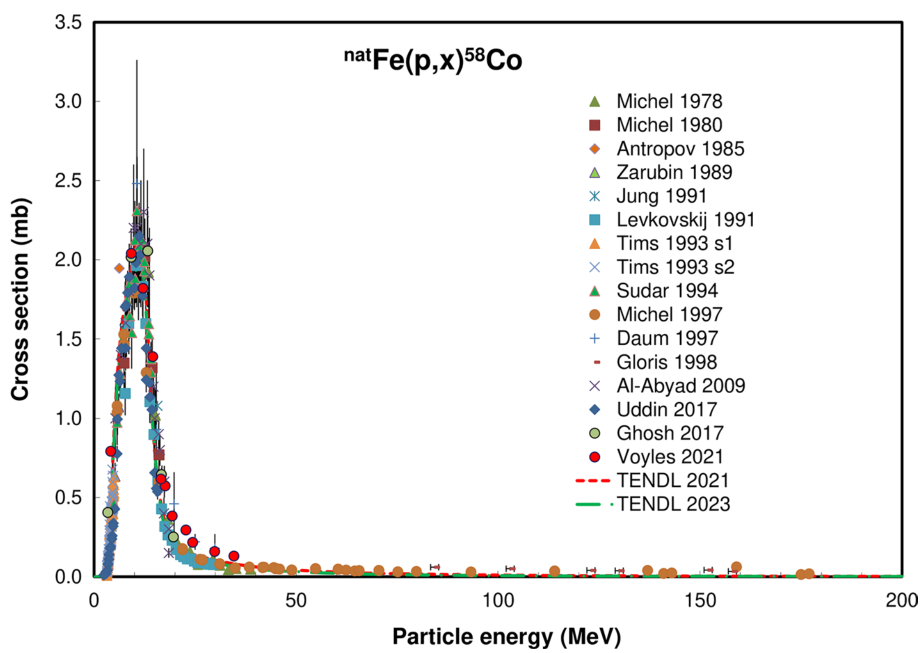

Fig. 16 $^{nat}Fe(p,x)^{58}Co$ reaction: all experimental data and the TENDL theoretical excitation functions

Tanaka [106], Brodzinski [87], Michel [90], Shoen [112], Michel [113], Zhao [96], Michel [114], Jung [118], Sudar [120], Michel [24], Gloris [97], Ditroi [99], Al-Abyad [100], Kim [101], Uddin [123], Lawriniang [124], Voyles [103].

Two outlying points were deleted: Shoen 1979 at 5.8 MeV (too low) and Lawriniang 2018 at 9.73 MeV.

The data of up to 50 MeV, from 17 publications were selected and fitted (Fig. 15). Both TENDL predictions are in good agreement with the experimental data over the entire energy domain and slightly overestimate the maximal experimental values of the $^{57}Fe(p,n)^{57}Co$ reaction. Only TENDL 2021 shows the small contribution of the $^{58}Fe(p,2n)$ reaction above 15 MeV.

The integral yields calculated from the recommended cross sections are shown in Fig. 18. One experimental yield data was found by Dmitriev [128].

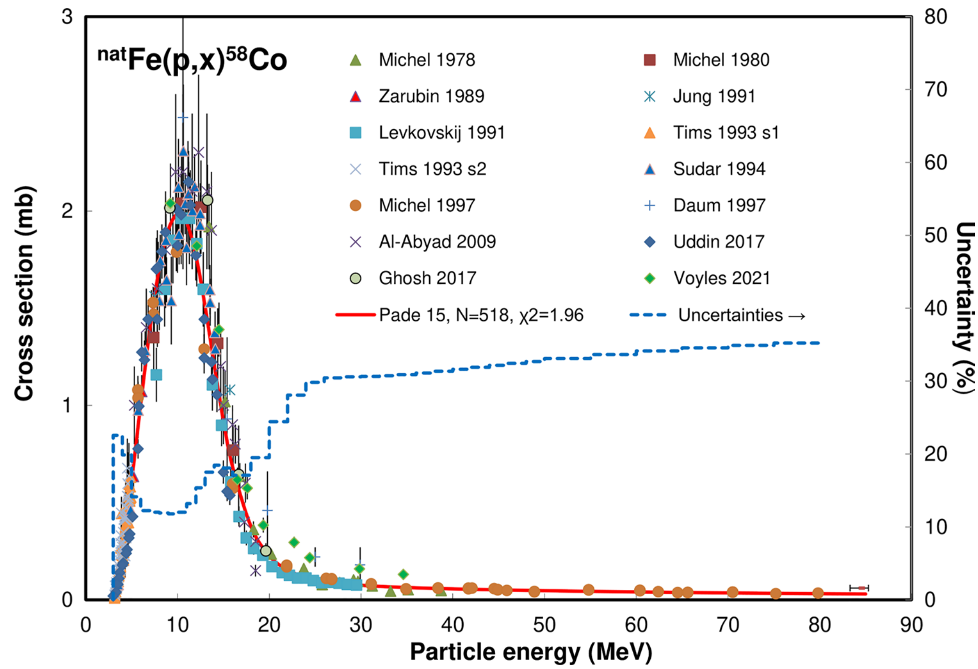

Fig. 17 $^{nat}Fe(p,x)^{58}Co$ reaction: selected experimental works and Padé fit (solid line) with total derived uncertainties, including 4% systematic uncertainty (dashed line, right-hand scale)

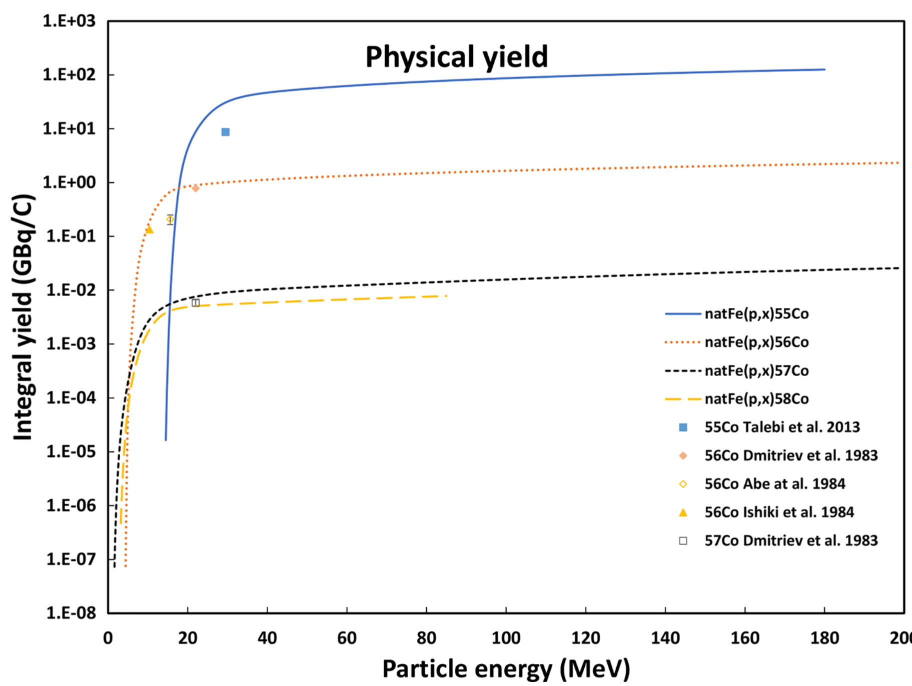

Fig. 18 Yield calculated from the recommended cross sections of the $^{nat}Fe(p,x)^{55}Co$, $^{nat}Fe(p,x)^{56}Co$, $^{nat}Fe(p,x)^{57}Co$ and $^{nat}Fe(p,x)^{58}Co$ reactions

$^{nat}Fe(p,x)^{58}Co$ reaction

Only the $^{58}Fe(p,n)$ reaction, with a threshold of 3.144 MeV, on low abundance ^{58}Fe (0.282%) contributes to the formation of ^{57}Co when irradiating ^{nat}Fe targets.

A total of 16 cross section data sets, covering the energy range from threshold up to 200 MeV, were found in literature and are displayed in Fig. 16: Michel [90], Michel [113], Antropov [115], Zarubin [129], Jung [118], Levkovskii [130], Tims [131], Sudar [120], Michel [24], Daum [92], Gloris [97], Al-Abyad [100], Uddin [123], Ghosh [132], Voyles [103].

Outlying data points of Antropov 1985 (at 6.24 MeV), Tims 1993 (at 3.895 MeV), Ghosh 2017 (at 3.38 MeV) and Voyles 2021 (at 4. 1 MeV) were deleted. As the two data points at 2.9 and 2.4 MeV of Uddin 2017 are below the reaction threshold they were removed.

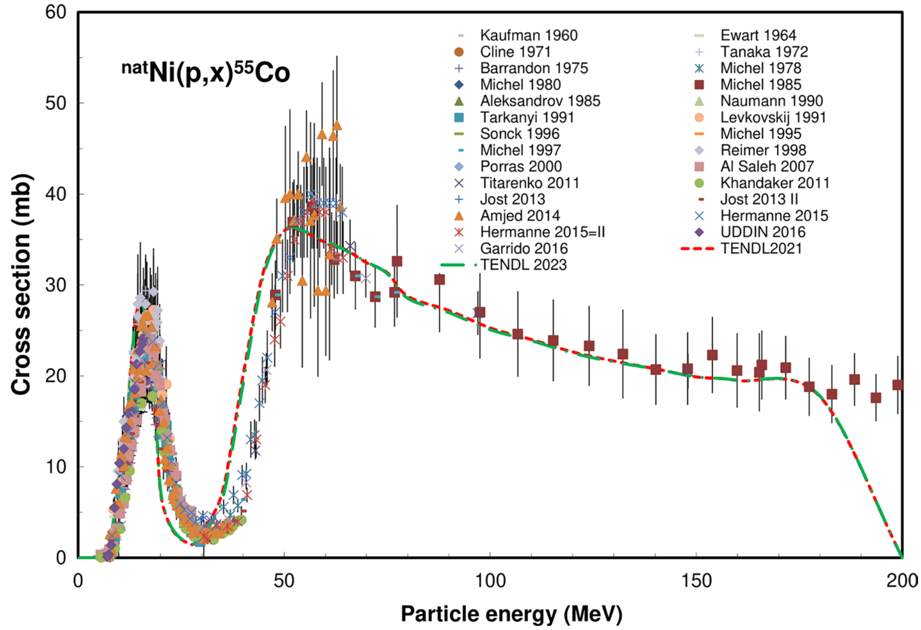

Fig. 19 $^{nat}Ni(p,x)^{55}Co$ reaction: all experimental data and the TENDL theoretical excitation functions

The data up to 85 MeV, the energy limit for interesting practical applications, of 14 publications were selected and fitted (Fig. 17). The two TENDL predictions are in very good agreement with the experimental data over the entire energy domain. The integral yields calculated from the recommended cross sections are shown in Fig. 18. One experimental yield data was found by Nickles [133], which is saturation yield on ^{58}Fe, so it is not shown in Fig. 18.

$^{nat}Ni(p,x)^{55}Co$ reaction

In principle five (p,2pxn) reactions on the stable target isotopes ^{58}Ni (abundance 68.077% in ^{nat}Ni, x = 2), ^{60}Ni (abundance 26.223% in ^{nat}Ni, n = 3), ^{61}Ni (abundance 1.1399% in ^{nat}Ni), ^{62}Ni (abundance 3.6346% in ^{nat}Ni), ^{64}Ni (abundance 0.9255% in ^{nat}Ni) can contribute to formation of ^{55}Co if high energy proton bombardment is performed.

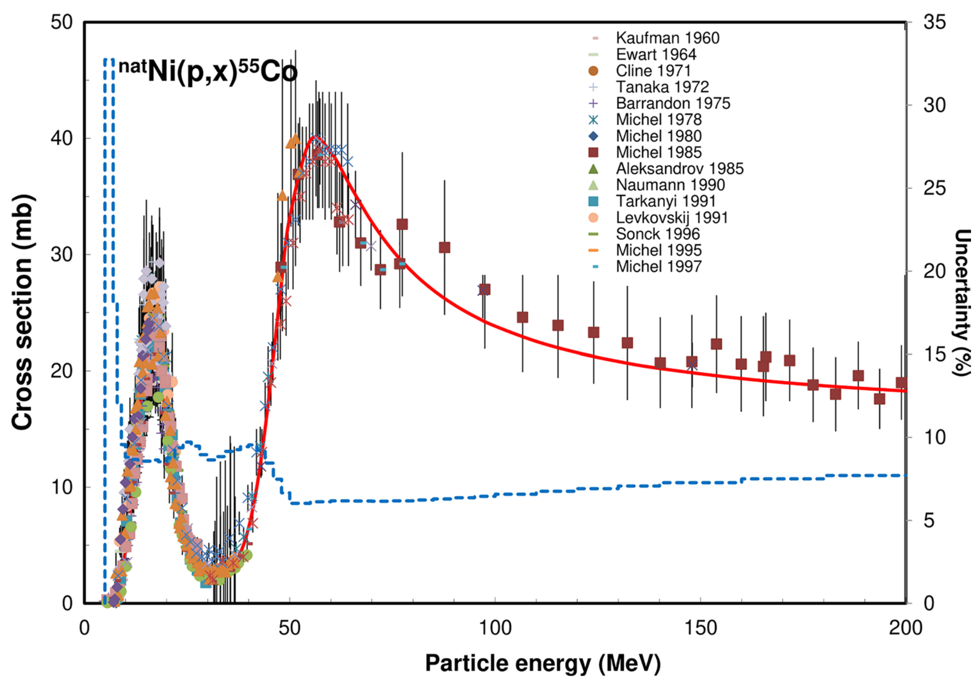

Fig. 20 $^{nat}Ni(p,x)^{55}Co$ reaction: selected experimental works and Padé fit (solid line) with total derived uncertainties, including 4% systematic uncertainty (dashed line, right-hand scale)

The threshold for reactions where at least 4 separate particles are emitted will be around 25 MeV but by clustering the (p,αyn) reaction is favored with 28 MeV lower thresholds.

A total of 27 cross section data sets, covering the energy range from threshold up to 200 MeV, were found in literature and are displayed in Fig. 19.

The publications are: Kaufman [134], Ewart [135], Cline [56], Tanaka [136], Barrandon [88], Michel [74], Michel [113], Michel [114], Aleksandrov [137], Neumann [98], Tarkanyi [138], Levkovskii [117], Sonck [139], Michel [65], Michel [24], Reimer [140], Porras [141], Al Saleh [142], Titarenko [71], Khandaker [143], Jost [144], Amjed [145], Hermanne [146], Uddin [147], Garrido [78].

All datasets were selected and fitted up to 200 MeV (Fig. 20). The two TENDL predictions represent well the overall behavior of the multiple contributing reactions but are systematically shifted to lower energy and overestimate the experimental data in the 30–80 MeV energy range.

The integral yields calculated from the recommended cross sections are shown in Fig. 31. Three experimental

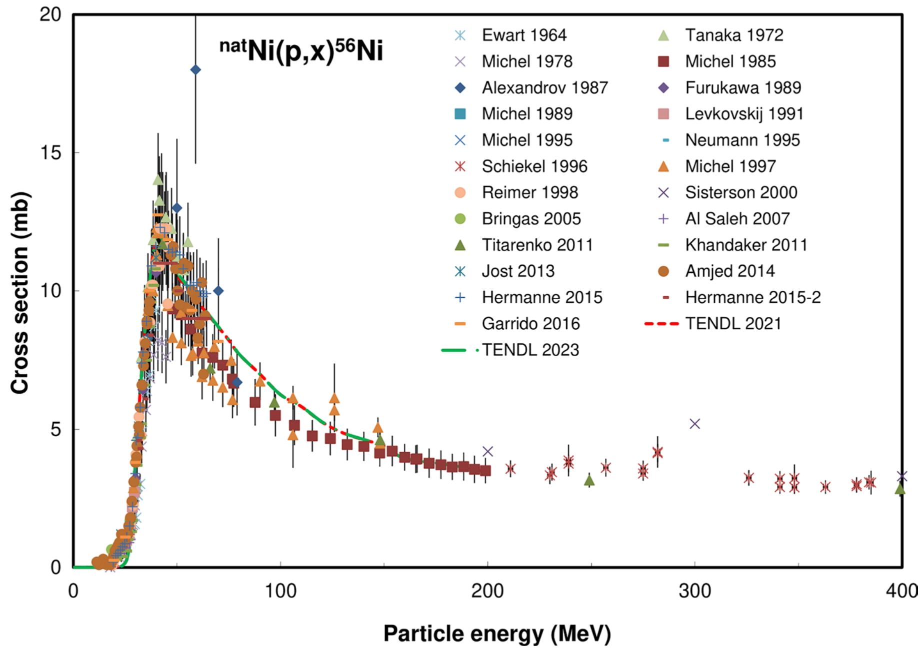

Fig. 21 $^{nat}Ni(p,x)^{56}Ni$ reaction: all experimental data and the TENDL theoretical excitation functions. TENDL stops here at 200 MeV

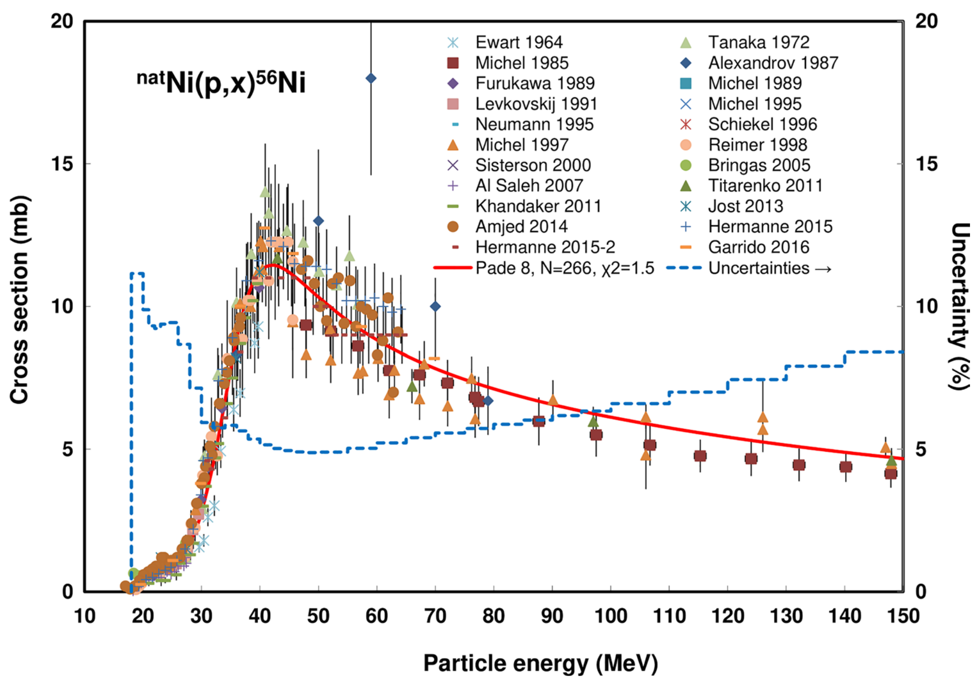

Fig. 22 $^{nat}Ni(p,x)^{56}Ni$ reaction: selected experimental works and Padé fit (solid line) with total derived uncertainties, including 4% systematic uncertainty (dashed line, right-hand scale)

yield data were found: Abe [84], Sadeghi [148], Le Van So [149].

$^{nat}Ni(p,x)^{56}Ni$ reaction

In principle five (p,pxn) reactions on the stable target isotopes ^{58}Ni (abundance 68.077% in ^{nat}Ni, x = 2), ^{60}Ni (abundance 26.223% in ^{nat}Ni, n = 3), ^{61}Ni (abundance 1.1399% in ^{nat}Ni), ^{62}Ni (abundance 3.6346% in ^{nat}Ni), ^{64}Ni (abundance 0.9255% in ^{nat}Ni) can contribute to formation of ^{55}Ni if high energy proton bombardment is performed. The threshold for the $^{58}Ni(p,p2n)^{56}Ni$ reaction with emission of 3 separate particles is 22.85 MeV but by clustering the $^{58}Ni(p,dn)^{56}Co$ reaction is favored with 20.59 MeV threshold. The same observation is valid for the reactions on other Ni isotopes.

A total of 23 cross section data sets, covering the energy range fom threshold up to 400 MeV, were found in literature and are displayed in Fig. 21: Ewart [135], Tanaka [136], Michel [150], Michel [114], Aleksandrov [151], Furukawa [152], Michel [63], Levkovskii [117], Michel [153], Neumann [98], Schiekel [66], Michel [24], Reimer [140], Sisterson [121], Bringas [154], Al Saleh [142], Titarenko [71], Khandaker [143], Jost [144], Amjed [145], Hermanne [146], Hermanne [155], Garrido [78].

The values of Michel 1978 are outlying and too low in the energy region of the maximum and were deselected. All other original datasets of 22 publications were selected up to 150 MeV and fitted (Fig. 22).

The two TENDL predictions are in good agreement with the overall shape of the excitation function, but overestimate the experimental data in the 50–150 MeV energy range. The integral yields calculated from the recommended cross sections are shown in Fig. 31. No experimental yield data was found.

$^{nat}Ni(p,x)^{56}Co$ reaction

In principle five (p,2pxn) reactions on the stable target isotopes ^{58}Ni (abundance 68.077% in ^{nat}Ni, x = 1), ^{60}Ni (abundance 26.223% in ^{nat}Ni, n = 3), ^{61}Ni (abundance 1.1399% in ^{nat}Ni), ^{62}Ni (abundance 3.6346% in ^{nat}Ni), ^{64}Ni (abundance 0.9255% in ^{nat}Ni) can contribute to formation of ^{56}Co if high energy proton bombardment is performed. The threshold for the $^{58}Ni(p,2pn)^{56}Co$ reaction with emission of 3 separate particles is 19.89 MeV but by clustering the $^{58}Ni(p,dp)^{55}Co$ reaction is favored with 17.62 MeV threshold. The same observation is valid for the reactions on other Ni isotopes.

A total of 15 cross section data sets, covering the energy range from threshold up to 200 MeV, were found in literature and are displayed in Fig. 23: Ewart [135], Tanaka [136], Aleksandrov [151], Levkovskii [117], Jung [118], Tarkanyi [138], Reimer [140], Michel [24], Sisterson [121], Al Saleh [142], Titarenko [156], Khandaker [143], Amjed [145], Hermanne [146], Garrido [78].

An additional set, only containing datapoints above 200 MeV is available but was not included further in the evaluation: Schiekel [66].

The total set of Ewart 1964 with too low values was deselected. The set of Hermanne 2015 consists of two series of data obtained in two irradiations with respectively 34 and 65 MeV incident proton beam energy. As results for the 65 MeV experiment are too low they were multiplied by a factor of 3 to be in good agreement with the values of Garrido 2016 and Michel 1997. Additionally, the 6 data points

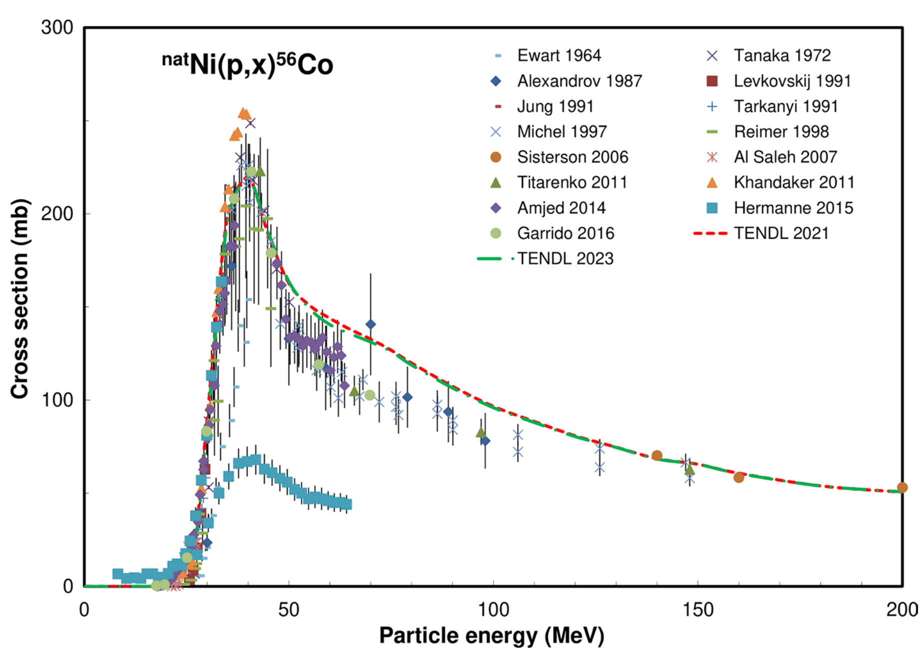

Fig. 23 $^{nat}Ni(p,x)^{56}Co$ reaction: all experimental data and the TENDL theoretical excitation functions

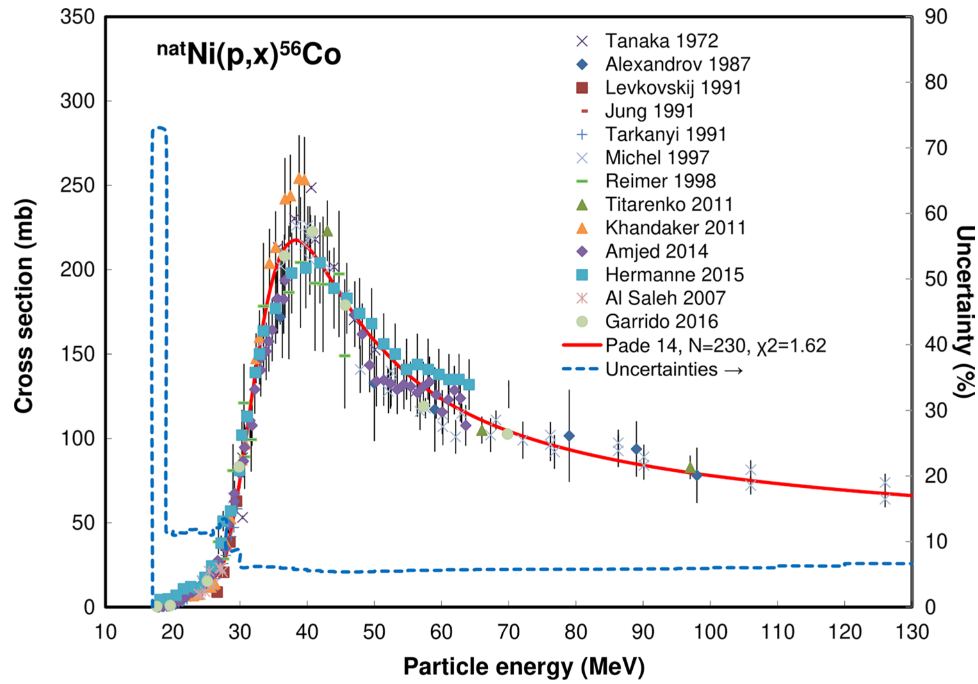

Fig. 24 $^{nat}Ni(p,x)^{56}Co$ reaction: selected experimental works and Padé fit (solid line) with total derived uncertainties, including 4% systematic uncertainty (dashed line, right-hand scale)

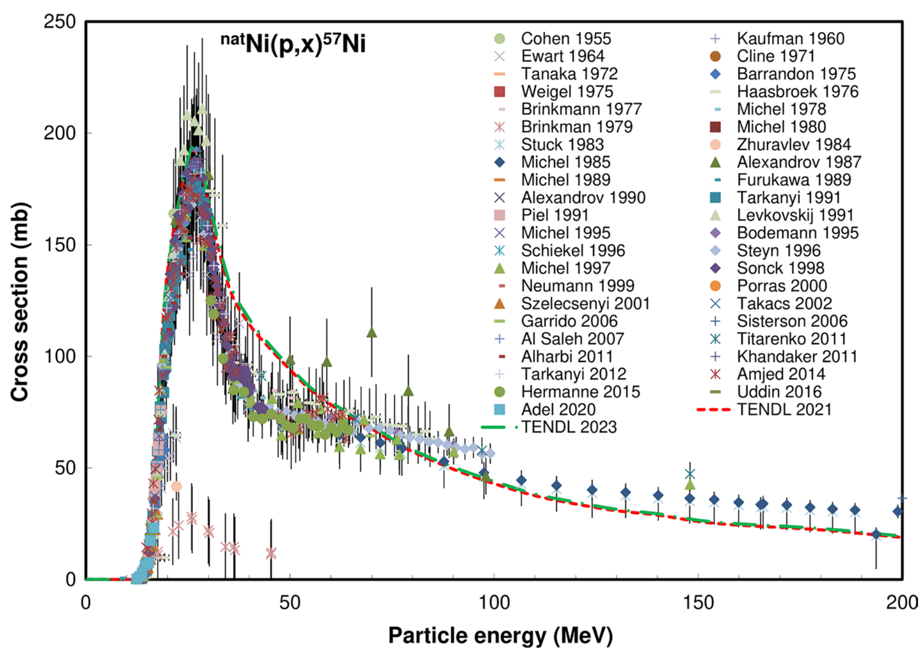

Fig. 25 $^{nat}Ni(p,x)^{57}Ni$ reaction: all experimental data and the TENDL theoretical excitation functions

below the practical 18 MeV threshold were deleted. The set of Reimer 1998 was energy-shifted and the two points at 26 and 24.5 MeV were deleted. Some outlying data points at energies below 30 MeV of Tanaka 1972, Aleksandrov 1987, Levkovski 1991 and Al Saleh 2007 were deleted.

The original and corrected datasets of 13 publications were selected up to 130 MeV and fitted (Fig. 24). The two TENDL predictions overestimate the experimental excitation functions above 40 MeV. The integral yields calculated from the recommended cross sections are shown in Fig. 31. Two experimental yield data were found Dmitriev [126] and Le Van So [149].

$^{nat}Ni(p,x)^{57}Ni$ reaction

In principle five (p,pxn) reactions on the stable target isotopes ^{58}Ni (abundance 68.077% in ^{nat}Ni, x = 1), ^{60}Ni (abundance 26.223% in ^{nat}Ni, n = 3), ^{61}Ni (abundance 1.1399% in ^{nat}Ni), ^{62}Ni (abundance 3.6346% in ^{nat}Ni), ^{64}Ni (abundance

0.9255% in ^{nat}Ni) can contribute to formation of ^{57}Ni if high energy proton bombardment is performed.

The threshold for the $^{58}Ni(p,pn)^{57}Ni$ reaction with the emission of 2 separate particles is 12.43 MeV but by clustering the $^{58}Ni(p,d)^{57}Co$ reaction is favored with 10.16 MeV threshold. The same observation is valid for the reactions on other Ni isotopes. A total of 43 cross section data sets, covering the energy range from threshold up to 200 MeV, were found in the literature and are displayed in Fig. 25:

Cohen [157], Kaufman [134], Ewart [135], Cline [56], Tanaka [136], Barrandon [88], Weigel [158], Haasbroek [159], Brinkman [160], Piel [161], Brinkmann [162], Michel [113], Stück [163], Zhuravlev [164], Michel [114], Aleksandrov [151], Michel [63], Furukawa [152], Aleksandrov [151], Tarkanyi [165], Levkovskii [117], Bodemann [166], Michel [65], Schiekel [66], Steyn [167], Michel [24], Sonck [168], Neumann [98], Porras [141], Szelecsenyi [169], Takacs [170], Garrido [78], Sisterson [121], Al Saleh [142], Titarenko [156], Alharbi [171], Khandaker [143], Amjed [145], Hermanne [155], Uddin [147], Adel [172].

Datapoints above 200 MeV were not included further in the evaluation. The outlying datasets of Cohen 1955, Kaufmann 1960, Ewart 1964, Tanaka 1972, Haasbroek 1977, Brinkmann 1977, Zhuravlev 1984 and Steyn 1996 data were deselected. The data of Aleksandrov 1987 are too high and the set was deselected. Additionally, the points with too low cross section values below 20 MeV of Barandon 1975, Szelecsenyi 2001 and Garrido 2016 were deleted. The remaining data from 31 publications were selected up to 200 MeV and fitted (Fig. 26). The two TENDL predictions estimated the maximal value around 26 MeV but overestimated the contribution of the reactions where multiple separate particles are emitted in the 30–60 MeV domain.

The integral yields calculated from the recommended cross sections are shown in Fig. 31. Four experimental yield data were found: Dmitriev [126], Abe [84], Sadeghi [148], Le Van So [149].

$^{nat}Ni(p,x)^{57}Co$ reaction

In principle five (p,2pxn) reactions on the stable target isotopes ^{58}Ni (abundance 68.077% in ^{nat}Ni, x = 0), ^{60}Ni (abundance 26.223% in ^{nat}Ni, n = 2), ^{61}Ni (abundance 1.1399% in ^{nat}Ni), ^{62}Ni (abundance 3.6346% in ^{nat}Ni), ^{64}Ni (abundance 0.9255% in ^{nat}Ni) can contribute to direct formation of ^{57}Co ($T_{1/2}$ = 271.74 d) if high energy proton bombardment is performed. Depending on the cooling time before measurement contribution of the shorter-lived ^{57}Ni ($T_{1/2}$ = 35.60 h) can contribute. The threshold for the $^{58}Ni(p,2p)^{57}Co$ reaction is 8.31 MeV, for the $^{60}Ni(p,\alpha)^{57}Co$ reaction (clustering) a low threshold of 0.268 MeV is seen and for $^{61}Ni(p,\alpha n)$ it is 8.22 MeV. The possible contribution of parent ^{57}Ni can only start at 10.16 MeV, the threshold of the $^{58}Ni(p,d)^{57}Ni$ reaction.

A total of 15 cross section data sets, covering the energy range from threshold up to 200 MeV, were found in the literature and are displayed in Fig. 27:

Cline [56], Michel [150], Michel [113], Aleksandrov [151], Tarkanyi [165], Jung [118], Schiekel [66], Michel

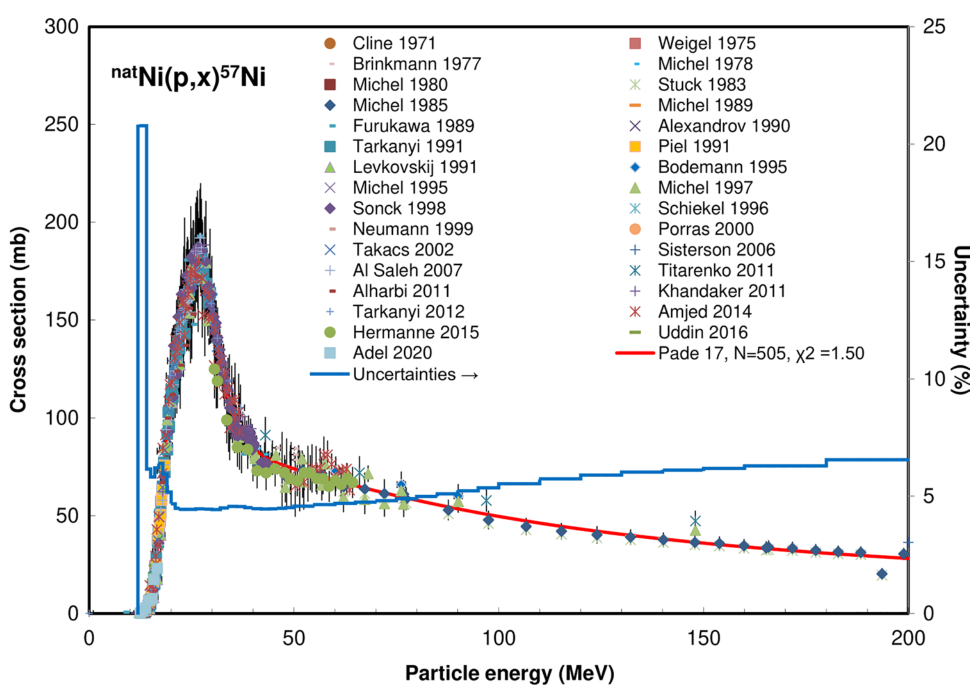

Fig. 26 $^{nat}Ni(p,x)^{57}Ni$ reaction: selected experimental works and Padé fit (solid line) with total derived uncertainties, including 4% systematic uncertainty (dashed line, right hand scale)

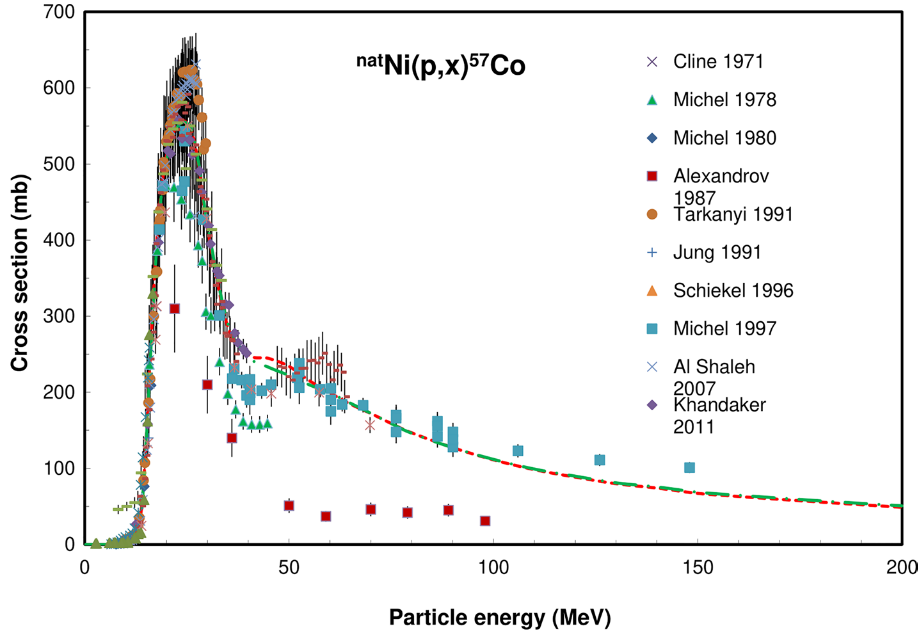

Fig. 27 $^{nat}Ni(p,x)^{57}Co$ reaction: all experimental data and the TENDL theoretical excitation functions

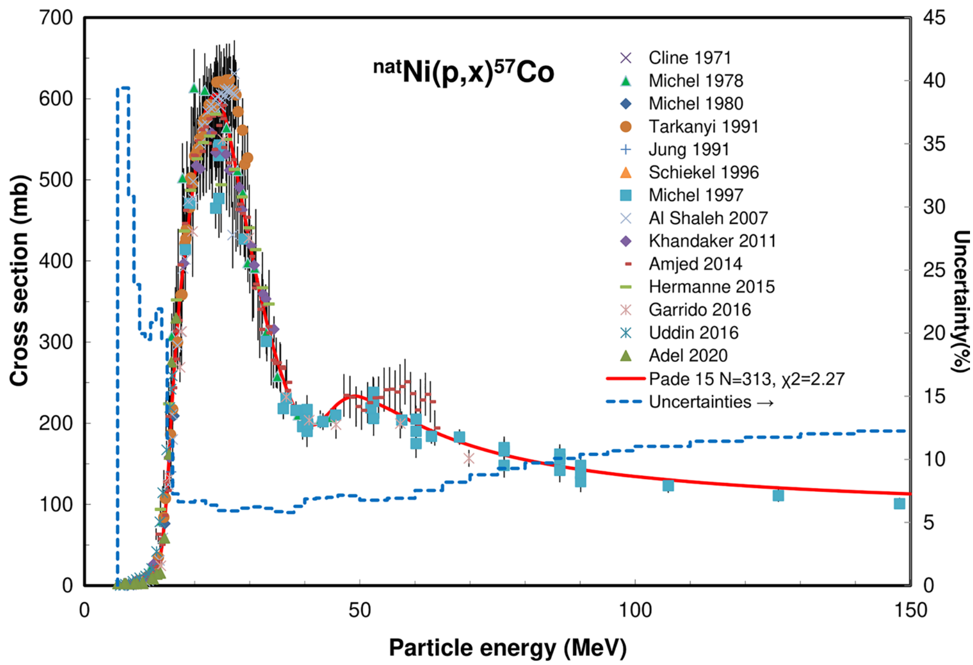

Fig. 28 $^{nat}Ni(p,x)^{57}Co$ reaction: selected experimental works and Padé fit (solid line) with total derived uncertainties, including 4% systematic uncertainty (dashed line, right-hand scale)

[24], Al Saleh [142], Khandaker [143], Amjed [145], Hermanne [146], Garrido [78], Uddin [147], Adel [172].

As far as can be deduced from the information in the original publications, full cumulative cross sections, after decay of ^{57}Ni, were reported. TENDL predictions allow us to calculate a contribution starting at 2% at 14 MeV, rising continuously to 85% at 35 MeV and decreasing to a value around 65% from 55 MeV on.

The outlying dataset of Aleksandrov 1987 was deleted. The whole set of Michel 1978 has a good shape but is too low and was multiplied with a factor of 1.3 to correspond to the data of Michel 1997, Garrido 2016 and Amjed 2014 in the 30–45 MeV region. Additionally, the too high values point at the lowest energies in Hermanne 2015 and Adel 2020 were deleted, while at higher energies all points Khandaker 2011 above 35 MeV and two values of Michel 1997 (at 24.4 and 23.8 MeV) were considered outlying.

The original and corrected datasets of 14 publications were selected up to 150 MeV and fitted (Fig. 28).

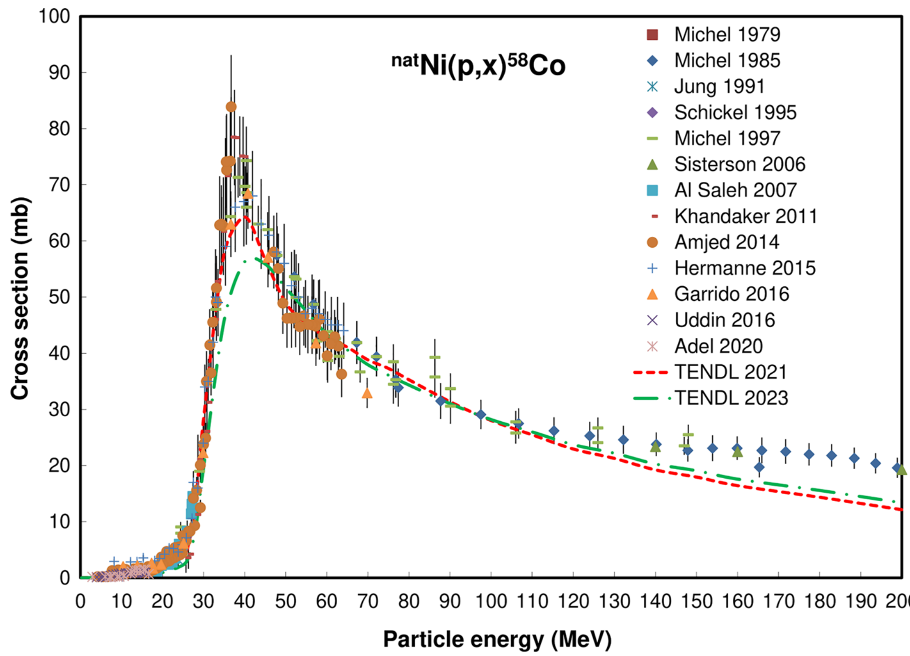

Fig. 29 $^{nat}Ni(p,x)^{58}Co$ reaction: all experimental data and the TENDL theoretical excitation functions

The two TENDL predictions are well estimating the maximal value around 26 MeV but are overestimating the contribution of the ^{57}Ni decay in the 35–55 MeV domain. The integral yields calculated from the recommended cross sections are shown in Fig. 31. Four experimental yield data were found Gruverman [173], Dmitriev [126]. Le Van So [149], Sadeghi [148].

$^{nat}Ni(p,x)^{58}Co$ reaction

In principle four (p,2pxn) reactions on the stable target isotopes ^{60}Ni (abundance 26.223% in ^{nat}Ni, n = 1), ^{61}Ni (abundance 1.1399% in ^{nat}Ni), ^{62}Ni (abundance 3.6346% in ^{nat}Ni), ^{64}Ni (abundance 0.9255% in ^{nat}Ni) can contribute to

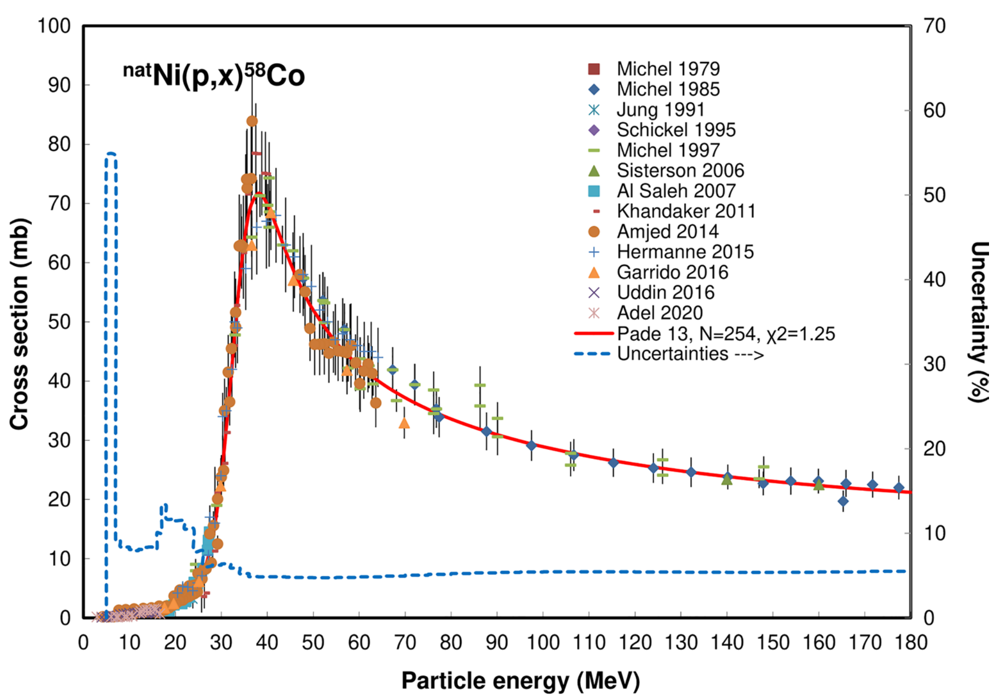

Fig. 30 $^{nat}Ni(p,x)^{58}Co$ reaction: selected experimental works and Padé fit (solid line) with total derived uncertainties, including 4% systematic uncertainty (dashed line, right hand scale)

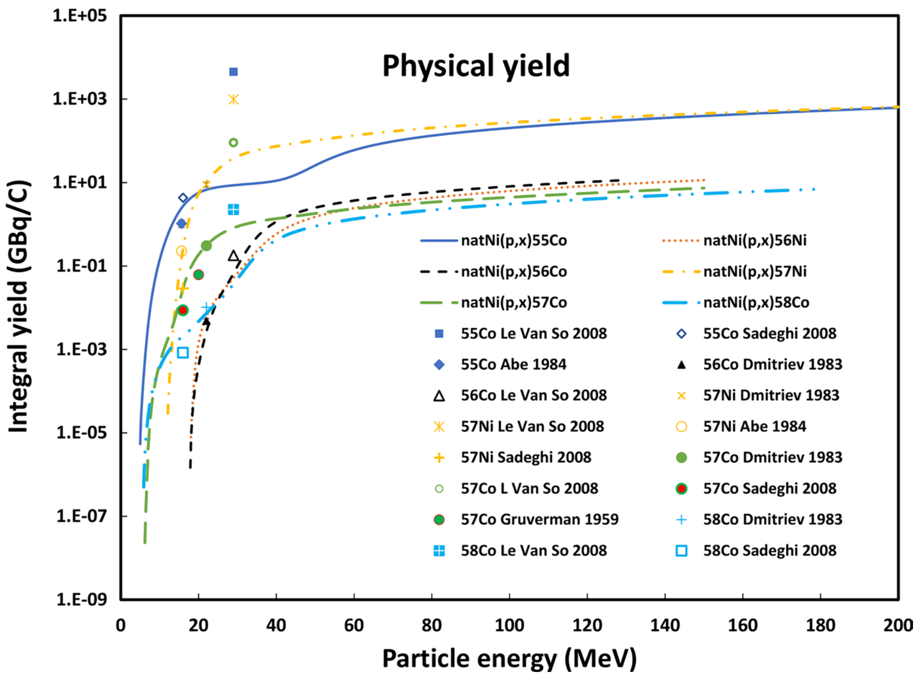

Fig. 31 Yield calculated from the recommended cross sections of the $^{nat}Ni(p,x)^{55}Co$, $^{nat}Ni(p,x)^{56}Ni$, $^{nat}Ni(p,x)^{56}Co$, $^{nat}Ni(p,x)^{57}Ni$, $^{nat}Ni(p,x)^{57}Co$ and $^{nat}Ni(p,x)^{58}Co$ reactions

formation of ^{58}Co if high energy proton bombardment is performed.

The threshold for the $^{60}Ni(p,2pn)^{58}Co$ reaction with the emission of 3 separate particles is around 12.47 MeV but by clustering the $^{61}Ni(p,\alpha)^{58}Co$ reaction with a positive Q-value of 0.489 MeV can contribute.

A total of 13 cross section data sets, covering the energy range from threshold up to 200 MeV, were found in literature and are displayed in Fig. 29: Michel [113], Michel [114], Jung [118], Schiekel [66], Michel [24]Targeted radionuclide therapy, Sisterson [121], Al Saleh [142], Khandaker [143], Amjed [145], Hermanne [146], Garrido [78], Uddin [147], Adel [172].

An additional set, only containing datapoints above 200 MeV is available but was not included further in the evaluation], Sisterson [121].

All sets were in acceptable agreement but some outlying datapoints were deleted: Hermanne 2015 (7 points below 20 MeV), Garrido 2016 (3 points below 18 MeV), Amjed 2014 (7 too high points between 13 and 7.5 MeV). The original and corrected datasets of 13 publications were selected up to 180 MeV and fitted (Fig. 30). The two TENDL predictions represent well the overall shape of the excitation function with an underestimation of the maximal value.

The integral yields calculated from the recommended cross sections are shown in Fig. 31. 3 experimental yield data was found: Dmitriev [126], Le Van So [149] and Sadeghi [148].

$^{nat}Cu(p,x)^{61}Cu$ reaction

As in 2020 updated abundances for the different γ-lines emitted in the decay of ^{61}Cu were adopted in NUDAT3.0 (see Table 2) nearly all data sets published before 2020 had to be attentively checked and corrections for used absolute abundances or ratios made. Moreover, new relative intensity values for the 656.008 keV line were found in a well-documented study published by Bleuel 2021 [174]. However, the ratio of the 656.008 keV (10.4%) to 282.956 keV (12.7%) intensities used in the present evaluation (ratio 0.820 (140), see Table 3) only differs by 3% from the proposed Bleuel 2021 data (ratio 0.793 (10)). On the other side practically in all compiled work, the cross section data were corrected by using the 282.956 keV line. Possible additional corrections for a new update of ENSDF accepted absolute abundance will hence be well within the 10–12% uncertainties on the used experimental data and the change in fit and recommended values will be small.

Two (p,pxn) reactions on the stable target isotopes ^{63}Cu (abundance 69.15% in ^{nat}Cu, n = 2), ^{65}Cu (abundance 30.85% in ^{nat}Cu, n = 4), can contribute to the formation of ^{61}Cu if high energy proton bombardment is performed.

The threshold for the $^{63}Cu(p,p2n)^{61}Cu$ reaction with the emission of 3 separate particles is 20.054 MeV while the $^{65}Cu(p,p4n)^{61}Cu$ reaction has a 38.15 MeV threshold. Above 30 MeV incident proton energy decay of short-lived ^{61}Zn ($T_{1/2}$ = 89.1 s), formed in the $^{63}Cu(p,3n)^{61}Zn$ reaction, will start cumulative formation.

A total of 20 cross section data sets, covering the energy range from threshold up to 200 MeV, were found in literature

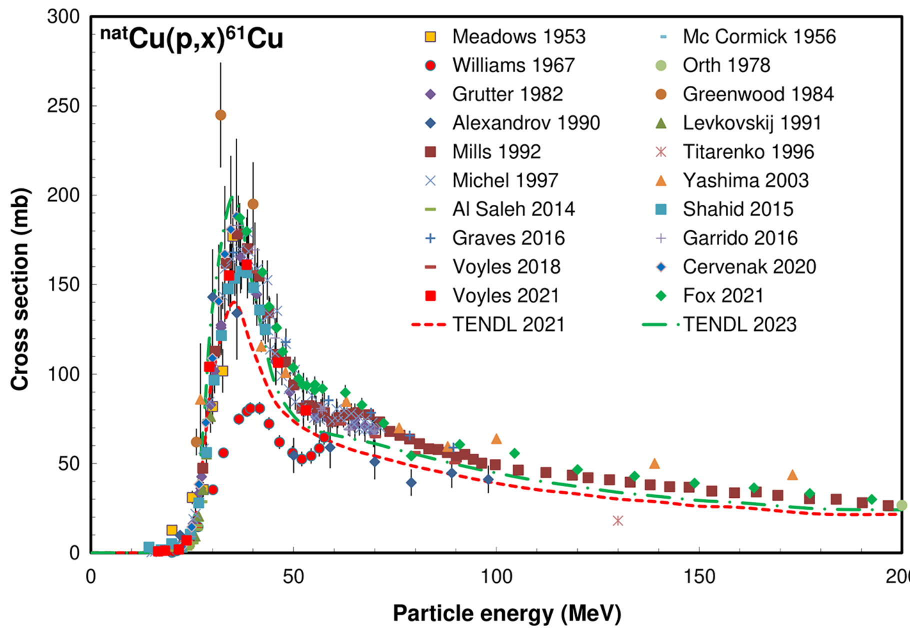

Fig. 32 $^{nat}Cu(p,x)^{61}Cu$ reaction: all experimental data and the TENDL theoretical excitation functions

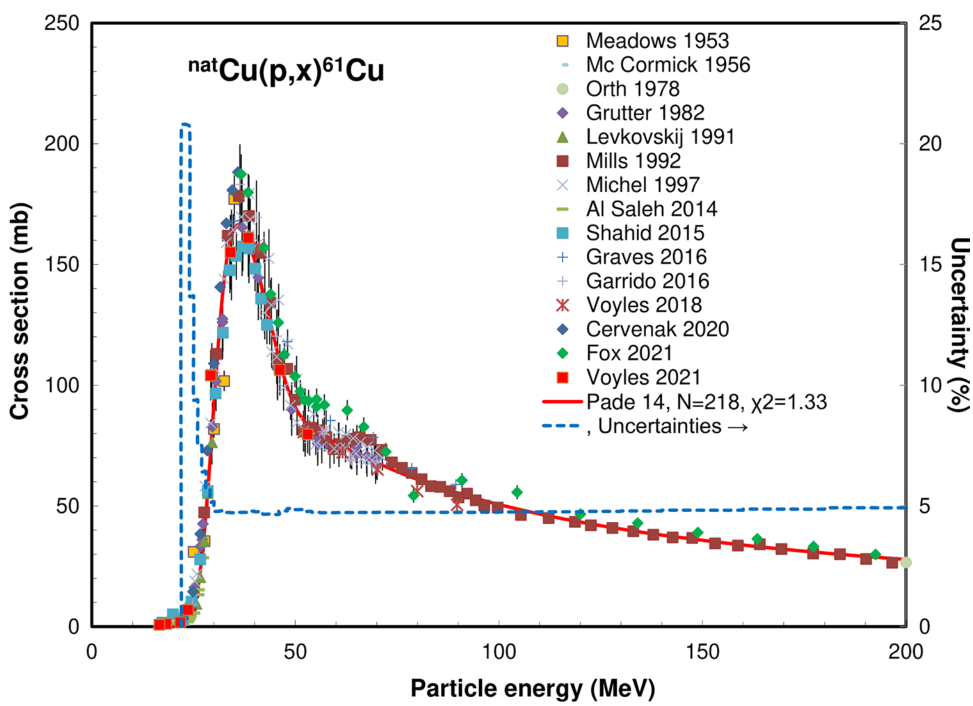

Fig. 33 $^{nat}Cu(p,x)^{61}Cu$ reaction: selected experimental works and Padé fit (solid line) with total derived uncertainties, including 4% systematic uncertainty (dashed line, right-hand scale)

and are displayed in Fig. 32: Meadows [175], McCormick [176], Williams [86], Orth [177], Grutter [61], Greenwood [178], Aleksandrov [151], Aleksandrov [137], Levkovskii [130], Mills [179], Titarenko [180], Michel [24], Yashima [69], Al Saleh [181], Shahid [182], Graves [102], Garrido [78], Voyles [183], Cervenak [81], Voyles [103], Fox [83].

An additional set, only containing datapoints above 200 MeV is available but is not included further in the evaluation: Alksandrov [95].

Five sets with outlying points were deselected: Williams 1967, Greenwood 1984, Aleksandrov 1987, Titerenko 1996, Yashima 2002. The two points at 20 and 23 MeV, too high values, of Meadows 1953 were deleted.

The original and corrected datasets of 15 publications were selected up to 200 MeV and fitted (Fig. 33).

The TENDL 2021 prediction underestimates the maximal value at a slightly energy-shifted position but the 2023 version more correctly describes the experimental values.

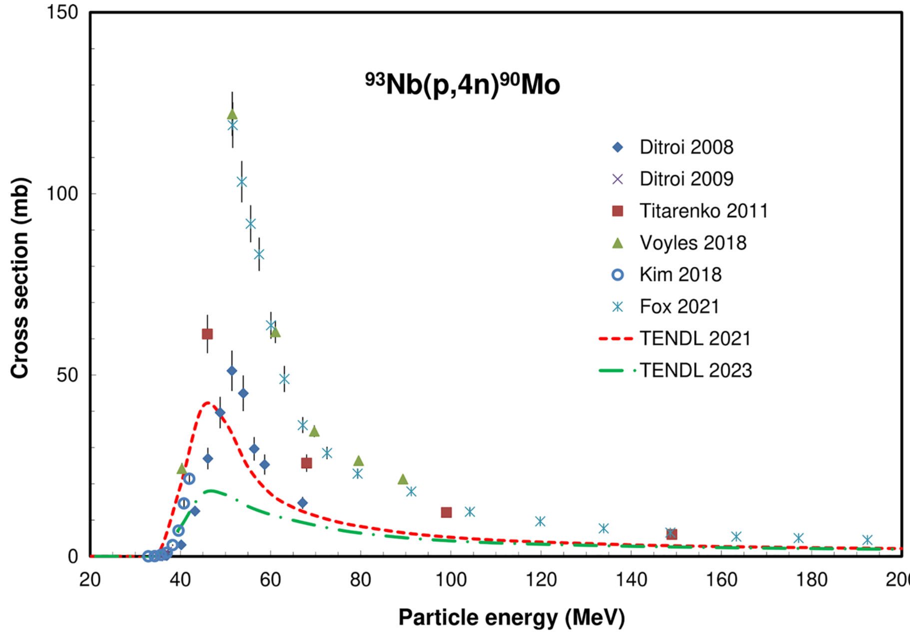

Fig. 34 $^{93}Nb(p,x)^{90}Mo$ reaction: all experimental data and the TENDL theoretical excitation functions

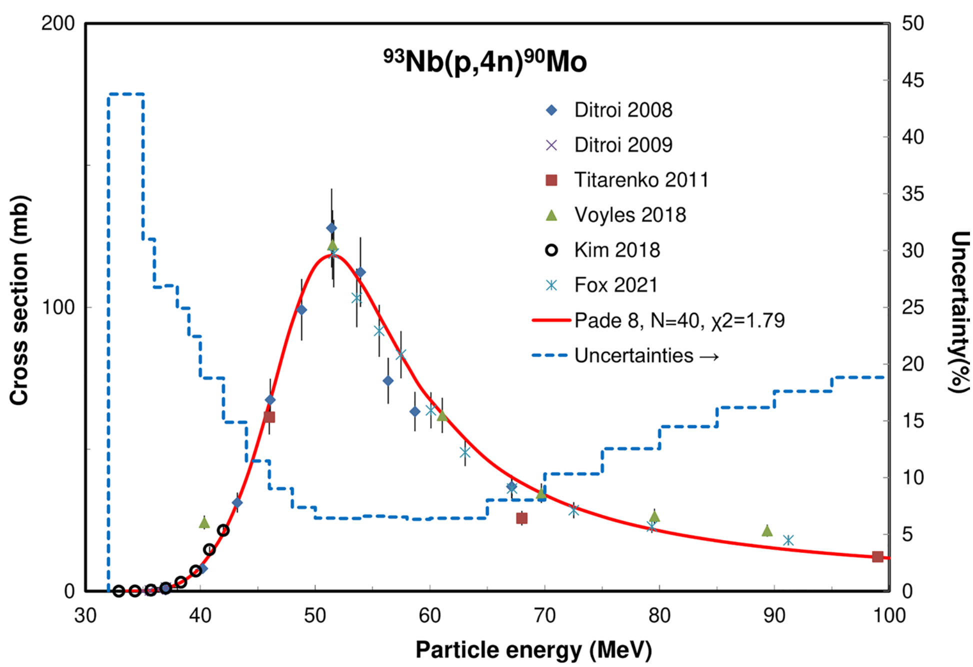

Fig. 35 $^{93}Nb(p,x)^{90}Mo$ reaction: selected experimental works and Padé fit (solid line) with total derived uncertainties, including 4% systematic uncertainty (dashed line, right-hand scale)

The integral yields calculated from the recommended cross sections are shown in Fig. 42. A single experimental yield data was found: Le Van So [149].

$^{93}Nb(p,4n)^{90}Mo$ reaction

As Nb is monoisotopic only the $^{93}Nb(p,4n)$ reaction with the threshold of 32.384 MeV contributes to the formation of ^{90}Mo. A total of 6 cross section data sets, covering the energy range from threshold up to 200 MeV, were found in

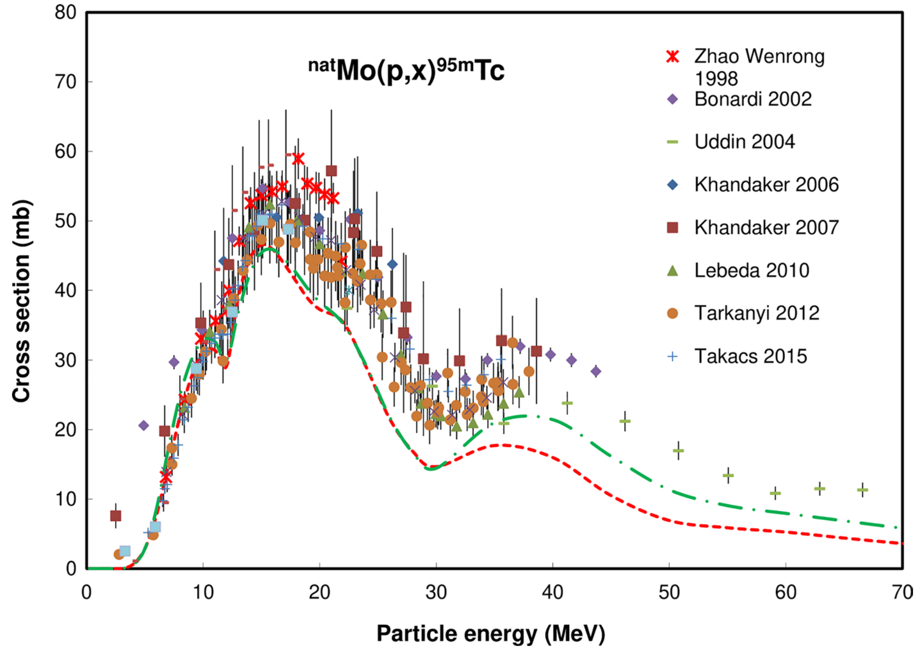

Fig. 36 $^{nat}Mo(p,x)^{95m}Tc$ reaction: all experimental data and the TENDL theoretical excitation functions

literature and are displayed in Fig. 34: Ditroi [184], Ditroi [185], Titarenko [156], Voyles [183], Kim [186], Fox [83]. The values of Ditroi 2008 are too low but the excitation function has a good overall shape and hence the set was multiplied by a factor of 2.5 to agree with the maximal values of 120 mb near 51.5 MeV given by Fox 2021 and Voyles 2018. As for several sets the uncertainties given in the original publication are well below 10% they were systematically increased to 12% for selection.

The original and corrected datasets of the 6 publications were selected up to 100 MeV and fitted (Fig. 35). While TENDL 2021 prediction underestimates the maximal value by a factor of 2.5–3, the new 2023 version is even a factor of two lower. Although the overall shape of the excitation curve is well represented, a 4 MeV energy shift is noted. The integral yields calculated from the recommended cross sections are shown in Fig. 42. No experimental yield data were found.

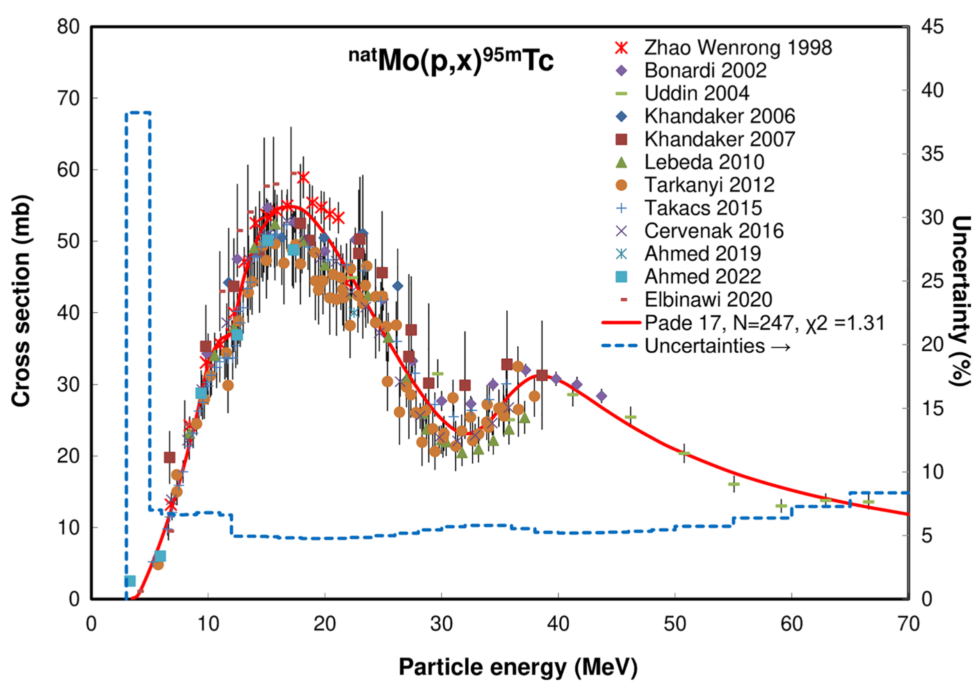

Fig. 37 $^{nat}Mo(p,x)^{95m}Tc$ reaction: selected experimental works and Padé fit (solid line) with total derived uncertainties, including 4% systematic uncertainty (dashed line, right hand scale)

$^{nat}Mo(p,x)^{95m}Tc$ reaction

In principle five (p,xn) reactions on the stable target isotopes ^{95}Mo (abundance 15.84% in ^{nat}Mo, n = 1), ^{96}Mo (abundance 16.67% in ^{nat}Mo, n = 2), ^{97}Mo (abundance 9.60% in ^{nat}Mo), ^{98}Mo (abundance 24.39% in ^{nat}Mo), ^{100}Mo (abundance 9.82% in ^{nat}Mo, n = 6) can contribute to formation of ^{95m}Tc if a high energy proton bombardment is performed.

The threshold for the $^{95}Mo(p,n)^{95m}Tc$ reaction is 2.499 MeV and it rises to 41.727 MeV for the $^{100}Mo(p,n)^{95m}Tc$ reaction.

A total of 12 cross section data sets, covering the energy range from threshold up to 70 MeV, were found in literature and are displayed in Fig. 36: Zhao Wenrong [187], Bonardi [188], Uddin [189], Khandaker [190], Khandaker [191], Lebeda [192], Tarkanyi [193], Takacs [194], Cervenak [195], Ahmed [196], Elbinawi [197], Ahmed [198]. The values of Uddin 2004 are low compared to other sets above

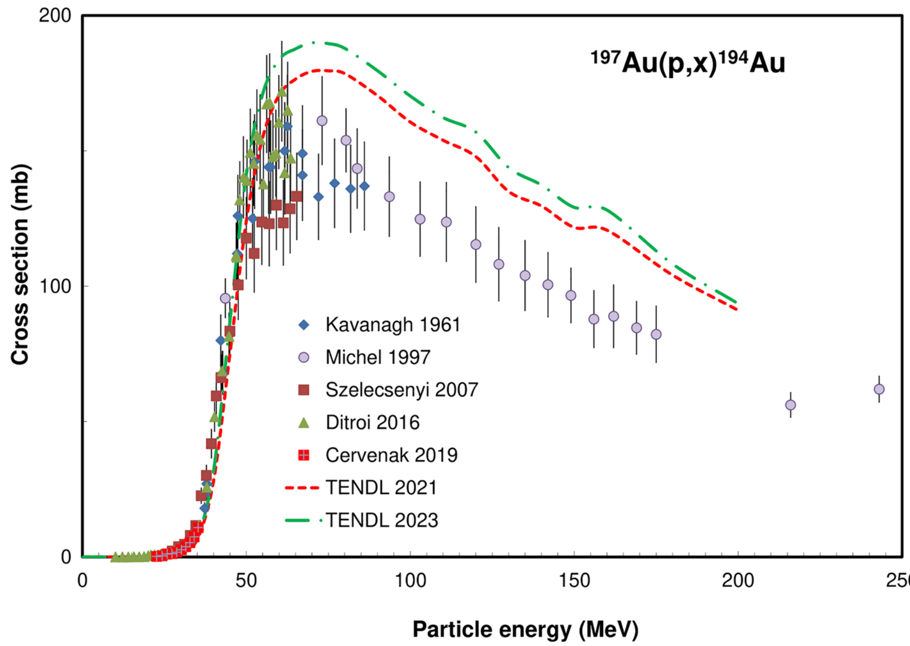

Fig. 38 $^{197}Au(p,x)^{194}Au$ reaction: all experimental data and the TENDL theoretical excitation functions

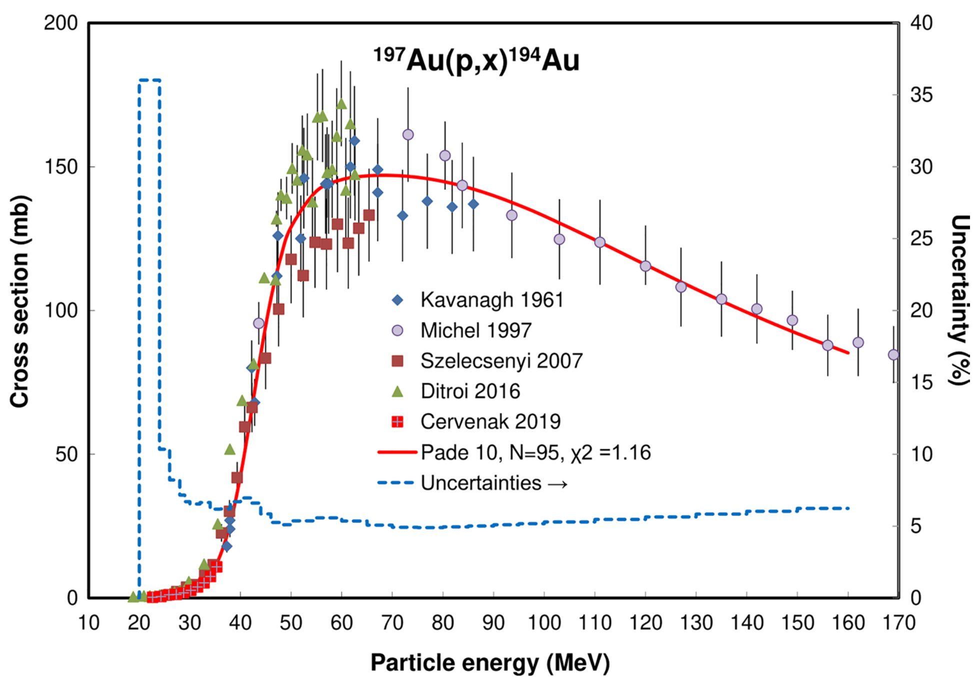

Fig. 39 $^{197}Au(p,x)^{194}Au$ reaction: selected experimental works and Padé fit (solid line) with total derived uncertainties, including 4% systematic uncertainty (dashed line, right-hand scale)

30 MeV and were multiplied by a factor of 1.2 to be in better agreement. Outlying datapoints at separate energies were deleted: Bonardi 2002 (at 4.9 and 7.5 MeV), Khandaker 2007 (at 2.5 and 21 MeV), Tarkanyi 2012 (at 2.78 MeV) (Fig. 37).

The original and corrected datasets of the 12 publications were selected up to 70 MeV and fitted (Fig. 13).

The TENDL predictions enhance better the separate contributions of the different stable target isotopes than the experimental results where only a secondary maximum near 40 MeV (probably (p,4n) on more abundant ^{98}Mo) can be seen. All maximum values are underestimated in the two versions.

The integral yields calculated from the recommended cross sections are shown in Fig. 42. Four experimental yield data were found: Dmitriev [199], Dmitriev [126], Lagunas-Solar [200], Bonardi (differential yield, not in figure) [188].

^{197}Au(p,x)^{194}Au reaction

As Au is monoisotopic only the ^{197}Au(p,p3n) reaction, with threshold for emission of single particles at 23.26 MeV, contributes to direct formation of ^{194}Au. As the threshold for the (p,^{3}H n) reaction is 14.73 MeV also small cross sections in the 15–24 MeV domain can be expected. Although the ^{197}Au(p,4n) reaction will result in formation of very long-lived parent ^{194}Hg ($T_{1/2}$ = 367 y) it will in practice not contribute to cumulative formation of ^{194}Au.

A total of 5 cross section data sets, covering the energy range from threshold up to 250 MeV, were found in literature and are displayed in Fig. 38: Kavanagh [201], Michel [24], Szelecsenyi [202], Ditroi [203], Cervenak [204]. All datasets of the 5 publications were selected up to 170 MeV and fitted (Fig. 39).

The two TENDL predictions agree well in overall shape but slightly overestimate the maximum value of the experimental points. The integral yields calculated from the recommended cross sections are shown in Fig. 42. Only 1 experimental yield data was found: Birattari [205] (differential yield, not in figure).

^{197}Au(p,x)^{196g}Au reaction

As Au is monoisotopic only the ^{197}Au(p,pn) reaction, with the threshold for emission of single particles at 8.114 MeV, contributes. As the threshold for (p,d) is 5.878 MeV also small cross section in the 6–9 MeV domain can be expected. The parallel formation of the two excited states, with respective half-lives of 9.7 h and 8.2 s, both decaying for 100% by IT to ^{196g}Au, will result in cumulative formation when using ^{196g}Au in practice for monitoring.

A total of 8 cross section data sets, covering the energy range from threshold up to 175 MeV, were found in literature and are displayed in Fig. 40: Yule [206], Gusakow [207], Kavanagh [201], Nagame [208], Michel [24], Szelecsenyi [209], Szelecsenyi [202], Ditroi [203].

The disagreeing set of Gusakov 1960 was deleted. The original sets of the remaining 7 publications were selected up to 150 MeV and fitted (Fig. 40). The two TENDL predictions agree well in overall shape but slightly overestimate the maximal value of the experimental points. The integral yields calculated from the recommended cross sections are shown in Fig. 41. Two experimental yield data point were

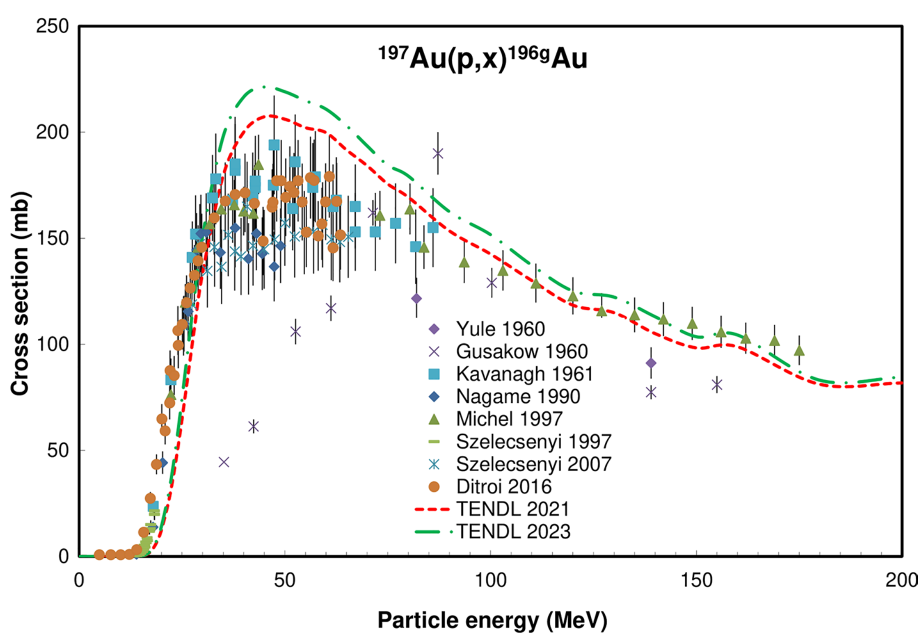

Fig. 40 ^{197}Au(p,x)^{196g}Au reaction: all experimental data and the TENDL theoretical excitation functions

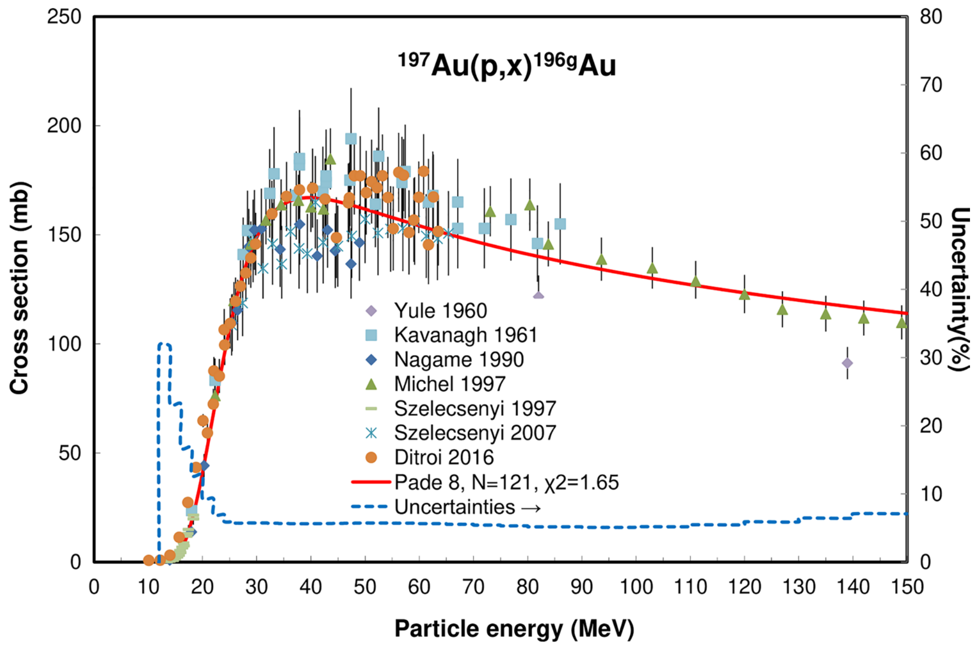

Fig. 41 $^{197}Au(p,x)^{196g}Au$ reaction: selected experimental works and Padé fit (solid line) with total derived uncertainties, including 4% systematic uncertainty (dashed line, right hand scale)

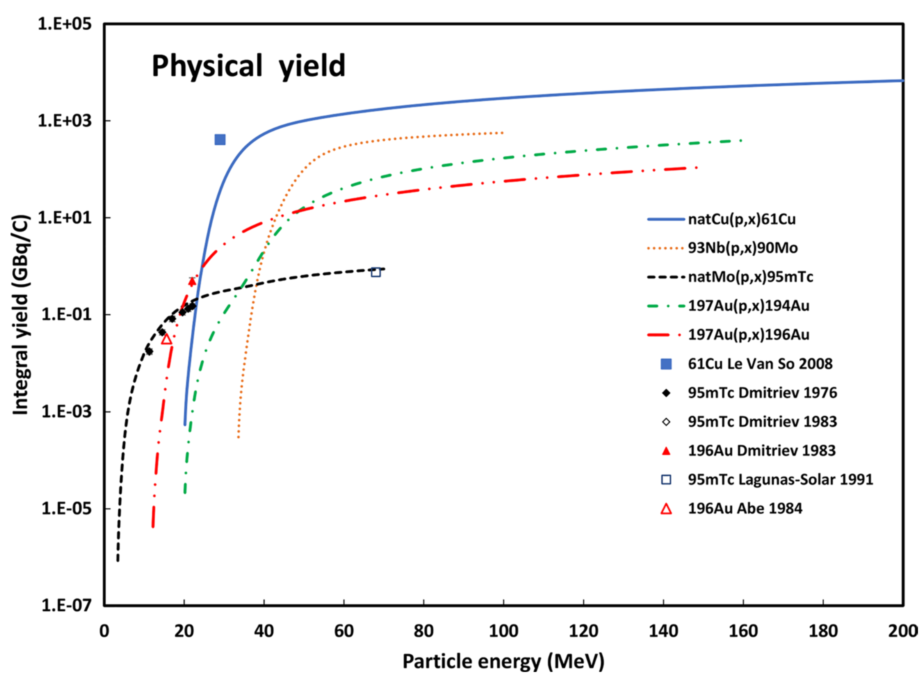

Fig. 42 Yield calculated from the recommended cross sections of the $^{nat}Cu(p,x)^{61}Cu$, $^{93}Nb(p,x)^{90}Mo$, $^{nat}Mo(p,x)^{95m}Tc$, $^{197}Au(p,x)^{194}Au$ and $^{197}Au(p,x)^{196g}Au$ reactions

found, Dmitriev [126], Abe [84] and Birattari (differential yield, not in figure) [205] (Fig. 42).

Evaluated deuteron-induced nuclear reactions

$^{nat}Ti(d,x)^{43}Sc$ reaction

Reactions of the general shape (d,αxn), with x between 1 and 5, on the five stable isotopes of Ti can contribute to direct ^{43}Sc formation (^{46}Ti abundance is 8.25%

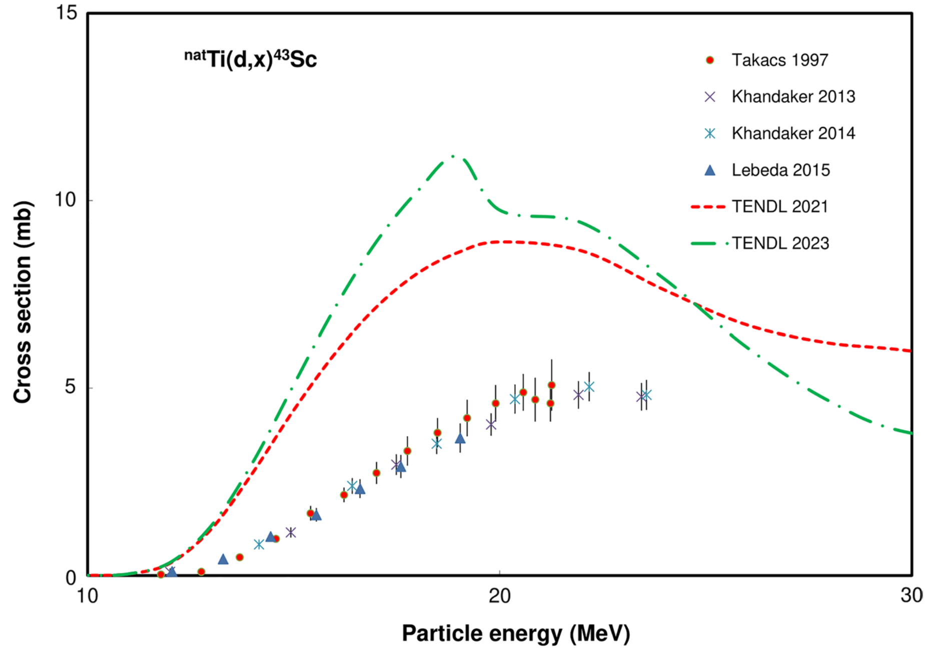

Fig. 43 $^{nat}Ti(d,x)^{43}Sc$ reaction: all experimental data and the TENDL theoretical excitation functions

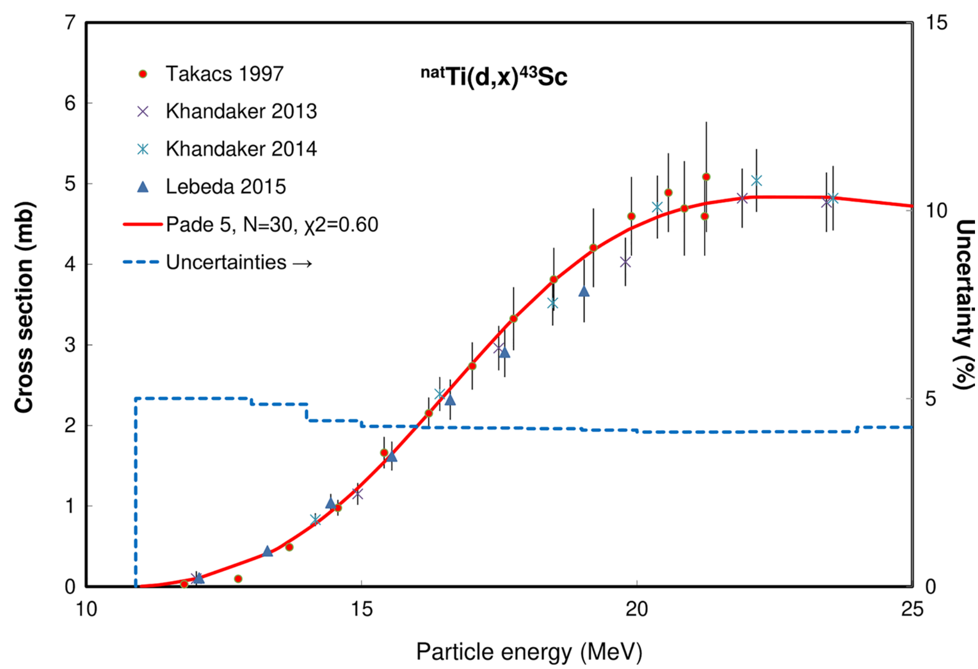

Fig. 44 $^{nat}Ti(d,x)^{43}Sc$ reaction: selected experimental works and Padé fit (solid line) with total derived uncertainties, including 4% systematic uncertainty (dashed line, right hand scale)

in natural Ti; ^{47}Ti abundance is 7.44%, ^{48}Ti abundance is 73.72%, ^{49}Ti abundance is 5.41%, ^{50}Ti abundance is 5.18%). The lowest threshold is for the $^{46}Ti(d,\alpha n)^{43}Sc$ reaction at 5.526 MeV while the $^{47}Ti(d,\alpha^2n)^{43}Sc$ reaction has a 14.772 MeV threshold. If only separate particles are emitted, for instance, the $^{46}Ti(d,2p3n)^{43}Sc$ reaction, the threshold is 35.029 MeV. Formation by partly clustered emission will occur at intermediate energies and the contribution of the interactions with the other isotopes at different energies will result in an excitation function with multiple local maxima. The formation of ^{43}Sc at energies above 43 MeV is always cumulative as it contains the full decay of very short-lived ^{43}Ti ($T_{1/2} = 0.5$ s) produced by (d,pxn) reactions on the different stable Ti isotopes. The threshold for the $^{46}Ti(d,p4n)^{43}Ti$ reaction is 43.011 MeV.

As only 4 cross section data sets, covering the energy range from threshold up to 24 MeV, were found in the literature, only the direct formation by $^{46}Ti(d,\alpha n)^{43}Sc$, with low contribution of the $^{47}Ti(d,\alpha_2n)^{43}Sc$ reaction, is available

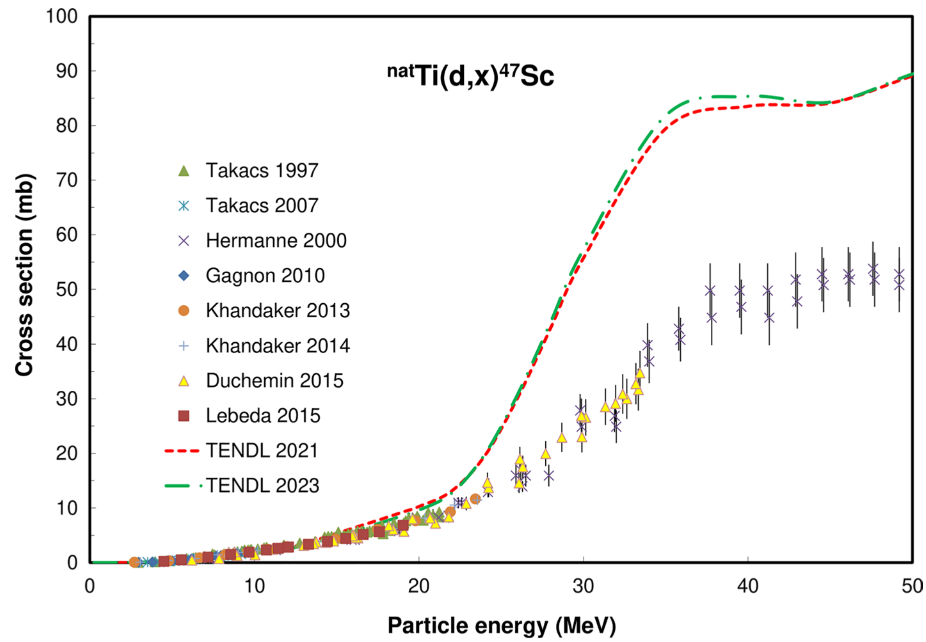

Fig. 45 $^{nat}Ti(d,x)^{47}Sc$ reaction: all experimental data and the TENDL theoretical excitation functions

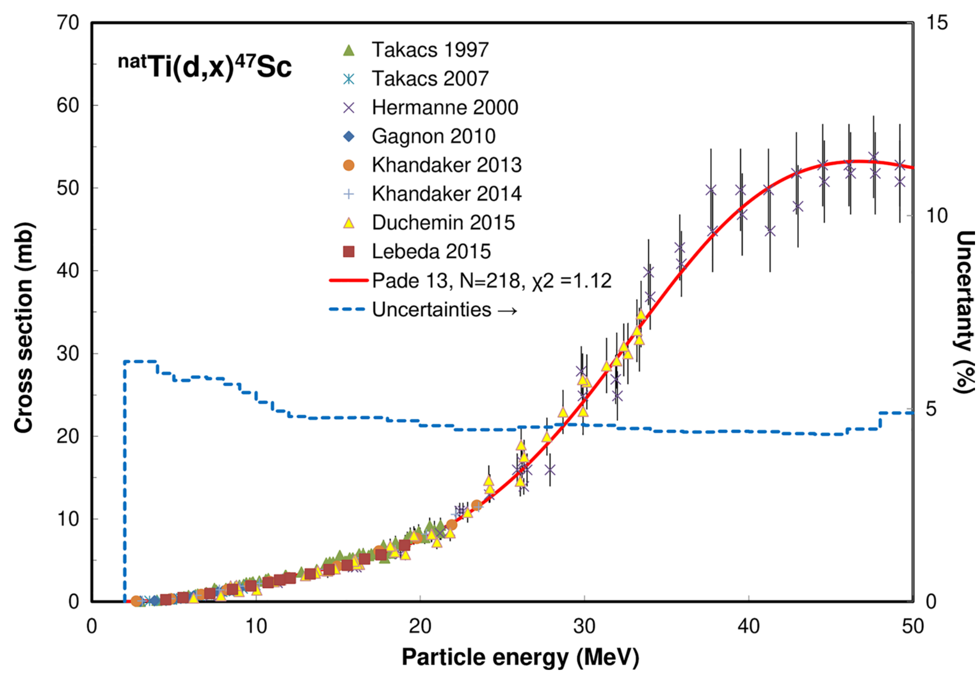

Fig. 46 $^{nat}Ti(d,x)^{47}Sc$ reaction: selected experimental works and Padé fit (solid line) with total derived uncertainties, including 4% systematic uncertainty (dashed line, right hand scale)

as displayed in Fig. 43: Takacs [210], Khandaker [211], Khandaker [212], Lebeda [213].

All sets were selected and fitted up to 25 MeV (Fig. 44). While the TENDL 2021 prediction does not show multiple reaction contributions in the 2023 version a pronounced local maximum of around 19 MeV is seen. The maximum value is nearly double that of the experiments. The integral yields calculated from the recommended cross sections are shown in Fig. 47. As the Khandaker 2013 data are derived from cross section they are not presented in Fig. 47 [211].

$^{nat}Ti(d,x)^{47}Sc$ reaction

Reactions of the general shape (d,2pxn), with x between 0 and 3, on four stable isotopes of Ti can contribute to direct ^{47}Sc formation (^{47}Ti abundance is 7.44%, ^{48}Ti abundance is 73.72%, ^{49}Ti abundance is 5.41%, ^{50}Ti abundance is 5.18%). The threshold for the $^{47}Ti(d,2p)^{47}Sc$ reaction is 5.526 MeV while for the $^{49}Ti(d,\alpha)^{47}Sc$ reaction a positive Q-value of 6.483 MeV is noted and the $^{50}Ti(d,2p3n)$ reaction with emission of not clustered particles would have a

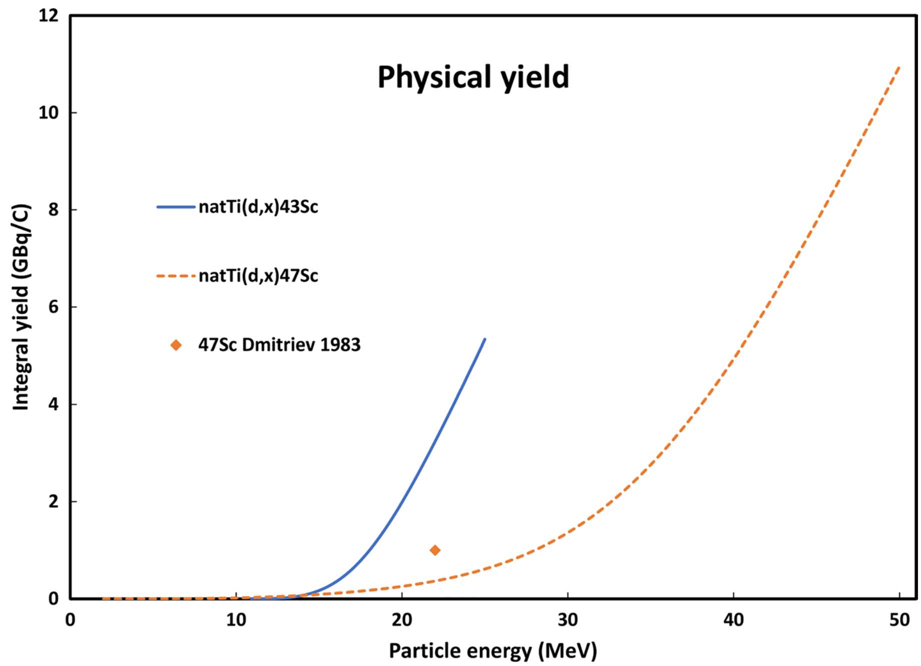

Fig. 47 Yield calculated from the recommended cross sections of the $^{nat}Ti(d,x)^{43}Sc$ and $^{nat}Ti(d,x)^{47}Sc$ reactions

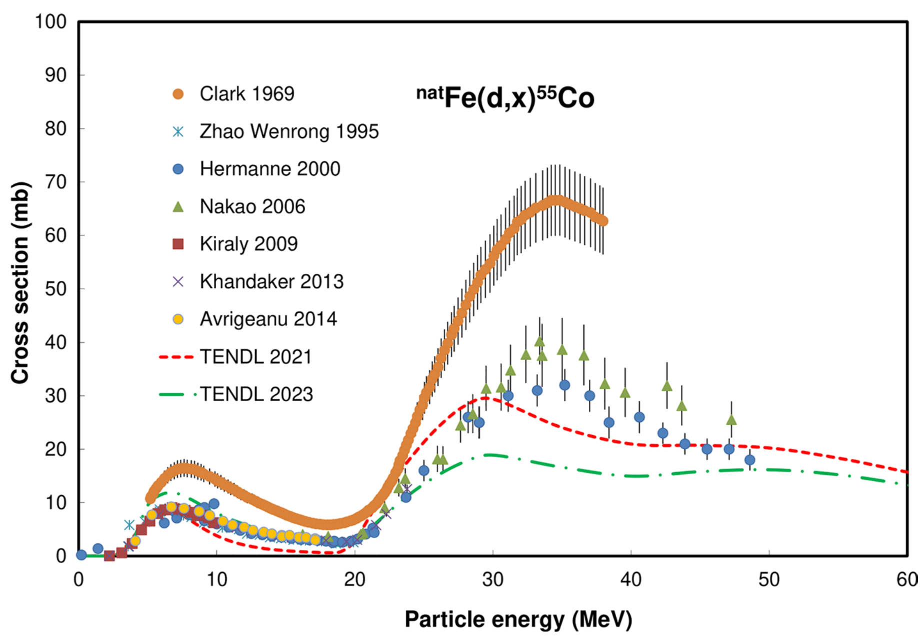

Fig. 48 $^{nat}Fe(d,x)^{55}Co$ reaction: all experimental data and the TENDL theoretical excitation functions

34.033 MeV threshold. Formation by partly clustered emission on the different target isotopes will occur at intermediate energies and should result in an excitation function with multiple local maxima. The parallel formation of parent, somewhat longer-lived, ^{47}Ca ($T_{1/2}$ = 4.536 d, 100% β^- decay) by the $^{50}Ti(d,\alpha p)^{47}Ca$ reaction with 5.887 MeV threshold or $^{49}Ti(d,3pn)$ with 23.942 MeV threshold could influence and disturb the practical use of this reaction for monitoring (Fig. 45).

All original datasets of the 8 publications were selected up to 50 MeV and fitted (Fig. 46): Takacs [210], Takacs [214], Hermanne [215], Gagnon [216], Khandaker [211], Khandaker [212], Duchemin [217], Lebeda [213].

The two TENDL predictions do not show multiple reaction contributions but above 15 MeV a steeper rise than the experimental values, increasing further above 45 MeV, is seen. The integral yields calculated from the recommended cross sections are shown in Fig. 47. A

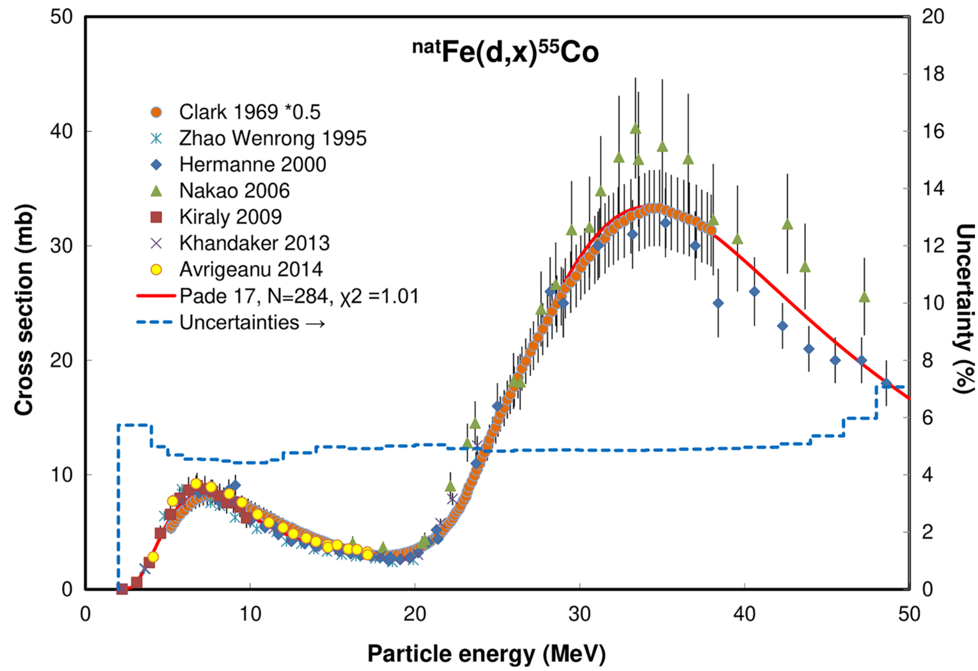

Fig. 49 $^{nat}Fe(d,x)^{55}Co$ reaction: selected experimental works and Padé fit (solid line) with total derived uncertainties, including 4% systematic uncertainty (dashed line, right-hand scale)

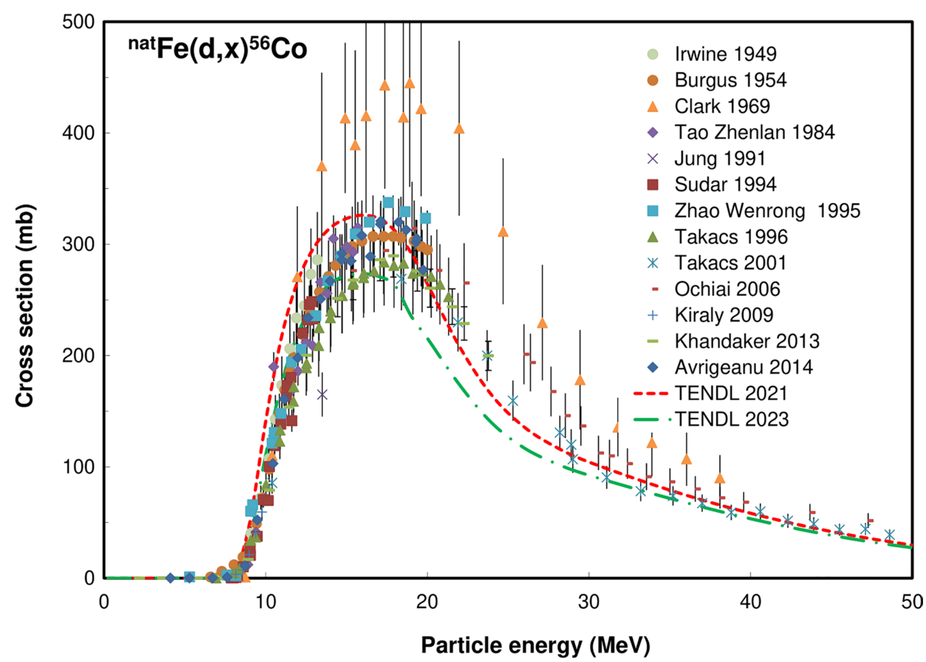

Fig. 50 $^{nat}Fe(d,x)^{56}Co$ reaction: all experimental data and the TENDL theoretical excitation function

single experimental yield data point was found: Dmitriev [218].

$^{nat}Fe(d,x)^{55}Co$ reaction

Four (d,xn) reactions on the stable target isotopes ^{54}Fe (abundance 5.845% in ^{nat}Fe) ^{56}Fe (abundance 91.754% in ^{nat}Fe), ^{57}Fe (2.119%) and ^{58}Fe (0.282%) contribute to the formation of ^{55}Co. At energies below 20 MeV the $^{54}Fe(d,n)^{55}Co$ reaction with a positive Q-value of 2.839 MeV will contribute while, due to the predominance of the ^{56}Fe isotope, the (d,3n) reaction, with the threshold of 18.270 MeV, will in practice be more important.

A total of 7 cross section data sets, covering the energy range from threshold up to 48 MeV, were found in literature and are displayed in Fig. 48: Clark [219], Zhao Wenrong [220], Hermanne [215], Nakao [221], Kiraly [222], Khandaker [211]. Avrigeanu [223]. As the overall shape of the excitation function published in Clark 1969 is acceptable but too high, all data points were multiplied by a factor

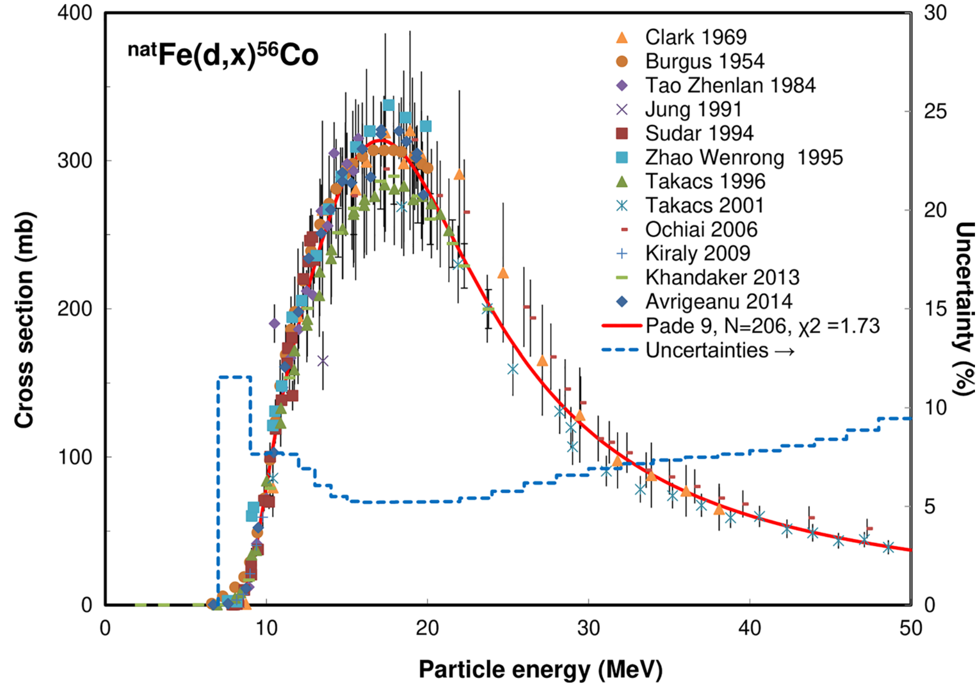

Fig. 51 $^{nat}Fe(d,x)^{56}Co$ reaction: selected experimental works and Padé fit (solid line) with total derived uncertainties, including 4% systematic uncertainty (dashed line, right-hand scale)

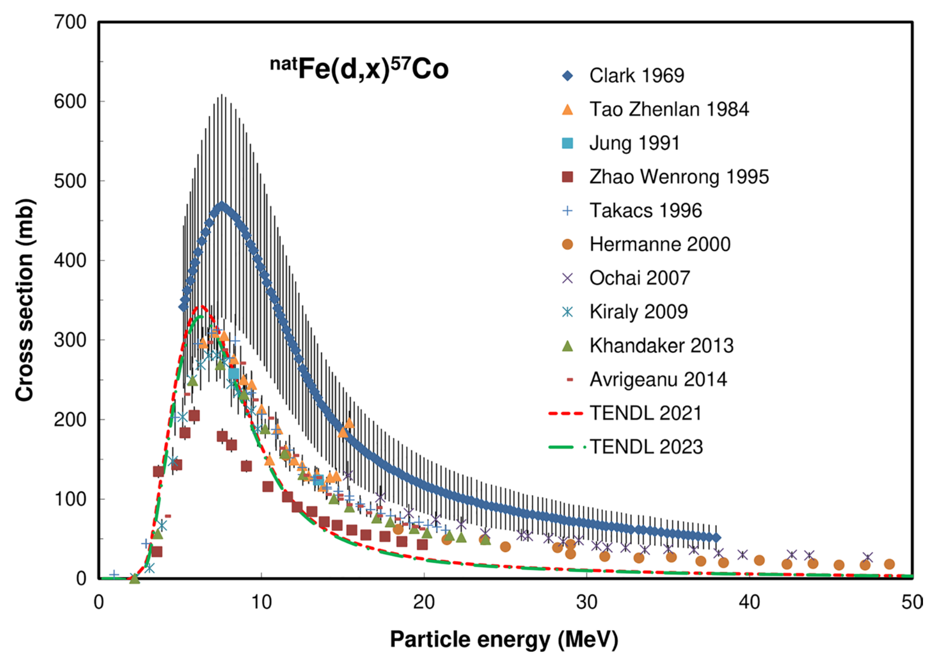

Fig. 52 $^{nat}Fe(d,x)^{57}Co$ reaction: all experimental data and the TENDL theoretical excitation functions

of 0.5 to agree with the two local maxima found in the other publications. In the lower energy domain, the outlying data points of Zhao Wenrong 1995 at 3.669 MeV and Hermanne 2000 (at 0.2, 1.4, 6.2, 7.1, 9.1 and 9.8 MeV) were deleted. The original and corrected datasets of the 7 publications were selected and fitted up to 50 MeV (Fig. 49).

The TENDL predictions represent well the overall shape of the combined reactions' excitation function but are energy-shifted above 20 MeV. The TENDL 2023 version is significantly lower in the 20–50 MeV domain. The integral yields calculated from the recommended cross sections are shown in Fig. 56. A single experimental yield data was found: Dmitriev [218].

$^{nat}Fe(d,x)^{56}Co$ reaction

Three (d,xn) reactions on the stable target isotopes ^{56}Fe(abundance 91.754% in ^{nat}Fe), ^{57}Fe (2.119%) and ^{58}Fe (0.282%) contribute to the formation of ^{55}Co. Due to the prominence of the ^{56}Fe isotope the $^{56}Fe(d,2n)^{56}Co$ reaction, with the threshold of 7.837 MeV, will be dominant.

A total of 13 cross section data sets, covering the energy range from threshold up to 50 MeV, were found in literature and are displayed in Fig. 50: Irwine [224], Burgus [225], Clark [219], Tao Zhenlan [226], Jung [227], Sudar [120], Zhao Wenrong [220], Takacs [228], Takacs [229], Ochiai [230], Kiraly [222], Khandaker [231], Zavorka [232], Avrigeanu [223]. As the Zavorka 2011 data (reported in a conference) are identical to the data of Avregianu 2014, only this last set is represented. The data of Irwine 1949 are outlying above 10 MeV and were deselected. The too high values of Clark 1969 data were normalized by a factor of 0.72 to bring them in agreement with the average value of the other publications near the maximum around 18 MeV. The original and corrected datasets of the 12 publications were selected up to 50 MeV and fitted (Fig. 51).

The TENDL predictions are well representing the shape of the experimental excitation function, with 10% lower maximum in the 2023 version, but are slightly

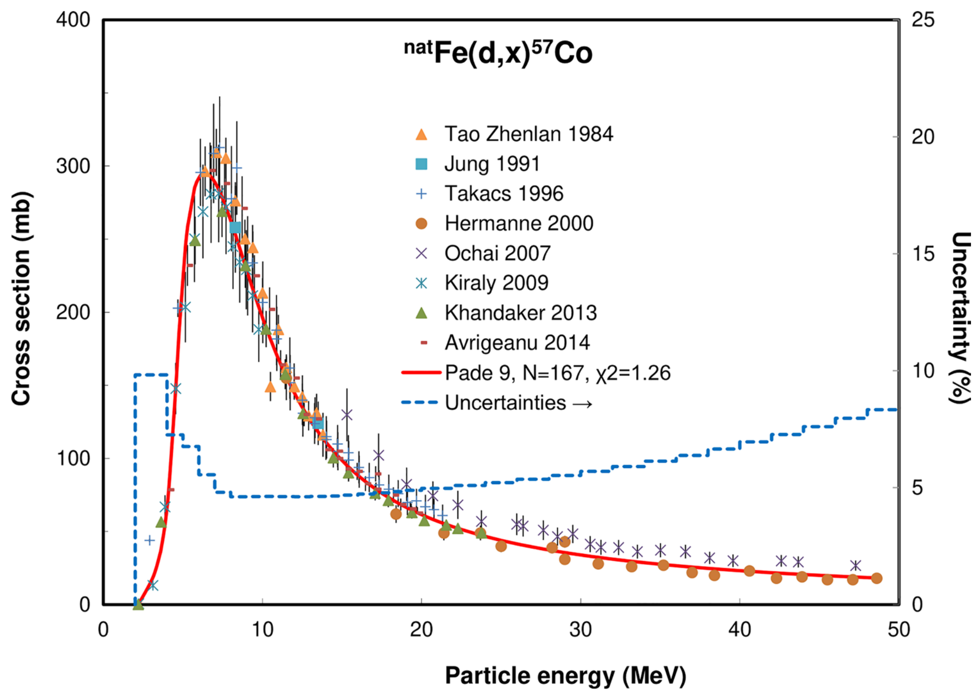

Fig. 53 $^{nat}Fe(d,x)^{57}Co$ reaction: selected experimental works and Padé fit (solid line) with total derived uncertainties, including 4% systematic uncertainty (dashed line, right-hand scale)

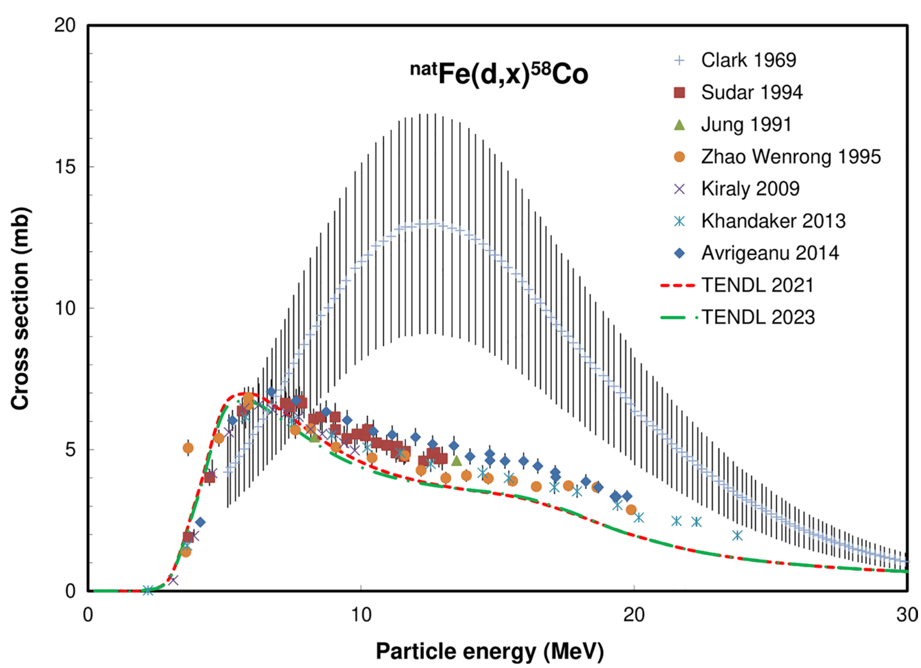

Fig. 54 $^{nat}Fe(d,x)^{58}Co$ reaction: all experimental data and the TENDL theoretical excitation functions

energy-shifted. The integral yields calculated from the recommended cross sections are shown in Fig. 56. A single experimental yield data point was found: Dmitriev [218] (Fig. 52).

$^{nat}Fe(d,x)^{57}Co$ reaction

Three (d,xn) reactions on the stable target isotopes ^{56}Fe (abundance 91.754% in ^{nat}Fe), ^{57}Fe (2.119%) and ^{58}Fe (0.282%) contribute to the formation of ^{55}Co. Due to the prominence of the ^{56}Fe isotope the $^{56}Fe(d,n)^{57}Co$ reaction, with a positive Q-value of 3.802 MeV, will be dominant.

A total of 10 cross section data sets, covering the energy range from threshold up to 49 MeV, were found in literature and are displayed in Fig. 52: Clark [219], Tao Zhenlan [226], Jung [227], Zhao Wenrong [220], Takacs [228], Hermanne [215], Ochai [230], Kiraly [222], Khandaker [231], Avrigeanu [223]. The too high and energy-shifted set of

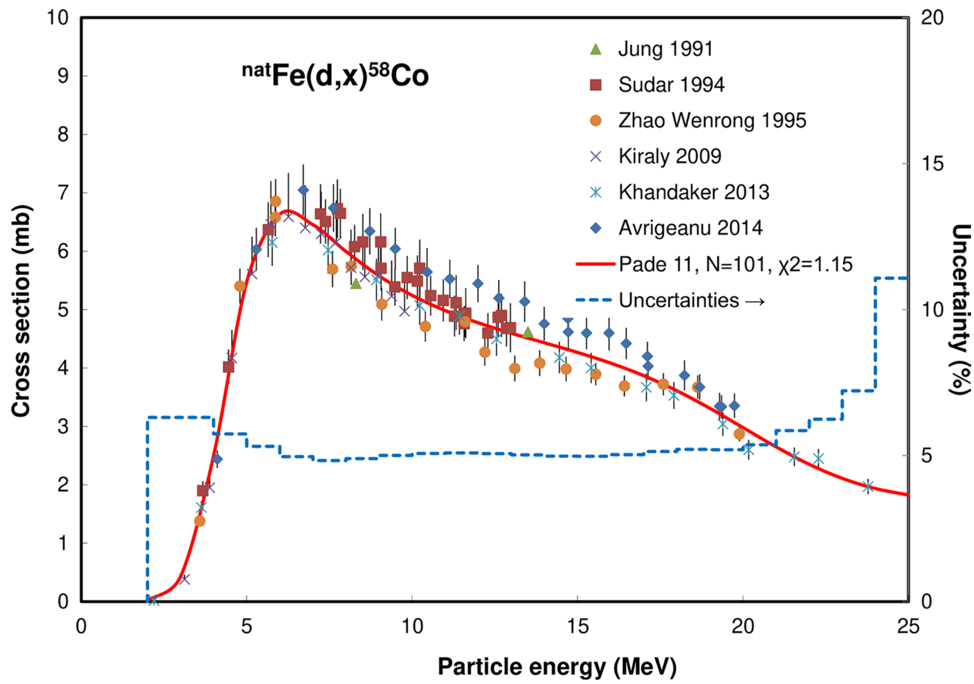

Fig. 55 $^{nat}Fe(d,x)^{58}Co$ reaction: selected experimental works and Padé fit (solid line) with total derived uncertainties, including 4% systematic uncertainty (dashed line, right-hand scale)

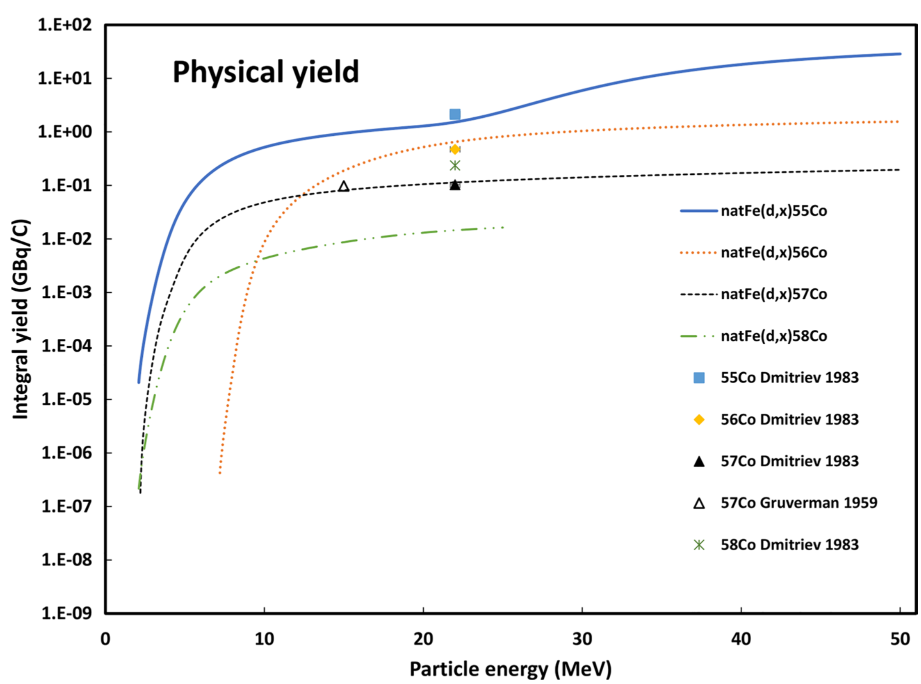

Fig. 56 Yield calculated from the recommended cross sections of the $^{nat}Fe(d,x)^{55}Co$, $^{nat}Fe(d,x)^{56}Co$, $^{nat}Fe(d,x)^{57}Co$ and $^{nat}Fe(d,x)^{58}Co$ reactions

Clark 1969 was deselected. The outlying sets of Zhao Wenrong 1995 and Ochai 2007 were normalized, respectively by a factor of 1.45 and by a factor of 0.8, to bring them in agreement with an average value of the other publications near a maximum of 300 mb around 7 MeV. Four wrongly rising points of Tao Zhenlan 1995 above 14 MeV were deleted. The too low dataset of Zhao Wenrong is deselected.

The original and corrected datasets of 8 publications were selected up to 49 MeV and fitted (Fig. 53).

The two TENDL predictions are well representing the shape of the experimental excitation function but are slightly energy-shifted and a 10% overestimation of the maximum cross section is seen. The integral yields calculated from the recommended cross sections are shown in Fig. 56.

Two experimental yield data was found: Dmitriev [218] and Gruverman [173].

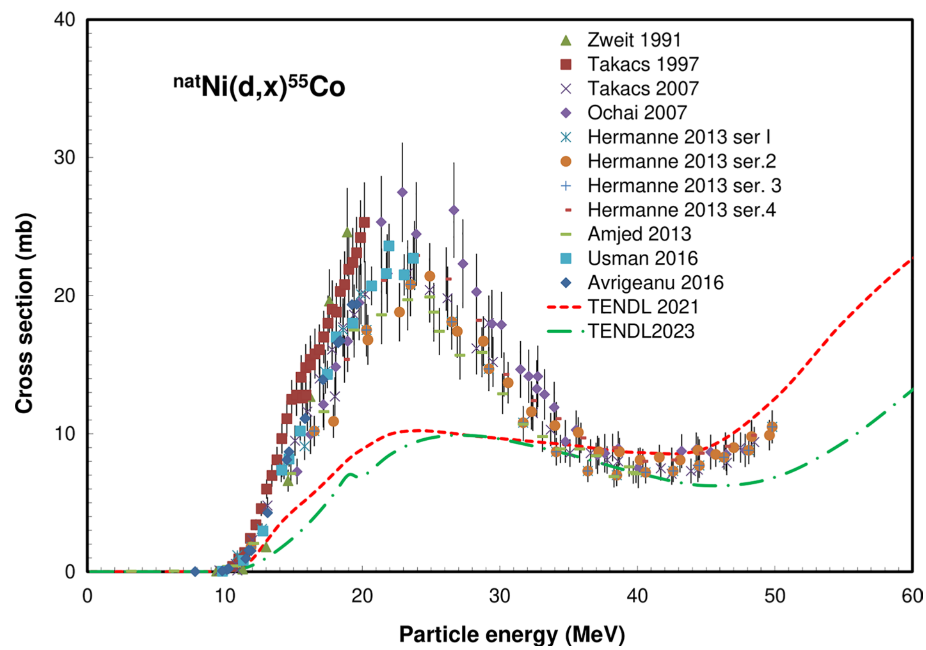

Fig. 57 $^{nat}Ni(d,x)^{55}Co$ reaction: all experimental data and the TENDL theoretical excitation functions

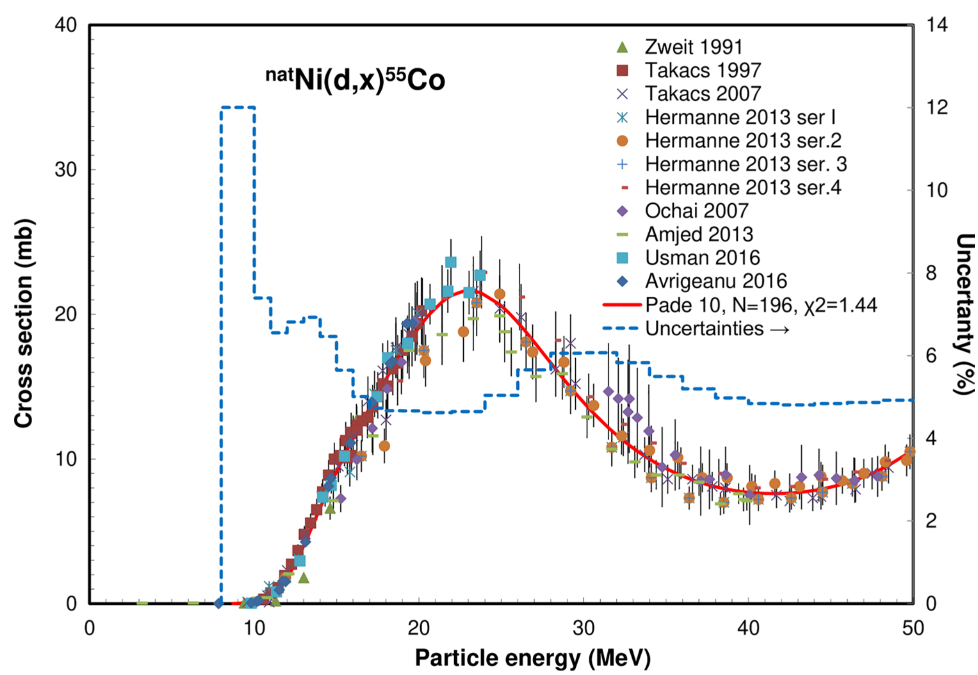

Fig. 58 $^{nat}Ni(d,x)^{55}Co$ reaction: selected experimental works and Padé fit (solid line) with total derived uncertainties, including 4% systematic uncertainty (dashed line, right-hand scale)

Fig. 59 $^{nat}Ni(d,x)^{56}Ni$ reaction: all experimental data and the TENDL theoretical excitation functions

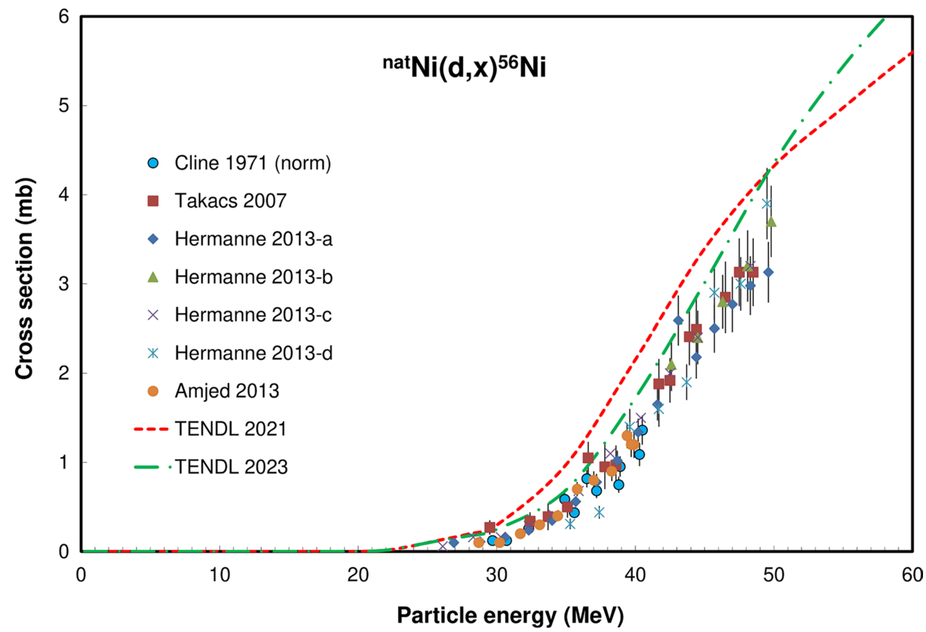

$^{nat}Fe(d,x)^{58}Co$ reaction

Only two (d,xn) reactions on the low abundance stable target isotopes, ^{57}Fe (2.119% abundance in ^{nat}Fe) and ^{58}Fe (0.282%), contribute to the formation of ^{58}Co. Due to the prominence of the ^{57}Fe isotope the $^{57}Fe(d,n)^{58}Co$ reaction, with a positive Q-value of 4.729 MeV, will be dominant.

A total of 7 cross section data sets, covering the energy range from threshold up to 30 MeV, were found in literature and are displayed in Fig. 54: Clark [219], Jung [227], Sudar [120], Zhao Wenrong [220], Kiraly [222], Khandaker [231], Avrigeanu [223].

The too high and energy-shifted set of Clark 1969 was deselected. The outlying point of Zhao Wenrong 1995 at 3.67 MeV was deleted. The original and corrected datasets of 6 publications were selected and fitted up to 25 MeV (Fig. 55).

The two TENDL predictions represent the shape of the experimental excitation function but are slightly energy-shifted. The integral yields calculated from the recommended cross sections are shown in Fig. 56. A single experimental yield data was found: Dmitriev [218].

$^{nat}Ni(d,x)^{55}Co$ reaction

In principle five (d,2pxn) reactions on the stable target isotopes ^{58}Ni (abundance 68.077% in ^{nat}Ni, x = 3), ^{60}Ni (abundance 26.223% in ^{nat}Ni, n = 5), ^{61}Ni (abundance 1.1399% in ^{nat}Ni), ^{62}Ni (abundance 3.6349% in ^{nat}Ni), ^{64}Ni (abundance 0.9255% in ^{nat}Ni) can contribute to formation of ^{55}Co if high energy deuteron bombardment is performed.

The threshold for the $^{58}Ni(d,2p3n)^{55}Co$ reaction with the emission of 5 separate particles is 32.924 MeV but by clustering the $^{58}Ni(d,\alpha n)^{55}Co$ reaction is favored with 3.678 MeV threshold. The same observation is valid for the reactions on other Ni isotopes.

A total of 11 cross section data sets, covering the energy range from threshold up to 50 MeV, were found in literature and are displayed in Fig. 57: Zweit [233], Takacs [234], Takacs [235], Ochiai [230], Hermanne ser.I-4[236], Amjed [237], Usman [238], Avrigeanu [239]. The data of Takacs 1997 are too high in the rising part of the excitation function and were multiplied by a factor of 0.8 before selection. Additionally, too high outlying points of Zweit 1991 at 17.6 and 18.9 MeV and the series of Ochai 2007 between 21 and 30 MeV were deleted. The original and corrected datasets of the 11 publications were selected up to 50 MeV and fitted (Fig. 58).

The two TENDL predictions strongly underestimate the maximal value observed around 24 MeV but represent well the rising excitation function above 42 MeV. The integral yields calculated from the recommended cross sections are shown in Fig. 69. Two experimental yield data were found: Zweit [233] Amjed [237].

$^{nat}Ni(d,x)^{56}Ni$ reaction

In principle five (d,pxn) reactions on the stable target isotopes isotopes ^{58}Ni (abundance 68.077% in ^{nat}Ni, x = 3), ^{60}Ni (abundance 26.223% in ^{nat}Ni, n = 5), ^{61}Ni (abundance 1.1399% in ^{nat}Ni), ^{62}Ni (abundance 3.6349% in ^{nat}Ni), ^{64}Ni

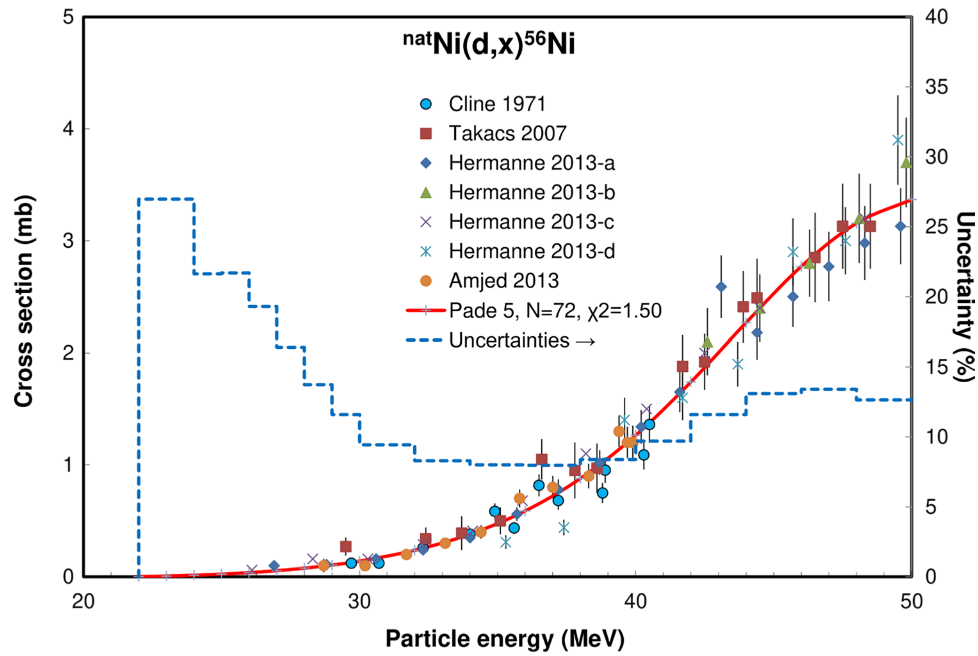

Fig. 60 $^{nat}Ni(d,x)^{56}Ni$ reaction: selected experimental works and Padé fit (solid line) with total derived uncertainties, including 4% systematic uncertainty (dashed line, right-hand scale)

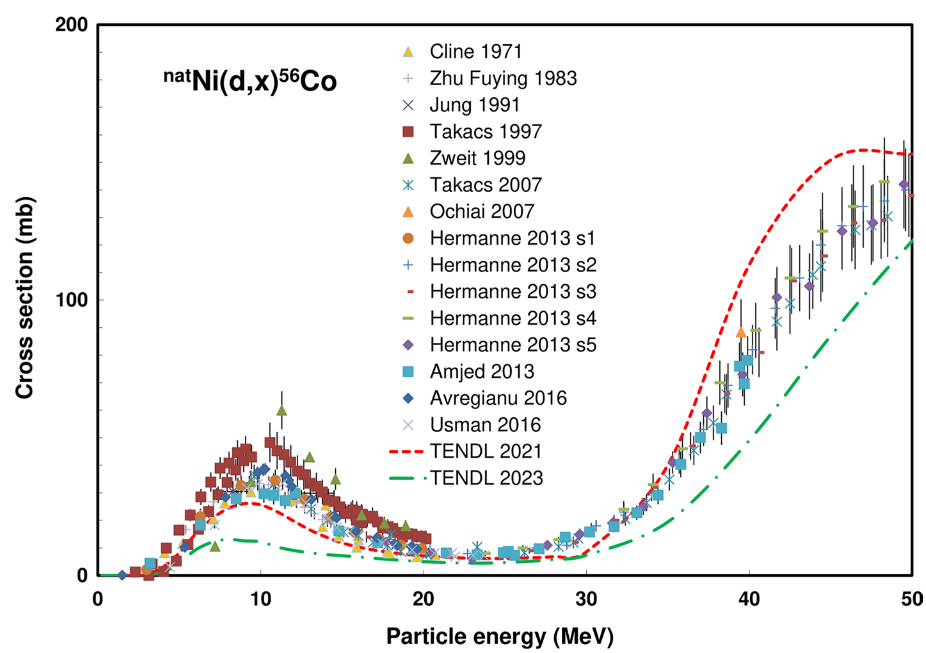

Fig. 61 $^{nat}Ni(d,x)^{56}Co$ reaction: all experimental data and the TENDL theoretical excitation functions

(abundance 0.9255% in ^{nat}Ni) can contribute to formation of ^{56}Ni if high energy deuteron bombardment is performed.

The threshold for the $^{58}Ni(d,p3n)^{56}Ni$ reaction with emission of 4 separate particles is 25.517 MeV while clustering allows the $^{58}Ni(d,^{3}Hn)^{56}Ni$ reaction with 16.750 MeV threshold. The same observation is valid for the reactions on other Ni isotopes.

A total of 7 cross section data sets, covering the energy range from threshold up to 50 MeV, were found in the literature and are displayed in Fig. 59: Cline 1971 (^{58}Ni norm) [240], Zhu Fuying [241], Takacs [235], Hermanne [236], Amjed [237].

The data of Cline 1971 are given for the $^{58}Ni(d,x)^{56}Ni$ reaction and were normalized for the ^{58}Ni abundance in ^{nat}Ni.

All 7 datasets were selected up to 50 MeV and fitted (Fig. 60). The TENDL predictions are overestimating, with observable differences between the two versions the excitation function over the entire energy domain. The integral

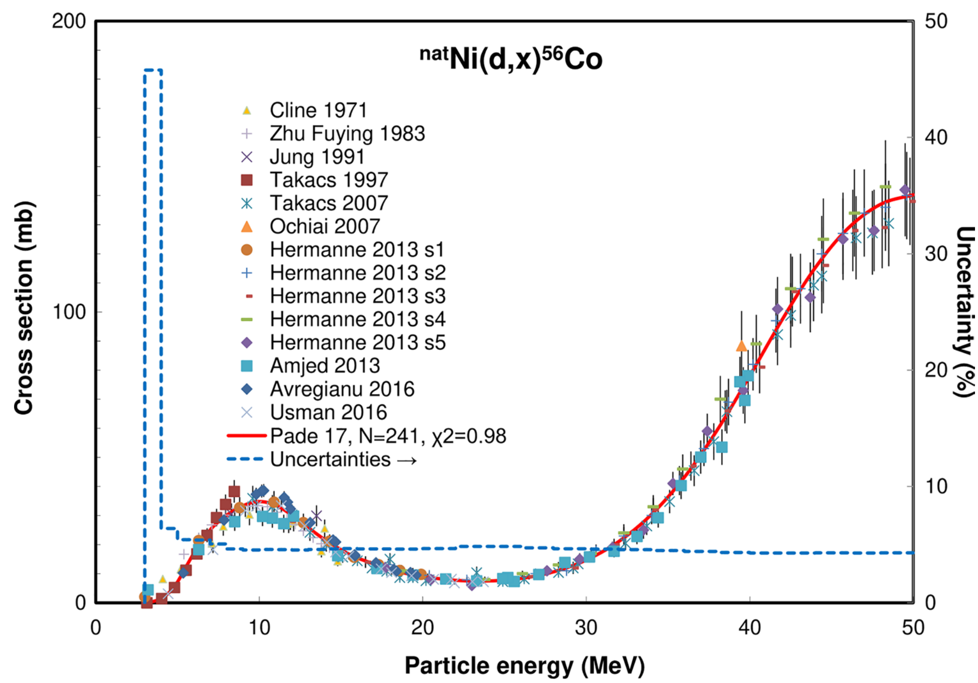

Fig. 62 $^{nat}Ni(d,x)^{56}Co$ reaction: selected experimental works and Padé fit (solid line) with total derived uncertainties, including 4% systematic uncertainty (dashed line, right-hand scale)

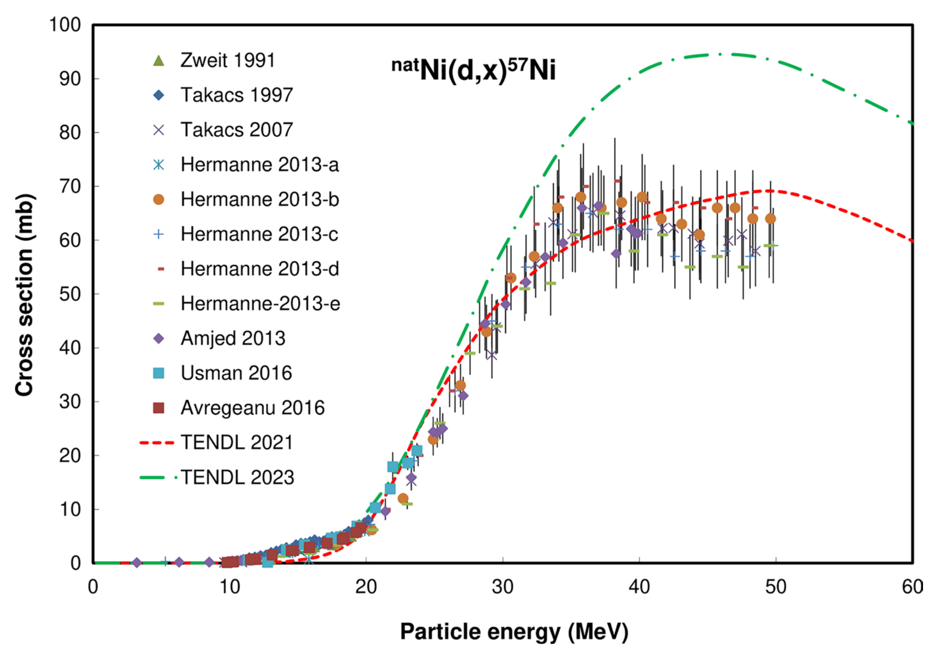

Fig. 63 $^{nat}Ni(d,x)^{57}Ni$ reaction: all experimental data and the TENDL theoretical excitation functions

yields calculated from the recommended cross sections are shown in Fig. 69. No experimental yield data are available.

^{nat}Ni(d,x)^{56}Co reaction

In principle five (d,2pxn) reactions on the stable target isotopes ^{58}Ni (abundance 68.077% in ^{nat}Ni, x = 3), ^{60}Ni (abundance 26.223% in ^{nat}Ni, n = 5), ^{61}Ni (abundance 1.1399% in ^{nat}Ni), ^{62}Ni (abundance 3.6349% in ^{nat}Ni), ^{64}Ni (abundance 0.9255% in ^{nat}Ni) can contribute to formation of ^{56}Co if high energy deuteron bombardment is performed.

The threshold for the ^{58}Ni(d,2p2n)^{56}Co reaction with the emission of 4 separate particles is 22.504 MeV but by clustering the ^{58}Ni(d,α)^{56}Co reaction is favored with a positive Q value of 6.522 MeV. The same observation is valid for the reactions on other Ni isotopes and hence a double-peaked excitation function, starting at low energies, can be expected. Taking into account that the threshold for the

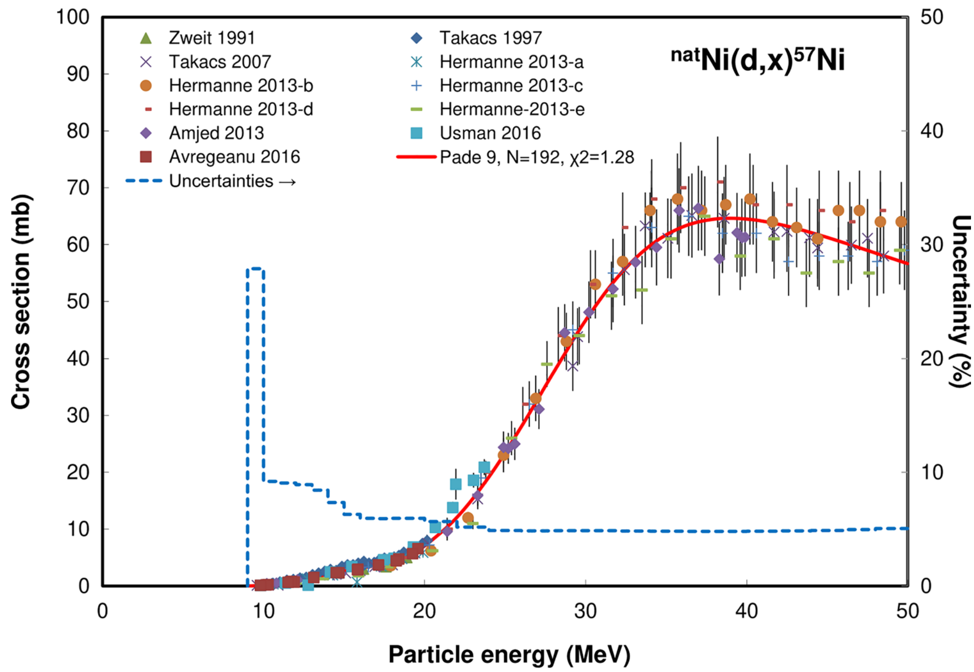

Fig. 64 natNi(d,x)57Ni reaction: selected experimental works and Padé fit (solid line) with total derived uncertainties, including 4% systematic uncertainty (dashed line, right-hand scale)

^{80}Ni(d,α2n)^{56}Co reaction is 14 MeV, the data sets of the publications reporting cross sections for the ^{58}Ni(d,α) reaction, using ^{58}Ni or ^{nat}Ni targets, were considered only up to 14 MeV.

A total of 14 cross section data sets, covering the energy range from threshold up to 50 MeV, were found in literature and are displayed in Fig. 61: Cline [240], Zhu Fuying [241], Jung [227], Takacs [234], Zweit [233], Takacs [235], Ochiai [230], Hermanne [236], Amjed [237], Avrigeanu [239].

All datasets were selected up to 50 MeV and fitted (Fig. 62). The TENDL predictions represent well the shape of the double peaked excitation function, but values differ significantly between the two versions. The integral yields calculated from the recommended cross sections are shown in Fig. 69. Two experimental yield data points are available: Dmitriev [218] and Amjed [237].

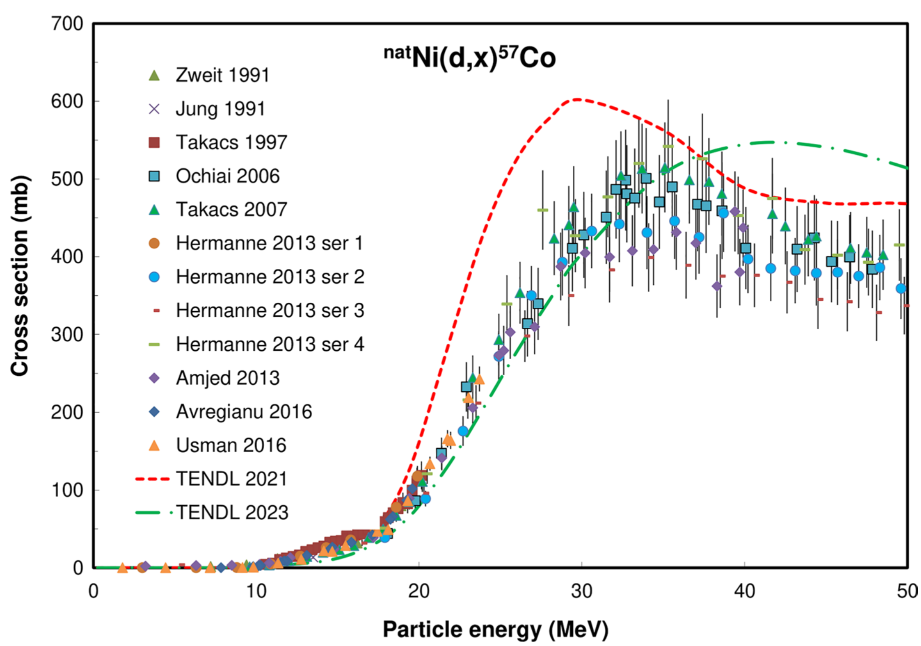

Fig. 65 natNi(d,x)57Co reaction: all experimental data and the TENDL theoretical excitation functions

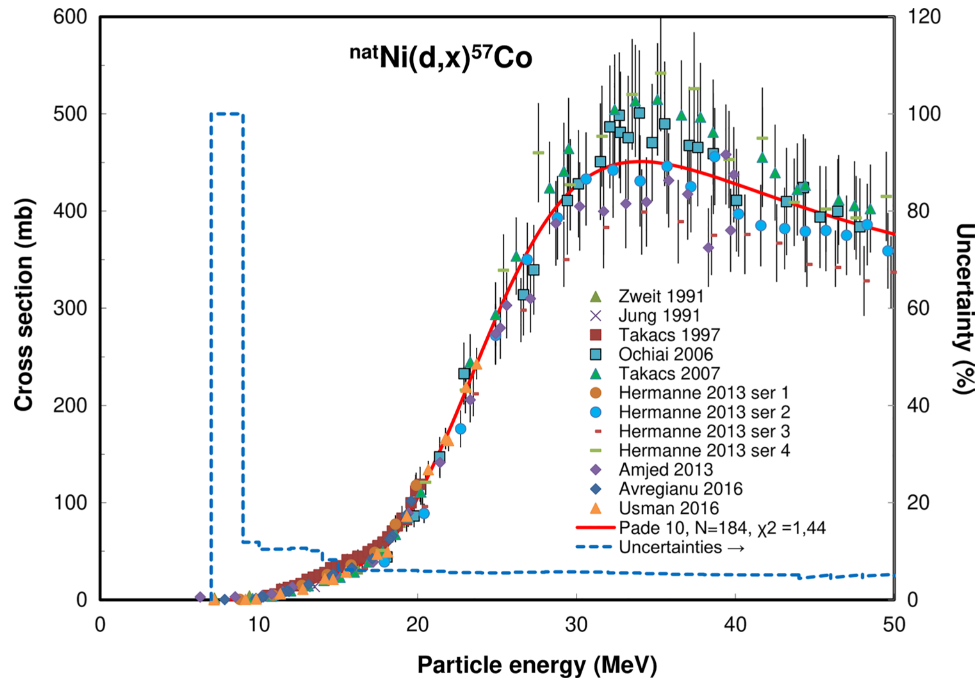

Fig. 66 $^{nat}Ni(d,x)^{57}Co$ reaction: selected experimental works and Padé fit (solid line) with total derived uncertainties, including 4% systematic uncertainty (dashed line, right-hand scale)

$^{nat}Ni(d,x)^{57}Ni$ reaction

In principle five (d,pxn) reactions on the stable target isotopes ^{58}Ni (abundance 68.077% in ^{nat}Ni, x = 3), ^{60}Ni (abundance 26.223% in ^{nat}Ni, n = 5), ^{61}Ni (abundance 1.1399% in ^{nat}Ni), ^{62}Ni (abundance 3.6349% in ^{nat}Ni), ^{64}Ni (abundance 0.9255% in ^{nat}Ni) can contribute to formation of ^{57}Ni if high energy deuteron bombardment is performed.

The threshold for the $^{58}Ni(d,p2n)^{57}Ni$ reaction with the emission of 3 separate particles is 14.925 MeV while clustering allows the $^{58}Ni(d,t)^{57}Ni$ reaction with a 6.159 MeV threshold. The same observation is valid for the reactions on other Ni isotopes.

A total of 11 cross section data sets, covering the energy range from threshold up to 50 MeV, were found in literature and are displayed in Fig. 63: Zweit [233], Takacs [234], Takacs [235], Hermanne [236], Amjed [237], Usman [238],

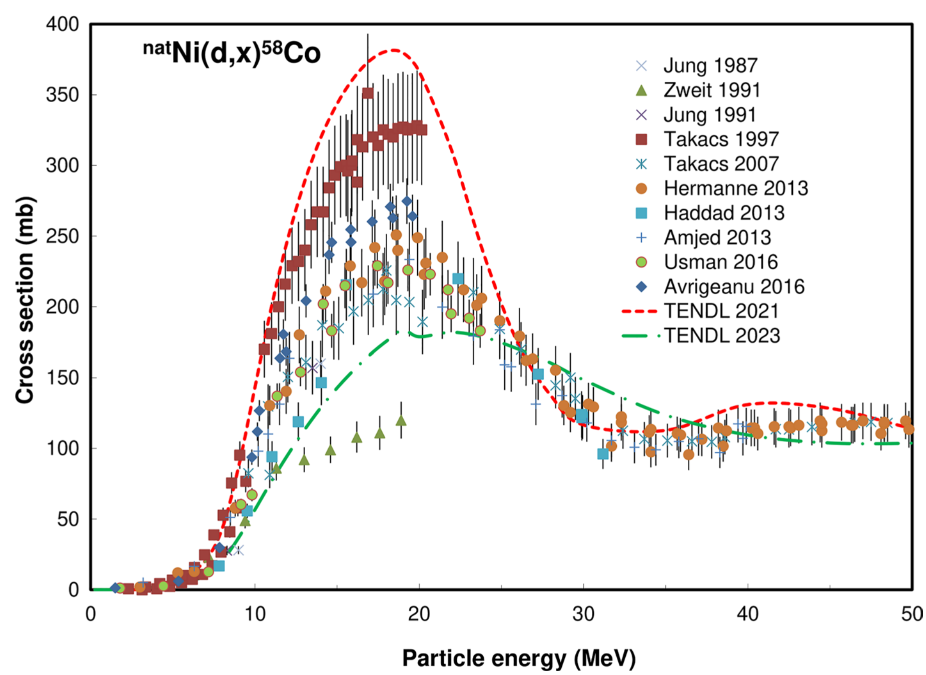

Fig. 67 $^{nat}Ni(d,x)^{58}Co$ reaction: all experimental data and the TENDL theoretical excitation functions

Avrigeanu [239]. Some outlying data points were deleted: Zweit 1991 at 13 MeV, Amjed 2013 (at 3.7 MeV, 6.3 MeV and 8.5 MeV), Hermanne 2013 (at 5.3 MeV, 15.8 and 15.9 MeV).

The original and corrected 11 published datasets were selected up to 50 MeV and fitted (Fig. 64).

While the TENDL 2021 prediction is low near the threshold, it is in good agreement with the experimental excitation function up to 40 MeV. The TENDL 2023 version better predicts the low energy part but significantly overestimates the experimental data from 25 MeV. The integral yields calculated from the recommended cross sections are shown in Fig. 69. Two experimental yield data points are available: Dmitriev [218] and Amjed [237].

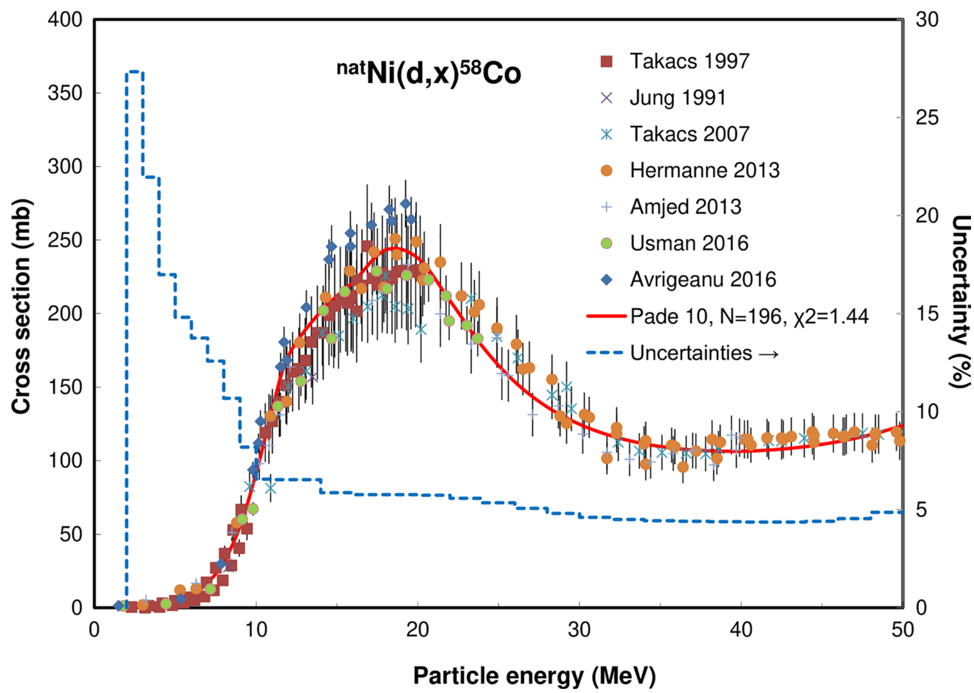

Fig. 68 $^{nat}Ni(d,x)^{58}Co$ reaction: selected experimental works and Padé fit (solid line) with total derived uncertainties, including 4% systematic uncertainty (dashed line, right-hand scale)

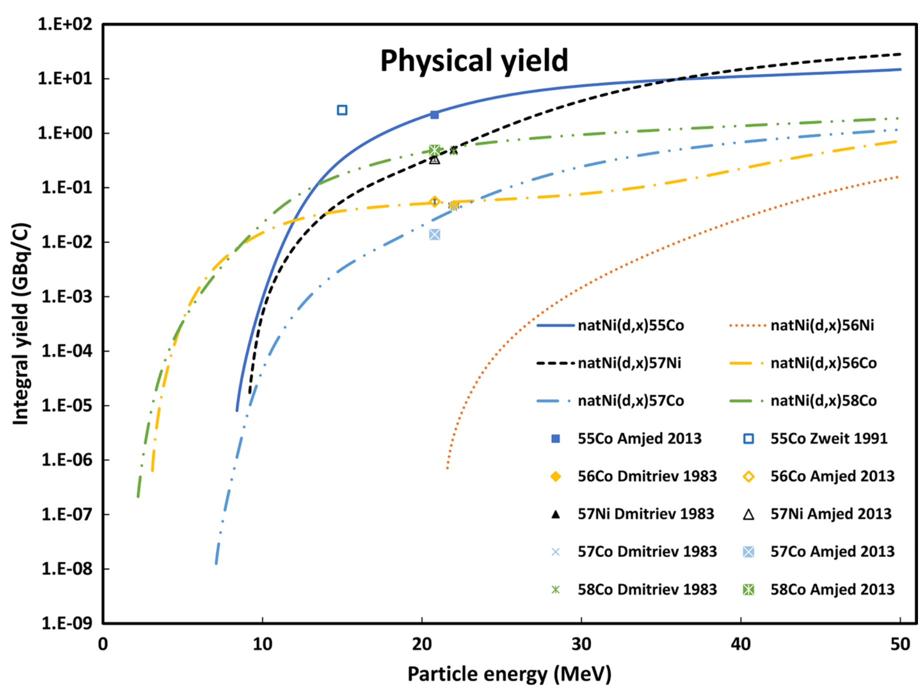

Fig. 69 Yield calculated from the recommended cross sections of the $^{nat}Ni(d,x)^{55}Co$ $^{nat}Ni(d,x)^{56}Ni$, $^{nat}Ni(d,x)^{56}Co$, $^{nat}Ni(d,x)^{57}Ni$, $^{nat}Ni(d,x)^{57}Co$ and $^{nat}Ni(d,x)^{58}Co$ reactions

$^{nat}Ni(d,x)^{57}Co$ reaction

In principle five (d,2pxn) reactions on the stable target isotopes ^{58}Ni (abundance 68.077% in ^{nat}Ni, x = 3), ^{60}Ni (abundance 26.223% in ^{nat}Ni, n = 5), ^{61}Ni (abundance 1.1399% in ^{nat}Ni), ^{62}Ni (abundance 3.6349% in ^{nat}Ni), ^{64}Ni (abundance 0.9255% in ^{nat}Ni) can contribute to formation of ^{55}Co if high energy deuteron bombardment is performed.

The threshold for the $^{58}Ni(d,2pn)^{57}Co$ reaction with the emission of 3 separate particles is 10.745 MeV but by clustering the $^{58}Ni(d,dp)^{57}Co$ reaction is possible with 8.446 MeV threshold. The same observation is valid for the reactions on other Ni isotopes.

A total of 12 cross section data sets, covering the energy range from threshold up to 50 MeV, were found in literature and are displayed in Fig. 65: Zweit [233], Jung [227], Takacs [234], Ochiai [230], Takacs [235], Hermanne [236], Amjed [237], Usman [238], Avrigeanu [239]. All data from the 9 publications were selected up to 50 MeV and fitted (Fig. 66).

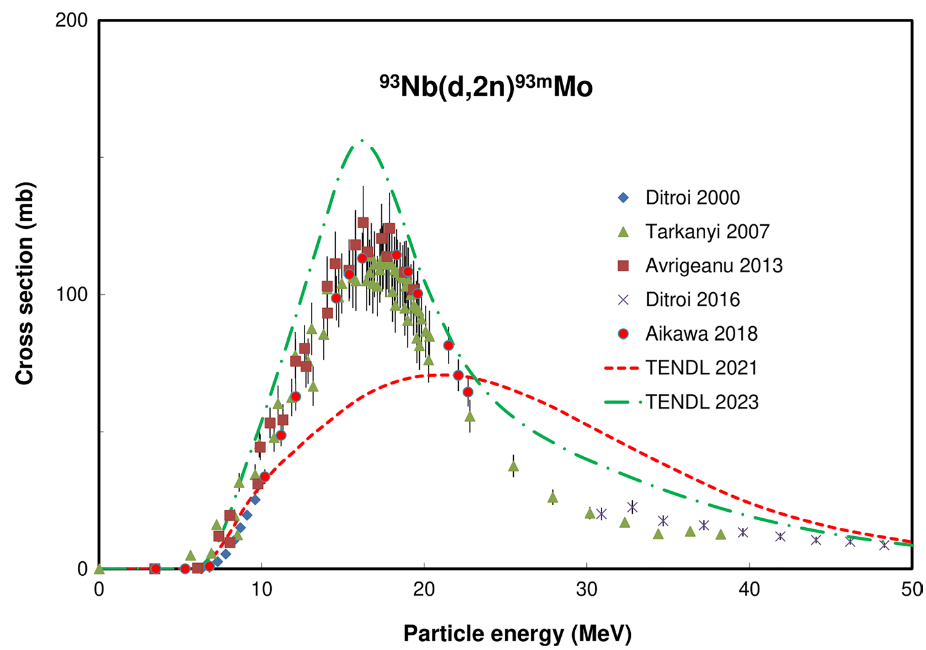

Fig. 70 $^{93}Nb(d,x)^{93m}Mo$ reaction: all experimental data and the TENDL theoretical excitation functions

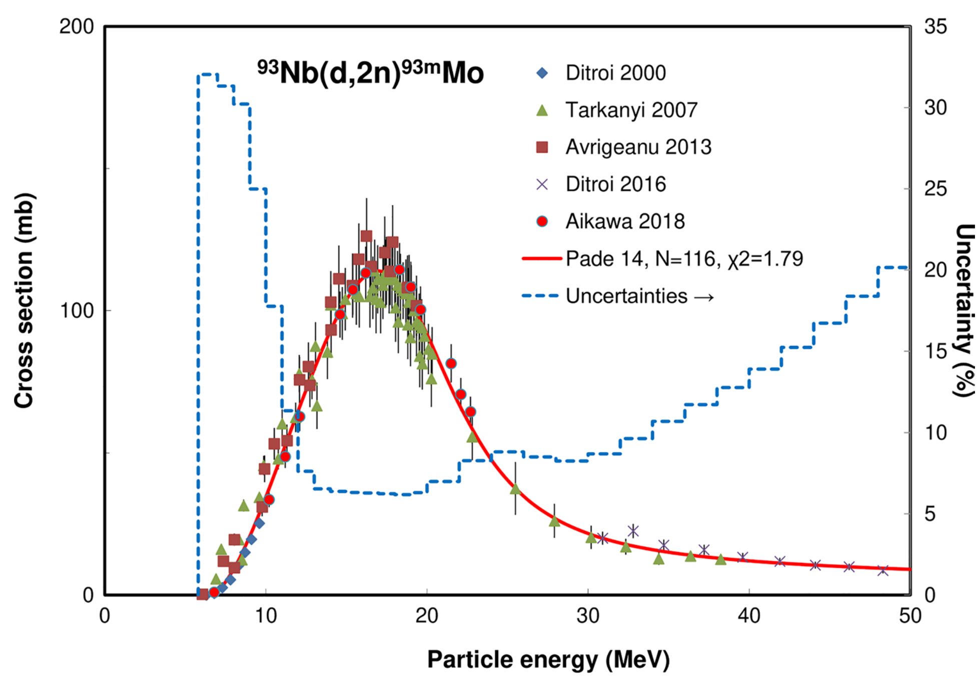

Fig. 71 $^{93}Nb(d,x)^{93m}Mo$ reaction: selected experimental works and Padé fit (solid line) with total derived uncertainties, including 4% systematic uncertainty (dashed line, right-hand scale)

The TENDL 2021 predictions are shifted above 18 MeV and are overestimating the maximal value by 15%. Good agreement can be found up to 30 MeV for the TENDL 2023, but the prediction does not follow the expected decreasing behavior as shown in the experimental data. The integral yields calculated from the recommended cross sections are shown in Fig. 69. Two experimental yield data points are available: Dmitriev [218] and Amjed [237].

$^{nat}Ni(d,x)^{58}Co$ reaction

In principle five (d,2pxn) reactions on the stable target isotopes ^{58}Ni (abundance 68.077% in ^{nat}Ni, x = 3), ^{60}Ni (abundance 26.223% in ^{nat}Ni, n = 5), ^{61}Ni (abundance 1.1399% in ^{nat}Ni), ^{62}Ni (abundance 3.6349% in ^{nat}Ni), ^{64}Ni (abundance 0.9255% in ^{nat}Ni) can contribute to the formation of ^{58}Co if high energy deuteron bombardment is performed.

The threshold for the $^{58}Ni(d,2p)^{58}Co$ reaction is 1.885 MeV but by clustering the $^{60}Ni(d,\alpha)^{58}Co$ reaction is possible with a positive Q-value of 6.084 MeV. The same observation is valid for the reactions on other Ni isotopes.

A total of 8 cross section data sets, covering the energy range from threshold up to 50 MeV, were found in literature and are displayed in Fig. 67: Jung [227], Zweit [233], Jung [118], Takacs [234], Takacs [235], Hermanne [236], Amjed [237], Usman [238], Avrigeanu [239].

As Jung 1987 data are identical with Jung 1991 only the most recent version is displayed and considered for evaluation. The values in Zweit 1991 are too low and do not show a good maximum structure, the set was hence deselected. The whole, too high, set of Takacs 1997 data was multiplied by a factor of 0.7 to be in acceptable agreement with the average value of 220 mb near the maximum at 19 MeV found in the other publications. The original and corrected datasets of 7 publications were selected up to 50 MeV and fitted (Fig. 68).

The overall shape of the excitation function predicted by TENDL 2021 is in good agreement with the experimental results but overestimates the maximal value around 19 MeV. The predictions of TENDL 2023 are lower by a factor of 2 near the maximum and do not represent well the expected shape of the excitation curve. The integral yields calculated from the recommended cross sections are shown in Fig. 69. Two experimental yield data points are available: Dmitriev [218] and Amjed [237].

$^{93}Nb(d,2n)^{93m}Mo$ reaction

As the element Nb is monoisotopic only the $^{93}Nb(d,2n)^{93m}Mo$ reaction with an effective threshold of 5.907 MeV (taking into account the excitation energy of 2.425 MeV of the metastable state) is possible. A total of 5 cross section data sets, covering the energy range from threshold up to 50 MeV, were found in the literature and are displayed in Fig. 70: Ditroi [242], Tarkanyi [243], Avrigeanu [244], Ditroi [245], Aikawa [246].

The data points below the threshold value of 6 MeV of Tarkanyi 2007, Avrigeanu 2013 and Aikawa 2018 were deleted. The original and corrected datasets of the 5 publications were selected up to 50 MeV (Fig. 71).

The TENDL 2021 prediction does not well represent the peak near 18 MeV and is largely underestimating the maximal value. For the TENDL 2023 version the peaked shape agreement is better and the maximum value is overestimated by 20%. The integral yields calculated from the

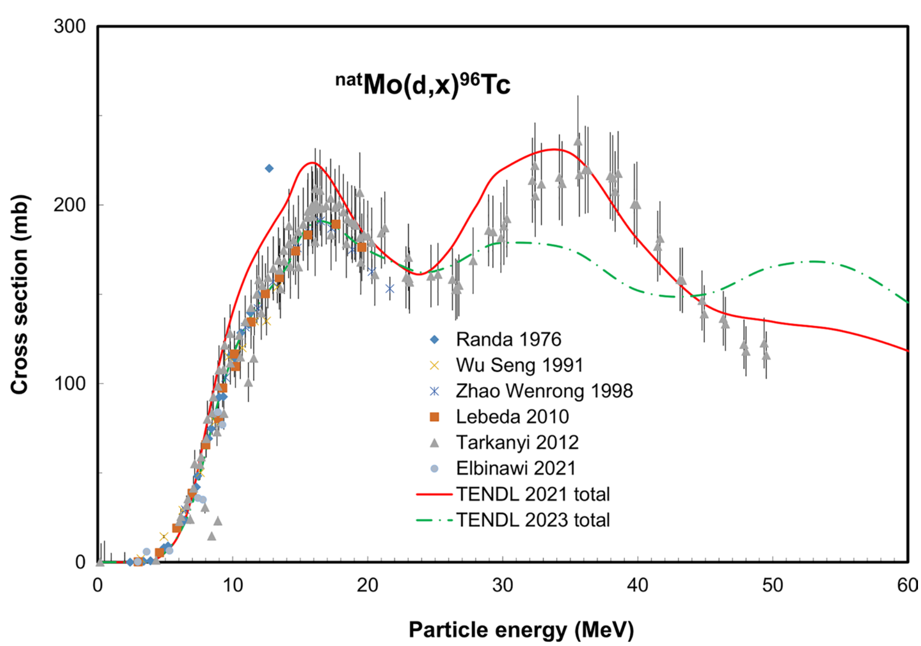

Fig. 72 $^{nat}Mo(d,x)^{96}Tc$ reaction: all experimental data and the TENDL theoretical excitation functions

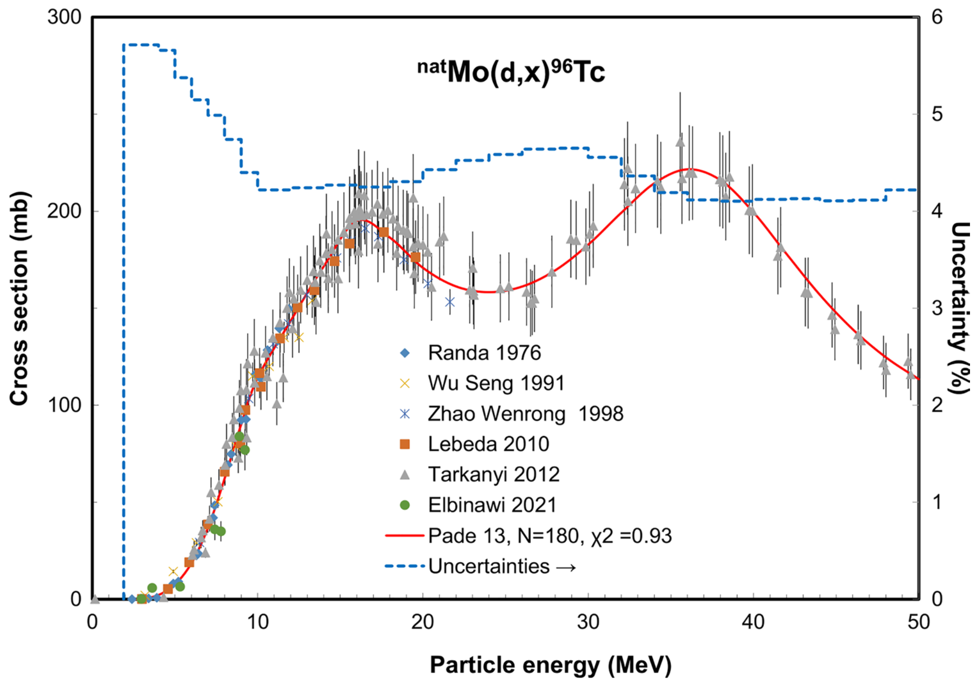

Fig. 73 $^{nat}Mo(d,x)^{96}Tc$ reaction: selected experimental works and Padé fit (solid line) with total derived uncertainties, including 4% systematic uncertainty (dashed line, right-hand scale)

recommended cross sections are shown in Fig. 80. One experimental yield data point is available: Dmitriev [218].

$^{nat}Mo(d,x)^{96}Tc$ reaction

In principle five (p,xn) reactions on the stable target isotopes ^{95}Mo (abundance 15.84% in ^{nat}Mo, n = 1), ^{96}Mo (abundance 16.67% in ^{nat}Mo, n = 2), ^{97}Mo (abundance 9.60% in ^{nat}Mo), ^{98}Mo (abundance 24.39% in ^{nat}Mo), ^{100}Mo (abundance 9.82% in ^{nat}Mo, n = 6) can contribute to formation of ^{96}Tc if high energy deuteron bombardment is performed. The $^{95}Mo(d,n)^{96}Tc$ reaction has a positive Q-value of 3.174 MeV and the threshold rises to 36.340 MeV for the $^{100}Mo(d,6n)^{96}Tc$ reaction.

A total of 6 cross section data sets, covering the energy range from threshold up to 50 MeV, were found in literature and are displayed in Fig. 72: Randa [247], Wu Sheng [248], Zhao Wenrong [249], Lebeda [192], Tarkanyi [250], Elbinawi [251]. Outlying data points of Randa 1976 (at 12.7 MeV), Tarkanyi 2012 (at 7.57, 7.94, 8.44, 8.9, 11.16 and 11.55 MeV) and Elbinawi 2021 (at 3.62 MeV) were deleted.

The original and corrected datasets of the 6 publications were selected up to 50 MeV and fitted (Fig. 73). While the TENDL 2021 predictions represent well the shape and amplitude of the multiple reaction excitation functions in the TENDL 2023 version the disagreements become significant above 25 MeV. The integral yields calculated from the recommended cross sections are shown in Fig. 80. Two experimental yield data points are available: Svoboda [252], Dmitriev [218].

$^{197}Au(d,x)^{194}Au$ reaction

As Au is monoisotopic only the $^{197}Au(d,p4n)$ reaction, with the threshold for emission of single particles at 25.595 MeV, contributes to direct formation of ^{194}Au. As the threshold for (p,^{3}H2n) is 17.037 MeV also low cross sections in the 18–26 MeV domain can be expected. Although the $^{197}Au(d,5n)$ reaction, with a threshold of 26.413 MeV, will result in the formation of very long-lived ^{194}Hg ($T_{1/2}$ = 367 y) it will in practice not contribute to the cumulative formation of ^{194}Au.

A total of 4 cross section data sets, covering the energy range from threshold up to 86 MeV, were found in the literature and are displayed in Fig. 74: Jahn [253], Ochiai [230], Tarkanyi [254], Tarkanyi [255]. Above 40 MeV the status of the experimental database is poor: the two available sets by Jahn 1973 and Tarkanyi 2015 show systematic disagreement. To get selected data they were normalized to each other taking into account acceptance of the Ochai 2007 and Tarkanyi 2011 cross section values at energies between 30 and 40 MeV.

The original and corrected datasets of the 4 publications were selected up to 86 MeV and fitted (Fig. 75). The two TENDL predictions show a more pronounced and higher maximum of around 80 MeV. The integral yields calculated from the recommended cross sections are shown in Fig. 80. No experimental yield data is available.

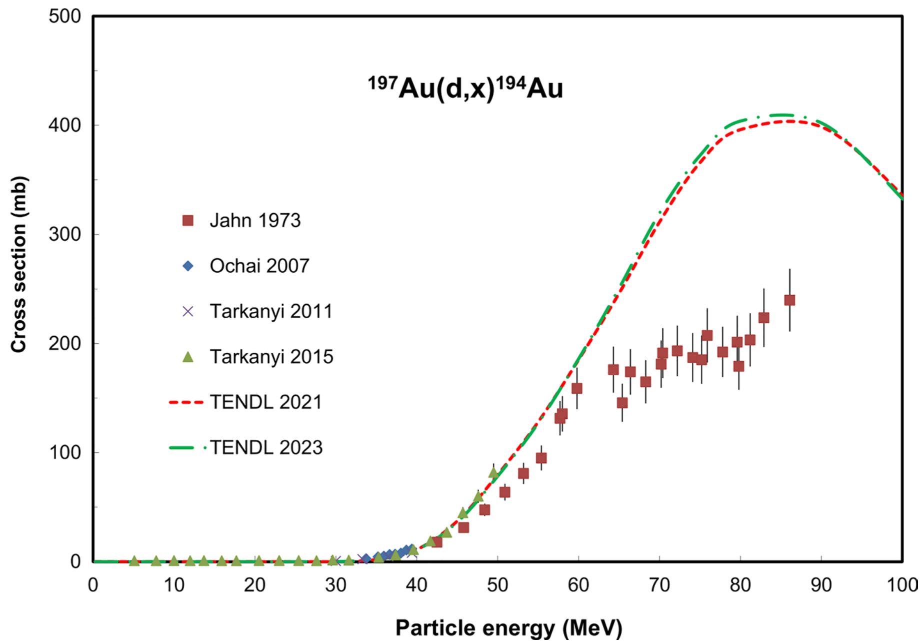

Fig. 74 ^{197}Au(d,x)^{194}Au reaction: all experimental data and the TENDL theoretical excitation functions

^{197}Au(d,x)^{196}Au reaction

As Au is monoisotopic only the ^{197}Au(d,p2n) reaction, with the threshold for emission of single particles at 10.390 MeV, contributes to the formation of ^{196}Au. As the threshold for (d,^{3}H) is only 1.832 MeV also low cross sections in the 3–12 MeV domain can be expected.

A total of 9 cross section data sets, covering the energy range from threshold up to 80 MeV, were found in the literature and are displayed in Fig. 76: Baron [256], Chevarier [257], Khrisanfov [258], Jahn [253], Long [259], Zhao Wenrong [260], Tarkanyi [254], Tarkanyi [255], Lebeda [261]. As all data points of Tarkanyi 2015 are too high, the whole set was multiplied by a factor of 0.8 for selection.

The original and corrected datasets of the 9 publications were selected up to 80 MeV and fitted (Fig. 77). The small local maximum suggested by the experimental data around 15–16 MeV is probably due to more than expected contribution of the clustered emission in the (d,^{3}H) and (d,dn) reactions. The two TENDL predictions do not show the contribution of clustered emission below 20 MeV and are overestimating the maximal value around 40 MeV by more than 40%. The integral yields calculated from the recommended cross sections are shown in Fig. 80. One experimental yield data is available: Dmitriev [218].

^{197}Au(d,x)^{198g}Au reaction

As Au is monoisotopic only the ^{197}Au(d,p) reaction, with a positive Q-value of 4.287 MeV contributes to the formation of ^{198g}Au. A total of 12 cross section data sets, covering the energy range from threshold up to 50 MeV, were found in literature and are displayed in Fig. 78: Baron [256], Sandoval [262], Nassiff [263], Chevarier [257], Khrisanfov [258], Jahn [253], Long [259], Zhao Wenrong [260], Tarkanyi [254], Tarkanyi [255], Ditroi [264], Lebeda [261].

As the cross sections for co-producing the metastable state parent with similar half-life, ^{198m}Au ($T_{1/2}$ = 2.876 d, IT 100%), is very low (less than 1 mb up to 20 MeV in Tarkanyi 2011 and Lebeda 2019) the contribution in the formation of the ground state is negligible and not further considered.

The two datasets with too low values at energies below 12 MeV (Nasiff 1966 and Khrisanfov 1972) were deselected. Also, the too low values of Chevarier 1971 at 9.51 MeV and four points of Tarkanyi 2015 (at 5.1, 7.8, 10 and 12 MeV) were deleted. The clearly outlying and too high sets of Tarkanyi 2015 and Lebeda 2019 were reduced by a factor of 0.8 while the really low set of Ditroi 2017 was multiplied by a factor of 10. The original and corrected datasets of 10 publications were selected up to 80 MeV and fitted (Fig. 79).

The two TENDL predictions are energy-shifted and strongly underestimate the maximal value. This is because a ratio for formation of metastable state to ground state of around 2.5–5 10^{-1} is predicted in the 5–20 MeV range while values derived from experimental results are 3–4 10^{-3}. The integral yields calculated from the recommended cross sections are shown in Fig. 80. One experimental yield data point is available: Dmitriev [218].

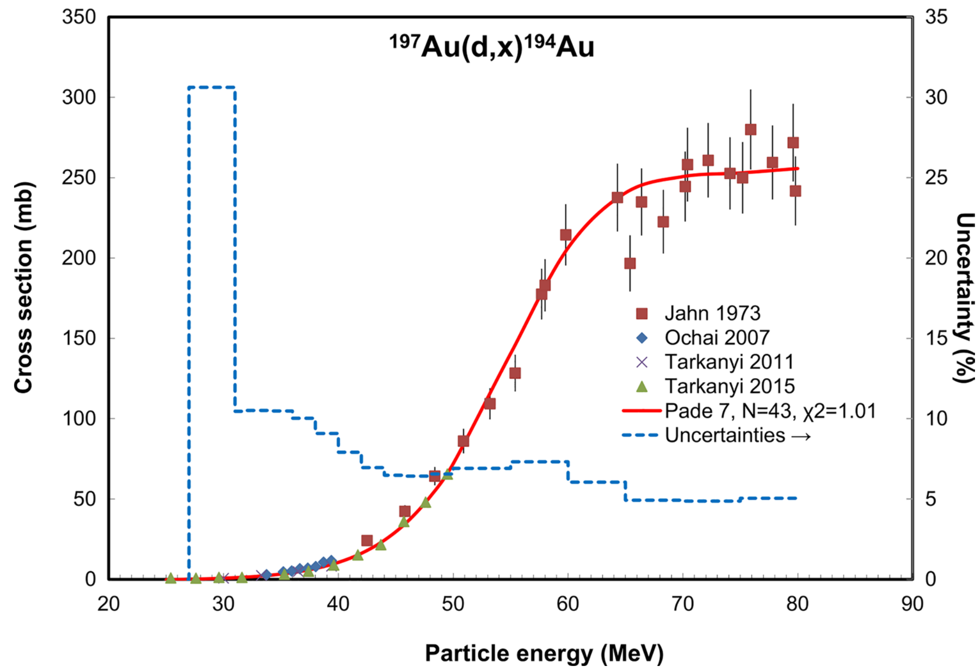

Fig. 75 $^{197}Au(d,x)^{194}Au$ reaction: selected experimental works and Padé fit (solid line) with total derived uncertainties, including 4% systematic uncertainty (dashed line, right-hand scale)

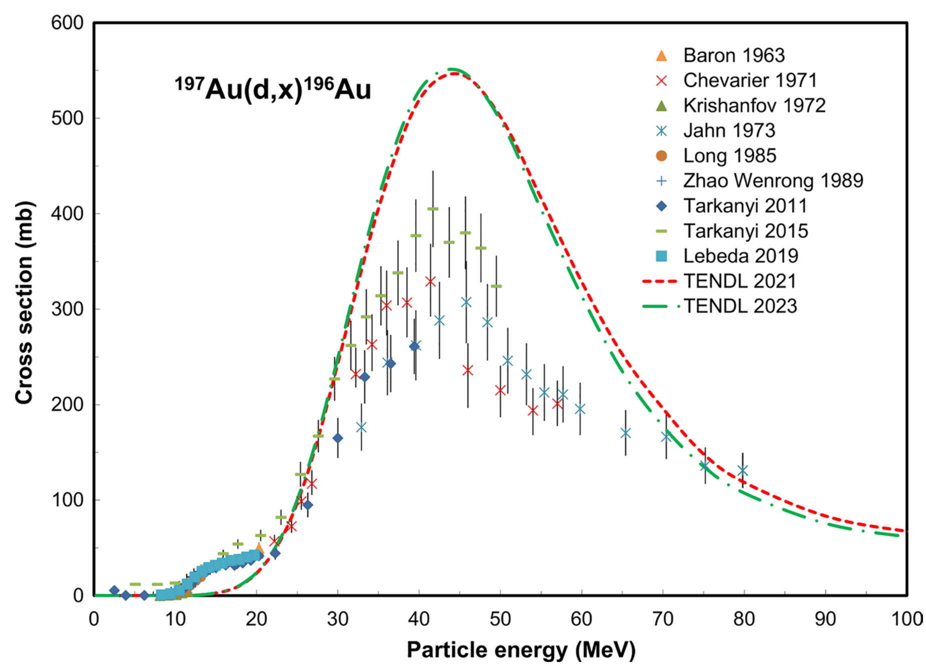

Fig. 76 $^{197}Au(d,x)^{196}Au$ reaction: all experimental data and the TENDL theoretical excitation functions

7. Evaluated ^{3}He-induced nuclear reactions

$^{nat}C(^{3}He,x)^{11}C$ reaction

Two reactions contribute to ^{11}C formation after ^{3}He bombardment of ^{nat}C: $^{12}C(^{3}He,\alpha)^{11}C$ (^{12}C abundance is 98.90%, positive Q-value of 1.856 MeV) and $^{13}C(^{3}He,\alpha n)^{11}C$ (^{13}C abundance is 1.10%, threshold 3.791 MeV). A total of 6

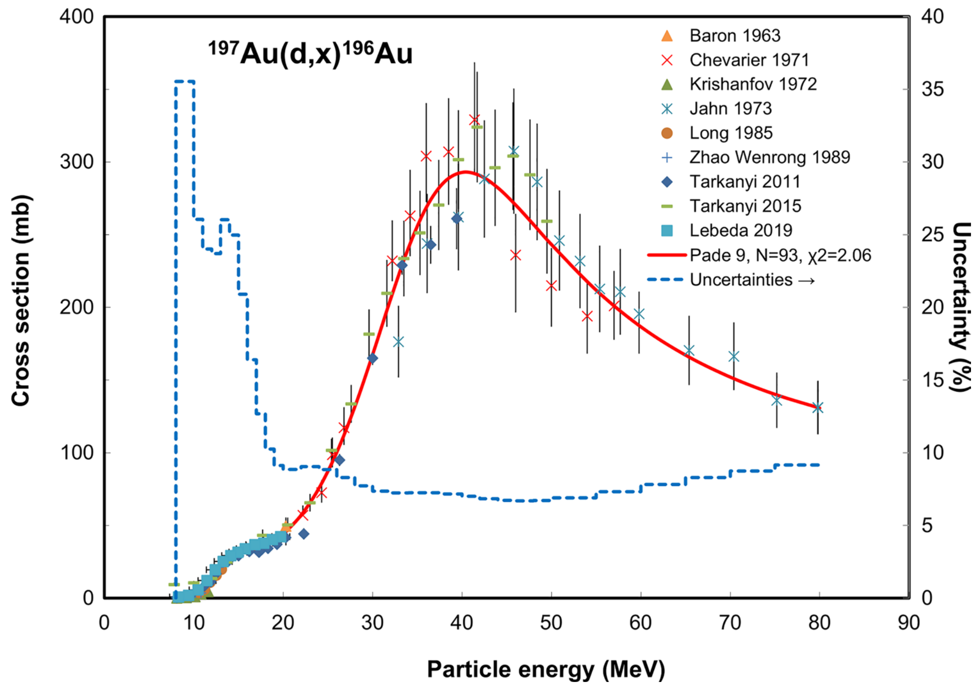

Fig. 77 $^{197}Au(d,x)^{196}Au$ reaction: selected experimental works and Padé fit (solid line) with total derived uncertainties, including 4% systematic uncertainty (dashed line, right-hand scale)

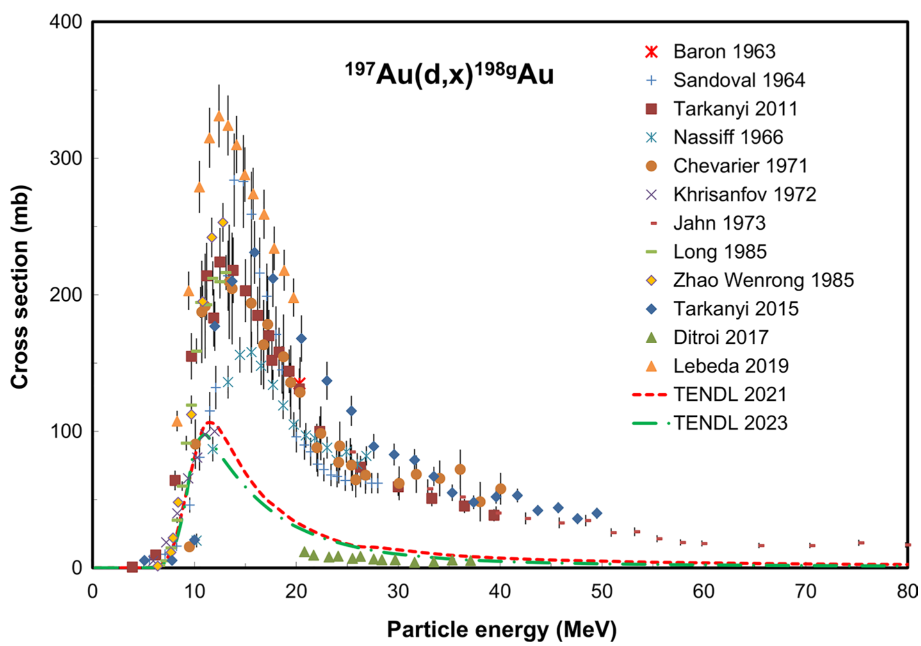

Fig. 78 $^{197}Au(d,x)^{198}Au$ reaction: all experimental data and the TENDL theoretical excitation functions

cross section data sets, covering the energy range from threshold up to 37 MeV, were found in the literature and are displayed in Fig. 81: Crandall [31], Brill [265], Hahn [266], Cirilov [267], Liebler s1-2 [268]. The too low point of Brill 1965 at 5.09 MeV was deleted. The original and corrected datasets of the 6 publications were selected and fitted up to 40 MeV (Fig. 82). No TENDL predictions are available for these low Z-value targets. The integral yields calculated from the recommended cross sections are shown in Fig. 93.

Two experimental yield data available: Krasnov [48], which is independent and Nozaki [269], which is derived saturation yield, that's why it was not presented in Fig. 93.

$^{nat}Ti(^{3}He,x)^{44m}Sc$ reaction

Reactions of the general shape (^{3}He,αpxn), with x between 0 and 3, on the five stable isotopes of Ti can contribute to direct ^{44m}Sc formation (^{46}Ti abundance is 8.22% in natural Ti, ^{47}Ti abundance is 7.44%, ^{48}Ti abundance is 73.72%,

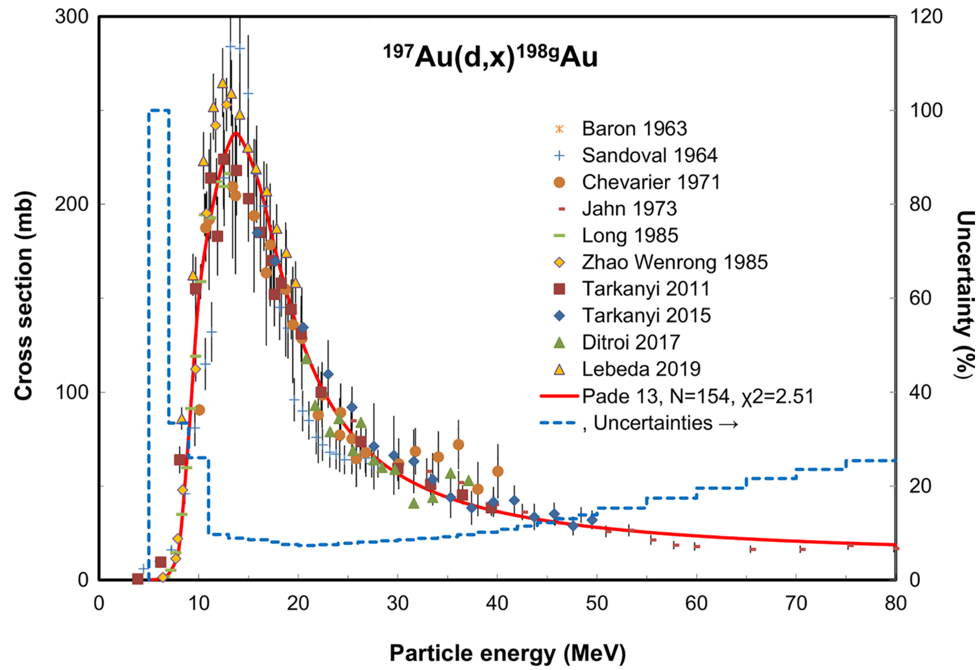

Fig. 79 ^{197}Au(d,x)^{198}Au reaction: selected experimental works and Padé fit (solid line) with total derived uncertainties, including 4% systematic uncertainty (dashed line, right-hand scale)

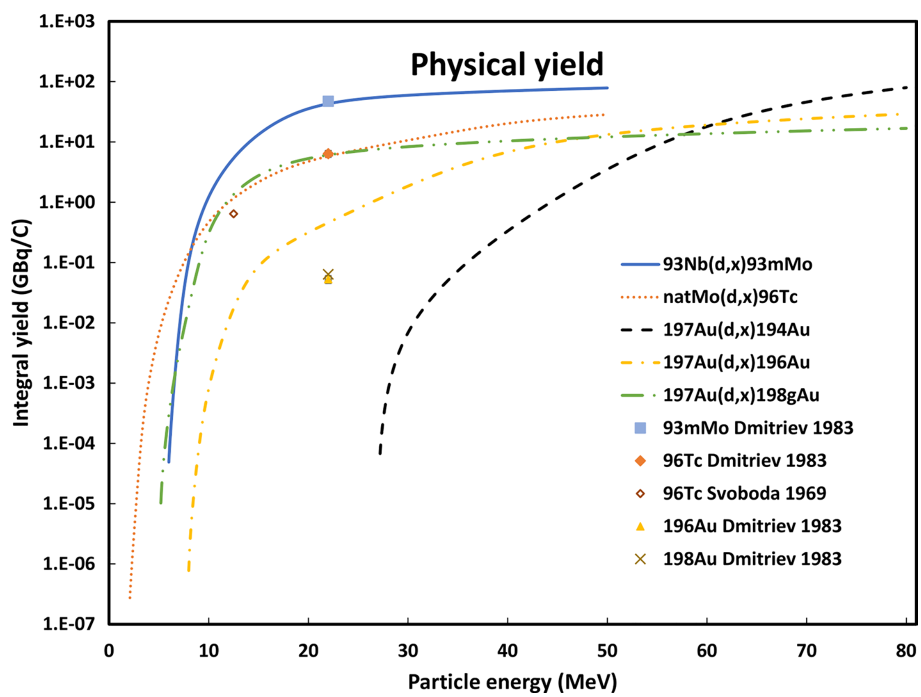

Fig. 80 ^{197}Au(d,x)^{198}Au reaction: selected experimental works and Padé fit (solid line) with total derived uncertainties, including 4% systematic uncertainty (dashed line, right-hand scale)

^{49}Ti abundance is 5.41%, ^{50}Ti abundance is 5.18%). The threshold for the ^{46}Ti(^{3}He,αp)^{44g}Sc reaction is 1.163 MeV while for the ^{50}Ti(^{3}He,αp4n) ^{44g}Sc reaction a threshold of 43.09 MeV is reached. A value of 0.2710 MeV, the excitation energy of the metastable state, should be added to these threshold values. More clustering with the emission of Li isotopes could also occur, the ^{47}Ti(^{3}He,^{6}Li)^{44g}Sc reaction has a threshold of 6.663 MeV.

A total of 4 cross section data sets, covering the energy range from threshold up to 135 MeV, were found in literature and are displayed in Fig. 83: Weinreich [270], Ditroi [271], Szelecsenyi [272], Khandaker [273]. The two lowest points of Weinreich 1980 at 4.9 and 9 MeV are deleted. The pronounced local maximum around 55 MeV is due to the most contributing reaction on dominant ^{48}Ti.

The original and corrected datasets of the 4 publications were selected up to 135 MeV and fitted (Fig. 84). The two

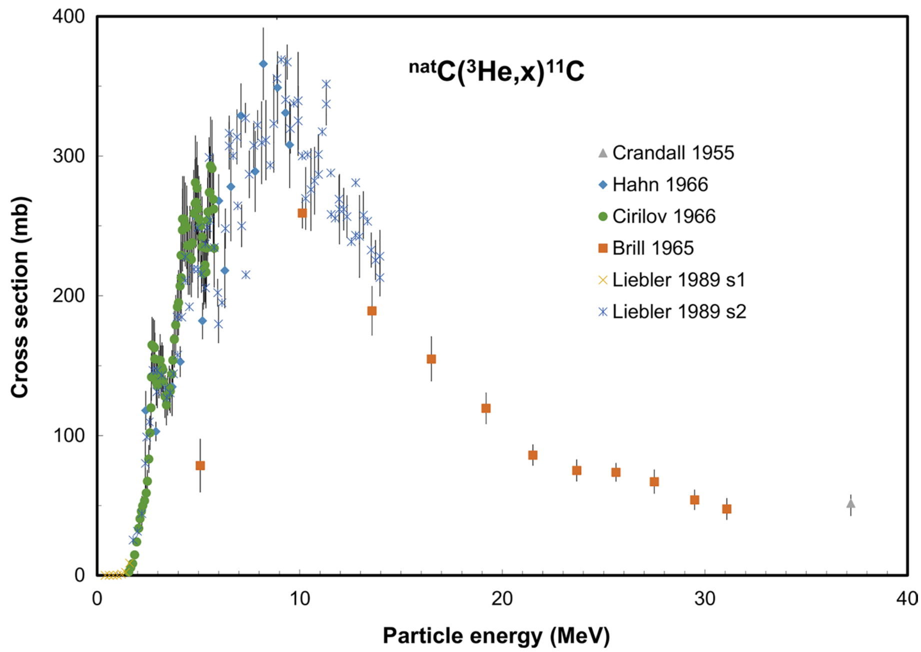

Fig. 81 $^{nat}C(^3He,x)^{11}C$ reaction: all experimental data

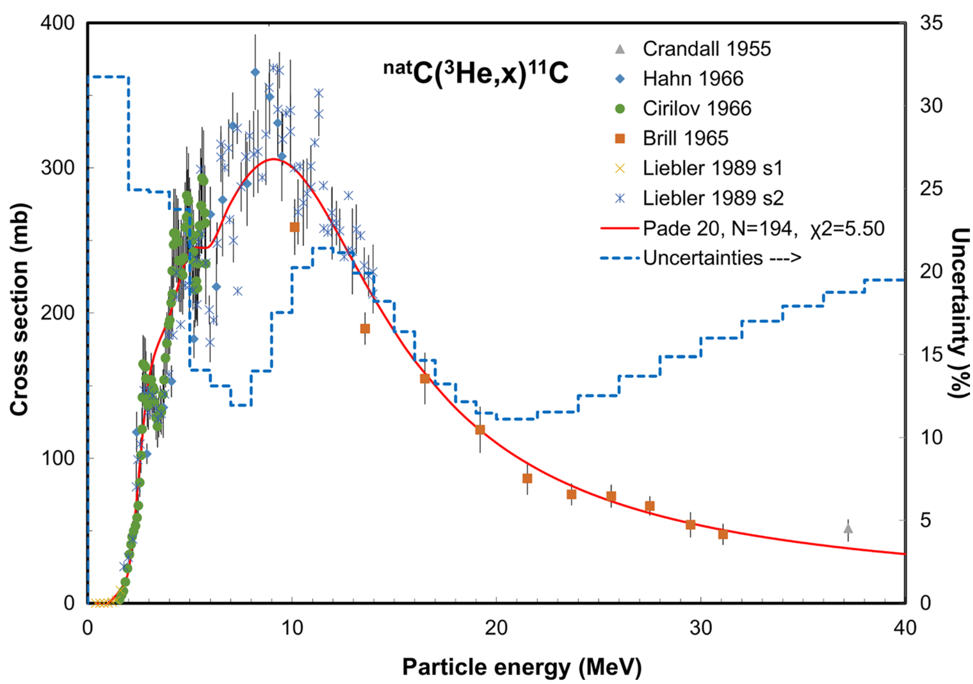

Fig. 82 $^{nat}C(^3He,x)^{11}C$ reaction: selected experimental works and Padé fit (solid line) with total derived uncertainties, including 4% systematic uncertainty (dashed line, right hand scale)

versions of the TENDL predictions reproduce the overall shape of the experimental data and show the local maxima of the contributing reactions on the different stable Ti isotopes but with an energy shift of 50 MeV for the dominant $^{48}Ti(3He,x)^{44m}Sc$ reaction. A difference by a factor of two between the two versions is noted. The integral yields calculated from the recommended cross sections are shown in Fig. 93. No experimental yield data are available.

$^{nat}Ti(^3He,x)^{46}Sc$ reaction

Reactions of the general shape (^3He,3pxn), with x between 1 and 5, on the five stable isotopes of Ti can contribute to direct ^{46}Sc formation (^{46}Ti abundance is 8.22% in natural Ti, ^{47}Ti abundance is 7.44%, ^{48}Ti abundance is 73.72%, ^{49}Ti abundance is 5.41%, ^{50}Ti abundance is 5.18%). The threshold for the $^{46}Ti(^3He,3p)^{46}Sc$ reaction is 9.887 MeV while for the maximal clustered emission $^{48}Ti(^3He,\alpha p)^{46}Sc$ reaction a threshold of 1.605 MeV is reached. More clustering

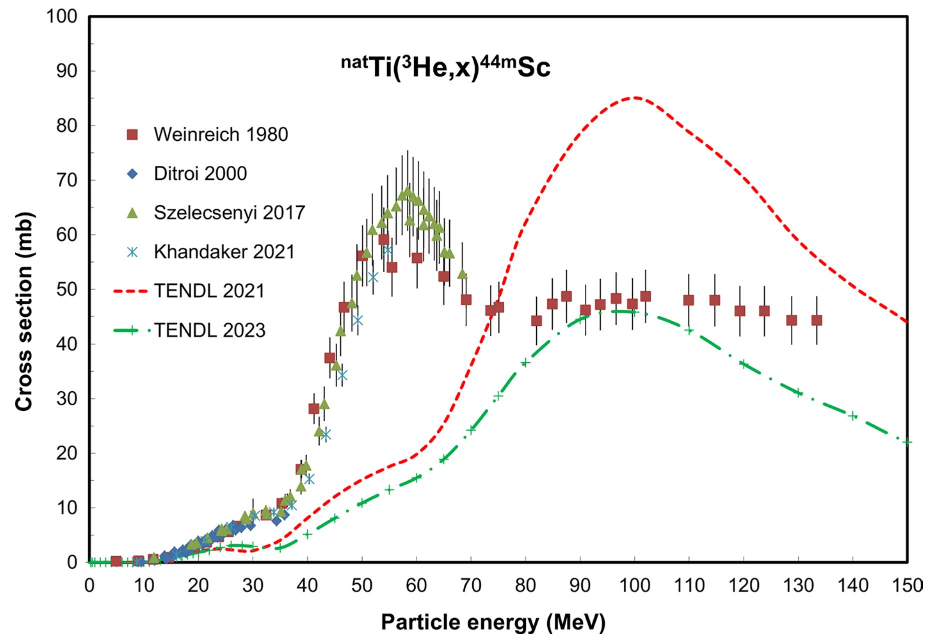

Fig. 83 $^{nat}Ti(^{3}He,x)^{44m}Sc$ reaction: all experimental data and the TENDL theoretical excitation functions

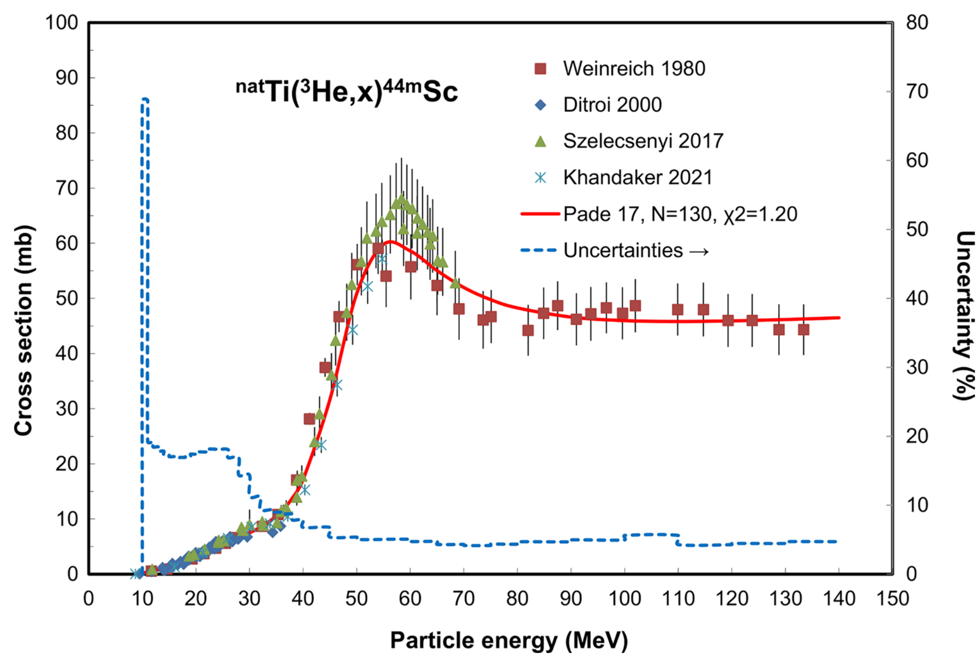

Fig. 84 $^{nat}Ti(^{3}He,x)^{44m}Sc$ reaction: all experimental data and the TENDL theoretical excitation functions

with the emission of Li isotopes could also occur, the $^{49}Ti(^{3}He,^{6}Li)^{46}Sc$ reaction has a threshold of 6.308 MeV.

A total of 4 cross section data sets, covering the energy range from threshold up to 135 MeV, were found in the literature and are displayed in Fig. 85: Weinreich [270], Ditroi [271], Szelecsenyi [272], Khandaker [274]. All sets were selected up to 100 MeV and fitted (Fig. 86).

The two TENDL predictions are well representing the overall shape but the values are a factor 3–7 too low. The integral yields calculated from the recommended cross sections are shown in Fig. 93. No experimental yield data are available.

$^{nat}Ti(^{3}He,x)^{47}Sc$ reaction

Reactions of the general shape (^{3}He,αpxn), with x between 0 and 3, on four stable isotopes of Ti can contribute to direct ^{47}Sc formation (^{47}Ti abundance is 7.44% in natural Ti, ^{48}Ti abundance is 73.72%, ^{49}Ti abundance is 5.41%, ^{50}Ti abundance is 5.18%). The threshold for the $^{47}Ti(^{3}He,3p)^{47}Sc$

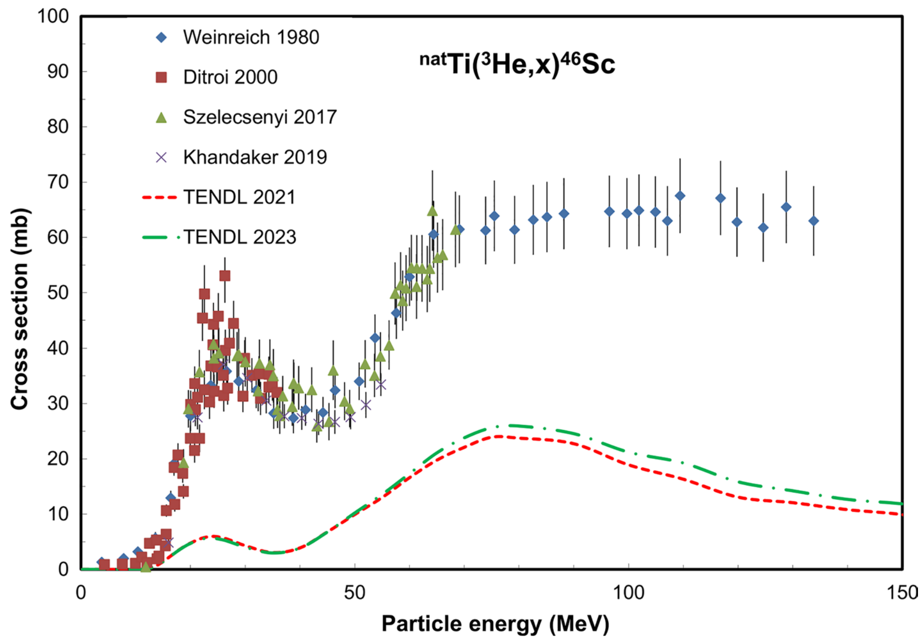

Fig. 85 $^{nat}Ti(^{3}He,x)^{46}Sc$ reaction: all experimental data and the TENDL theoretical excitation functions

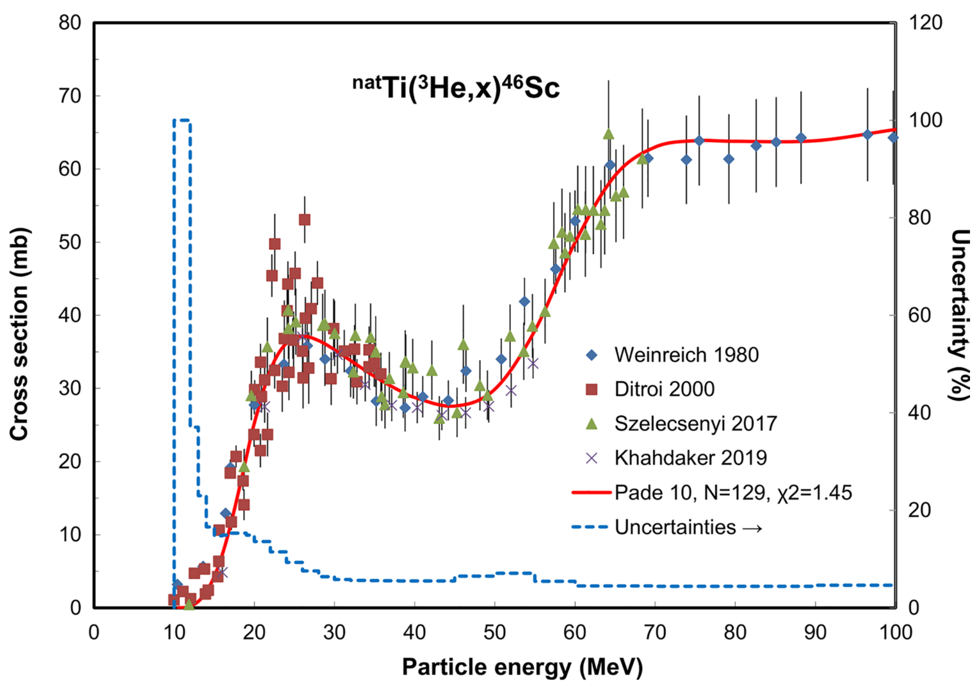

Fig. 86 $^{nat}Ti(^{3}He,x)^{46}Sc$ reaction: selected experimental works and Padé fit (solid line) with total derived uncertainties, including 4% systematic uncertainty (dashed line, right-hand scale)

reaction is 8.000 MeV while for the $^{49}Ti(^{3}He,\alpha p)^{47}Sc$ reaction a positive Q-value of 990 keV is obtained.

A total of 4 cross section data sets, covering the energy range from threshold up to 135 MeV, were found in literature and are displayed in Fig. 87. Weinreich [270], Ditroi [271], Szelecsenyi [272], Khandaker [274]. The excitation function obtained from the data set of Weinreich [270] was energy corrected.

The original and corrected datasets of the 4 publications were selected up to 140 MeV and fitted (Fig. 88). The two TENDL predictions represent well the overall shape up to 60 MeV but the values are a factor of 3–5 too low. The integral yields calculated from the recommended cross sections are shown in Fig. 93. No experimental yield data are available.

$^{nat}Ti(^{3}He,x)^{48}Cr$ reaction

Reactions of the general shape (^{3}He, xn), with x between 1 and 5, on the five stable isotopes of Ti can contribute to

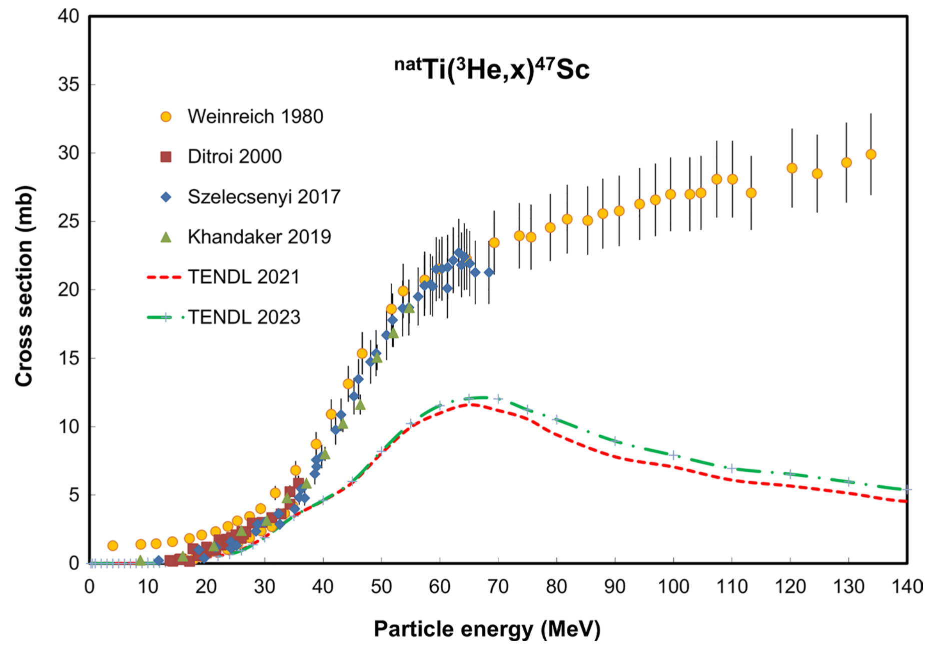

Fig. 87 $^{nat}Ti(^{3}He,x)^{47}Sc$ reaction: all experimental data and the TENDL theoretical excitation functions

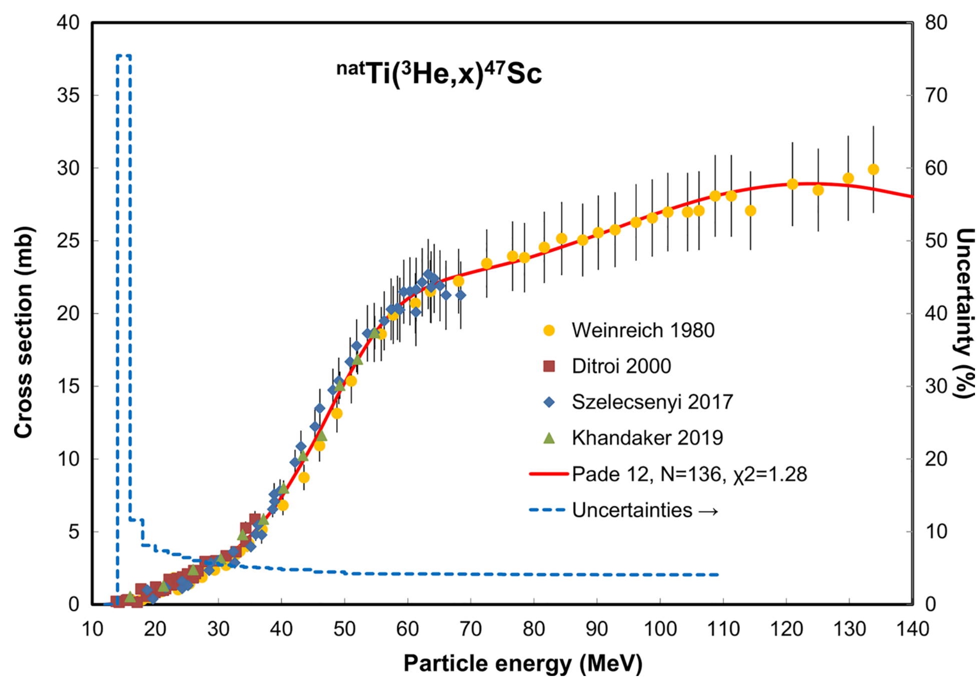

Fig. 88 $^{nat}Ti(^{3}He,x)^{47}Sc$ reaction: selected experimental works and Padé fit (solid line) with total derived uncertainties, including 4% systematic uncertainty (dashed line, right-hand scale)

direct ^{48}Cr formation (^{46}Ti abundance is 8.22%, ^{47}Ti abundance is 7.44%, ^{48}Ti abundance is 73.72%, ^{49}Ti abundance is 5.41%, ^{50}Ti abundance is 5.18%). The $^{46}Ti(^{3}He,n)^{48}Cr$ reaction has a positive Q-value of 5.553 MeV while for the $^{50}Ti(^{3}He,5n)$ ^{48}Cr reaction a threshold of 35.998 MeV is reached.

A total of 5 cross section data sets, covering the energy range from threshold up to 135 MeV, were found in literature and are displayed in Fig. 89: Weinreich [270], Ditroi [271], Szelecsenyi [272], Khandaker [274], Lebeda [275].

The excitation function obtained from the data set of Weinreich is energy-shifted in the lower energy domain and has too low cross section values near the maximum. A negative, linearly decreasing towards accepted energy of 134.7 MeV correction was applied (−1.2 MeV at 9.4 MeV original) and all values were multiplied by a factor of 1.2. The original and corrected datasets of the 5 publications were selected up to 135 MeV, and fitted up to 100 MeV (Fig. 90).

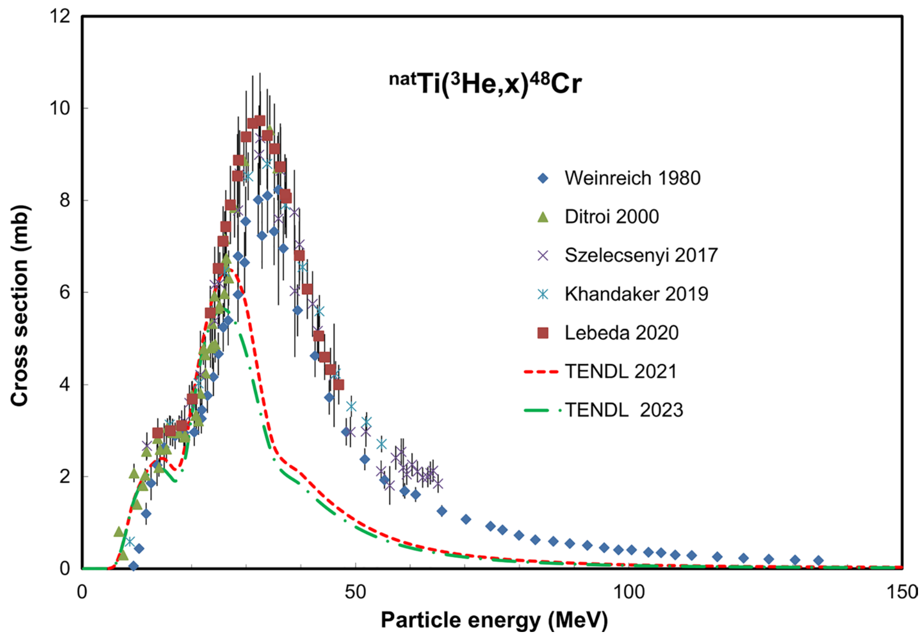

Fig. 89 $^{nat}Ti(^{3}He,x)^{48}Cr$ reaction: all experimental data and the TENDL theoretical excitation functions

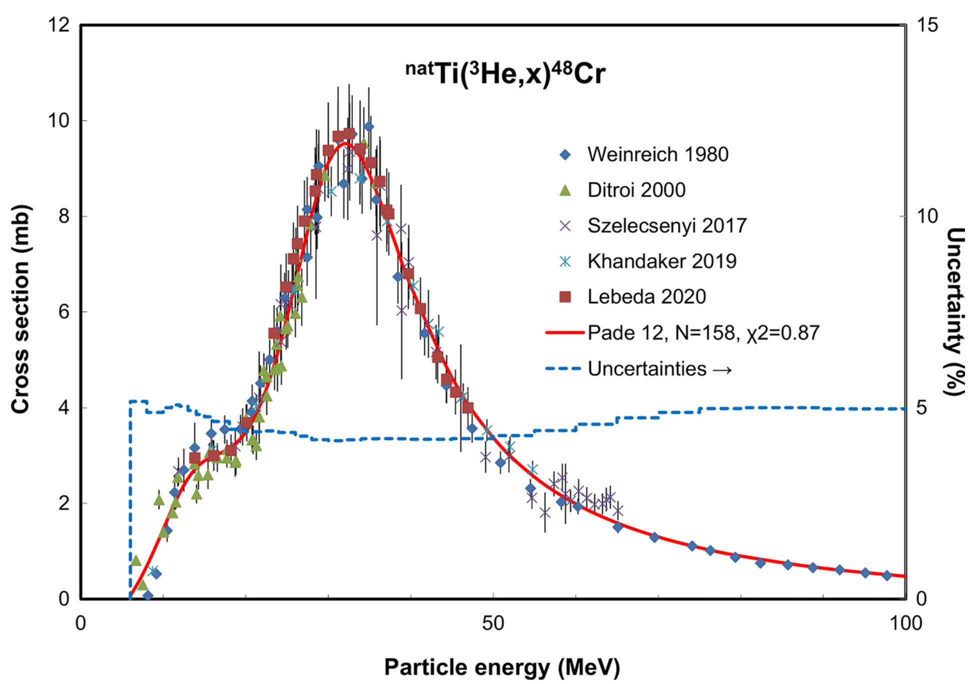

Fig. 90 $^{nat}Ti(^{3}He,x)^{48}Cr$ reaction: selected experimental works and Padé fit (solid line) with total derived uncertainties, including 4% systematic uncertainty (dashed line, right-hand scale)

The two TENDL predictions have a more pronounced dip in the 14–19 MeV region before the dominant contribution of the $^{48}Ti(^{3}He,3n)^{48}Cr$ reaction with a 15.854 MeV threshold is starting. The excitation curve is however shifted to lower energy and underestimates the maximal value by 40%. The integral yields calculated from the recommended cross sections are shown in Fig. 93. No experimental yield data are available.

$^{nat}Ti(^{3}He,x)^{51}Cr$ reaction

Reactions of the general shape (^{3}He,xn), with x is 1 or 2, on two stable isotopes of Ti, can contribute to direct ^{41}Cr formation (^{49}Ti abundance is 5.41% in natural Ti, ^{50}Ti abundance is 5.18%). The $^{49}Ti(^{3}He,n)^{81}Cr$ reaction has a positive Q-value of 9.746 MeV while for the $^{50}Ti(^{3}He, 2n)\ ^{51}Cr$ reaction a threshold of 1.261 MeV is reached.

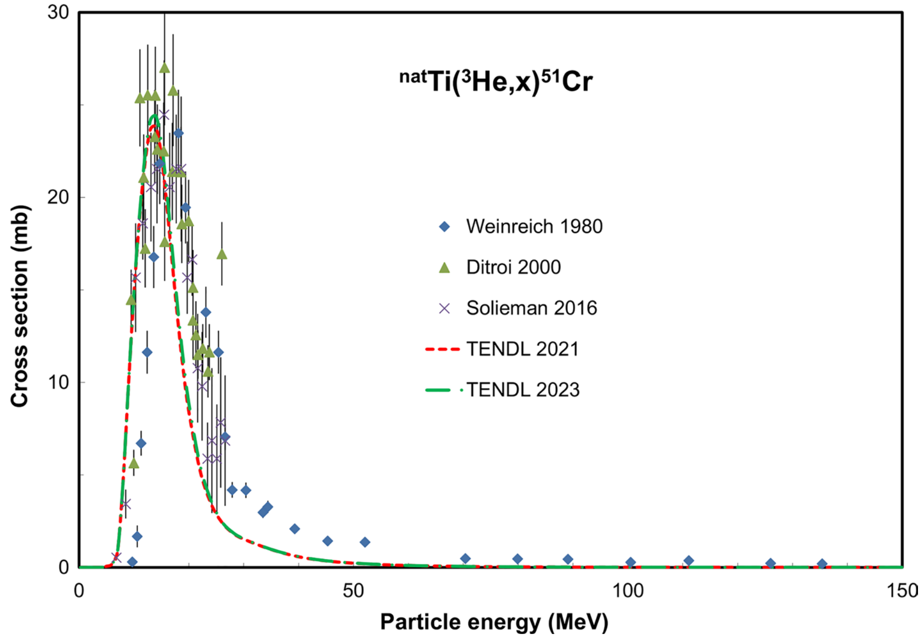

Fig. 91 $^{nat}Ti(^{3}He,x)^{51}Cr$ reaction: all experimental data and the TENDL theoretical excitation functions

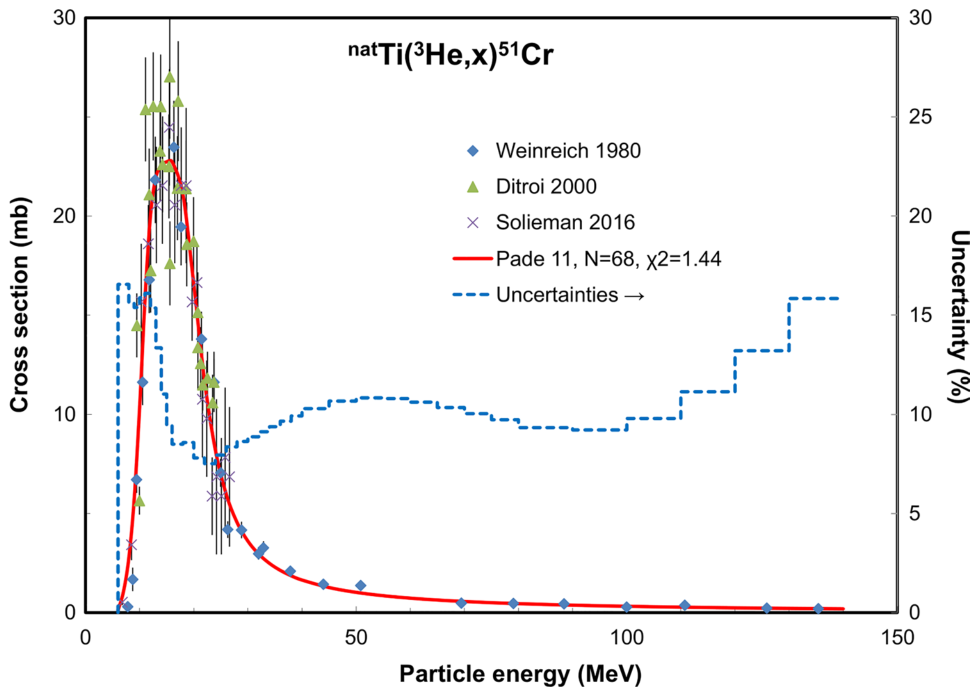

Fig. 92 $^{nat}Ti(^{3}He,x)^{51}Cr$ reaction: selected experimental works and Padé fit (solid line) with total derived uncertainties, including 4% systematic uncertainty (dashed line, right-hand scale)

A total of 3 cross section data sets, covering the energy range from threshold up to 135 MeV, were found in the literature and are displayed in Fig. 91: Weinreich [270], Ditroi [271], Solieman [276].

The excitation function obtained from the data set of Weinreich is energy-shifted in the lower energy domain. A negative, linearly decreasing towards accepted energy of 134.7 MeV), the correction was applied (− 1.9 MeV at 9.4 MeV original,—0.7 at 90 MeV).

The original and corrected datasets of the 3 publications were selected and fitted up to 135 MeV, the energy limit for interesting practical application (Fig. 92). The TENDL predictions are in good agreement with the available experimental results in the maximum, confirm a practical threshold of 6 MeV, but above the maximum are shifted to low energies. The integral yields calculated from the recommended cross sections are shown in Fig. 93. No experimental yield data are available.

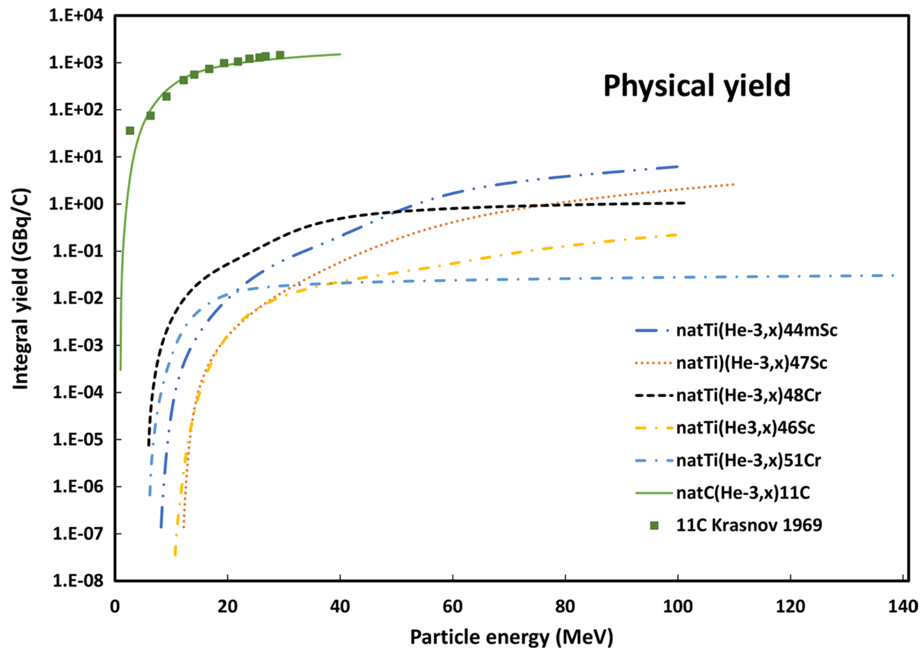

Fig. 93 Yield calculated from the recommended cross sections of the $^{nat}Ti(^{3}He,x)^{44m}Sc$ $^{nat}Ti(^{3}He,x)^{46}Sc$ $^{nat}Ti(^{3}He,x)^{47}Sc$ $^{nat}Ti(^{3}He,x)^{48}Cr$ and $^{nat}Ti(^{3}He,x)^{51}Cr$ reactions

Evaluated alpha-induced nuclear reactions

$^{27}Al(\alpha,x)^{28}Mg$ reaction

As Al is monoisotopic only the $^{27}Al(a,3p)$ reaction with a threshold of 24.665 MeV contributes to ^{28}Mg formation.

A total of 13 cross section data sets, covering the energy range from threshold up to 170 MeV, were found in literature and are displayed in Fig. 94: Hudis [277], Nethaway [278], Martens [279], Nozaki [280], Probst [281], Rattan [282], Rattan [283], Vysotskiy [284], Rattan [285], Karamyan [286], Kirov [287], Lange [288], Paul [289].

The energy scale of Probst 1976 was positively, linearly decreasing with the accepted original value at 155 MeV, corrected. The single points of Hudis 1957 and Kirov 1992 were deleted while the too low data point of Vysotskiy 1989 at 52 MeV was deselected.

The original and corrected datasets of 11 publications were selected up to 160 MeV and fitted (Fig. 95). The maximum cross section in both versions of the TENDL predictions is more than a factor 6 lower than the experimental

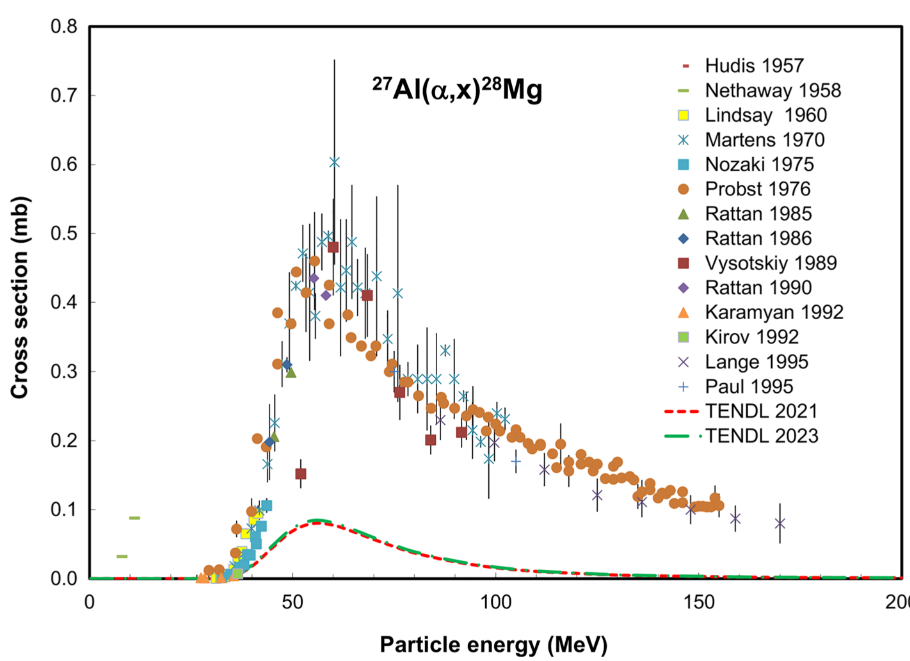

Fig. 94 $^{27}Al(\alpha,x)^{28}Mg$ reaction: all experimental data and the TENDL theoretical excitation functions

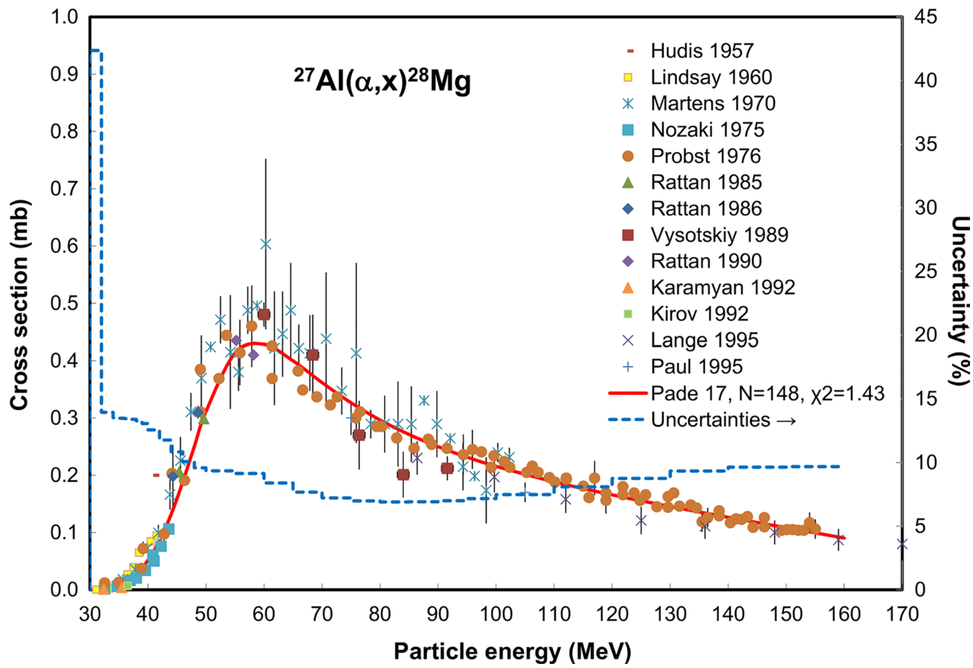

Fig. 95 ^{27}Al(α,x)^{28}Mg reaction: selected experimental works and Padé fit (solid line) with total derived uncertainties, including 4% systematic uncertainty (dashed line, right-hand scale)

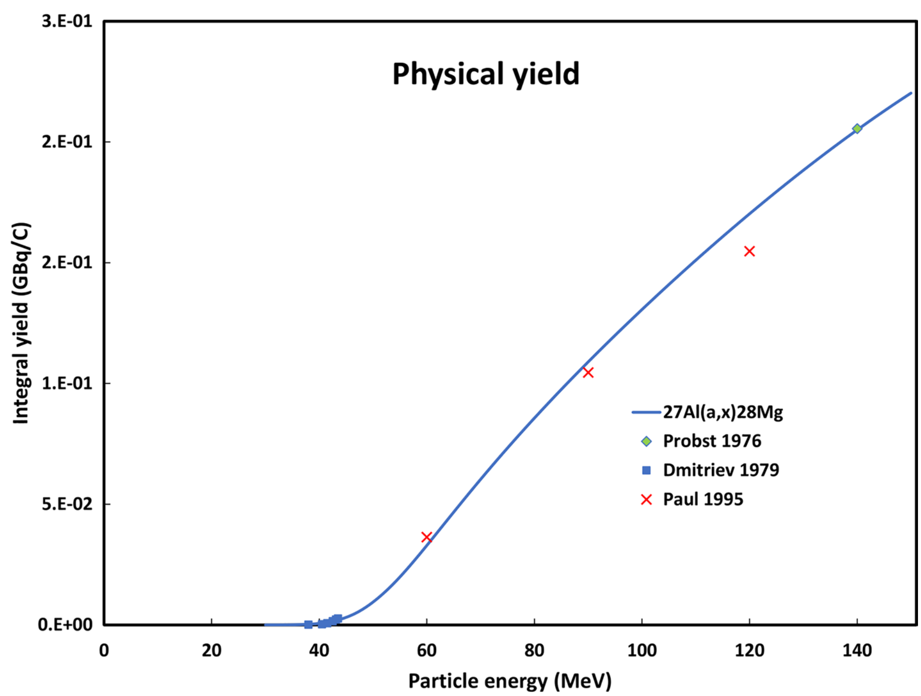

Fig. 96 Yield calculated from the recommended cross sections of the ^{27}Al(α,x)^{28}Mg reaction

maximum. The integral yields calculated from the recommended cross sections are shown in Fig. 96. Three experimental yield data are available: Dmitriev [290], Paul [289] and Probst [281].

^{nat}Ni(α,x)^{57}Ni reaction

In principle five (α,αxn) reactions on the stable target isotopes ^{58}Ni (abundance 68.077% in ^{nat}Ni, x = 1), ^{60}Ni (abundance 26.223% in ^{nat}Ni, n = 3), ^{61}Ni (abundance 1.1399% in ^{nat}Ni), ^{62}Ni (abundance 3.6346% in ^{nat}Ni), ^{64}Ni (abundance 0.9255% in ^{nat}Ni) can contribute to direct formation of ^{57}Ni if high energy α-particle bombardment is performed. The

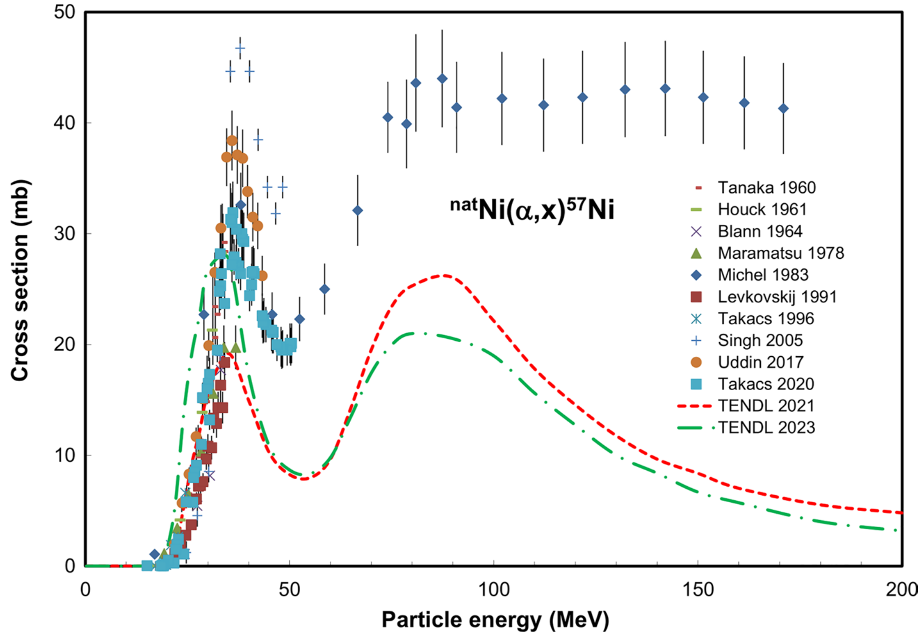

Fig. 97 $^{nat}Ni(\alpha,x)^{57}Ni$ reaction: all experimental data and the TENDL theoretical excitation functions

threshold of the $^{58}Ni(\alpha,\alpha n)^{57}Ni$ reaction is 12.967 MeV while the reaction with un-clustered particle emission $^{58}Ni(\alpha,2p3n)^{57}Ni$ can start at 43.104 MeV.

A total of 10 cross section data sets, covering the energy range from threshold up to 170 MeV, were found in literature and are displayed in Fig. 97: Tanaka [291], Houck [292], Blann [293], Muramatsu [294], Michel [153], Levkovskii [130], Takacs [295], Singh [296], Uddin [297], Takacs [298]. Two datasets in the rising part of the excitation function (Blann 1964 and Levkovskii 1991) are too low and were multiplied by a factor of 2. The set of Singh 2005 is considered to be too high near the maximum and is deleted as is the too low point of Muramatsu 1978 (at 36.8 MeV).

The original and corrected datasets of 9 publications were selected and fitted up to 150 MeV (Fig. 98). The increase of the excitation function above 50 MeV is due to the start of reactions with single particle emissions. The two TENDL predictions confirm the double region excitation function but are energy-shifted and oppositely describe the relative importance of clustered and single particle emissions.

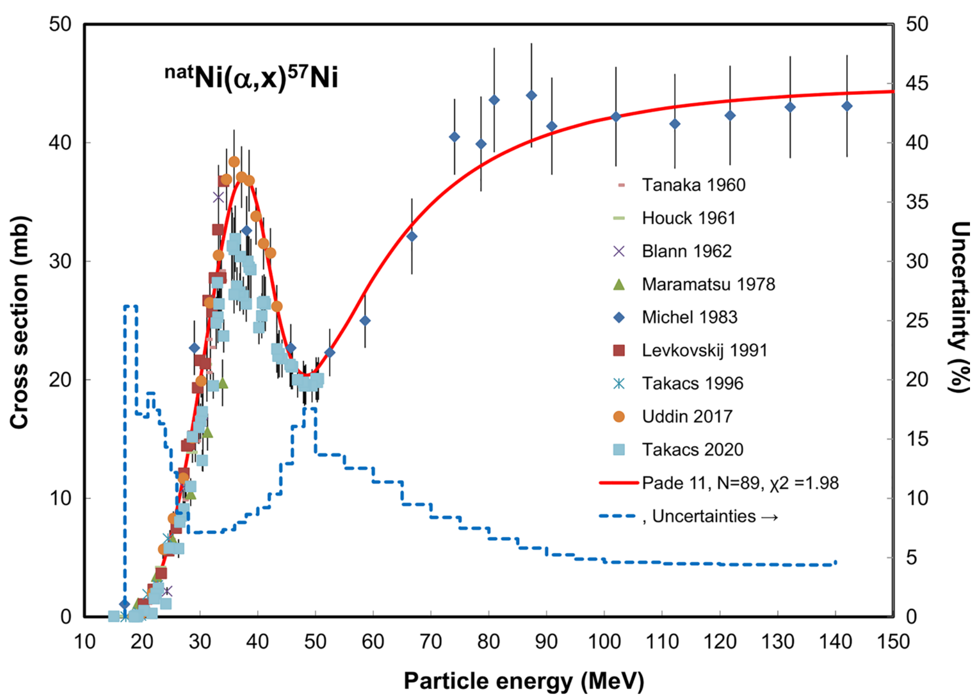

Fig. 98 $^{nat}Ni(\alpha,x)^{57}Ni$ reaction: selected experimental works and Padé fit (solid line) with total derived uncertainties, including 4% systematic uncertainty (dashed line, right-hand scale)

The integral yields calculated from the recommended cross sections are shown in Fig. 111. A single experimental yield data point is available: Paul [289].

^{nat}Ni(α,x)^{57}Co reaction

In principle five (α,αpxn) reactions on the stable target isotopes ^{58}Ni (abundance 68.077% in ^{nat}Ni, x = 0), ^{60}Ni (abundance 26.223% in ^{nat}Ni, n = 2), ^{61}Ni (abundance 1.1399% in ^{nat}Ni), ^{62}Ni (abundance 3.6346% in ^{nat}Ni), ^{64}Ni (abundance 0.9255% in ^{nat}Ni) can contribute to direct formation of ^{57}Co ($T_{1/2}$ = 271.74 d) if high energy α-particle bombardment is performed. The threshold for the ^{58}Ni(α,αp)^{57}Co reaction is 8.172 MeV. Depending on the cooling time before measurement contribution of the shorter-lived ^{57}Ni ($T_{1/2}$ = 35.60 h), formed by (α,xn) reactions with as lowest threshold 12.967 MeV, can contribute (see previous section).

A total of 10 cross section data sets, covering the energy range from threshold up to 145 MeV, were found in literature and are displayed in Fig. 99: Tanaka [291], Houck [292],

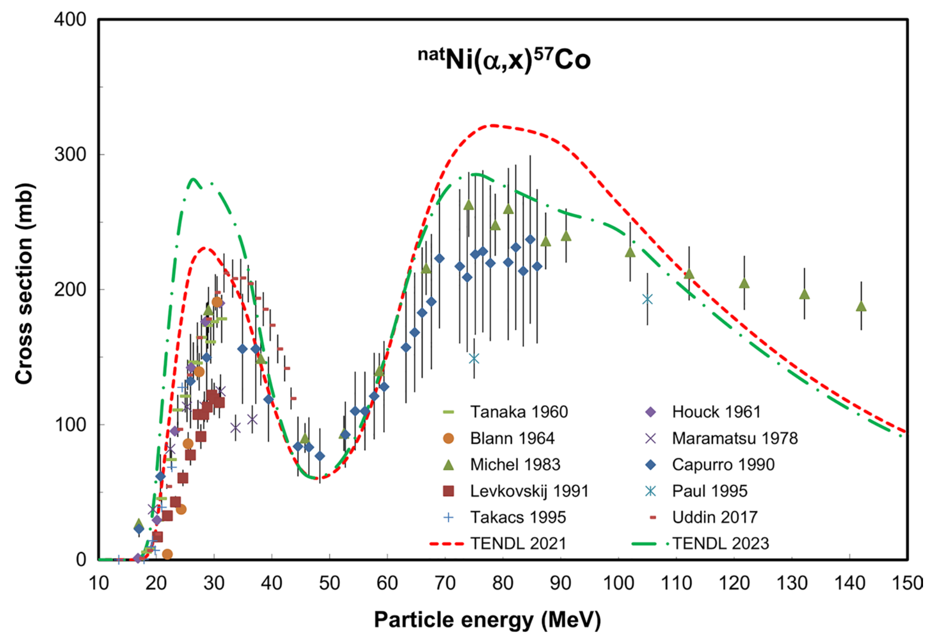

Fig. 99 ^{nat}Ni(α,x)^{57}Co reaction: all experimental data and the TENDL theoretical excitation functions

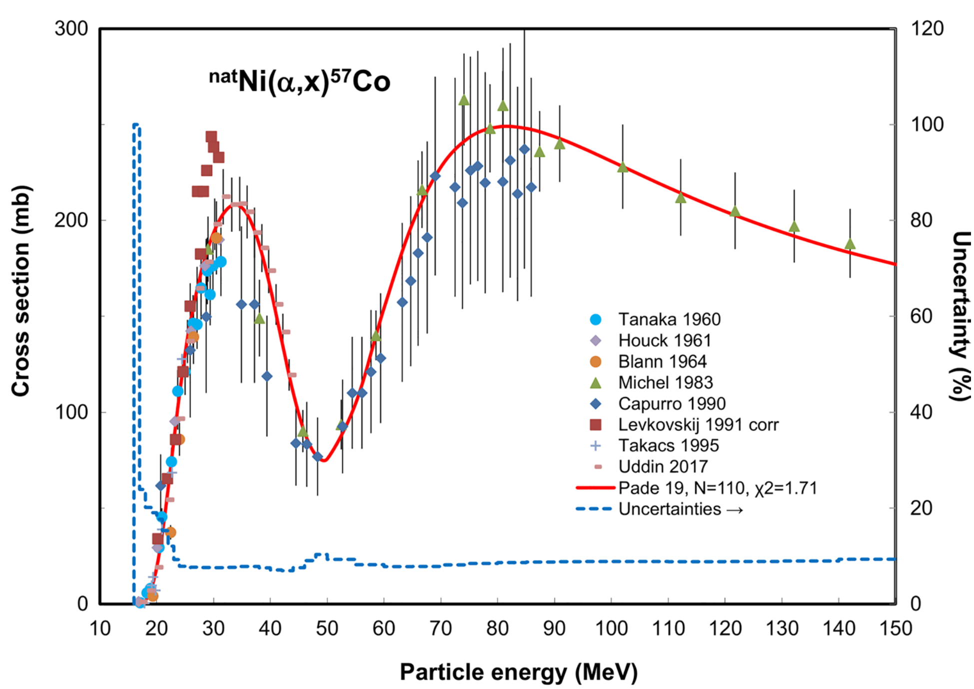

Fig. 100 ^{nat}Ni(α,x)^{57}Co reaction: selected experimental works and Padé fit (solid line) with total derived uncertainties, including 4% systematic uncertainty (dashed line, right-hand scale)

Blann [293], Muramatsu [294], Michel [153], Capurro [299], Levkovskii [130], Paul [289], Takacs [295], Uddin [297].

The two outlying data sets of Muramatsu 1978 and Paul 1995 were deselected. To be in acceptable agreement with the other data the set of Levkovskii 1991 was multiplied by a factor of two while the set of Blann 1964 was energy shifted. The too high data points at 17 MeV of Michel 1983 and Capurro 1990 were deleted.

The original and corrected datasets of 8 publications were selected and fitted up to 150 MeV (Fig. 100). The increase of the excitation function above 50 MeV is due to the reactions with single particle emissions.

As already remarked in the previous section the two TENDL predictions confirm the double region excitation function but are energy-shifted and oppositely describe the relative importance of clustered and single particle emissions. The integral yields calculated from the recommended cross sections are shown in Fig. 111. A single experimental yield data point is available: Paul [289].

$^{nat}Ni(\alpha,x)^{60}Cu$ reaction

In principle five (α,pxn) reactions on the stable target isotopes ^{58}Ni (abundance 68.077% in ^{nat}Ni, x = 1), ^{60}Ni (abundance 26.223% in ^{nat}Ni, n = 3), ^{61}Ni (abundance 1.1399% in ^{nat}Ni), ^{62}Ni (abundance 3.6346% in ^{nat}Ni), ^{64}Ni (abundance 0.9255% in ^{nat}Ni) can contribute to direct formation of ^{60}Cu if high energy α-particle bombardment is performed. The threshold of the $^{58}Ni(\alpha,pn)^{60}Cu$ reaction is 15.730 MeV while the reaction with clustered particle emission $^{58}Ni(\alpha,d)^{60}cu$ can start at 13.369 MeV. Depending on the cooling time before measurement contribution of the shorter-lived ^{60}Zn ($T_{1/2}$ = 2.38 min), formed by $^{nat}Ni(\alpha,xn)$ reactions with as lowest threshold 20.988 MeV, can contribute.

A total of 8 cross section data sets, covering the energy range from threshold up to 50 MeV, were found in literature and are displayed in Fig. 101: Tanaka ser 1–2 [291], Muramatsu [294], Levkovskii [130], Takacs [295], Yadav [300], Uddin [301], Takacs [298]. The three outlying and energy-shifted sets of Tanaka 1960 ser1, Levkovskii 1991 and. Yadav 2008 (all obtained on ^{58}Ni targets but published results normalized to ^{nat}Ni) were deselected. The values in Uddin 2018 are too low and were multiplied by a factor of 1.3. The original and corrected datasets of 4 publications were selected up to 50 MeV and fitted (Fig. 102). Both TENDL predictions are representing well the overall excitation function. The integral yields calculated from the recommended cross sections are shown in Fig. 111. A single experimental yield data is available: Muramatsu [294].

$^{nat}Ni(\alpha,x)^{61}Cu$ reaction

As in 2020 updated abundances for the different γ-lines emitted in the decay of ^{61}Cu were adopted in NUDAT3.0 (see Table 2) nearly all data sets published before 2020 had to be attentively checked and corrections for used absolute abundances or ratios made. Moreover, new relative intensity values for the 656.008 keV line were found in a well-documented study published by Bleuel [174]. However, the ratio of the 656.008 keV (10.4%) to 282.956 keV (12.7%) intensities used in the present evaluation (ratio 0.820 (140), see Table 3) only differs by 3% from the proposed Bleuel 2021 data (ratio 0.793 (10)). On the other side practically in

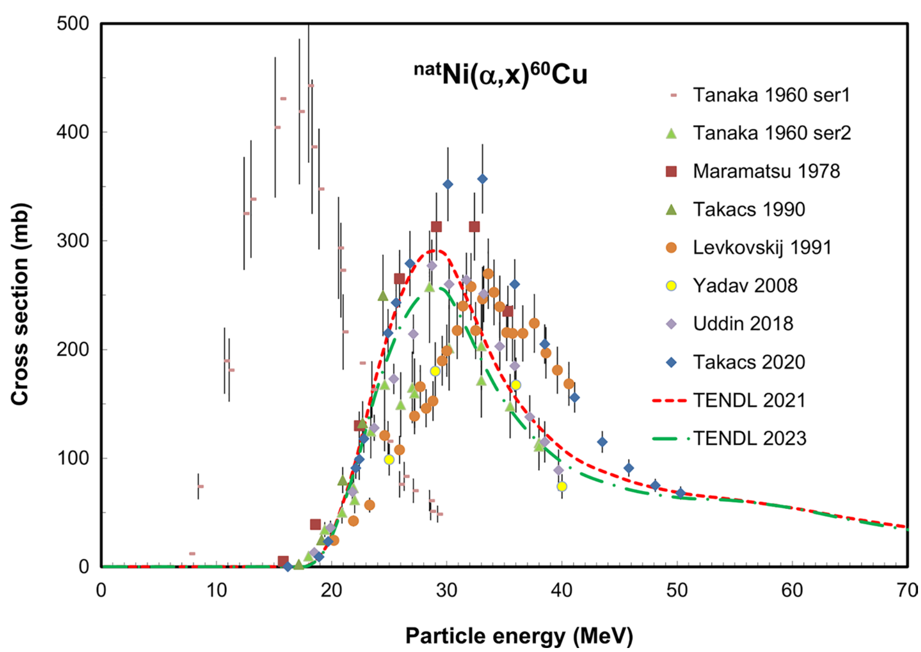

Fig. 101 $^{nat}Ni(\alpha,x)^{60}Cu$ reaction: all experimental data and the TENDL theoretical excitation functions

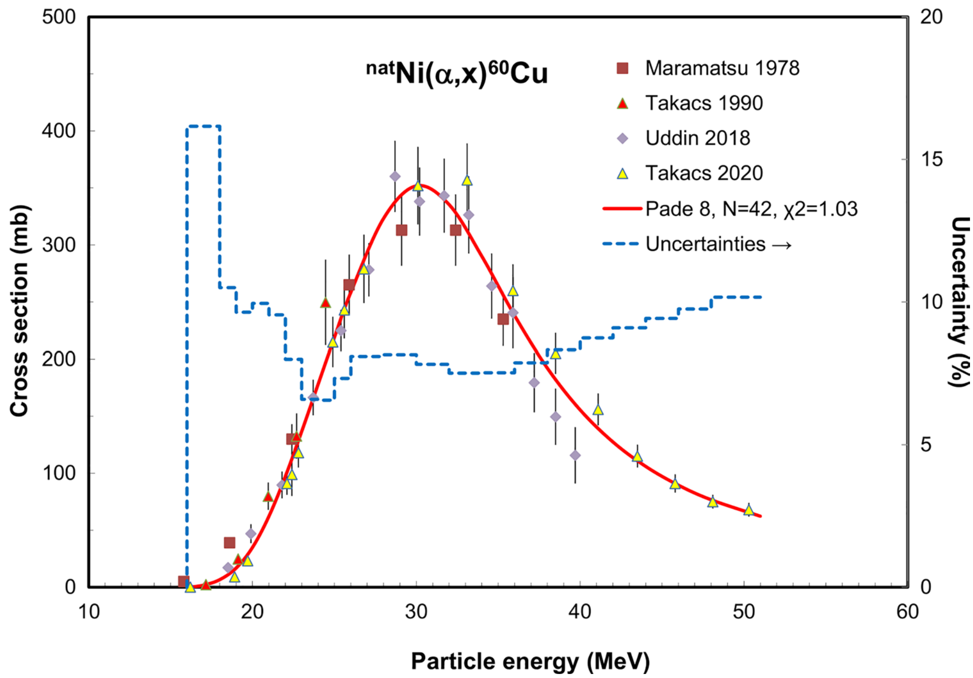

Fig. 102 $^{nat}Ni(\alpha,x)^{60}Cu$ reaction: selected experimental works and Padé fit (solid line) with total derived uncertainties, including 4% systematic uncertainty (dashed line, right-hand scale)

all compiled work, the cross section data were corrected by using the 282.956 keV line, when it was possible. Possible additional corrections for a new update of ENSDF accepted absolute abundance will hence be well within the 10–12% uncertainties on the used experimental data and the change in fit and recommended values will be small.

In principle five (α,pxn) reactions on the stable target isotopes ^{58}Ni (abundance 68.077% in ^{nat}Ni, x = 0), ^{60}Ni (abundance 26.223% in ^{nat}Ni, n = 2), ^{61}Ni (abundance 1.1399% in ^{nat}Ni), ^{62}Ni (abundance 3.6346% in ^{nat}Ni), ^{64}Ni (abundance 0.9255% in ^{nat}Ni) can contribute to direct formation of ^{57}Ni if high energy α-particle bombardment is performed. The threshold of the $^{58}Ni(\alpha,p)^{61}Cu$ reaction is 3.300 MeV while the reaction with clustered particle emission $^{60}Ni(\alpha,^{3}H)^{61}Cu$ can start at 15.903 MeV. As the half-life of the parent ^{61}Zn ($T_{1/2}$ = 89.1 s) is very short and is formed by the $^{58}Ni(\alpha,n)^{61}Cu$ reaction with a positive Q-value of 3.364 MeV, probably always cumulative formation of ^{61}Cu will be measured. All measured cross sections have hence to be assumed as for ^{61}Cu(cum).

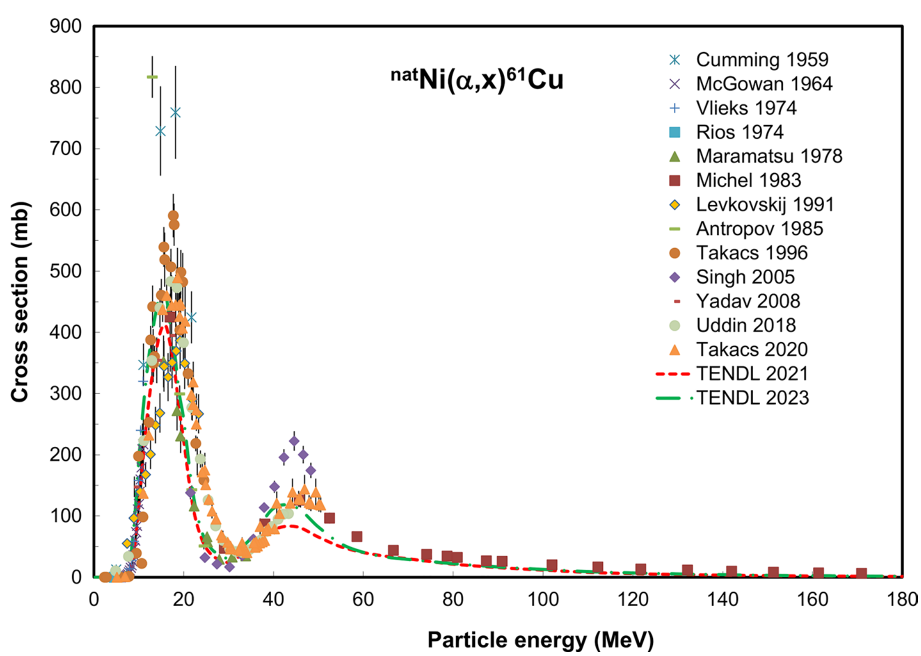

Fig. 103 $^{nat}Ni(\alpha,x)^{61}Cu$ reaction: all experimental data and the TENDL theoretical excitation functions

A total of 13 cross section data sets, covering the energy range from threshold up to 170 MeV, were found in the literature and are displayed in Fig. 103:

Cumming [302], McGowan [303], Vlieks [304], Rios [305], Muramatsu [294], Michel [153], Levkovskii [130], Antropov [115], Takacs [295], Singh [296], Yadav [300], Uddin [301], Takacs [298].

The outlying data sets of Cumming 1959, Muramatsu 1978, Antropov 1985, Levkovskii 1991, and Singh 2005 were deselected. The original datasets of the remaining 8 publications were selected and fitted up to 100 MeV (Fig. 104).

The two TENDL predictions describe well the overall shape of the excitation function but are energy-shifted and give too low maximal values. The integral yields calculated from the recommended cross sections are shown in Fig. 111. Three experimental yield data are available: Muramatsu [294], Abe [84] and Paul [289].

$^{nat}Ni(\alpha,x)^{62}Zn$ reaction

In principle four (α,xn) reactions on the stable target isotopes ^{60}Ni (abundance 26.223% in ^{nat}Ni, n = 2), ^{61}Ni (abundance 1.1399% in ^{nat}Ni), ^{62}Ni (abundance 3.6346% in ^{nat}Ni), ^{64}Ni (abundance 0.9255% in ^{nat}Ni) can contribute to direct formation of ^{62}Zn if high energy α-particle bombardment is performed. The threshold of the $^{60}Ni(\alpha,2n)^{62}Zn$ reaction is 18.031 MeV.

A total of 12 cross section data sets, covering the energy range from threshold up to 122 MeV, were found in the literature and are displayed in Fig. 105: Ghoshal [306], Tanaka [291], Neirinckx [307], Muramatsu [294], Michel [153], Levkovskii [130], Paul [289], Takacs [295], Singh [296], Yadav [300], Uddin [297], Takacs [298]. The outlying sets of Ghoshal 1950, Muramatsu 1978 and Singh 2005 were deleted.

As the data of Neirinckx 1977 follow the shape of the excitation function but are energy shifted a linearly decreasing positive correction was applied (highest energy point at 31.9 MeV maintained). Data points at specific energies were deleted in two sets: Michel 1983 (at 16.96 and 29.02 MeV) and Takács 2020 (at 50.5 MeV). The original and corrected datasets of the remaining 9 publications were selected and fitted up to 120 MeV (Fig. 106). The TENDL predictions describe well the overall shape of the excitation function but are energy-shifted and give a too low maximum value. The integral yields calculated from the recommended cross sections are shown in Fig. 111. Two experimental yield data are available: Neirinckx [307], Paul [289].

$^{nat}Ni(\alpha,x)^{63}Zn$ reaction

In principle four (α,xn) reactions on the stable targets ^{60}Ni (abundance 26.223% in ^{nat}Ni, n = 1), ^{61}Ni (abundance 1.1399% in ^{nat}Ni), ^{62}Ni (abundance 3.6346% in ^{nat}Ni), ^{64}Ni (abundance 0.9255% in ^{nat}Ni) can contribute to direct formation of short-lived ^{63}Zn if high energy α-particle bombardment is performed. The threshold of the $^{60}Ni(\alpha,n)^{63}Zn$ reaction is 8.374 MeV.

A total of 9 cross section data sets, covering the energy range from threshold up to 51 MeV, were found in the literature and are displayed in Fig. 107: Ghoshal [306], Cumming

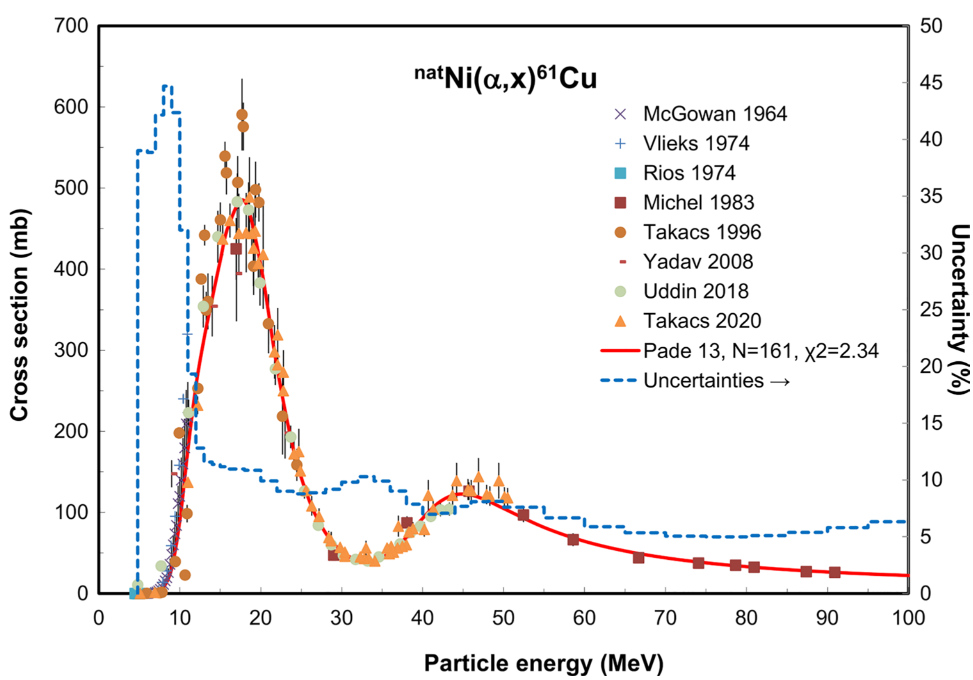

Fig. 104 $^{nat}Ni(\alpha,x)^{61}Cu$ reaction: selected experimental works and Padé fit (solid line) with total derived uncertainties, including 4% systematic uncertainty (dashed line, right-hand scale)

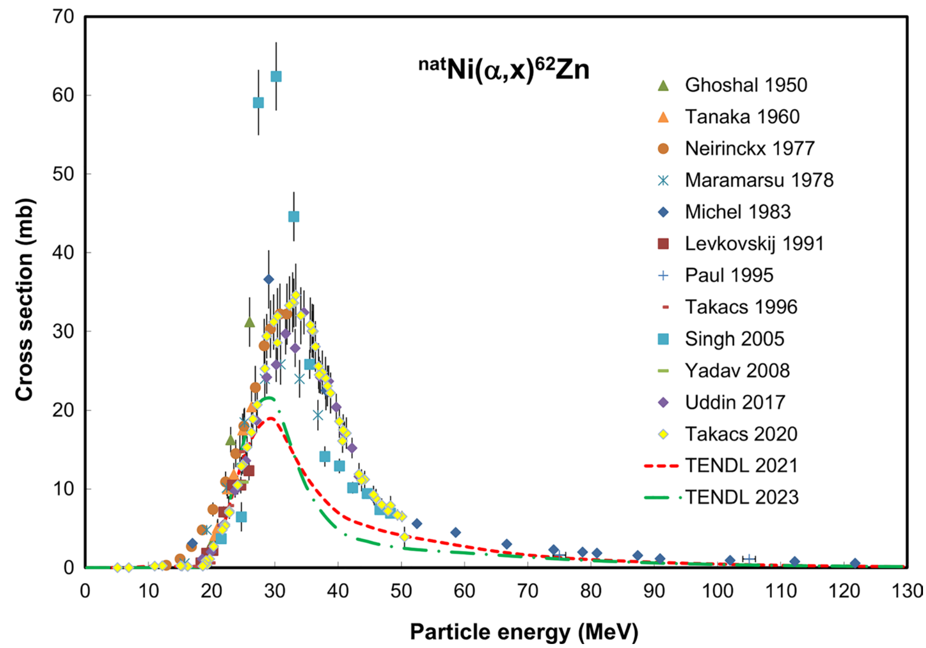

Fig. 105 $^{nat}Ni(\alpha,x)^{62}Zn$ reaction: all experimental data and the TENDL theoretical excitation functions

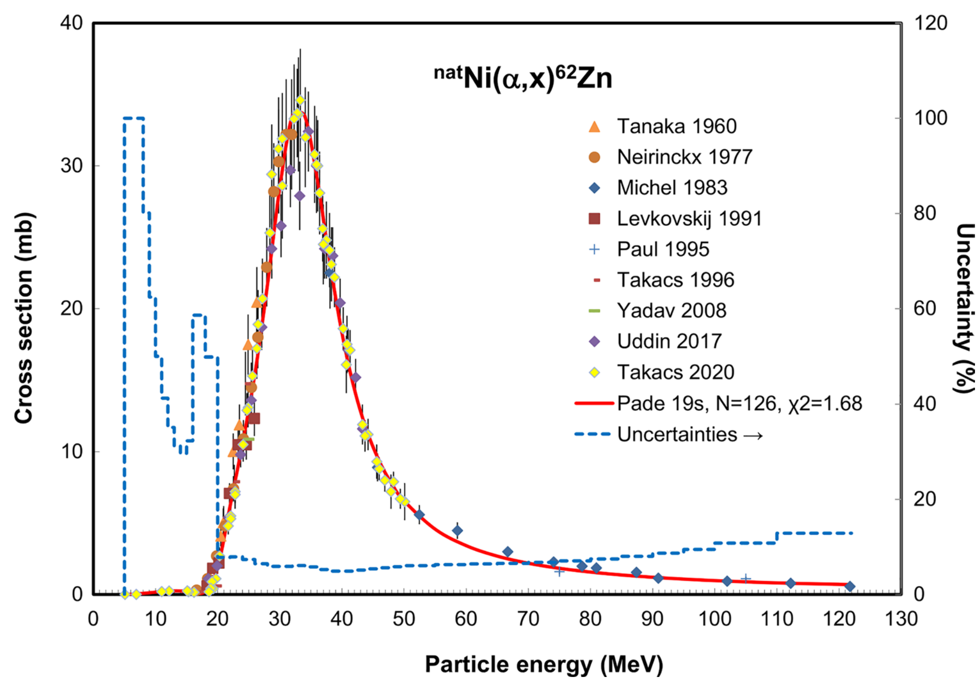

Fig. 106 $^{nat}Ni(\alpha,x)^{62}Zn$ reaction: selected experimental works and Padé fit (solid line) with total derived uncertainties, including 4% systematic uncertainty (dashed line, right-hand scale)

[302], Tanaka [291], Stelson [308], Muramatsu [294], Levkovskii [130], Takacs [295], Uddin [297], Takacs [298].

As the overall shape of the excitation function is acceptable but the cross section values near the maximum at 18 MeV are too low for three sets a correction was performed before selection: Muramatsu 1978 (is multiplied by a factor of 1.3), Levkovskii 1991 (multiplied by a factor of 2) and Uddin 2017 (multiplied by a factor of 1.3). Additionally, some outlying data points at specific energies were deleted: Goshal 1950 (at 12.6 and 15.4 MeV) and Levkovskii 1991 (at 7.4, 8.9 and 10.4 MeV). The original and corrected datasets of the 9 publications were selected up to 51 MeV and fitted (Fig. 108). The two TENDL predictions describe properly the overall shape of the excitation function but are energy-shifted and give too low maximal values. The integral yields calculated from the recommended cross sections are shown in Fig. 111. No experimental yield data are available.

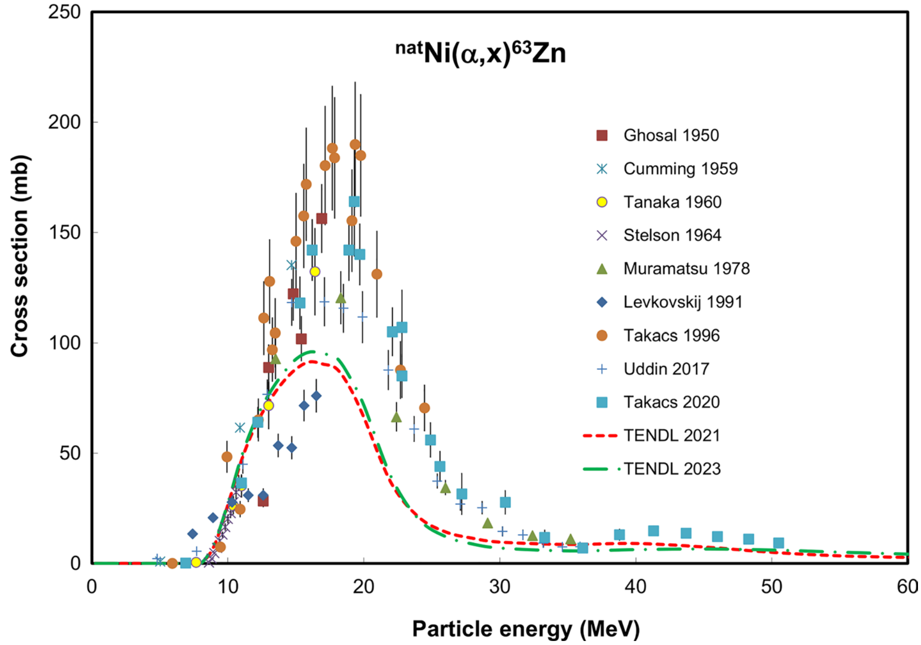

Fig. 107 $^{nat}Ni(\alpha,x)^{63}Zn$ reaction: all experimental data and the TENDL theoretical excitation functions

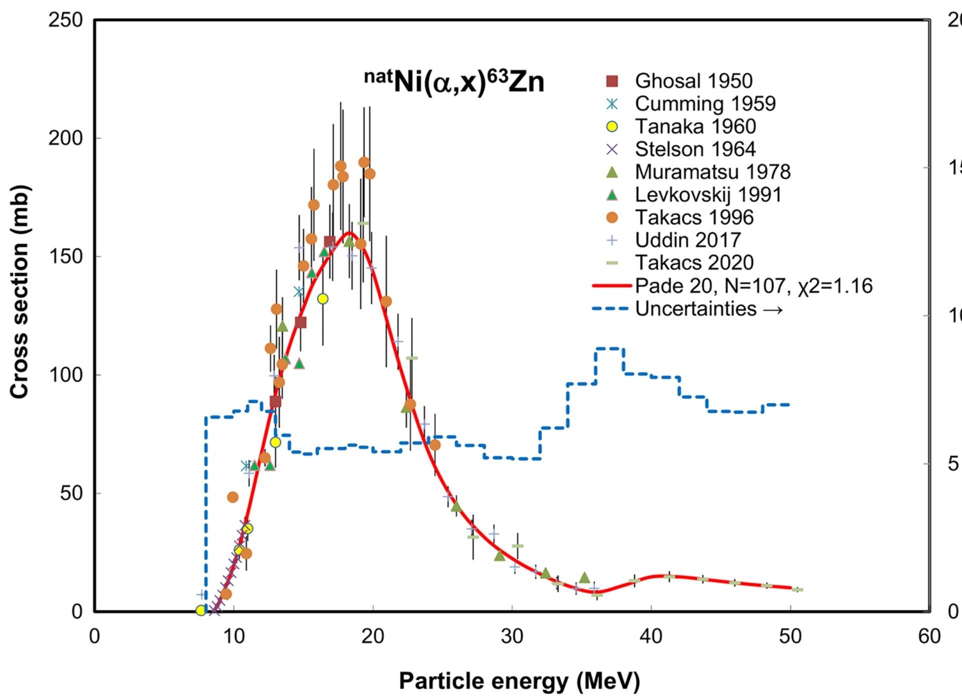

Fig. 108 $^{nat}Ni(\alpha,x)^{63}Zn$ reaction: selected experimental works and Padé fit (solid line) with total derived uncertainties, including 4% systematic uncertainty (dashed line, right-hand scale)

$^{nat}Ni(\alpha,x)^{65}Zn$ reaction

Only two (α,xn) reactions on the stable target isotopes ^{62}Ni (abundance 3.6346% in ^{nat}Ni), ^{64}Ni (abundance 0.9255% in ^{nat}Ni) can contribute to the direct formation of long-lived ^{65}Zn if α-particle bombardment is performed. The threshold of the $^{62}Ni(\alpha,n)^{65}Zn$ reaction is 6.850 MeV while the reaction on very low abundance ^{64}Ni can start at 24.240 MeV.

A total of 8 cross section data sets, covering the energy range from threshold up to 88 MeV, were found in the literature and are displayed in Fig. 109: Tanaka [291], Stelson [308], Muramatsu [294], Zyskind [309], Michel [153], Levkovskii [130], Takacs [295], Uddin [297].

The energy shifted and too low set of Levkovskii 1991 was deselected. The 5 data points of Muramatsu 1978 between 9 and 22.5 MeV were deleted. The original and corrected datasets of 7 publications, showing the contribution of

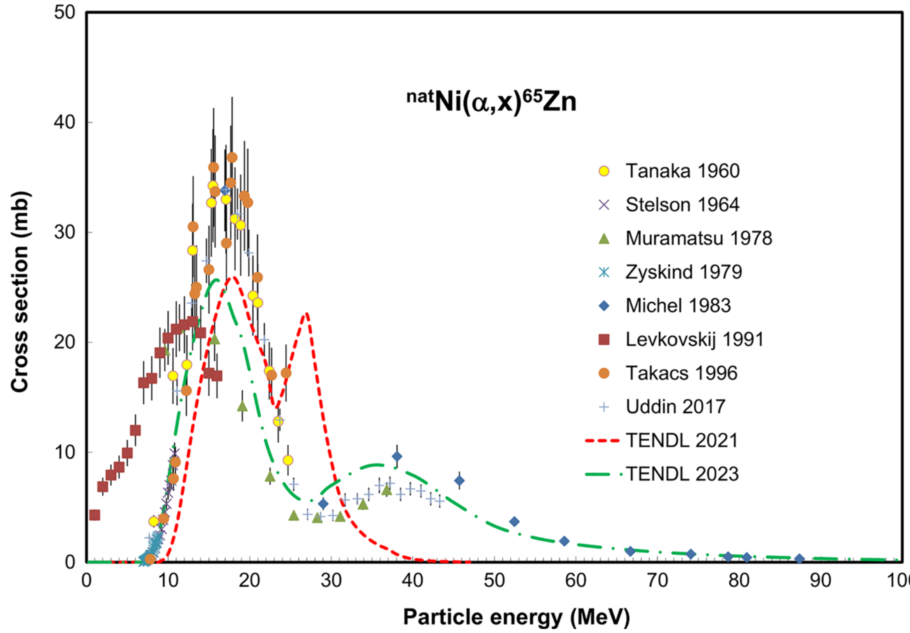

Fig. 109 $^{nat}Ni(\alpha,x)^{65}Zn$ reaction: all experimental data and the TENDL theoretical excitation functions

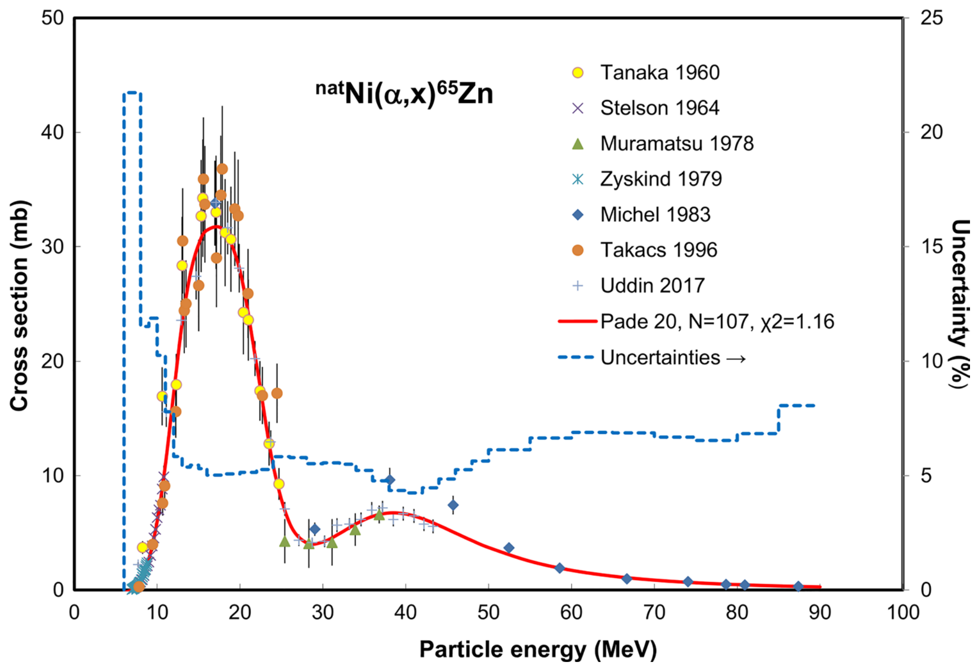

Fig. 110 $^{nat}Ni(\alpha,x)^{65}Zn$ reaction: selected experimental works and Padé fit (solid line) with total derived uncertainties, including 4% systematic uncertainty (dashed line, right-hand scale)

the two reactions in separate energy domains, were selected up to 88 MeV and fitted (Fig. 110). The TENDL 2023 predictions agree well with the overall shape and values. The TENDL 2021 description is acceptable up to 25 MeV, but the prediction of the higher energy part is too sharp and overestimated. The integral yields calculated from the recommended cross sections are shown in Fig. 111. No experimental yield data are available.

$^{nat}Mo(\alpha,xn)^{95}Ru$ reaction

In principle seven (α,xn) reactions on the stable target isotopes ^{92}Mo (abundance 14.53% in ^{nat}Mo, n = 1), ^{94}Mo (abundance 9.15% in ^{nat}Mo, n = 3), ^{95}Mo (abundance 15.84% in ^{nat}Mo, n = 4), ^{96}Mo (abundance 16.67% in ^{nat}Mo, n = 5), ^{97}Mo (abundance 9.60% in ^{nat}Mo), ^{98}Mo (abundance 24.39% in ^{nat}Mo), ^{100}Mo (abundance 9.82% in ^{nat}Mo, n = 9) can contribute to formation of ^{95}Ru if high energy α-particle bombardment is performed.

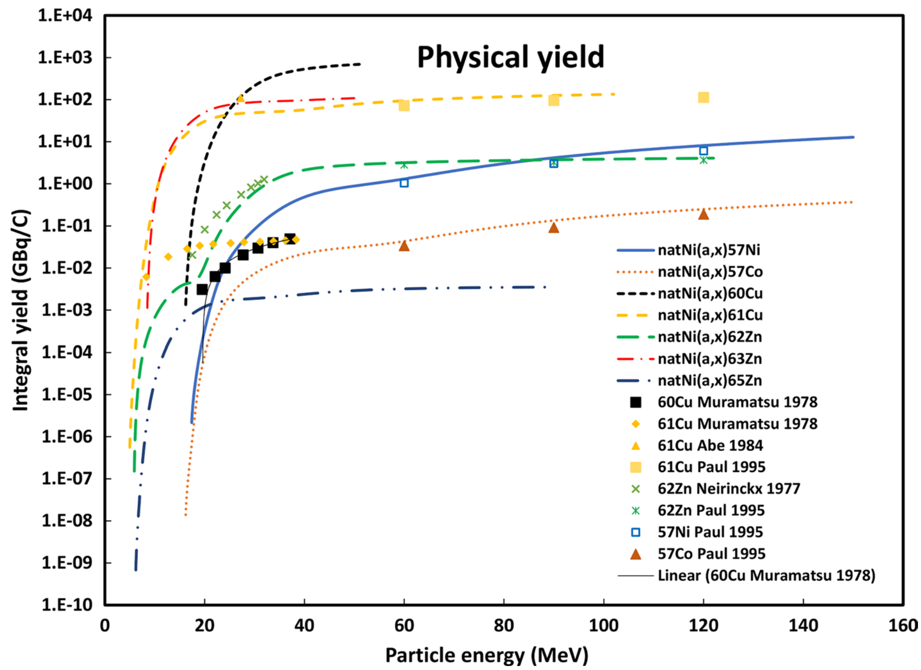

Fig. 111 Yield calculated from the recommended cross sections of the $^{nat}Ni(\alpha,x)^{57}Ni$, $^{nat}Ni(\alpha,x)^{57}Co$, $^{nat}Ni(\alpha,x)^{60}Cu$, $^{nat}Ni(\alpha,x)^{61}Cu$, $^{nat}Ni(\alpha,x)^{62}Zn$, $^{nat}Ni(\alpha,x)^{63}Zn$ and $^{nat}Ni(\alpha,x)^{65}Zn$ reactions

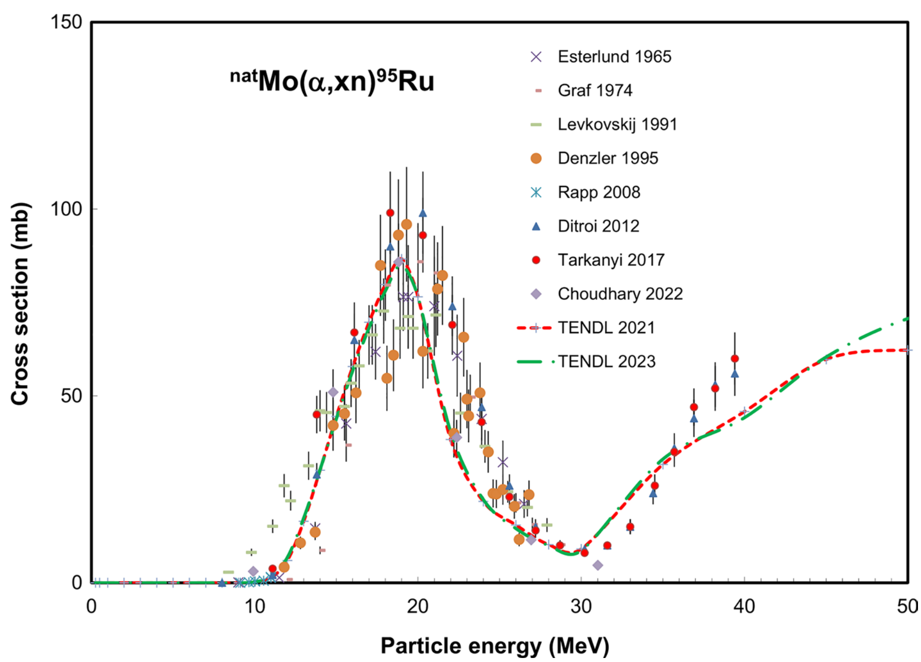

Fig. 112 $^{nat}Mo(\alpha,xn)^{95}Ru$ reaction: all experimental data and the TENDL theoretical excitation function

The threshold for the $^{92}Mo(\alpha,n)^{95}Ru$ reaction is 9.321 MeV, for the $^{94}Mo(\alpha,3n)^{95}Ru$ reaction it is 27.682 MeV and it rises to 75.321 MeV for the $^{100}Mo(\alpha,9n)^{95}Ru$ reaction.

A total of 8 cross section data sets, covering the energy range from threshold up to 40 MeV, were found in literature and are displayed in Fig. 112: Esterlund [310], Graf [311], Levkovskii [130], Denzler [312], Rapp [313], Ditroi [314], Tarkanyi [315], Choudhary [316]. All datasets were selected, showing the single contribution of the $^{92}Mo(\alpha,n)^{95}Ru$ reaction up to 28 MeV, and fitted (Fig. 113). The TENDL predictions agree well with the shape and cross sections values of the experimental excitation function. The integral yields calculated from the recommended cross sections are shown in Fig. 118. A single experimental yield data point is available: Abe [84].

$^{nat}Mo(\alpha,xn)^{96g}Tc$ (m+) reaction

In principle six (α,pxn) reactions on the stable target isotopes ^{94}Mo (abundance 9.15% in ^{nat}Mo, n = 1), ^{95}Mo (abundance

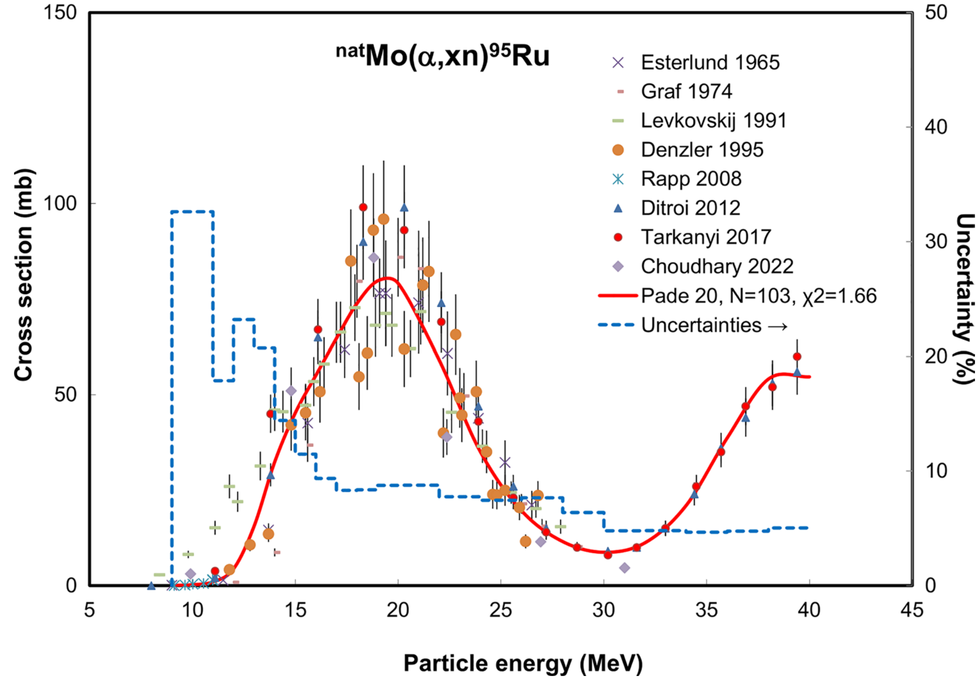

Fig. 113 $^{nat}Mo(\alpha,xn)^{95}Ru$ reaction: selected experimental works and Padé fit (solid line) with total derived uncertainties, including 4% systematic uncertainty (dashed line, right-hand scale)

15.84% in ^{nat}Mo, n = 2), ^{96}Mo (abundance 16.67% in ^{nat}Mo, n = 3), ^{97}Mo (abundance 9.60% in ^{nat}Mo), ^{98}Mo (abundance 24.39% in ^{nat}Mo), ^{100}Mo (abundance 9.82% in ^{nat}Mo, n = 7) can contribute to the formation of ^{96}Tc if high energy α-particle bombardment is performed. The formation of ^{96}Tc will always be a cumulative ground state as the short-lived metastable state ($T_{1/2}$ = 51.5 min) decays for 98% by IT to ^{96g}Tc.

The threshold for the $^{94}Mo(\alpha,pn)^{96}Tc$ reaction is 16.072 MeV, for the $^{95}Mo(\alpha,p2n)^{96}Tc$ reaction it is 23.689 MeV (reduced to 14.914 MeV for the clustered emission $^{95}Mo(\alpha,^{3}H)$ reaction) and it rises to 63.739 MeV for the $^{100}Mo(\alpha,p7n)^{96}Tc$ reaction.

A total of 4 cross section data sets, covering the energy range from threshold up to 67 MeV, were found in literature and are displayed in Fig. 114: Ditroi [314], Tarkanyi [315], Sitarz [317], Choudhary [316]. The outlying datapoint at 20 MeV of Tarkanyi 2017 was deleted. The original and corrected datasets of the 4 publications were selected and fitted up to 70 MeV (Fig. 115).

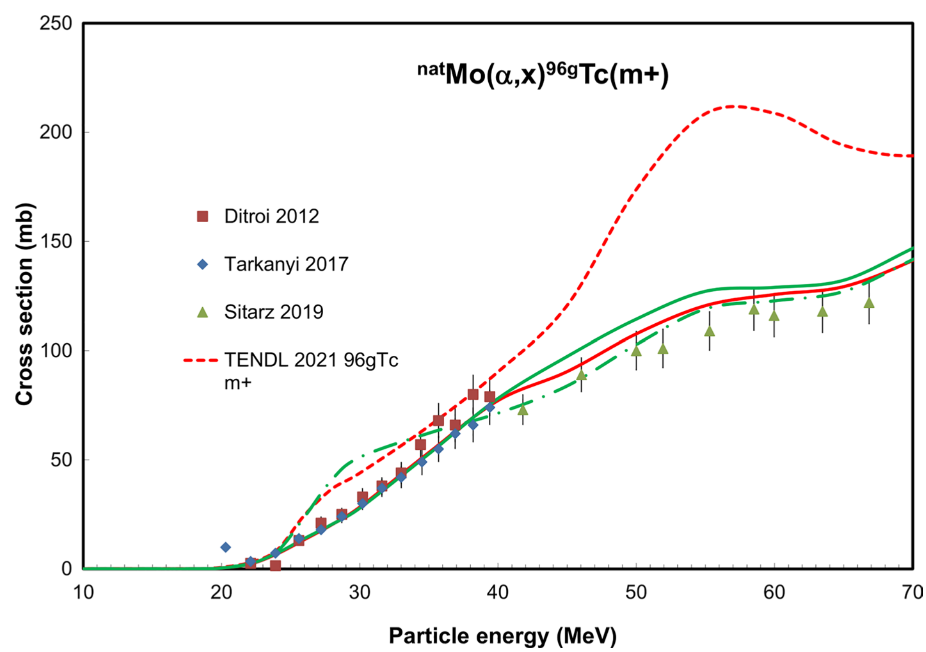

Fig. 114 $^{nat}Mo(\alpha,xn)^{96g}Tc$ m + reaction: all experimental data and the TENDL theoretical excitation functions

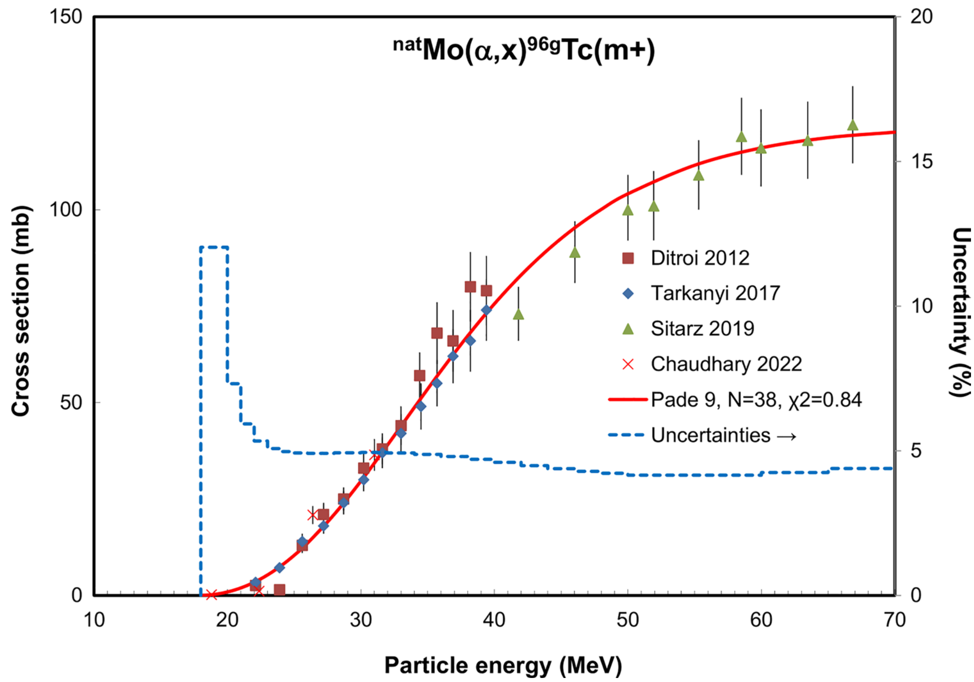

Fig. 115 $^{nat}Mo(\alpha,xn)^{96}Tc$ reaction: selected experimental works and Padé fit (solid line) with total derived uncertainties, including 4% systematic uncertainty (dashed line, right-hand scale)

The TENDL 2023 predictions are higher than the experimental values up to 40 MeV but agree well at higher energies. In the case of TENDL 2021 the values of the ^{96g}Tc m + are surprisingly higher compared to ^{96}Tc total, due to the overestimation of the production of the meta state (Fig. 114). The integral yields calculated from the recommended cross sections are shown in Fig. 118. A single experimental yield data point is available: Dmitriev [199].

$^{nat}Mo(\alpha,xn)^{97}Ru$ reaction

In principle seven (α,xn) reactions on the stable target isotopes ^{94}Mo (abundance 9.15% in ^{nat}Mo, n = 1), ^{95}Mo (abundance 15.84% in ^{nat}Mo, n = 2), ^{96}Mo (abundance 16.67% in ^{nat} Mo, n = 3), ^{97}Mo (abundance 9.60% in ^{nat} Mo), ^{98}Mo (abundance 24.39% in ^{nat} Mo), ^{100}Mo (abundance 9.82% in ^{nat} Mo, n = 7) can contribute to formation of ^{97}Ru if high energy α-particle bombardment is performed.

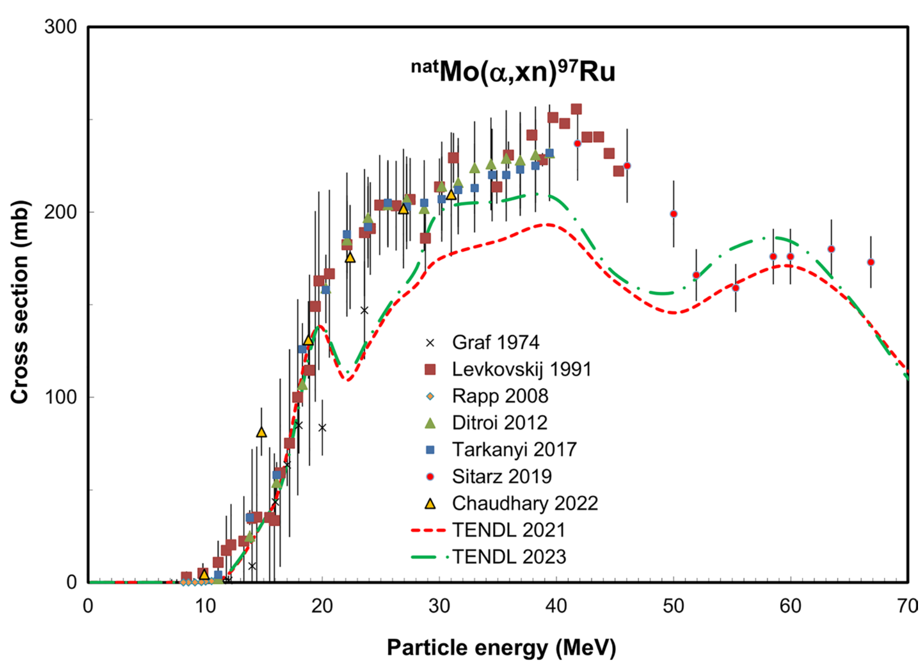

Fig. 116 $^{nat}Mo(\alpha,xn)^{97}Ru$ reaction: all experimental data and the TENDL theoretical excitation functions

The threshold for the $^{94}Mo(\alpha,n)^{97}Ru$ reaction is 8.218 MeV and it rises to 55.905 MeV for the $^{100}Mo(\alpha,7n)^{97}Ru$ reaction.

A total of 6 cross section data sets, covering the energy range from threshold up to 67 MeV, were found in the literature and are displayed in Fig. 116: Graf [311], Levkovskii [130], Rapp [313], Ditroi [314], Tarkanyi [315], Sitarz [317], Choudhary [316]. The set of Graf 1974 with too low values was deselected. The two outlying data points of Chaudhary 2022 at 10 and 16 MeV were deleted.

The original and corrected datasets of 6 publications were selected up to 67 MeV and fitted (Fig. 117). The two TENDL predictions show more explicitly the contributions of the reactions on the different stable target isotopes but are from 20 MeV on underestimating the cross section values. The integral yields calculated from the recommended cross

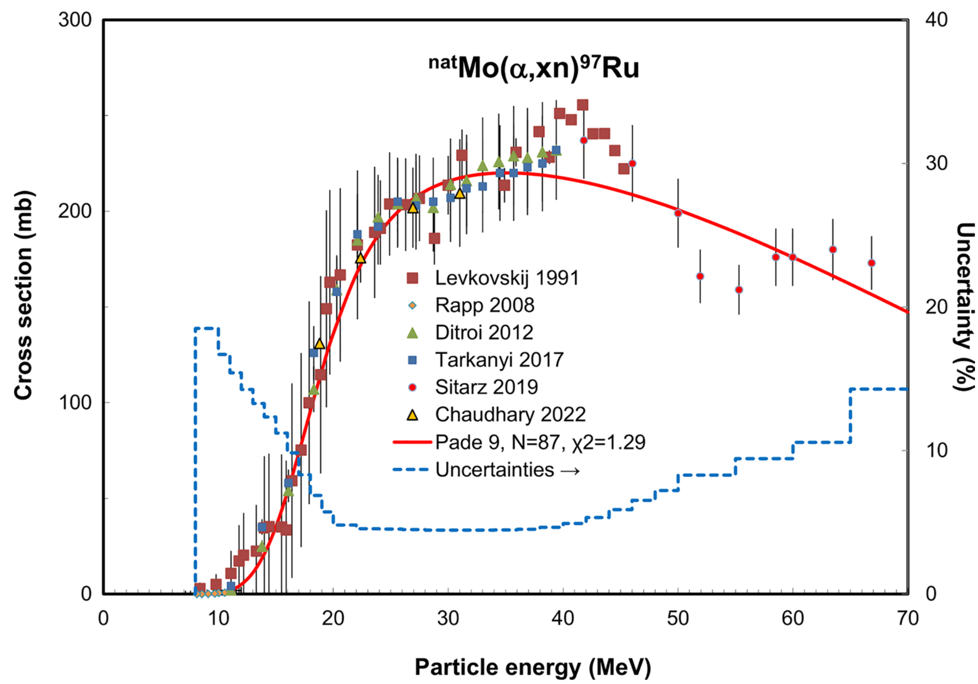

Fig. 117 $^{nat}Mo(\alpha,xn)^{97}Ru$ reaction: selected experimental works and Padé fit (solid line) with total derived uncertainties, including 4% systematic uncertainty (dashed line, right-hand scale)

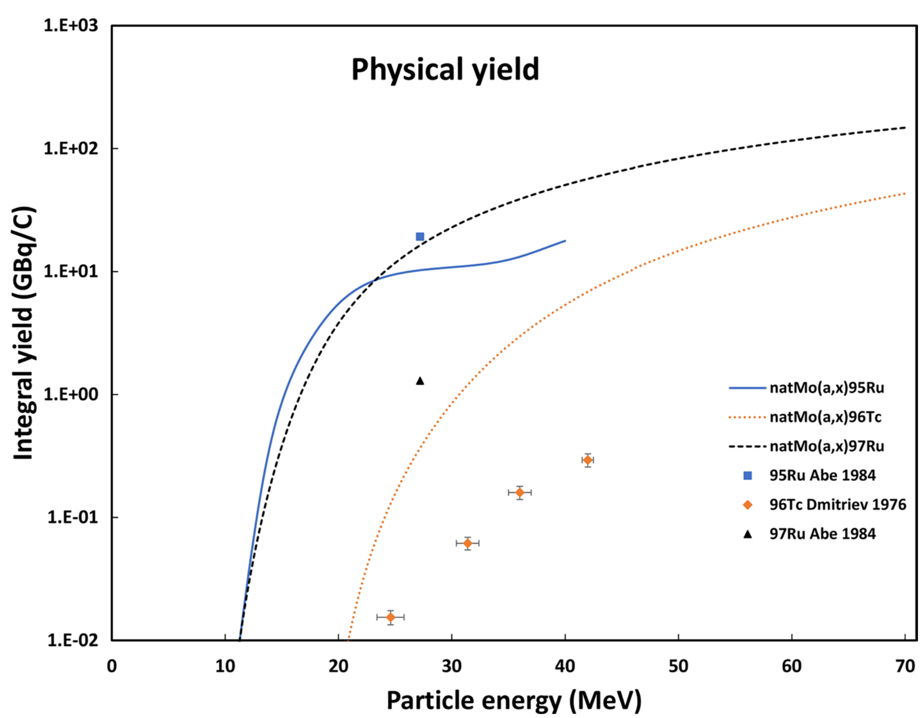

Fig. 118 Yield calculated from the recommended cross sections of the $^{nat}Mo(\alpha,xn)^{95}Ru$, $^{nat}Mo(\alpha,x)^{96}Tc$ and $^{nat}Mo(\alpha,xn)^{97}Ru$ reactions

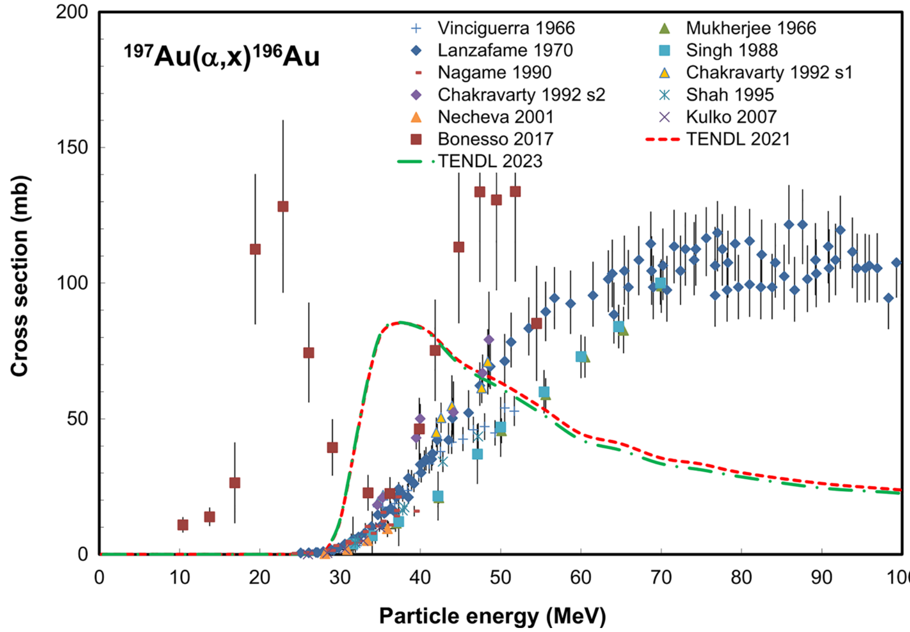

Fig. 119 ^{197}Au(α,x)^{196}Au reaction: all experimental data and the TENDL theoretical excitation functions

sections are shown in Fig. 118. A single experimental yield data point is available: Abe [84].

^{197}Au(α,x)^{196}Au reaction

Only the ^{197}Au(α,αn) reaction with a threshold of 8.175 MeV, or the reaction with not clustered emission ^{197}Au(α,2p3n) with a threshold of 36.83 MeV, contributes to the formation of ^{196}Au. A total of 11 cross section data sets, covering the energy range from threshold up to 99 MeV, were found in the literature and are displayed in Fig. 119:

Vinciguerra [318], Mukherjee [319], Lanzafame [320], Singh [321], Nagame [208], Chakravarty s1-2 [322], Shah [323], Necheva [324], Kulko [325], Bonesso [326].

The sets of Mukherjee 1995 and Singh 1988 with too low values were deselected. Although the double-peaked set of Bonesso 2017 can be explained by the separate contribution of clustered and not clustered emission, this fact is not confirmed by all the other available data sets. A practical

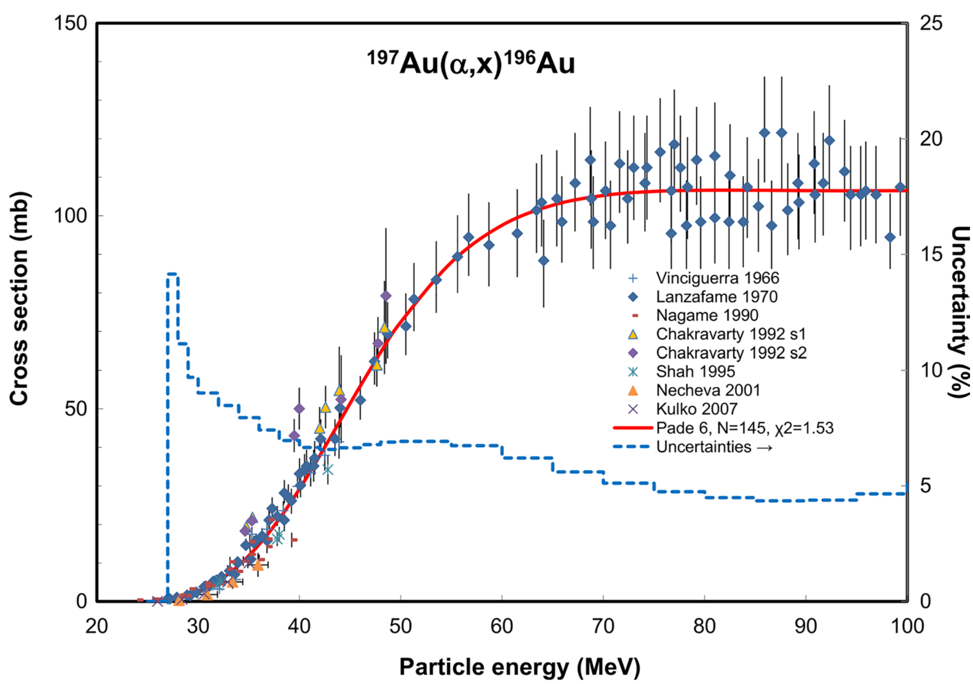

Fig. 120 ^{197}Au(α,x)^{196}Au reaction: selected experimental works and Padé fit (solid line) with total derived uncertainties, including 4% systematic uncertainty (dashed line, right-hand scale)

threshold of around 25 MeV is indicated by 10 publications and hence the set of Bonesso 2017 was deselected. The too low data points of Vinciguerra 1966 (last 6 points) and Shah 1995 (last point) were deleted. The original and corrected datasets of 8 publications were selected up to 99 MeV, the energy, and fitted (Fig. 120). The two TENDL predictions show a single peak near 38 MeV and do not correspond to the shape of the experimental excitation function. The integral yields calculated from the recommended cross sections are shown in Fig. 125. No experimental yield data are available.

^{197}Au(α,x)^{199}Tl reaction

Only the ^{197}Au(α,2n) reaction with a threshold of 17.01 MeV contributes to the formation of ^{199}Tl.

A total of 18 cross section data sets, covering the energy range from threshold up to 115 MeV, were found in literature

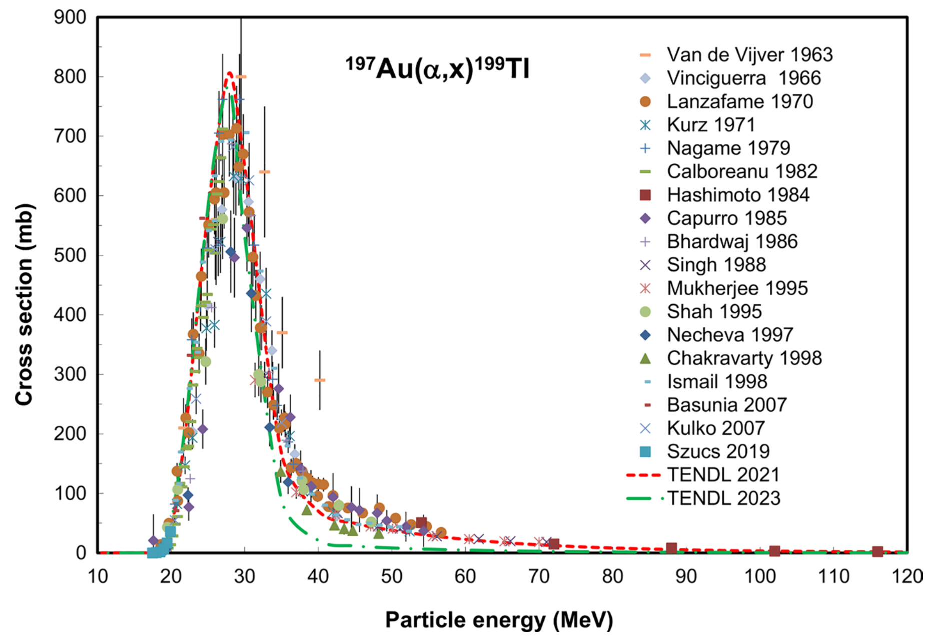

Fig. 121 ^{197}Au(α,x)^{199}Tl reaction: all experimental data and the TENDL theoretical excitation functions

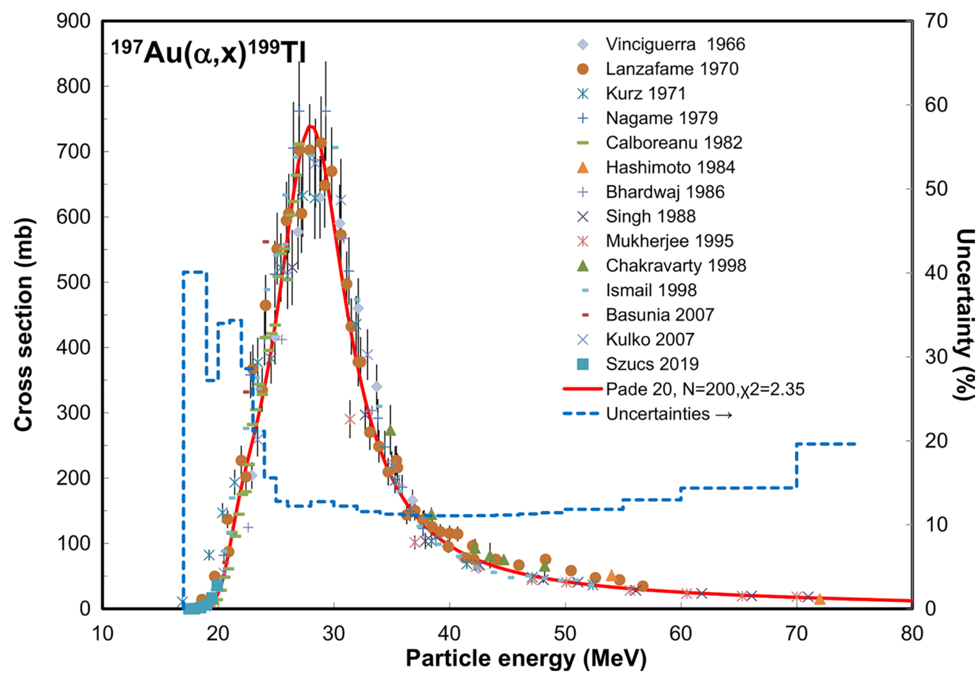

Fig. 122 ^{197}Au(α,x)^{199}Tl reaction: selected experimental works and Padé fit (solid line) with total derived uncertainties, including 4% systematic uncertainty (dashed line, right-hand scale)

and are displayed in Fig. 121: Van de Vijver [327], Vinciguerra [318], Lanzafame [320], Kurz [328], Nagame [208], Calboreanu [329], Hashimoto [330], Capurro [331], Bhardwaj [332], Singh [321], Mukherjee [319], Shah [323], Necheva [324], Chakravarty [333], Ismail [334], Basunia [335], Kulko [325], Szucs [336].

The 4 sets with too low values, especially in the rising part of the excitation function, of Van de Vijver 1963, Capurro 1985, Shah 1995 and Necheva 1997 were deselected. The set of Kurz 1971 was energy corrected while the data of Chakravarty 1998 were multiplied by a factor of 2.

The original and corrected datasets of 14 publications were selected and fitted up to 80 MeV (Fig. 122). The TENDL 2021 prediction is in very good agreement with the experimental excitation function while the 2023 version is too low above 30 MeV. The integral yields calculated from the recommended cross sections are shown in Fig. 125. No experimental yield data are available.

^{197}Au(α,n)^{200}Tl reaction

Only the ^{197}Au(α,n) reaction with a threshold of 9.86 MeV contributes to the formation of ^{200}Tl. A total of 18 cross section data sets, covering the energy range from threshold up to 80 MeV, were found in the literature and are displayed in Fig. 123: Van de Vijver [327], Vinciguerra [318], Lanzafame [320], Kurz [328], Nagame [208], Calboreanu [329], Capurro [331], Bhardwaj [332]. Singh [321], Mukherjee [319], Shah [323], Necheva [324], Chakravarty [333], Ismail [334], Basunia [335], Kulko [325], Sharma [337], Szucs [336].

The 8 sets giving maximal cross section values under 25 mb were deselected: Van de Vijver 1963, Vinciguerra 1966, Kurz 1971, Capurro 1985, Singh 1988, Ismai 1988, Shah 1995, Necheva 1997.

All data points in the remaining 10 publications were selected up to 80 MeV and fitted (Fig. 124). The two TENDL predictions represent well the overall shape of the excitation function but TENDL 2021 gives significantly higher cross sections. The integral yields calculated from the recommended cross sections are shown in Fig. 125. No experimental yield data are available.

Summary and conclusions

Evaluations of production cross sections and their uncertainties were performed on sixty reactions for charged particle beam monitor reactions on C, Al, Ti, Fe, Ni, Cu, Nb, Mo and Au targets. The experimental data in some cases show large disagreements and were selected based on many factors, not only statistically. In such a way the reliability of the recommended data is different for different reactions and the obtained uncertainties refer only to the selected data. Despite this, the deduced recommended data will be useful for different applications. Validation of the recommended data with properly made integral measurements would be very useful. The collected experimental data were compared with the theoretical predictions found in the TENDL-2021 and 2023 libraries, but still, in some cases, significant disagreements in the magnitude and shape of the resulting excitation functions exist (especially when considering isomeric states or deuteron-induced reactions).

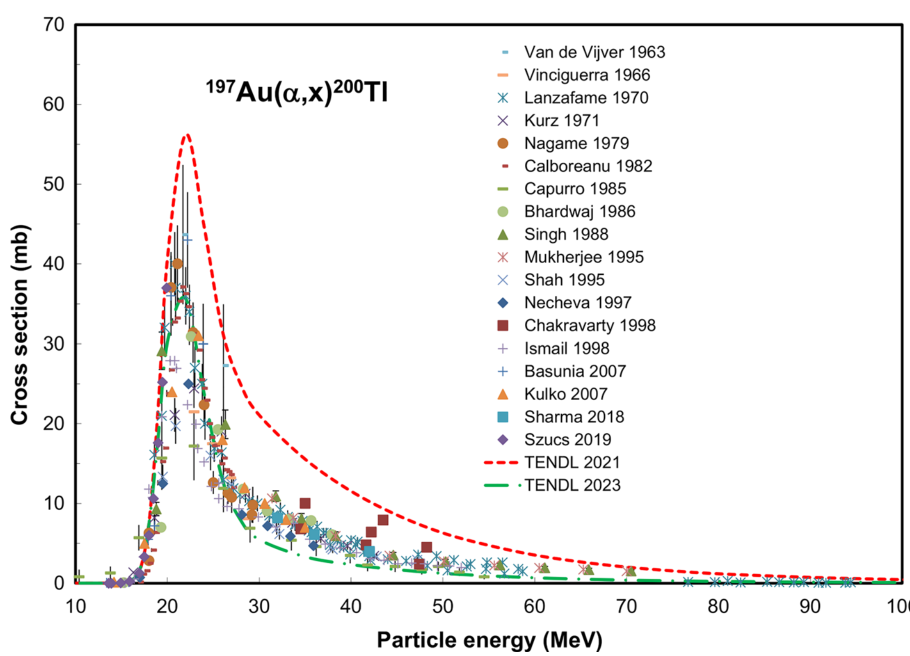

Fig. 123 ^{197}Au(α,x)^{200}Tl reaction: all experimental data and the TENDL theoretical excitation functions

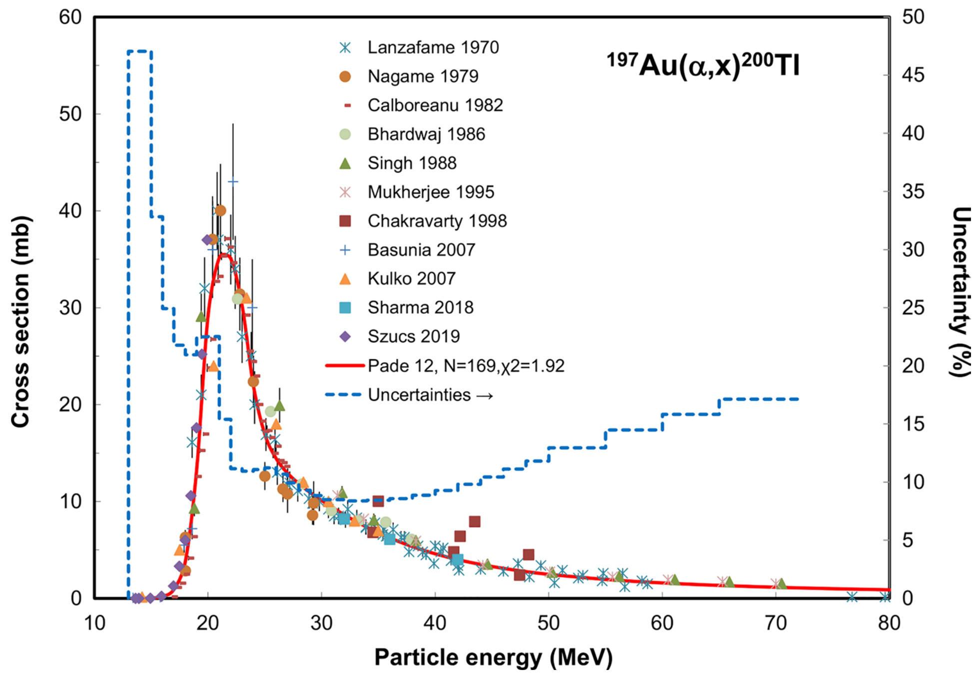

Fig. 124 ^{197}Au(α,x)^{200}Tl reaction: selected experimental works and Padé fit (solid line) with total derived uncertainties, including 4% systematic uncertainty (dashed line, right-hand scale)

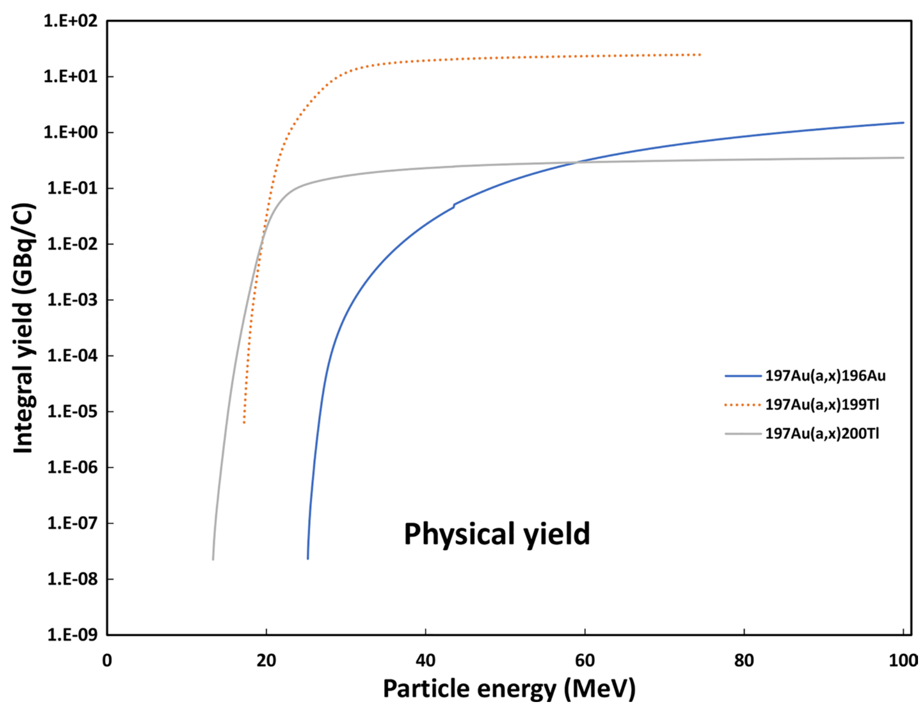

Fig. 125 Yield calculated from the recommended cross sections of the ^{197}Au(α,x)^{196}Au, ^{197}Au(α,x)^{199}Tl and ^{197}Au(α,x)^{200}Tl reactions

A Padé fitting method was applied to the selected datasets, and uncertainties for all recommended cross-section data were deduced. The recommended cross-section data have been used to determine integral yields for practical radionuclide production. In the literature, only very few experimental data and intercomparison exist to validate the recommended cross section data. The recommended cross section data and the deduced integral yields may also be useful in other fields of non-energy related nuclear studies (e.g., accelerator technology, activation analysis and thin layer activation) and further development of the theory of nuclear reactions.

Acknowledgements This work was partly supported by Project No. NKTA-42, which has been implemented with the support provided by the Ministry of Innovation and Technology of Hungary from the

National Research, Development and Innovation Fund, financed under the TKP2021 funding scheme.

Funding Open access funding provided by HUN-REN Institute for Nuclear Research.

References

1. Wiedemann H (2015) Particle accelerator physics, 4th edn. Springer International Publishing AG, Switzerland
2. Hermanne A, Ignatyuk AV, Capote R, Carlson BV, Engle JW, Kellett MA, Kibedi T, Kim G, Kondev FG, Hussain M, Lebeda O, Luca A, Nagai Y, Naik H, Nichols AL, Nortier FM, Suryanarayana SV, Takacs S, Tarkanyi FT, Verpelli M (2018) Reference cross sections for charged-particle monitor reactions. Nucl Data Sheets 148:338–382
3. IAEA (2001) Medical radioisotope database, IAEA, https://www-nds.iaea.org/medical/monitor_reactions.html
4. Gul K, Hermanne A, Mustafa MG, Nortier FM, Oblozinsky P, Qaim SM, Scholten B, Shubin YN, Takács S, Tárkányi F, Zhuang Y (2001) Charged particle cross-section database for medical radioisotope production diagnostic radioisotopes and monitor reactions. Charged particle cross-section database for medical radioisotope production: diagnostic radioisotopes and monitor reactions. Vienna, IAEA. IAEA-TECDOC-1211, http://www.nds.or.at/medical), IAEA, Vienna
5. Engle JW, Nichols AI, Capote Noy R (2018) Summary report : technical meeting on nuclear data for medical applications. IAEA, Vienna
6. Schwerer O, Okamoto K (1989) Status report on cross-sections of monitor reactions for radioisotope production. IAEA, Vienna
7. Otuka N, Dupont E, Semkova V, Pritychenko B, Blokhin AI, Aikawa M, Babykina S, Bossant M, Chen G, Dunaeva S, Forrest RA, Fukahori T, Furutachi N, Ganesan S, Ge Z, Gritzay OO, Herman M, Hlavač S, Katō K, Lalremruata B, Lee YO, Makinaga A, Matsumoto K, Mikhaylyukova M, Pikulina G, Pronyaev VG, Saxena A, Schwerer O, Simakov SP, Soppera N, Suzuki R, Takács S, Tao X, Taova S, Tárkányi F, Varlamov VV, Wang J, Yang SC, Zerkin V, Zhuang Y (2014) Towards a more complete and accurate experimental nuclear reaction data library (EXFOR): international collaboration between nuclear reaction data centres (NRDC). Nucl Data Sheets 120:272–276
8. NNDC (2022) NUDAT 3.0, Brookhaven National Laboratory, https://www.nndc.bnl.gov/nudat3/
9. NNDC (2020) Evaluated Nuclear Structure Data File (ENSDF), NNDC, https://www.nndc.bnl.gov/ensdf/
10. Pade HE (1892) Sur la représentation d'une fonction par des fractions rationnelles. Ann L'Ecole Norm 9:3–93
11. Baker GA Jr (1970) The padé approximants in theoretical physics. Academic Press, New York
12. Graves-Morris PR (1973) Padé approximants and their applications. Academic Press, New York
13. Otuka N, Takács S (2015) Definitions of radioisotope thick target yields. Radiochim Acta 103:1–6
14. Koning AJ, Rochman D, Sublet JC, Dzysiuk N, Fleming M, van der Marck S (2019) TENDL: complete nuclear data library for innovative nuclear science and technology. Nucl Data Sheets 155:1–55
15. Dickson JM, Randle TC (1951) The excitation function for the production of 7Be by the bombardment of 12C by protons. Proc Phys Soc Sect A 64:902
16. Lefort M, Simonoff GN, Tarrago X (1961) Re´actions nucle´aires de spallation induites sur le thorium par des protons de 150 et 82 MeV. Nucl Phys 25:216–247
17. Gauvin H, Lefort M, Tarrago X (1962) Emission of alpha particles in spallation reactions. Nuc Phys. https://doi.org/10.1016/0029-5582(62)90403-0
18. Brun C, Lefort M, Tarrago X (1962) Détermination des intensités de faisceaux de protons de 40 à 150 Mev. J Phys Radium 23:371–376
19. Rayudu GVS (1964) Formation cross sections of various radionuclides from Ni, Fe, Si, Mg, O, AND C for protons of energies between 130 and 400 MeV. Can J Chem 42:1149–1154
20. Vdovin AI, Golikov IG, Zhukov MN, Loschakov II, Ostroumov VI (1979) reaction cross-sections under influence of protons with 50 MeV energy on C-12, N-14, O-16 nuclei. Izv Akad Nauk Ser Fiz 43:148–150
21. Williams IR, Fulmer CB (1967) Cross section for formation of ^{7}Be by 20–155-MeV proton-induced reactions in carbon. Phys Rev 154:1005–1007
22. Aleksandrov VN (1990) The production of Be-7 at middle energy protons interaction with light nuclei. Vopr Atomn Nauki i Tekhn Ser Yad Fiz Issledo 8(16):17
23. Bodemann R, Lange H, Leya I, Michel R, Schiekel T, Rosel R, Herpers U, Hoffmann H, Dittrich B, Suter M, Wolfli W, Holmovist B, Conde H, Malmborg P (1993) Production of residual nuclei by proton-induced reactions on C N, O, MG, AL AND SI. Nucl Inst Methods Phys Res Sect B-Beam Inter Mater Atoms 82:9–31
24. Michel R, Bodemann R, Busemann H, Daunke R, Gloris M, Lange HJ, Klug B, Krins A, Leya I, Lüpke M, Neumann S, Reinhardt H, Schnatz-Büttgen M, Herpers U, Schiekel T, Sudbrock F, Holmqvist B, Condé H, Malmborg P, Suter M, Dittrich-Hannen B, Kubik PW, Synal HA, Filges D (1997) Cross sections for the production of residual nuclides by low- and medium-energy protons from the target elements C, N, O, Mg, Al, Si, Ca, Ti, V, Mn, Fe Co, Ni, Cu, Sr, Y, Zr, Nb, Ba and Au. Nucl Instrum Methods Phys Res Sect B 129:153–193
25. Fassbender M, Scholten B, Qaim S (1998) Radiochemical studies of (p,^{7}Be) reactions on biologically relevant elements in the proton energy range of 50 to 350 MeV. Radiochim Acta 81:1–10
26. Bäumer C, Bäcker C, Gerhardt M, Grusell E, Koska B, Kröninger K, Nitsch C, Rullkötter H, Siregar H, Timmermann B, Verbeek N, Wulff J, Yazgan A (2019) Measurement of absolute activation cross sections from carbon and aluminum for proton therapy. Nuc Inst Methods Phys Res Sect B-Beam Inter Mater Atoms 440:75–81
27. Bäcker C, Bäumer C, Gerhardt M, Kröninger K, Nitsch C, Siregar H, Timmermann B, Verbeek N, Weingarten J, Wulff J, Yazgan A (2019) Measurement of nuclear activation cross sections of protons on natural carbon for proton beam energies between 100 and 220 MeV. Nucl Inst Methods Phys Res Sect B-Beam Inter Mater Atoms 454:50–55

28. Hintz NM, Ramsey NF (1952) Excitation functions to 100 Mev. Phys Rev 88:19–27
29. Aamodt RL, Peterson V, Phillips R (1952) ^{12}C(p, pn)^{1}1C cross section from threshold to 340 Mev. Phys Rev 88:739–744
30. Burcham WE, Symonds JL, Young JD (1955) The production of 11C from carbon by protons of energy between 200 and 950 MeV. Proc Phys Soc Sect A 68:1001
31. Crandall WE, Millburn GP, Pyle RV, Birnbaum W (1956) C12(x, xn)C11 and Al27(x, x2pn)Na24 cross sections at high energies. Phys Rev 101:329–337
32. Measday DF (1966) The 12C(p, pn)11C reaction from 50 to 160 MeV. Nucl Phys 78:476–480
33. Symonds JL, Warren J, Young JD (1957) Excitation functions up to 980 MeV for proton-induced reactions in some light elements. Proc Phys Soc Sect A 70:824
34. Rosenfeld AH, Swanson RA, Warshaw SD (1956) Cross section for C^{12}(p, pn)C^{11}. Phys Rev 103:413–419
35. Whitehead AB, Foster JS (1958) Activation cross sections for C12(p, pn)C11, O16(p, α)N13, and F19(p, pn)F18. Can J Phys 36:1276–1285
36. Parikh V (1960) Absolute cross-sections of C12(p, pn)C11 from 288 to 383 MeV. Nucl Phys 18:628–637
37. Goebel K, Harting D, Kluyver JC, Kusumegi A, Schultes H (1961) The C12(p, pn)C11 and Al27(p, 3pn)Na24 cross-sections at 591 MeV. Nucl Phys 24:28–35
38. Cumming JB (1963) Absolute cross section for the C12(p, pn) C11 reaction at 50 MeV. Nucl Phys 49:417–423
39. Kavanagh TM, Lee JKP, Link WT (1964) A precise measurement of the C11 production cross section for 98-MeV protons on carbon. Can J Phys 42:1429–1436
40. Andrews PT, Butler PG, Christy A, James AN, Kirkby P, Lowe BG, Renwick BW (1968) Measurement of the production cross section of 11C from natural carbon for 385 MeV protons. Nucl Phys 109:689–693
41. Hogstrom KR (1976) ^{12}C(p, pn)^{1}1C cross section at 800 MeV. Phys Rev C 14:753–754
42. Kostjuchenko V, Nichiporov D (1993) Measurement of the 12C(p, pn)11C reaction from 95 to 200 MeV. Appl Radiat Isot 44:1173–1175
43. Kettern K, Shubin Y, Steyn G, van der Walt T, Coenen H, Qaim S (2004) Formation of short-lived positron emitters in reactions of protons of energies up to 200 MeV with the target elements carbon, nitrogen and oxygen. Appl Radiat Isot 60:939–945
44. Akagi T, Yagi M, Yamashita T, Murakami M, Yamakawa Y, Kitamura K, Ogura K, Kondo K, Kawanishi S (2013) Experimental study for the production cross sections of positron emitters induced from 12C and 16O nuclei by low-energy proton beams. Radiat Meas 59:262
45. Matsushita K, Nishio T, Tanaka S, Tsuneda M, Sugiura A, Ieki K (2016) Measurement of proton-induced target fragmentation cross sections in carbon. Nucl Phys A 946:104–116
46. Horst F, Adi W, Aricò G, Brinkmann K, Durante M, Reidel C, Rovituso M, Weber U, Zaunick H, Zink K, Schuy C (2019) Measurement of PET isotope production cross sections for protons and carbon ions on carbon and oxygen targets for applications in particle therapy range verification. Phys Med Biol 64:205012
47. Rodríguez-González T, Guerrero C, Bäcker C, Bauer J, Bäumer C, Brons S, Jentzen W, Jiménez-Ramos M, Millán-Callado M, Schömers C, Timmermann B, Quesada J, Capote R (2023) Production of ^{11}C,^{13}N and ^{15}O in proton-induced nuclear reactions up to 200 MeV. Nucl Data Sheets 187:579–596
48. Krasnov NN, Dmitriev PP, Dmitrieva ZP, Konstantinov IO, Molin GA (1969) N13, C11, and F18 yields from charged particle irradiation of carbon and oxygen, Soviet. At Energ 27:832–835
49. Dmitriev PP (1983) Systematics of nuclear reaction yields for thick target at 22 MeV proton energy. Vop At Nauki i Tekhn SerYadernye Konstanty 57:2
50. Marquez L, Perlman I (1951) Observations on lithium and beryllium nuclei ejected from heavy nuclei by high energy particles. Phys Rev 81:953–957
51. Lavrukhina AK, Moskaleva LP, Malyshev VV, Satarova LM (1962) production of light nuclei by bombarding heavy elements with 660 Mev protons, Zhur. Eksptl. i Teoret. Fiz., Vol: 43 C1 - Research Org.: Inst. of Geochemistry and Analytical Chemistry, Academy of Sciences, USSR
52. Neuzil EF, Lindsay RH (1963) Emission of Be^7 and competition processes at 30 to 42 MeV. Phys Rev 131:1697–1701
53. Ligonniere M, Vassent B, Bernas R (1964) Production cross section of beryllium-7 from Al, V, Ta and Au induced by 155 and 550 MeV protons. Comptes Rendus 259:1406
54. Furukawa M, Kume S, Ogawa M (1965) Excitation functions for the formation of 7Be and 22Na in proton induced reactions on 27Al. Nucl Phys 69:362–368
55. Lafleur MS, Porille NT, Yaffe L (1966) Formation of ^{7}Be in nuclear reactions induced by 85-MeV protons. Can J Chem 44:2749
56. Cline JE, Nieschmidt EB (1971) Measurements of spallation cross sections for 590 MeV protons on thin targets of copper, nickel, iron and aluminum. Nucl Phys A 169:437–448
57. Bimbot R, Gauvin H (1972) Reactions de spallation de noyaux legers induites par des protons de 50, 100 et 153 Me. Comptes Rendus Serie B 273:1054
58. Miyano K (1973) The ^{7}Be, ^{22}Naand ^{24}Na production cross sections with 52- to22-MeV proton on ^{27}Al. J Phys Soc Jpn 34:853
59. Bogatin VI, Litvin VF, Lozhkin OV, Perfilov NA, Yakovlev YP (1976) Isotopic effects in high-energy nuclear-reactions and isospin correlations of fragmentation cross-sections. Nucl Phys A 260:446–460
60. Heydegger HR, Turkevich AL, Van Ginneken A, Walpole PH (1976) Production of ^{7}Be, ^{22}Na and ^{28}Mg from Mg, Al, and SiO_2 by protons between 82 and 800 MeV. Phys Rev C 14:1506–1514
61. Grütter A (1982) Excitation functions for radioactive isotopes produced by proton bombardment of Cu and Al in the energy range of 16 to 70 MeV. Nucl Phys A 383:98–108
62. Grütter A (1982) Cross sections for reactions with 593 and 540 MeV protons in aluminium, arsenic, bromine, rubidium and yttrium. Int J Appl Radiat Isot 33:725–732
63. Michel R, Dittrich B, Herpers U, Peiffer F, Schiffmann T, Cloth P, Dragovitsch P, Filges D (1989) Proton-induced spallation at 600 MeV. Analyst 114:287–293
64. Scholten B, Qaim SM, Stocklin G (1994) Radiochemical studies of proton-induced Be-7 emission reactions in the energy-range of 40 to 100 Mev. Radiochim Acta 65:81–86
65. Michel R, Gloris M, Lange HJ, Lupke LIM, Herpers U, Dittrichhannen B, Rosel R, Schiekel T, Filges D, Dragovitsch P, Suter M, Hofmann HJ, Wolfli W, Kubik PW, Baur H, Wieler R (1995) Nuclide production by proton-induced reactions on elements (6 <=Z <= 29) in the energy-range from 800 to 2600 Mev. Nucl Inst Methods Phys Res Sect B-Beam Inter Mater Atoms 103:183–222
66. Schiekel T, Sudbrock F, Herpers U, Gloris M, Lange HJ, Michel LIR, DittrichHannen B, Synal HA, Suter M, Kubik PW, Blann M, Filges D (1996) Nuclide production by proton-induced reactions on elements in the energy range from 200MeV to 400MeV. Nucl Inst Methods Phys Res Sect B-Beam Inter Mater Atoms 114:91–119
67. Sisterson JM, Kim K, Beverding A, Emglert PAJ, Caffee MW, Vincent J, Castaneda C, Reedy RC (1996) Measuring excitation

functions needed to inter-pretcosmogenic nuclide production in lunar rocks. In: Conf. on Appl. of Accel. in Res. and Ind.,, Denton, Texas, USA, pp 811
68. Taddeucci TN, Ullmann J, Rybarcyk LJ, Butler GW, Ward TE (1997) Total cross sections for production of ^{7}Be, ^{22}Na, and ^{24}Na in p+^{7}Li and p+^{27}Al reactions at 495 and 795 MeV. Phys Rev C 55:1551
69. Yashima H, Uwamino Y, Sugita H, Nakamura T, Ito S, Fukumura A (2002) Projectile dependence of radioactive spallation products induced in copper by high-energy heavy ions. Phys Rev C 66:044607
70. Titarenko YE, Shvedov OV, Batyaev VF, Karpikhin AA, Zhivun EI, Koldobsky VM, Mulambetov AB, Sosin RD, Shubin AN, Yu AVL, Ignatyuk N, Mashnik VP, S. G., Prael TAGRE, Blann M (2003) Experimental and theoretical study of the yields of radioactive product nuclei in Tc-99 thin targets irradiated with 100–2600 MeV protons, USSR report to the I.N.D.C., pp 86
71. Titarenko YE, Batyaev VF, Titarenko AY, Butko MA, Pavlov KV, Florya SN, Tikhonov RS, Zhivun VM, Ignatyuk AV, Mashnik SG, Leray S, Boudard A, Cugnon J, Mancusi D, Yariv Y, Nishihara K, Matsuda N, Kumawat H, Mank G, Gudowski W (2011) Measurement and simulation of the cross sections for nuclide production in 56Fe and natCr targets irradiated with 0.04- to 2.6-GeV protons. Phys Atomic Nucl 74:523–536
72. F. Szelecsényi, G.F. Steyn, F.M. Nortier, Z. Kovács, New cross sections for the 27Al(p,x)7Be nuclear process: Monitoring proton beam energy via the 22Na/7Be cross-section ratio between 45 and 200 MeV, EPJ Web Conf., 146 (2017).
73. Meigo S, Matsuda H, Iwamoto H (2017) Cross section measurement in J-PARC for neutronics of the ADS, In: 13th Int. Meeting on Nucl.Appl.of Accel.,, Quebec, Canada, pp 396
74. Michel R, Brinkmann G, Weigel H, Herr W (1978) Proton-induced reactions on titanium with energies between 13 and 45 MeV. J Inorg Nucl Chem 40:1845–1851
75. Kopecky P, Szelecsényi F, Molnar T, Mikecz P, Tárkányi F (1993) Excitation-functions of (P, Xn) reactions on (Nat)Ti - monitoring of bombarding proton-beams. Appl Radiat Isot 44:687–692
76. Zarie K, Al-Hammad N, Azzam A (2006) Experimental study of excitation functions of some proton induced reactions on Ti-nat for beam monitoring purposes. Radiochim Acta 94:795–799
77. Khandaker MU, Kim K, Lee MW, Kim KS, Kim GN, Cho YS, Lee YO (2009) Investigations of the natTi(p, x)43,44m,44g,46,47,48Sc,48V nuclear processes up to 40MeV. Appl Radiat Isot 67:1348–1354
78. Garrido E, Duchemin C, Guertin A, Haddad F, Michel N, Metivier V (2016) New excitation functions for proton induced reactions on natural titanium, nickel and copper up to 70 MeV. Nucl Inst Methods Phys Res Sect B-Beam Inter Mater Atoms 383:191–212
79. Shahid M, Kim K, Kim G, Naik H (2018) Measurement of excitation functions of residual radionuclides from natTi(p, x) reactions up to 44 MeV. J Radioanal Nucl Chem 318:2049–2057
80. Azzam A, Hamada M, Said S, Mohamed G, Al-abyad M (2020) Excitation functions for proton-induced reactions on Te and Ti-nat targets: Measurements and model calculations special relevant to the Te-128(p, n)I-128 reaction. Nucl Phys a 999:121790
81. Cervenak J, Lebeda O (2020) New cross-section data for proton-induced reactions on Ti-nat and Cu-nat with special regard to the beam monitoring. Nucl Inst Methods Phys Res Sect B-Beam Inter Mater Atoms 480:78–97
82. Liu B, Han R, Yuan C, Sun H, Chen Z, Tian G, Shi F, Zhang X, Luo P, Jia H (2021) Excitation functions of proton induced reactions on titanium and copper. Appl Radiat Isotopes 173:109713
83. Fox MB, Voyles AS, Morrell JT, Bernstein LA, Batchelder JC, Birnbaum ER, Cutler CS, Koning AJ, Lewis AM, Medvedev DG, Nortier FM, O'Brien EM, Vermeulen C (2021) Measurement and modeling of proton-induced reactions on arsenic from 35 to 200 MeV. Phys Rev C 104:064615
84. Abe K, Iizuka A, Hasegawa A, Morozumi S (1984) Induced radioactivity of component materials by 16-Mev protons and 30-Mev alpha-particles. J Nucl Mater 123:972–976
85. Lavrukhina AK, Revina LD, Malyshev VV, Satarova LM (1963) Spallation of Fe nuclei induced by 150 MeV protons. J Exp Theor Phys 17:960
86. Williams IR, Fulmer CB (1967) Excitation functions for radioactive isotopes produced by protons below 60 MeV on Al Fe, and Cu. Phys Rev 162:1055–1061
87. Brodzinski RL, Rancitelli LA, Cooper JA, Wogman NA (1971) High-energy proton spallation of iron. Phys Rev C 4:1257–1265
88. Barrandon JN, Debrun JL, Kohn A, Spear RH (1975) Study of level of Ti, V, Cr, Fe, Ni, Cu and Zn by activation with protons whose energy is limited to 20 MeV. Nucl Inst Methods 127:269–278
89. Orth CJ, O'Brien HA, Schillaci ME, Dropesky BJ, Cline JE, Nieschmidt EB, Brodzinski RL (1976) Interlaboratory comparison of spallation-reaction cross sections for iron and copper with 590-MeV protons. J Inorg Nucl Chem 38:13–17
90. Michel R, Brinkmann G, Weigel H, Herr W (1979) Measurement and hybrid-model analysis of proton-induced reactions with V, Fe and Co. Nucl Phys A 322:40–60
91. Lagunas-Solar MC, Jungerman JA (1979) Cyclotron production of carrier-free cobalt-55, a new positron-emitting label for bleomycin. Appl Radiat Isot 30:25–32
92. Daum E (1997) Investigation of light ion induced activation cross sections in iron. Proton induced activation cross sections, Fed. Rep.Germ.report to the I.N.D.C., Germany, pp 4
93. Aleksandrov YV, Bogdanov AI, Vasilev SK, Ivanov RB, Kocherov NP, Mikhailova MA, Popova TI, Prikhodtseva VP (1989) Yields of Nuclides Produced in Interactions of 1 GeV Protons with Cylindrical Iron Target. In: 39. Conf. Nucl. Spectrosc. and Nucl.Struct., Tashkent, USSR, pp 536
94. Fassbender M, Shubin YN, Qaim SM (1999) Formation of activation products in interactions of medium energy protons with Na, Si, P, S, CI, Ca and Fe. Radiochim Acta 84:59–68
95. Aleksandrov YV, Bogdanov AI, Vasilev SK, Ivanov RB, Mikhailova MA, Popova TI, Prikhodtseva VP (1990) Cross Section for the Production of Radioactive Nuclides Under Bombardment of Intermediate-Mass Nuclei with 1-GeV Protons. In; 40. Conf. Nucl. Spectroscopy Nucl. Struct., Leningrad USSR, pp 496
96. Zhao W, Lu H, Yu W (1993) Measurement of cross sections by bombarding Fe with protons up to 19 MeV. Chin J Nucl Phys 15:337–340
97. Gloris M (1998) Proton-induced production of residual nuclei in heavy elements at medium energies. University of Hannover, Physics
98. S. Neumann (1999) Activation experiments with medium-energy neutrons and the production of cosmogenic nuclides in extraterrestrial matter (dissertation)
99. Ditrói F, Tárkányi F, Csikai G, Uddin MS, Hagiwara M, Baba M (2004) Investigation of activation cross sections of the proton induced nuclear reactions on natural iron at medium energies, International Conference on Nuclear Data for Science and Technology, AIP, Santa Fe, USA, pp 1011
100. Al-Abyad M, Comsan MNH, Qaim SM (2009) Excitation functions of proton-induced reactions on natFe and enriched 57Fe with particular reference to the production of 57Co. Appl Radiat Isot 67:122–128

101. Kim K, Khandaker MU, Naik H, Kim G (2014) Excitation functions of proton induced reactions on Fe-nat in the energy region up to 45 MeV. Nucl Inst Methods Phys Res Sect B-Beam Inter Mater Atoms 322:63–69
102. Graves SA, Ellison PA, Barnhart TE, Valdovinos HF, Birnbaum ER, Nortier FM, Nickles RJ, Engle JW (2016) Nuclear excitation functions of proton-induced reactions (Ep=35–90MeV) from Fe Cu, and Al. Nucl Inst Methods Phys Res Sect B 386:44–53
103. Voyles AS, Lewis AM, Morrell JT, Basunia MS, Bernstein LA, Engle JW, Graves SA, Matthews EF (2021) Proton-induced reactions on Fe, Cu, and Ti from threshold to 55 MeV. Eur Phys J A 57:94
104. Talebi M, Kakavand T, Mirzaii M (2013) Nuclear aspects and cyclotron production of the positron emitter 55Co. Kerntechnik 78:204–208
105. Remsberg LP, Miller JM (1963) Study of (p, pn) reactions in medium weight nuclei at 370 MeV. Phys Rev 130:2069–2076
106. Tanaka S, Furukawa M (1959) Excitation functions for (p, n) reactions with titanium, vanadium, chromium, iron and nickel up to E_p=14 MeV. J Phys Soc Japan 14:1269–1275
107. Read JBJ (1968) (p, xn) Reactions of 56Fe, 57Fe and 58Fe at 370 MeV. J Inorg Nucl Chem 30:2039–2046
108. Lavrukhina AK, Revina LD, Malyshev VV, Satarova LM, Hung-Kuei S, Kalicheva IS, Firsova LD (1963) Further investigation of the products of the spallation of iron by 660 MeV protons. Soviet Radiochem 5:682
109. Rayudu GVS (1968) Formation cross sections of various radionuclides from Ni, Fe, Si, Mg, O and C for protons of energies between 0.5 and 2.9 GeV. J Inorganic Nucl Chem 30:2311–2315
110. Jenkins IL, Wain AG (1970) Excitation functions for the bombardment of 56Fe with protons. J Inorg Nucl Chem 32:1419–1425
111. Gadioli E, Grassi Strini AM, Bianco GL, Strini G, Tagliaferri G (1974) Excitation functions of ^{51}V, ^{56}Fe, ^{65}Cu(p, n) reactions between 10 and 45 MeV. Nuovo Cimento A 22:547
112. Schoen NC, Orlov G, Mcdonald RJ (1979) Excitation-functions for radioactive isotopes produced by proton-bombardment of Fe Co, and W in the energy-range from 10 to 60 Mev. Phys Rev C 20:88–92
113. Michel R, Brinkmann G (1980) On the depth-dependent production of radionuclides (44<=A<=59) by solar protons in extraterrestrial matter. J Radioanal Chem 59:467–510
114. Michel R, Peiffer F, Stuck R (1985) Measurement and hybrid model analysis of integral excitation-functions for proton-induced reactions on vanadium, manganese and cobalt up to 200 Mev. Nucl Phys A 441:617–639
115. Antropov AE, Zarubin PP, Aleksandrov YA, Gorshkov IY (1985) Study of the Cross Section for the Reactions (p,n),(α,pn),(α,xn) onMedium Weight Nuclei. In: 35. Conf. Nucl. Spectr. and Nucl. Struct., Leningrad, USSR, pp 369
116. Neumann W, Woelfli W, Heimgartner P, Streicher RM (1990) Thin-layer activation of hip-joint prostheses for tribological tests. Nucl Instrum Methods Phys Res, Sect B 50:57–61
117. Levkovskii VN (1991) Activation cross sections for the nuclides of medium mass region (A=40-100) with medium energy (E=10-50 MeV) protons and alpha-particles (experiment and systematics). Inter-Vesti, Moscow
118. Jung P (1991) Cross sections for the production of helium and long-living radioactive isotopes by protons and deuterons. Julich Report, Julich, p 352
119. Takács S, Vasváry L, Tárkányi F (1994) Remeasurement and compilation of excitation-function of proton-induced reactions on iron for activation techniques. Nucl Inst Methods Phys Res Sect B-Beam Inter Materials Atoms 89:88–94
120. Sudár S, Qaim SM (1994) Excitation functions of proton and deuteron induced reactions on iron and alpha-particle induced reactions on manganese in the energy region up to 25 MeV. Phys Rev C 50:2408–2419
121. Sisterson JM, Vincent J (2006) Cross section measurements for proton-induced reactions in Fe and Ni producing relatively short-lived radionuclides at Ep=140–500MeV. Nucl Instrum Methods Phys Res, Sect B 251:1–8
122. Zherebchevsky VI, Alekseev IE, Gridnev KA, Krymov EB, Lazareva TV, Maltsev NA, Panin RB, Prokofyev NA, Torilov SY, Shtamburg AI (2016) The study of the nuclear reactions for the production of antimony isotopes. Bull Russ Acad Sci Phys 80:888–893
123. Uddin MS, Chakraborty AK, Spellerberg S, Spahn I, Shariff MA, Rashid MA, Qaim SM (2017) Excitation functions of proton induced nuclear reactions on natFe up to 16 MeV, with emphasis on radiochemical determination of low cross sections. Radiochim Acta 105:985–992
124. Lawriniang B, Badwar S, Ghosh R, Jyrwa B, Naik H, Suryanarayana SV, Naik YP (2018) Excitation functions of proton-induced reactions on natFe and natZr targets for the production of cobalt and niobium isotopes. Eur Phys J A 54:141
125. Acerbi E, Birattari C, Castiglioni M, Resmini F (1976) Nuclear applied physics at milan cyclotron. J Radioanal Chem 34:191–217
126. Dmitriev PP, Molin GA (1982) Radionuclide yields for thick targets at 22 MeV proton energy, International Atomic Energy Agency (IAEA), pp 10
127. Isshiki M, Fukuda Y, Igaki K (1984) Proton activation-analysis of trace impurities in purified cobalt. J Radioanal Nucl Chem 82:135–142
128. Dmitriev PP (1986) Radionuclide yield in reactions with protons, deuterons, alfa particles and helium-3. IAEA, Vienna
129. Zarubin PP, Sergeev VO (1989) Gamma-ray spectra and production cross-sections of Ag isotopes in the reactions ^{104,105,106,108,110}Pd(p, nγ), In: 39th Ann. Conf. Nucl. Spectrosc. Struct. At. Nuclei, Tashkent, pp 1
130. Levkovskii VN (1991) The cross-sections of activation of nuclides of middle-range mass (A=40-100) by protons and alpha particles of middle range energies (E=10-50 MeV). Inter-Vesy, Moscow
131. Tims SG, Scott AF, Morton AJ, Hansper VY, Sargood DG (1993) Cross sections of the reactions 58Fe(p, γ)59Co, 58Fe(p, n)58Co, 55Mn(α, n)58Co, 55Mn(α, p)58Fe and 57Fe(p, n)57Co. Nucl Phys A 563:473–493
132. Ghosh R, Badwar S, Lawriniang B, Jyrwa B, Naik H, Naik Y, Suryanarayana SV, Ganesan S (2017) Measurement of Fe58(p, n)Co58 reaction cross-section within the proton energy range of 3.38 to 19.63 MeV. Nucl Phys A 964:86–92
133. Nickles RJ (1991) A shotgun approach to the chart of the nuclides. Radiotracer production with an 11 MeV proton cyclotron. Acta Radiol Suppl 376:69–71
134. Kaufman S (1960) Reactions of Protons with Ni^{58} and Ni^{60}. Phys Rev 117:1532–1538
135. Ewart HE, Blann M (1964) Private communication
136. Tanaka S, Furukawa M, Chiba M (1972) Nuclear reactions of nickel with protons up to 56 MEV. J Inorg Nucl Chem 34:2419–2426
137. Aleksandrov YV, Astapov AA, Vasilev SK, Zelinski A, Ivanov RB, Kolachkovski A, Misiak R, Mikhailova MA, Novgorodov AF, Popova TI, Prikhodtseva VP (1990) Production Cross Sections of Spallation Radioactive Nuclides in Thin Targets of Co,Ni,Cu and Zn Irradiated by 660 MeV Protons. In: 40. Conf. Nucl. Spectroscopy Nucl. Struct., Leningrad, USSR, pp 498
138. Tárkányi F, Szelecsényi F, Kopecky P (1991) Excitation-functions of proton-induced nuclear-reactions on natural nickel

for monitoring beam energy and intensity. Appl Radiat Isot 42:513–517
139. Sonck M, VanHoyweghen J, Hermanne A (1996) Determination of the external beam energy of a variable energy. Multi cyclotron Appl Radiat Isot 47:445–449
140. Reimer P, Qaim SM (1998) Excitation functions of proton induced reactions on highly enriched 58ni with special relevance to the production of 55Co and 57Co. Radiochim Acta 80:113–120
141. Porras E, Sánchez F, Reglero V, Cordier B, Dean AJ, Lei F, Pérez JM, Swinyard BM (2000) Production rate of proton-induced isotopes in different materials. Nucl Instrum Methods Phys Res, Sect B 160:73–125
142. Al Saleh FS, Al Mugren KS, Azzam A (2007) Excitation functions of (p, x) reactions on natural nickel between proton energies of 2.7 and 27.5MeV. Appl Radiation Isotopes 65:104–113
143. Khandaker MU, Kim K, Lee M, Kim KS, Kim G (2011) Excitation functions of (p, x) reactions on natural nickel up to 40MeV. Nucl Instrum Methods Phys Res, Sect B 269:1140–1149
144. Jost CU, Griswold JR, Bruffey SH, Mirzadeh S, Stracener DW, Williams CL (2013) Measurement of cross sections for the 232Th(P,4n) 229Pa reaction at low proton energies. In: AIP Conference Proceedings, pp 520–524
145. Amjed N, Tarkanyi F, Hermanne A, Ditroi F, Takacs S, Hussain M (2014) Activation cross-sections of proton induced reactions on natural Ni up to 65 MeV. Appl Radiat Isot 92:73–84
146. Hermanne A, Adam Rebeles R, Tárkányi F, Takács S (2015) Excitation functions of proton induced reactions on natOs up to 65MeV: Experiments and comparison with results from theoretical codes. Nucl Inst Methods Phys Res Sect B Beam Inter Mater Atoms 345:58–68
147. Uddin MS, Chakraborty AK, Spellerberg S, Shariff MA, Das S, Rashid MA, Spahn I, Qaim SM (2016) Experimental determination of proton induced reaction cross sections on natNi near threshold energy. Radiochim Acta 104:305–314
148. Sadeghi M, Amiri M, Roshanfarzad P, Avila M, Tenreiro C (2008) Radiochemical studies relevant to the no-carrier-added production of 61,64Cu at a cyclotron. Radiochim Acta 96:399–402
149. Van So L, Pellegrini P, Katsifis A, Howse J, Greguric I (2008) Radiochemical separation and quality assessment for the 68Zn target based 64Cu radioisotope production. J Radioanal Nucl Chem 277:451–466
150. Michel R, Weigel H, Herr W (1978) Proton-induced reactions on nickel with energies between 12 and 45 MeV. Zeitschrift für Physik A Atoms and Nuclei 286:393–400
151. Aleksandrov VN, Semenova MP, Semenov VG (1987) Production cross-section of radionuclides in (P, X) reactions at copper and nickel nuclei. Soviet At Energ 62:478–481
152. Furukawa M, Shinohara A, Narita M, Kojima S (1990) Production of cosmic-ray induced radionuclides, ^{49}Vand ^{59,63}Ni from Fe, Co and Ni irradiated with protons up to Ep=40 MeV, Univ. Tokyo, Inst. for Nucl. Study, Annual Report, Tokyo, pp 32
153. Michel R, Brinkmann G, Stück R (1983) Integral excitation functions of α-induced reactions on titanium, iron and nickel. Radiochim Acta 32:173–190
154. Bringas F, Yamashita MT, Goldman ID, Pascholati PR, Sciani V (2005) Measurement of Proton-Induced Reaction Cross Sections in Ti, Ni and Zr near the Threshold. In: Intern.Conf. Nuclear Data for Science and Technology, AIP, Santa Fe, pp 1374–1377
155. Hermanne A, Adam-Rebeles R, Tarkanyi F, Takacs S, Ditroi F (2015) Proton and deuteron induced reactions on Ga-nat: Experimental and calculated excitation functions. Nucl Inst Methods Phys Res Sect B-Beam Inter Mater Atoms 359:145–154
156. Titarenko YE, Batyaev VF, Titarenko AY, Butko MA, Pavlov KV, Florya SN, Tikhonov RS, Zhivun VM, Ignatyuk AV, Mashnik SG, Leray S, Boudard A, Cugnon J, Mancusi D, Yariv Y, Nishihara K, Matsuda N, Kumawat H, Mank G, Gudowski W (2011) Measurement and simulation of the cross sections for nuclide production in Nb-93 and Ni-nat targets irradiated with 0.04- to 2.6-GeV protons. Phys Atomic Nuclei 74:537–550
157. Cohen BL, Newman E, Handley TH (1955) (p, pn)+(p, 2n) and (p, 2p) cross sections in medium weight elements. Phys Rev 99:723–727
158. Weigel H, Michel R, Herpers U, Herr W (1975) Survey of 600 MeV proton cross-sections for spallogenic radionuclides in quartz- Fe-, Co- and Ni-targets. Radiochem Radioanal Lett 21:293
159. Haasbroek FJ, Steyn J, Neirinckx RD, Burdzik GF, Cogneau M, Wanet P (1976) Excitation functions and thick-target yields for radioisotopes induced in natural Mg, Co, Ni and Ta by medium energy protons, in: Laboratory NPR (Ed.), CSIR, South Africa, pp 27
160. Brinkman GA, Helmer J, Lindner L (1977) Nickel and copper foils as monitors for cyclotron beam intensities. Radiochem Radioanal Lett 28:9–19
161. Piel H (1991) Bestimmung der anregungsfunktionen von (p, xn)-reaktionen an Ni-isotopen. Universitet zu Köln, Cologne
162. Brinkmann G (1979) Integrale anregungsfunktionen für protonen- and alpha-induzierte reaktionen an targetelementen 22<Z<28. Universitat zu Köln, Cologne
163. Stück R (1983) Protonen-induzierte reaktionen an Ti, V, Mn, Fe, Co und Ni messung und hybrid modell analyse integraler anregungsfunktionen und ihre anwendung in modellrechnungen zur produktion kosmogener nuklide. Universitat zu Köln, Cologne
164. Zhuravlev BV, Grusha OV, Ivanova SP, Trykova VI, Shubin YN (1984) Analysis of neutron-spectra in interaction of 22 MeV protons with nuclei. Soviet J Nucl Phys-Ussr 39:164–168
165. Tárkányi F, Szelecsényi F, Kopecký P (1992) Cross section data for proton, 3He and α-particle induced reactions on natNi, natCu and natTi for monitoring beam performance, nuclear data for science and technology. Springer, Berlin, pp 529–532
166. Bodemann R, Michel R, Roesel R, Herpers U, Holmqvist B, Conde H, Malmborg P (1995) Production of radionuclides from target elements (22<Z<29) by proton-induced reactions up to 100 MeV. In: Qaim S (ed) Progress report on nuclear data research in the federal republic of germany for the period April 1, 1994 to March 31. Elsevier, Amsterdam, p 27
167. Steyn GF, Mills SJ, Nortier FM (1669) Private communication
168. Sonck M, Hermanne A, Szelecsényi F, Takács S, Tárkányi F (1998) Study of the Ni-nat(p, x)Ni-57 process up to 44 MeV for monitor purposes. Appl Radiat Isot 49:1533–1536
169. Szelecsényi F, Tárkányi F, Takács S, Hermanne A, Sonck M, Shubin Y, Mustafa MG, Zhuang YX (2001) Excitation function for the Ti-nat(p, x)V-48 nuclear process: evaluation and new measurements for practical applications. Nucl Inst Methods Phys Res Sect B-Beam Inter Mater Atoms 174:47–64
170. Takács S, Tárkányi F, Sonck M, Hermanne A (2002) New cross-sections and intercomparison of proton monitor reactions on Ti Ni and Cu. Nucl Inst Methods Phys Res Sect B-Beam Inter Mater Atoms 188:106–111
171. Alharbi AA, Alzahrani J, Azzam A (2011) Activation cross-section measurements of some proton induced reactions on Ni, Co and Mo for proton activation analysis (PAA) purposes. Radiochim Acta 99:763–770
172. Adel D, Mohamed GY, Yousef Z, El Wahab MA, Ditrói F, Takács S, Al-abyad M (2020) Experimental investigation and theoretical evaluation of proton induced nuclear reactions on nickel. Appl Radiat Isot 159:109094

173. Gruverman IJ, Kruger P (1959) Cyclotron-produced carrier-free radioisotopes: thick target yield data and carrier-free separation procedures. Int J Appl Radiat Isot 5:21–31
174. Bleuel DL, Bernstein LA, Marsh RA, Morrell JT, Rusnak B, Voyles AS (2021) Precision measurement of relative γ-ray intensities from the decay of 61Cu. Appl Radiat Isot 170:109625
175. Meadows JW (1953) Excitation functions for proton-induced reactions with copper. Phys Rev 91:885–889
176. McCormick GH, Blosser HG, Cohen BL, Newman E (1956) (p, He3) and (p, t) cross-section measurements. J Inorg Nucl Chem 2:269–270
177. Orth CJ, Dropesky BJ, Williams RA, Giesler GC, Hudis J (1978) Pion-induced spallation of copper across the (3,3) resonance. Phys Rev C 18:1426–1435
178. Greenwood LR, Smithe RK (1984) Measurement of Cu spallation cross sections at IPNS, United States, pp 11–17
179. Mills SJ, Steyn GF, Nortier FM (1992) Experimental and theoretical excitation functions of radionuclides produced in proton bombardment of copper up to 200 MeV. Int J Radiation Appl Inst Part A Appl Radiation Isotopes 43:1019–1030
180. Titarenko YE, Karpikhin EI, Smolyakov AF, Igumnov MM, Shvedov OV, Stepanov NV, Kazarizki VD, Batyaev VF, Mashnik SG, Gabriehl TA (1996) Experimental and calculative research of radioactive nuclei formation-products of target and constructional materials of electronuclear facilities irradiated by protons with energies 1.5 GeV and 130 MeV, Worksh. Exact Meas. in Nucl. Spect., Sarov, Russia, pp 184
181. Al-Saleh FS, Al-Harbi AA, Azzam A (2006) Excitation functions of proton induced nuclear reactions on natural copper using a medium-sized cyclotron. Radiochim Acta 94:391–396
182. Shahid M, Kim K, Naik H, Zaman M, Yang S-C, Kim G (2015) Measurement of excitation functions in proton induced reactions on natural copper from their threshold to 43MeV. Nucl Instrum Methods Phys Res, Sect B 342:305–313
183. Voyles AS, Bernstein LA, Birnbaum ER, Engle JW, Graves SA, Kawano T, Lewis AM, Nortier FM (2018) Excitation functions for (p, x) reactions of niobium in the energy range of Ep = 40–90 MeV. Nucl Instrum Methods Phys Res, Sect B 429:53–74
184. Ditroi F, Takacs S, Tarkanyi F, Baba M, Corniani E, Shubin YN (2008) Study of proton induced reactions on niobium targets up to 70 MeV. Nucl Inst Methods Phys Res Sect B-Beam Inter Mater Atoms 266:5087–5100
185. Ditroi F, Hermanne A, Corniani E, Takacs S, Tarkanyi F, Csikai J, Shubin YN (2009) Investigation of proton induced reactions on niobium at low and medium energies. Nucl Inst Methods Phys Res Sect B-Beam Inter Mater Atoms 267:3364–3374
186. Kim K, Kim G, Shahid M, Zaman M, Yang S-C, Uddin MS, Naik H (2018) Excitation functions of 93Nb(p, x) reactions from threshold to 42.5 MeV. J Radioanaly Nucl Chem 317:1021–1031
187. Zhao W, Yu W, Han X, Lu H (1998) Excitation functions of reactions from d + Ti, d + Mo, p + Ti and p +Mo, Beijing National Tandem Accelerator Laboratory, 1996–1997, Ann.Rept., pp 10
188. Bonardi M, Birattari C, Groppi F, Sabbioni E (2002) Thin-target excitation functions, cross-sections and optimised thick-target yields for Mo-nat(p, xn) Tc-94g, Tc-95m, Tc-95g, Tc-96(m+g) nuclear reactions induced by protons from threshold up to 44 MeV No carrier added radiochemical separation and quality control. Appl Radiation Isotopes 57:617–635
189. Uddin MS, Hagiwara M, Tárkányi F, Ditrói F, Baba M (2004) Experimental studies on the proton-induced activation reactions of molybdenum in the energy range 22–67 MeV. Appl Radiat Isot 60:911–920
190. Khandaker MU, Meaze AKMMH, Kim K, Son D, Kim G (2006) Measurements of the proton-induced reaction cross-sections of Mo-nat by using the MC50 cyclotron at the Korea institute of radiological and medical sciences. J Korean Phys Soc 48:821–826
191. Khandaker MU, Uddin MS, Kim KS, Lee YS, Kim GN (2007) Measurement of cross-sections for the (p, xn) reactions in natural molybdenum. Nucl Inst Methods Phys Res B 262:171
192. Lebeda O, Pruszynski M (2010) New measurement of excitation functions for (p, x) reactions on ^{na}tMo with special regard to the formation of ^{95}mTc, $^{96m+}$gTc, ^{99}mTc and ^{9}9Mo. Appl Radiat Isot 68:2355–2365
193. Tárkányi F, Ditrói F, Hermanne A, Takács S, Ignatyuk AV (2012) Investigation of Activation Cross Sections of Proton Induced Nuclear Reactions on ^{nat}Mo up to 40 MeV: New data and evaluation. Nucl Inst Methods Phys Res Sect B-Beam Inter Mater Atoms 280:45–73
194. Takacs S, Hermanne A, Ditroi F, Tarkanyi F, Aikawa M (2015) Reexamination of cross sections of the Mo-100(p,2n)Tc-99m reaction. Nucl Inst Methods Phys Res Sect B-Beam Inter Mater Atoms 347:26–38
195. Červenák J, Lebeda O (2016) Experimental cross-sections for proton-induced nuclear reactions on natMo. Nucl Instrum Methods Phys Res, Sect B 380:32–49
196. Anees Ahmed A, Wrońska A, Magiera A, Bartyzel M, Mietelski JW, Misiak R, Wąs B (2019) Reexamination of proton-induced reactions on ^{nat}Mo at 19–26 MeV and study of target yield of resultant radionuclides. Acta Phys Pol, B 50:1583–1596
197. Elbinawi A, Al-Abyad M, Bashter I, Seddik U, Ditrói F (2019) Study of proton induced nuclear reactions on molybdenum: cross section measurements and theoretical calculations. Radiochim Acta 108(1):1–9
198. Ahmed AA, Wrońska A, Magiera A, Misiak R, Bartyzel M, Mietelski JW, Waas B (2022) Study of 99Mo and long-lived impurities produced through (p, x) reactions in the natMo. Radiation Phys Chem 190:109774
199. Dmitriev PP, Molin GA, Dmitrieva ZP, Panarin MV (1976) Yields of ^{95m}Tc, ^{96}Tc, and ^{97m}Tc from irradiation of molybdenum and niobium. Soviet At Energ 40:75–77
200. Lagunas-Solar MC, Kiefer PM, Carvacho OF, Lagunas CA, Cha YP (1991) Cyclotron production of Nca Tc-99m and Mo-99 - an alternative non-reactor supply source of instant Tc-99m and Mo-99]Tc-99m generators. Appl Radiat Isot 42:643–657
201. Kavanagh TM, Bell RE (1961) Cross sections of (p, pxn) reactions in Au-197. Can J Phys 39:1172
202. Szelecsényi F, Steyn GF, Kovács Z, van der Walt TN (2007) Application of Au + p nuclear reactions for proton beam monitoring up to 70 MeV. In: International Conference on Nuclear Data for Science and Technology 2007, EDP Sciences, Nice, France, pp 1259
203. Ditroi F, Tarkanyi F, Takacs S, Hermanne A (2016) Activation cross sections of proton induced nuclear reactions on gold up to 65 MeV. Appl Radiat Isot 113:96–109
204. Červenák J, Lebeda O (2019) Measurement of cross-sections of proton-induced nuclear reactions on 197Au focused on the production of the theranostic pair 197m, gHg. Nucl Instrum Methods Phys Res Sect B 458:118–125
205. Birattari C, Bonardi M (1980) Excitation functions for nuclear reactions (p,xn) and (p,pxn) on targets of gold and study of the production of the ultra-short-lived radioisotope Au-195-m, INFN Reports/Various Techniques Series, IFNF, Italy
206. Yule HP, Turkevich A (1960) Radiochemical studies of the (p, pn) reaction in complex nuclei in the 80–450-MeV range. Phys Rev 118:1591
207. Gusakow M, Legoux Y, Sergolle H (1960) Spallation reaction (p, n+p),(p,2n+p) and (p,3n) on gold production effective cross section at variation proton energy. Comptes Rendus De L Academie Des Sciences 251:70

208. Nagame Y, Sueki K, Baba S, Nakahara H (1990) Isomeric yield ratios in proton-, ^{3}He-, and alpha-particle-induced reactions on ^{197}Au. Phys Rev C 41:889–897
209. Szelecsényi F, Takács S, Fenyvesi A, Szûcs Z, Tárkányi F, Heselius SJ, Bergman J, Boothe TE (1997) Study of the 197Au(p,pn)196ml,m2,gAu and 197Au(p,n)197mHg reactions and their application for proton beam monitoring in radioisotope production. In: International Conference on Nuclear Data for Science and Technology, Italian Physical Society, Trieste, Italy, pp 1483
210. Takács S, Sonck M, Scholten B, Hermanne A, Tárkányi F (1997) Excitation functions of deuteron induced nuclear reactions on Ti-nat up to 20 MeV for monitoring deuteron beams. Appl Radiat Isot 48:657–665
211. Khandaker M, Haba H, Kanaya J, Otuka N (2013) Excitation functions of (d, x) nuclear reactions on natural titanium up to 24 MeV. Nucl Inst Methods Phys Res Sect B-Beam Int Mater Atoms 296:14–21
212. Khandaker MU, Haba H, Kanaya J, Otuka N, Kassim HA (2014) Activation cross-sections of deuteron-induced nuclear reactions on natural titanium. Nucl Data Sheets 119:252–254
213. Lebeda O, Stursa J, Ralis J (2015) Experimental cross-sections of deuteron-induced reaction on Y-89 up to 20 MeV; comparison of Ti-nat(d, x)V-48 and Al-27(d, x)Na-24 monitor reactions. Nucl Inst Methods Phys Res Sect B-Beam Int Mater Atoms 360:118–128
214. Takács S, Király B, Tárkányi F, Hermanne A (2007) Evaluated activation cross sections of longer-lived radionuclides produced by deuteron induced reactions on natural titanium. Nucl Inst Methods Phys Res Sect B-Beam Int Mater Atoms 262:7–12
215. Hermanne A, Sonck M, Takács S, Tárkányi F (2000) Experimental study of excitation functions for some reactions induced by deuterons (10–50 Mev) on natural Fe and Ti. Nucl Inst Methods Phys Res Sect B-Beam Int Mater Atoms 161:178–185
216. Gagnon K, Avila-Rodriguez M, Wilson J, McQuarrie S (2010) Experimental deuteron cross section measurements using single natural titanium foils from 3 to 9 MeV with special reference to the production of V-47 and Ti-51. Nucl Inst Methods Phys Res Sect B-Beam Int Mater Atoms 268:1392–1398
217. Duchemin C, Guertin A, Haddad F, Michel N, Metivier V (2015) Cross section measurements of deuteron induced nuclear reactions on natural titanium up to 34 MeV. Appl Radiat Isot 103:160–165
218. Dmitriev PP, Krasnov NN, Molin GA (1983) Yields of Radioactive Nuclides Formed by Bombardment of a Thick Target with 22-MeV Deuterons, INDC(CCP)-210/L
219. Clark JW, Fulmer CB, Williams IR (1969) Excitation functions for radioactive nuclides produced by deuteron-induced reactions in iron. Phys Rev 179:1104–1108
220. Zhao W, Lu H, Yu W, Cheng J (1995) Excitation functions for reactions induced by deuteron in iron. Chin J Nucl Phys 17:163–166
221. Nakao M, Hori J, Ochiai K, Kubota N, Sato S, Yamauchi M, Ishioka NS, Nishitani T (2006) Measurements of deuteron-induced activation cross-sections for IFMIF accelerator structural materials. In: Proceedings of the 7th International Conference on Accelerator Applications, 562, pp 785–788
222. Kiraly B, Takacs S, Ditroi F, Tarkanyi F, Hermanne A (2009) Evaluated activation cross sections of longer-lived radionuclides produced by deuteron induced reactions on natural iron up to 10 MeV. Nucl Inst Methods Phys Res Sect B-Beam Int Mater Atoms 267:15–22
223. Avrigeanu M, Avrigeanu V, Bém P, Fischer U, Honusek M, Katovsky K, Mănăilescu C, Mrázek J, Šimečková E, Závorka L (2014) Low energy deuteron-induced reactions on Fe isotopes. Phys Rev C 89:044613
224. Goodman C (1949) The science and engineering of nuclear power, V2. Addison-Wesley Press Inc., Cambridge
225. Burgus WH, Cowan GA, Hadley JW, Hess W, Shull T, Stevenson ML, York HF (1954) Cross sections for the reactions Ti^{48}(d, 2n)V^{48}; Cr^{52}(d, 2n)Mn^{52}; and Fe^{56}(d, 2n)Co^{56}. Phys Rev 95:750–751
226. Tao Z, Zhu F, Qiu H, Wang G (1984) Excitation function of deuteron-induced reactions on natural iron. Atomic Energy Sci Technol 18:506
227. Jung P (1987) Helium production and long-term activation by protons and deuterons in metals for fusion reactor application. J Nucl Mater 144:43–50
228. Takacs S, Tarkanyi F, Sonck M, Hermanne A, Sudar S (1997) Study of deuteron induced reactions on natural iron and copper and their use for monitoring beam parameters and for thin layer activation technique. AIP Conf Proc 392:659–662
229. Takács S, Szelecsényi F, Tárkányi F, Sonck M, Hermanne A, Shubin Y, Dityuk A, Mustafa MG, Zhuang YX (2001) New cross-sections and intercomparison of deuteron monitor reactions on Al Ti, Fe, Ni and Cu. Nucl Inst Methods Phys Res Sect B-Beam Int Mater Atoms 174:235–258
230. Ochiai K, Nakao M, Kubota N, Sato, Yamauchi M, Ishioka NH, Nishitani T, Konno C (2007) Deuteron induced activation cross section measurement for IFMIF. In: Conf. on Nucl. Data for Sci. and Technology, Nice, France, pp 1011
231. Khandaker MU, Haba H, Kanaya J, Otuka N (2013) Activation cross-sections of deuteron-induced nuclear reactions on natural iron up to 24 MeV. Nucl Inst Methods Phys Res B 316:33
232. Zavorka L, Simeckova E, Honusek M, Katovsky K (2011) The activation of Fe by deuterons at energies up to 20 MeV. J Korean Phys Soc 59:1961
233. Zweit J, Smith AM, Downey S, Sharma HL (1991) Excitation functions for deuteron induced reactions in natural nickel: Production of no-carrier-added 64Cu from enriched 64Ni targets for positron emission tomography. Int J Radiation Appl Inst Part A Appl Radiation Isotopes 42:193–197
234. Takács S, Sonck M, Azzam A, Hermanne A, Tárkányi F (1997) Activation cross section measurements of deuteron induced reactions on Ni-nat with special reference to beam monitoring and production of Cu-61 for medical purpose. Radiochim Acta 76:15–24
235. Takács S, Tárkányi F, Király B, Hermanne A, Sonck M (2007) Evaluated activation cross sections of longer-lived radionuclides produced by deuteron induced reactions on natural nickel. Nucl Inst Methods Phys Res Sect B-Beam Int Mater Atoms 260:495–507
236. Hermanne A, Takacs S, Adam-Rebeles R, Tarkanyi F, Takacs MP (2013) New measurements and evaluation of database for deuteron induced reaction on Ni up to 50 MeV. Nucl Inst Methods Phys Res B 299:8
237. Amjed N, Tarkanyi F, Ditroi F, Takacs S, Yuki H (2013) Activation cross-sections of deuteron induced reaction of natural Ni up to 40 MeV. Appl Radiat Isot 82:87–99
238. Usman A, Khandaker M, Haba H, Murakami M, Otuka N (2016) Measurements of deuteron-induced reaction cross-sections on natural nickel up to 24 MeV. Nuc Inst Methods Phys Res Sect B-Beam Inter Mater Atoms 368:112–119
239. Avrigeanu M, Šimečková E, Fischer U, Mrázek J, Novak J, Štefánik M, Costache C, Avrigeanu V (2016) Deuteron-induced reactions on Ni isotopes up to 60 MeV. Phys Rev C 94:014606
240. Cline CK (1971) Reaction mechanisms and shell structure effects in 54Fe+6Li and 58Ni+d reactions at medium energies. Nucl Phys A 174:73–96

241. Zhu F, Zhenlan T, Zhenxia W (1983) Measurements of excitation functions for Ni-58(d, a) Ni-58(d, a+n) and Ni-58(d, t). Chin J Nucl Phys 5:166
242. Ditroi F, Tarkanyi F, Ali M (2000) Investigation of deuteron induced nuclear reactions on niobium. Nucl Inst Methods Phys Res Sect B-Beam Inter Mater Atoms 161:172–177
243. Tarkanyi F, Hermanne A, Ditroi F, Takacs S, Kiraly B, Baba M, Ohtsuki T, Kovalev SF, Ignatyuk AV (2007) Production of longer lived radionuclides in deuteron induced reactions on niobium. Nucl Inst Methods Phys Res Sect B-Beam Inter Mater Atoms 255:297–303
244. Avrigeanu M, Avrigeanu V, Bem P, Fischer U, Honusek M, Koning AJ, Mrazek J, Simeckova E, Stefanik M, Zavorka L (2013) Low-energy deuteron-induced reactions on Nb-93. Phys Rev C 88:014612
245. Ditroi F, Tarkanyi F, Takacs S, Hermanne A, Ignatyuk AV (2016) Activation cross sections of deuteron induced reactions on niobium in the 30–50 MeV energy range. Nucl Ins Methods Phys Res Sect B-Beam Inter Mater Atoms 373:17–27
246. Aikawa M, Komori Y, Haba H (2018) Activation cross sections of deuteron-induced reactions on niobium up to 24 MeV. Nucl Instrum Methods Phys Res Sect B 436:217–220
247. Randa Z, Svoboda K (1976) Excitation-functions and yields of (D, N) and (D,2n) reactions on natural molybdenum. J Inorg Nucl Chem 38:2289–2295
248. Sheng W, Xianguan L, Xiufeng P, Fuqing H, Mantian L (1990) Excitation Functions for the natMo(d,x)95mTC, natMo(d,x)96gTc and natMo(d,x)97Tc Reactions, Inst. of Nucl. Sci. and Techn., Sichuan Univ., NST-004
249. Wenrong Z, Weixiang Y, Xiaogang H, Hanlin L (1998) Excitation functions of reactions from d + Ti, d + Mo, p + Ti and p + Mo. Atomic Energy Press, Beijing
250. Tárkányi F, Ditrói F, Takács S, Király B, Hermanne A, Sonck M, Baba M, Ignatyuk AV (2012) Investigation of activation cross-sections of deuteron induced nuclear reactions on ^{nat}Mo up to 50 MeV. Nucl Inst Methods Phys Res Sect B-Beam Inter Mater Atoms 274:1–25
251. Elbinawi A, Ali BM, Mohamed GY, Ditrói F, Al-abyad M (2021) Deuteron induced nuclear reactions on Mo up to 10 MeV: experimental investigation and nuclear model calculations. Eur Phys J A 57:312
252. Svoboda K, Řanda Z, Hrubý J (1969) Interaction products of 12·5 deuterons with molybdenum and their isolation possibilities from worn-out cyclotron parts. Isotopenpraxis Isot Environ Health Stud 5:247–252
253. Jahn P, Probst HJ, Djaloeis A, Davidson WF, Mayer-Boricke C (1973) Measurement and interpretation of 197Au-(d, xnyp) excitation functions in the energy range from 25 to 86 MeV. Nucl Phys A 209:333
254. Tarkanyi F, Ditroi F, Hermanne A, Takacs S, Kiraly B, Yamazaki H, Baba M, Mohammadi A, Ignatyuk AV (2011) Activation cross-sections of deuteron induced nuclear reactions on gold up to 40 MeV. Nucl Inst Methods Phys Res Sect B-Beam Inter Mater Atoms 269:1389–1400
255. Tarkanyi F, Hermanne A, Ditroi F, Takacs S, Rebeles RA, Ignatyuk AV (2015) New data on cross-sections of deuteron induced nuclear reactions on gold up to 50 MeV and comparison of production routes of medically relevant Au and Hg radioisotopes. Nucl Inst Methods Phys Res Sect B-Beam Inter Mater Atoms 362:116–132
256. Baron N, Cohen BL (1963) Activation cross-section survey of deuteron-induced reactions. Phys Rev 129:2636–2642
257. Chevarier N, Chevarier A, Demeyer A, Duc TM (1971) Reactions induitessurl'or par des deutons de 10 a 70 MeV. J Phys (Paris) 32:483
258. Khrisanfov YV, Padalko VY, Zarubin PP (1973) Excitation functions for 197Au + d reactions. Bull Acad Sci USSR Phys Ser 36:580
259. Long X, Peng X, He F (1985) Activation cross-sections of Au-197 with deuterons, Inst.of Nucl.Sci.and Technol.,Sichuan U. Reports
260. Zhao W, Lu H (1989) Measurements of cross sections for ^{197}Au(d, x) reaction. Chin J Nucl Phys 11:83
261. Lebeda O, Červenák J (2019) Measurement of deuteron-induced nuclear reactions cross-sections on 197Au and on natCu focused on the theranostic 197m, gHg. Nucl Instrum Methods Phys Res Sect B 461:105–113
262. Sandoval E, Paez E (1964) Cross section for the Au197(d, p) Au198 reaction. Phys Rev B 415:136
263. Nassiff SJ, Quel E, Testoni J (1966) Excitation function for the reaction 197Au(d, p)198Au. Nucl Phys 88:344
264. Ditrói F, Tárkányi F, Takács S, Hermanne A (2017) Extension of activation cross section data of long lived products in deuteron induced nuclear reactions on platinum up to 50 MeV. Nucl Inst Methods Phys Res Sect B-Beam Inter Mater Atoms 401:56–70
265. Brill OD (1965) He3-light nucleus interaction cross sections. Sov J Nucl Phys 1:34
266. Hahn RL, Ricci E (1966) Interactions of ^{3}He particles with ^{9}Be, ^{12}C, ^{16}O, and ^{1}9F. Phys Rev 146:650
267. Cirilov SD, Newton JO, Schapira JP (1966) Total cross sections for the reaction 12C(3He, α)11C and 12C(3He, n)14O. Nucl Phys 77:472–476
268. Liebler V, Bethge K, Krauskopf J, Meyer JD, Misaelides P, Wolf G (1989) Determination of excitation functions for carbon detection by charged particle activation analysis. Nucl Instrum Methods Phys Res, Sect B 36:7–13
269. Nozaki T, Iwamoto M (1981) Yield of 14O for the reactions 14N(p, n) 14O, 12C(3He, n) 14O and 12C(α, 2n)14O. Radiochim Acta 29:57–60
270. Weinreich R, Probst HJ, Qaim SM (1980) Production of chromium-48 for applications in life sciences. Int J Appl Radiat Isot 31:223–232
271. Ditroi F, Tarkanyi F, Ali M, Ando L, Heselius S, Yu S, Zhuang Y, Mustafa M (2000) Investigation of He-3-induced reactions on natural Ti for nuclear analytical and radionuclide production purposes. Nucl Inst Methods Phys Res Sect B-Beam Inter Mater Atoms 168:337–346
272. Szelecsényi F, Kovács Z, Nagatsu K, Zhang MR, Suzuki K (2017) Production cross sections of radioisotopes from 3He-particle induced nuclear reactions on natural titanium. Appl Radiat Isot 119:94–100
273. Uddin Khandaker M, Kumer Chakraborty A, Nagatsu K, Obata H, Minegishi K, Zhang M-R, Okhunov AA (2021) The formation of isomeric pair in the natTi(3He, x)44m, gSc reactions: effect of spin cut-off parameter on the isomeric ratio. Nucl Inst Methods Phys Res Sect B Beam Inter Mater Atoms 499:1–6
274. Khandaker MU, Nagatsu K, Obata H, Minegishi K, Zhang M-R (2019) Excitation functions of helion-induced nuclear reactions on natural titanium up to 55 MeV. Nucl Instrum Methods Phys Res, Sect B 445:69–76
275. Lebeda O, Ráliš J, Štursa J (2020) Excitation functions of the 165Ho(3He, xn)166,165,163Tm and natTi(3He, x)48V,48Cr reactions. Appl Radiat Isot 156:108988
276. Solieman AHM, Al-Abyad M, Ditrói F, Saleh ZA (2016) Experimental and theoretical study for the production of 51Cr using p, d, 3He and 4He projectiles on V, Ti and Cr targets. Nucl Instrum Methods Phys Res Sect B 366:19–27
277. Hudis J (1957) Production of carrier-free Mg28 from aluminium. J Inorg Nucl Chem 4:237–238

278. Nethaway DR, Caretto AA (1958) New Isotope, Sulfur-38. Phys Rev 109:504–508
279. Martens U, Schweimer GW (1970) Production of7Be,22Na,24Na and28Mg by irradiation of27Al with 52 MeV deuterons and 104 MeV alpha particles. Zeitschrift für Physik A Hadrons and nuclei 233:170–177
280. Nozaki T, Furukawa M, Kume S, Seki R (1975) Production of 28Mg by triton and α-particle induced reactions. Int J Appl Radiat Isot 26:17–20
281. Probst HJ, Qaim SM, Weinreich R (1976) Excitation functions of high-energy α-particle induced nuclear reactions on aluminium and magnesium: production of 28Mg. Int J Appl Radiat Isot 27:431–441
282. Rattan SS, Singh RJ (1985) Alpha induced fission of 209Bi. Radiochim Acta 38:69–72
283. Rattan SS, Singh RJ, Sahakundu SM, Prakash S, Ramaniah MV (1986) Alpha particle induced reactions of 209Bi and 63,65Cu. Radiochim Acta 39:61–64
284. Vysotskiy ON, Gaydaenko SA, Gonchar AV, Gorpinic OK, Kadkin EP, Kondratev SN, Prokopenko VS, Rakitin SB, Saltykov LS, Sklyarenko VD, Strizh YS, Tokarevskiy VV (1989) The Absolute Cross Sections Production of Long-Lived Radionuclides in Reactions of Alpha-Particles on Aluminium-Nuclei. In: 39. Conf. Nucl. Spectrosc. and Nucl. Struct., Tashkent USSR, pp 365
285. Rattan SS, Ramaswami A, Singh RJ, Prakash S (1990) Alpha particle induced reactions on 27Al at 55.2 and 58.2 MeV. Radiochim Acta 51:55–58
286. Karamyan SA, Oganesyan YT, Tonchev A, Vinogradov VG (1992) Activation of Aluminum Foils by ^{4}He Ions in 25–45 MeV Energy Region. In: Int. Conf. Nucl. Spectroscopy Nucl. Struct, Alma-Ata, pp 291
287. Kirov A, Nenoff N, Kolev D (1992) Excitation functions and isomeric ratios in the reaction130Te (α, xpyn) for α-particle energies between 15 and 37 MeV. Zeitschrift für Physik A Hadrons and Nuclei 341:443–452
288. Lange HJ, Hahn T, Michel R, Schiekel T, Rösel R, Herpers U, Hofmann HJ, Dittrich-Hannen B, Suter M, Wölfli W, Kubik PW (1995) Production of residual nuclei by α-induced reactions on C, N, O, Mg, Al and Si up to 170 MeV. Appl Radiat Isot 46:93–112
289. Paul RL, Harris LJ, Englert PAJ, Goldman ID, Jackson C, Larimer R-M, Lesko KT, Napier B, Norman EB, Sur B (1995) Production of cosmogenic nuclides in thick targets by alpha bombardment. Part I — short-lived radioisotopes. Nucl Inst Methods Phys Res Sect B Beam Inter Mater Atoms 100:464–470
290. Dmitriev PP, Molin GA (1979) Yields of28Mg upon the irradiation of magnesium and aluminum by alpha particles. Soviet At Energ 46:216–218
291. Tanaka S (1960) Reactions of nickel with alpha-particles. J Phys Soc Jpn 15:2159–2167
292. Houck FS, Miller JM (1961) Reactions of alpha particles with iron-54 and nickel-58. Phys Rev 123:231
293. Blann M, Merkel G (1964) Evidence of nuclear shell effects in Ni58 reactions induced with 0–48 MeV alpha particles. Nucl Phys 52:673–691
294. Muramatsu H, Shirai E, Nakahara H, Muramaki Y (1978) Alpha-particle bombardment of natural nickel target for production of CU-61. Int J Appl Radiat Isot 29:611–614
295. Takács S, Tárkányi F, Kovacs Z (1996) Excitation function of alpha-particle induced nuclear reactions on natural nickel. Nucl Inst Methods Phys Res Sect B-Beam Inter Mater Atoms 113:424–428
296. Singh NL, Mukherjee S, Gadkari MS (2005) Excitation functions of alpha induced reactions on natural nickel up to 50 MeV. Int J Modern Phys E 14:611–629
297. Uddin MS, Kim KS, Nadeem M, Sudár S, Kim GN (2017) Excitation function of alpha-particle-induced reactions on natNi from threshold to 44 MeV. Eur Phys J A 53:100
298. Takács S, Aikawa M, Haba H, Komori Y, Ditrói F, Szűcs Z, Saito M, Murata T, Sakaguchi M, Ukon N (2020) Cross sections of alpha-particle induced reactions on natNi: production of 67Cu. Nucl Instrum Methods Phys Res Sect B 479:125–136
299. Capurro OA, Tavelli MJ, Nassiff SJ (1990) (α, 3 pxn) Reactions on natural nickel. J Radioanal Nucl Chem 139:15–24
300. Yadav A, Singh PP, Sharma MK, Singh DP, Unnati BP, Singh R, Prasad MMM (2008) Large pre-equilibrium contribution in alpha+natNi interactions at 8–40 MeV. Phys Rev C 78:044606
301. Uddin MS, Kim K, Nadeem M, Sudár S, Kim G (2018) Measurements of excitation functions of α-particle induced reactions on natNi: possibility of production of the medical isotopes 61Cu and 67Cu. Radiochim Acta 106:87–93
302. Cumming JB (1959) Decay of Zn^{61}. Phys Rev 114:1600–1604
303. McGowan FK, Stelson PH, Smith WG (1964) Cross sections for the Ni58(alpha, p) Ni58(alpha, gamma), and Co59(alpha, n) reactions. Phys Rev 133:B907–B910
304. Vlieks AE, Morgan JF, Blatt SL (1974) Total cross sections for some (α, n) and (α, p) reactions in medium-weight nuclei. Nucl Phys A 224:492–502
305. Rios M, Anderson BD, Schweitzer JS (1974) The 46Ti(p, γ)47V, 50Cr(p, γ)51Mn, 58Ni(α, γ)62Zn and 58Ni(α, p)61Cu cross sections. Nucl Phys A 236:523–532
306. Ghoshal SN (1950) An experimental verification of the theory of compound nucleus. Phys Rev 80:939–942
307. Neirinckx RD (1977) Excitation function for the 60Ni (α,2n) 62Zn reaction and production of 62Zn bleomycin. Int J Appl Radiat Isot 28:808–809
308. Stelson PH, McGowan FK (1964) Cross sections for (alpha, n) reactions for medium-weight nuclei. Phys Rev 133:B911–B919
309. Zyskind JL, Davidson JM, Esat MT, Shapiro MH, Spear RH (1979) Competition cusps in (α, γ) reactions. Nucl Phys A 331:180–192
310. Esterlund EA, Pate BD (1965) Analysis of excitation functions via the compound statistical model. Nucl Phys 69:401
311. Graf H, Muenzel H (1974) Excitation functions for α-particle reactions with molybdenum isotopes. J Inorg Nucl Chem 36:3647–3657
312. Denzler FO, Rosch F, Qaim SM (1995) Excitation-functions of alpha-particle induced nuclear-reactions on highly enriched ^{92}Mo - comparative-evaluation of production routes for ^{94m}Tc. Radiochim Acta 68:13–20
313. Rapp W, Dillmann I, Kaeppeler F, Giesen U, Klein H, Rauscher T, Hentschel D, Hilpp S (2008) Cross section measurements of alpha-induced reactions on (92,94)Mo and (112)Sn for p-process studies. Phys Rev C 78:025804
314. Ditroi F, Hermanne A, Tarkanyi F, Takacs S, Ignatyuk AV (2012) Investigation of the alpha-particle induced nuclear reactions on natural molybdenum. Nucl Inst Methods Phys Res Sect B-Beam Inter Mater Atoms 285:125–141
315. Tarkanyi F, Hermanne A, Ditroi F, Takacs S, Ignatyuk A (2017) Investigation of activation cross section data of alpha particle induced nuclear reaction on molybdenum up to 40 MeV: review of production routes of medically relevant Ru-97, Ru-103. Nucl Inst Methods Phys Res Section B-Beam Inter Mater Atoms 399:83–100
316. Choudhary M, Gandhi A, Sharma A, Singh N, Dubey P, Upadhyay M, Dasgupta S, Datta J, Kumar A (2022) Measurement of alpha-induced reaction cross-sections on ^{nat}Mo with detailed covariance analysis. Eur Phys J A 58:95
317. Sitarz M, Nigron E, Guertin A, Haddad F, Matulewicz T (2019) New cross-sections for natMo(α, x) reactions and medical 97Ru

production estimations with radionuclide yield calculator. Instruments 3:7
318. Vinciguerra D, Kotajima K, Van de Vijver RE (1966) Excitation functions of the reactions induced by 23 to 52 MeV alpha particles on 197Au. Nucl Phys 77:337–346
319. Mukherjee S, Singh NL (1995) Pre-equilibrium nucleon and alpha-particle emission in the alpha-particle-induced reactions on heavy nuclei. Il Nuovo Cimento A 1965–1970(108):269–279
320. Lanzafame FM, Blann M (1970) Reactions of Au-197 with 19 to 100 MeV He-4 Ions. Equilib Statis model analy Nucl Phys A 142:545
321. Singh NL, Mohan Rao AV, Mukherjee S, Upadhyay R, Jain RK, Bose SK, Chaturvedi L, Rama Rao J (1988) Alpha-induced reactions on gold. J Phys G Nucl Phys 14:931
322. Chakravarty N, Sarkar PK, Ghosh S (1992) Pre-equilibrium emission effects in the measured isomeric yield ratios in alpha-induced reactions on $^{197}\mathrm{Au}$. Phys Rev C 45:1171–1188
323. Shah DJ, Patel HB, Singh NL, Mukherjee S, Chintalapudi SN (1995) Measurement and analysis of alpha particle induced reactions on gold. Pramana 44:535–544
324. Necheva C, Kolev D (1997) Excitation functions of α-induced reactions on gold for α-particle energies between 11 and 36 MeV. Appl Radiat Isot 48:807–813
325. Kulko AA, Demekhina NA, Kalpakchieva R, Muzychka YA, Penionzhkevich YE, Rassadov DN, Skobelev NK, Testov DA (2007) Excitation functions for complete-fusion and transfer reactions in 4He interaction with 197Au nuclei. Phys At Nucl 70:613–618
326. Bonesso OA, Capurro MJ, Ozafran MJ, Tavelli M, De La Vega Vedoya, Wasilevsky C, Nassiff SJ (2017) Cross-sections and thick target yields of alpha-induced reactions, Argentine report to the I.N.D.C.
327. Van De Vijver RE (1963) Excitation functions for alpha-induced reactions on gold. Physica 29:1214–1218
328. Kurz HE, Jasper EW, Fischer K, Hermes F (1971) Measurement and equilibrium statistical-model calculation of excitation functions of the 197Au(α, xn) reactions in the energy range from 16 to 103 MeV. Nucl Phys A 168:129–138
329. Calboreanu A, Pencea C, Salagean O (1982) The effect of gamma de-excitation competition on the (α, n) and (α, 2n) reactions on gold and antimony. Nucl Phys A 383:251–263
330. Hashimoto O, Hamagaki H, Yonehara H, Shida Y (1984) Excitation functions of the 197Au(α, 2p)199Au and 197Au(α, 2n)199Tl reactions. Nucl Phys A 413:432–438
331. Capurro OA, Vedoya MD, Wasilevsky C, Nassiff SJ (1985) Au-197(Alpha, Xn) Tl-201-X reactions. J Radioanal Nucl Chem 89:519–529
332. Bhardwaj HD, Prasad R (1986) Excitation functions for 197Au(α, xn) reactions in the 10–40 MeV energy range. Nucl Instrum Methods Phys Res, Sect A 242:286–290
333. Chakravarty N, Sarkar P, Nandy M, Ghosh S (1998) Excitation function measurement and reaction mechanism analysis for alpha-induced reactions on ¹⁹⁷Au. J Phys G-Nucl Part Phys 24:151–166
334. Ismail M (1998) Measurement and analysis of the excitation function and isomeric cross section ratios forα-induced reaction on Ir, Au, Re and Ta nuclei. Pramana 50:173–189
335. Basunia MS, Shugart HA, Smith AR, Norman EB (2007) Measurement of cross sections for alpha-induced reactions on ^{197}Au and thick-target yields for the alpha, gamma) process on ^{6}4Zn and ^{6}3Cu. Phys Rev C 75:015802
336. Szücs T, Mohr P, Gyürky G, Halász Z, Huszánk R, Kiss GG, Szegedi TN, Török Z, Fülöp Z (2019) Cross section of alpha-induced reactions on ^{197}Au at sub-Coulomb energies. Phys Rev C 100:065803
337. Sharma MK, Kumar M, Shuaib M, Sharma VR, Yadav A, Singh PP, Singh DP, Singh BP, Prasad R (2018) Analysis of experimental cross-section for (α, n) reactions in odd A and odd Z heavy nuclei: a systematics on pre-compound emission. Eur Phys J A 54:205